UCRL-9969

cy. 2

University of California

Ernest O. Lawrence Radiation Laboratory

CONTROLLED THERMONUCLEAR RESEARCH SEMIANNUAL REPORT July through December 1961

DISCLAIMER

UCRL-9969
Controlled Thermo-
nuclear Processes
TID-4500(17th Ed.)

UNIVERSITY OF CALIFORNIA
Lawrence Radiation Laboratory
Berkeley, California

Contract No. W-7405-eng-48

CONTROLLED THERMONUCLEAR RESEARCH SEMIANNUAL REPORT

July through December 1961

January 19, 1962

Printed in USA. Price $3.00. Available from the
Office of Technical Services
U. S. Department of Commerce
Washington 25, D.C.

CONTROLLED THERMONUCLEAR RESEARCH SEMIANNUAL REPORT

July through December 1961

Contents

*Preceding (Quarterly) Reports: UCRL-9777, UCRL-9598

CONTROLLED THERMONUCLEAR RESEARCH SEMIANNUAL REPORT

July through December 1961

Lawrence Radiation Laboratory
University of California
Berkeley and Livermore, California

January 19, 1962

INTRODUCTION

C. M. Van Atta

The period July 1 to December 31, 1961 was one of intense research activity and great stimulation, enhanced significantly by participation in two international conferences, the Fifth International Conference on Ionization Phenomena in Gases at Munich and the IAEA Conference on Plasma Physics and Controlled Nuclear Fusion Research at Salzburg. The conferences provided an incentive to obtain reportable results at a specific deadline, so that the period before departure for the conferences was one of particularly intense effort. The conferences not only provided information on results obtained in controlled fusion research in other countries but also generated serious discussion, indeed at times even heated debate, on the significance and validity of implications inferred from the results reported. LRL contributions to the programs of the two conferences are listed in the Talks and Publications section at the end of this report.

Some of the more significant events of the past six months are briefly summarized below.

1. In the multiple compression (Toy Top) facility diagnostic measurements demonstrated that in the 9-inch-bore third stage the plasma responded normally to magnetic compression for the first 90 μsec of the cycle but drifted radially as a body striking the wall at the end of this period. Neutrons produced during this period were clearly shown to be produced by d-d fusion events in the hot plasma. The side drift of the plasma (approx 2×10^5 cm/sec) was shown to be correlated with asymmetries in the fields produced by the two transfer coils.

To remove the asymmetries, a new set of multiturn coils on a 6-inch-bore section was installed in place of the 9-inch-bore system. With the new system the neutron-production time has been extended by a factor of about 2, but still is far short of the 270 μsec compression time. Diagnostic measurements now indicate erratic radial loss of the plasma without any strong azimuthal consistency. During these experiments the large neutron-production rate has been an invaluable aid in diagnosing the history of the hot plasma.

2. The ALICE facility for injecting a beam of 20-kev neutral atoms into a steady-state mirror field is essentially completed and will be in operation early in the next report period. The ion beam neutralizer, beam tube, and burial chamber for disposal of the unused beam of energetic atoms have been assembled and successfully operated with a beam of 70 ma of 20-kev neutral atoms, which is ample for initial plasma buildup experiments.

3. In the Table Top magnetic mirror compression facility the character of the velocity-space instability previously mentioned has been more clearly defined. The critical density at which the instability occurs is lower by at least two orders of magnitude than that corresponding to the "mirror" instability, which had previously been postulated as the mode of the instability. Radial current and electrostatic probes show that in the unstable mode the plasma usually develops a single radial projection which exhibits charge separation and rotates at speeds of 10^5 to 10^6 revolutions/sec. These results suggest the presence of an interchange instability, usually with a single rotating flute. It is also observed that under certain circumstances the plasma is quasi-stable in the sense that the instability does not occur unless it is triggered by any of several different types of disturbances. The detailed structure of the plasma when it becomes unstable and the mechanism and rate of growth of the instability are subjects for further study.

4. Significant results obtained during preliminary operation of the levitron were reported previously. During bakeout of the liner at 450°C to improve the vacuum, trouble developed in two areas. Cracking of the inconel inner liner occurred near the hard-soldered joints, and the insulating epoxy coat on the inside surface of the outer shell failed owing to inadequate heat transfer. The levitron is now being reassembled with many substitutions of materials which should eliminate the difficulties and permit operation at substantially lower base pressure than was possible with the original construction.

5. Resistive instability calculations have resulted in the prediction that within the Astron E layer a B_θ field will be spontaneously generated. What effect if any this process will have on E-layer buildup and stability is not clear. It has also been shown that in a beam-plasma column formed by a high-energy electron beam passing through a gas the usual electrostatic two-stream mechanism in a weakly ionized medium is less important than a resistive instability of lower growth rate for which dissipative effects do not suppress collective interaction.

6. Extensive calculations of single-particle injection and confinement in a bumpy torus field have been carried out. Particles injected through the split coil of the torus behave qualitatively as originally predicted, but a more nearly optimum set of injection parameters has been determined. Experimental evidence for the drift surface diffusion previously predicted for the motion of particles in a bumpy torus field has been obtained by studying the effects of stationary probes on the current of particles escaping through the mirror at one end of a distorted mirror field. Engineering design for the bumpy torus apparatus for injection and trapping of 100-kev electrons is nearing completion, and some components of the apparatus have been constructed.

7. In the ion cyclotron resonance experiment (Hothouse II) the structure of the rotational hydromagnetic wave has been determined in greater detail by the use of a seven-coil magnetic probe allowing observation of the b_θ field component at seven positions simultaneously. The results confirm the conclusion reported previously on the basis of shot-to-shot observations that a substantial fraction of the 8.5 Mc power from the oscillator is transmitted along the plasma column in the form of a torsional wave. Large variations in wave amplitude with z position and in azimuth, however, are now apparent, and are interpreted as evidence of plasma turbulence on reflection of the wave from the magnetic beach region.

8. A terminal report on the ion magnetron device is included in the section on the Berkeley program. Many features of this interesting $E \times B$ type of discharge have been investigated and deserve further study. However, in the interest of pursuing projects that give greater promise of results of thermonuclear application, the ion magnetron project has been terminated.

I. PYROTRON (MAGNETIC MIRROR) PROGRAM

1. INTRODUCTION AND SUMMARY

Richard F. Post

Experimental study of plasma instabilities and their anatomy, and final preparations for putting the ALICE experiment into operation, were the main items of activity in this report period. In the Toy Top experiment the existence of a slow plasma drift to the chamber walls was shown, through its influence on the neutron yield from the plasma and the onset of light emitted from the chamber walls. The drift was found not to be random in direction, but to be correlated with asymmetries in the pulsed fields used for manipulating the plasma. New coils have been installed with smaller asymmetry. This has resulted in approximately doubling the confinement time, even though the chamber diameter is now smaller (6 in. instead of 9 in.). However, abnormal losses still persist and their nature is being studied.

New Table Top III was put into operation, with greatly improved vacuum conditions and with a lengthened field-holding time (0.2 sec). The first experiments with Table Top III have been concerned with further study of the plasma instabilities associated with the high-ratio magnetic compression mode of operation (as used in Table Top II). Some particularly interesting features of the instability have been discovered, and evidence of the apparent existence of nonlinear phenomena in its initiation has been seen. It has been found that, in its fully developed form, the instability appears to be a rapidly rotating "flute," carrying with it a dipole-like charge distribution consistent with its observed rotation and the transport of particles across the confining field.

As before, the instability is suppressed when the injected plasma density is increased. Of considerable interest is the fact that, under the proper conditions of density, the instability can be "latent," not appearing until many milliseconds after the initiation of compression, and then only when triggered by an electrostatic perturbing signal, which may apparently be small and of very short duration. This seems to show that nonlinear effects are operative, such that a minimum initial amplitude, larger than normal fluctuation levels, must be present for the instability to occur. If, in fact, the observed instability turns out to be "the" hydromagnetic interchange instability of the mirror machine, this property could be of substantial importance in understanding and --one would hope-- achieving adequately stable plasma states.

Most of the preparations for the ALICE neutral injection experiment are now complete, and final assembly is now under way. A neutral beam of nearly the supposed required intensity was transmitted successfully throughout the entire apparatus. Also, some very interesting and encouraging measurements were made in the use of gettering and cryogenic vacuum pumping techniques. Some studies of the use of transient plasma bursts to "boost" the initial buildup rate were also made, with encouraging results.

In summary, we are now fully in the middle of studies which bear crucially on the question of stable, long-time confinement of plasmas in a mirror machine. Although not all has proceeded without a hitch, we are encouraged by the increase in experimental data, by our new knowledge of the anatomy of plasma instabilities, and by the promise of a new method of plasma formation (neutral injection) about to be tested.

2. MULTISTAGE HIGH-COMPRESSION EXPERIMENTS

Frederic H. Coensgen, William F. Cummins, William E. Nexsen, Jr., Arthur E. Sherman, and Robert E. Ellis

Introduction

In the period covered by this report we have worked with two different multistage compression experiments. The first of these was, of course, the one (9-inch three-stage experiment) described in the preceding quarterly report.[1] All the results from the 9-inch three-stage system are reported in UCRL-6381 Addendum.[2] During September, at the time of the Salzburg meeting, the 9-inch three-stage experiment was dismantled and a 6-inch three-stage experiment installed. The 6-inch system was designed to eliminate certain asymmetries present in the 9-inch magnetic fields, and thus to check the fundamental nature of the observed cross-field plasma drift found in the 9-inch system. Investigation of the plasma behavior in the 6-inch system is still in progress.

9-Inch Three-Stage Experiment

Throughout the investigations from June to September, the magnetic field at the injection point in the 18-inch chamber was 600 gauss, and the dc magnetic field in the transfer section of the 9-inch volume was 2400 gauss. The dc field beyond the transfer section could be maintained at the 2400-gauss value (flat field configuration) or raised to about 10,000 over the third-stage region. Furthermore, the third-stage pulsed magnets located at 18, 12, 15, and 8 inches could be used to provide (essentially constant) large magnetic barriers in the third-stage region as well as be used in the more conventional third-stage compression. Three pulsed magnets were used in the transfer (second-stage) region. First, the single-turn gate coil at 74 inches followed by two 20-inch transfer magnets. One-inch separations were used between the gate coil and first transfer magnet, between the two transfer magnets, and between the end of the second transfer magnet and the first of the third-stage magnets.

---

[1] Frederic H. Coensgen, in Controlled Thermonuclear Research Quarterly Report, UCRL-9777, August 1961, p. 4.

[2] F. H. Coensgen, W. F. Cummins, W. E. Nexsen, Jr., and A. E. Sherman, UCRL-6381 Addendum, presented at the Conference on Plasma Physics and Controlled Nuclear Fusion, Salzburg, Austria, September 1961.

Optimum operation, as judged by neutron production, was obtained for the following timing sequence: injection at 0 μsec, gate and first transfer magnet pulsed at 14 μsec, second transfer magnet pulsed at 20 μsec, and first third-stage magnet pulsed at 50 μsec while the third third-stage magnet was pulsed early and was used as a dc barrier. The sequence viewed from the plasma is first mainly one of trapping, followed by a rapid radial compression which slows down as the second transfer magnet current attains its maximum value at 70 μsec. Also, in the period from 50 to 70 μsec the plasma is being transferred into the third-stage compression region where the radial compression is continued at a slower rate to 300 μsec, when the third-stage magnet currents have attained full value. As reported earlier, the compression process as judged from the rate of neutron production proceeds as expected at about 70 μsec, when it starts to decline rapidly and by 100 μsec it has decreased essentially to zero. This sudden break in the neutron production and its subsequent decline despite the continuing compression is in sharp contrast with the expected continued plasma heating and compression. Plasma loss due to excessive longitudinal compression and energy loss from the hot ions to cold electrons could be expected to slow the increase of the reaction rate, but could not be expected to lead to a catastrophic quenching of neutron production. Although the total neutron production could be changed by changing the timing sequence, capacitor bank potentials, and injection conditions, the reaction history remained essentially unchanged for all conditions. Indeed, early in July the evidence strongly supported the existence of losses of plasma or ion energy or both by processes other than classical, i. e., supported the existence of instabilities or other co-operative effects.

Early in July the character of the investigation changed from a study of the effect of parametric changes upon the total neutron production and reaction history to a more detailed study of the plasma behavior for one operating condition. The system was viewed transversely by a photomultiplier located at the final compression chamber. Large light bursts were found at the time the neutron-production rate decreased. An electrostatic probe was introduced which detected plasma near the wall at the time the neutron production decreased. It was established that the light and probe signals were exactly time-correlated and that as these signals increased the rate of neutron production decreased. Multiple-probe arrays were made which could be rotated and moved in the longitudinal direction, thus allowing a detailed investigation of the plasma bombardment of the wall. To facilitate interpretation of the data, most of the probe studies were made by using only one plasma injector located on axis. Investigations in the final compression region indicated that the plasma reached the wall at preferred azimuthal locations. The flute-like nature of the plasma flow was also verified.

As the preferred location appeared to be somewhat correlated with the leads of the transfer magnets, a "flat"-field experiment was performed. In this experiment the dc field was maintained flat at 2400 gauss throughout the entire 9-inch glass section, i. e., in both the transfer and third-stage regions. An "end" magnetic barrier was provided by pulsing one of the third-stage magnets early in time. In the absence of the end magnetic barrier, no probe signals or light signals were obtained for any operating sequence of the second-stage magnets. With the stopping magnetic barrier and only

one transfer magnet the location of the plasma bombardment of the wall was found to be strongly correlated with the lead position of the transfer magnet. Fortunately, the leads for the two transfer magnets were on opposite sides (i.e., 180° azimuthal separation). It was found that the plasma drifted as a body toward the low-field region at the lead side of the magnets. The drift velocity was found to be 2×10^5 cm/sec. The azimuthal extent of the plasma, as determined from multiple probe arrays, at a radial position of 3 in., was 2 in. to 3 in., which is consistent with the expected diameter of the plasma column. The time dependence of the probe signals was consistent with the diameter of the plasma column and the drift velocity.

Even before it was known that the plasma drifted to the wall, the persistent similarity of the tails of the various neutron histograms cast doubt on the validity of identification of the counts observed at the late times with late d-d reactions. Therefore, simultaneously with the probe investigations just described, a complete duplicate of the final compression section was fabricated and installed in the Cockcroft-Walton target area. The 500-kev D^+ beam from this accelerator was allowed to bombard deuterated targets placed in the final containment region of this duplicate system. These targets were bombarded for 50 μsec and the counting rate was measured by using the same counters in the same relative positions as used to obtain the neutron histograms. The decay of the counting rate in this experiment was found to be the same as that of the counting rate after 100 μsec in the plasma experiments. We conclude that the counts later than 100 μsec are due primarily to γ rays from the capture of neutrons which have been slowed down and have been rattling around in the large mass of plastic and copper of the pulsed and dc magnet systems. Previously, the late counts were identified as neutrons by measuring their absorption length in lead. Because the counting rate is low, the detector could not be moved very far from the system, so it was known that the counting geometry was "poor" and that the observed absorption length would be greater than the 2-cm value one would expect if "good counting geometry" could have been used. The absorption length obtained was 10 cm, which was assumed to be sufficiently greater than 2 cm to indicate that the late counts were neutrons. For the extended γ-ray source represented by the magnet system and close position of the recoil counters this assumption is now believed incorrect, and the plasma containment time in the 9-inch three-stage experiment must be revised downward from 900 to 90 μsec. It is possible that late counts could be due to capture γ rays arising from neutrons which slow down in the scintillator and are captured there. This effect was evaluated in the Cockcroft-Walton runs by noting the apparent broadening in our counter of a neutron pulse of known width. The broadening was found to be less than 7 μsec.

As the plasma is known to bombard the walls, the question arises whether or not the observed reactions are in the plasma or due to wall bombardment. Only 10^{10} fast (50- to 1000-kev) D^+ ions/cm^3 in the plasma would produce, through wall bombardment, the total observed number of neutrons. The following observations are evidence that the reactions occur within the plasma. First, as stated above, from neutron histograms taken simultaneously with the probe data, the rate of neutron production was found to reach its maximum value about the time the plasma was first detected by the probe, and as the probe signal increased the neutron rate rapidly decreased. Second, the peak of the rate is 20 μsec earlier when the wall

probes are in position. As the probes extend 3 cm from the walls, the drifting plasma would be expected to encounter them 20 μsec before striking the wall. Thus the 20-μsec shift in the peak of neutron production is consistent with the hypothesis that the reactions are quenched upon striking the probe or wall.

Finally, the following experiment was carried out to check neutron production by wall bombardment. It was found that the neutron production was about 10^4 n/pulse if the plasma was simply compressed and transferred into the third-stage region without the use of any compression in that region (that is, without use of the third-stage pulsed magnetic fields). Under these conditions the plasma ions have attained their maximum energy by the time they enter the third stage. If the neutron production is simply due to wall bombardment because the plasma drifts, then the same production should be obtained if ions encountered the wall immediately upon entering the third-stage region. Such a wall was introduced by mounting a glass plate at the position of lowest field in the third-stage region, so that every ion entering the region encountered the plate on its first traversal. No neutrons were observed. When the plate was moved into the higher-field regions near the "end" magnetic barrier, some of the plasma ions could not strike it and neutrons were detected. The neutron production increased as the plate was moved into the barrier field. We conclude that at least 90% of the reactions occur within the contained plasma. This experiment also sets an upper limit of 10^9 fast ions per cm^3 in the plasma, which is confirming evidence supporting the previous conclusion that the d-d reactions arise from the plasma ions of the previously measured energy distribution rather than from a small number of exceedingly hot ions.

6-Inch Three-Stage Experiment

It had been shown that in the 9-inch three-stage experiment the plasma drifted toward the lead side of the transfer magnets. As these magnets were constructed of five wide turns in series, the symmetry of the field should be similar to that of a single-turn magnet. Asymmetries up to 5% were subsequently found by differential field measurements, confirming the earlier hypothesis of field asymmetries in the 9-inch transfer fields. Although the actual field shape is quite complex, the essential feature is the weak-field region at the lead side of the magnet.

The question arose whether the plasma drift was due only to strong driving forces or was a hydromagnetic instability (m = 1) which, because of the asymmetric field, developed in a preferred direction. To answer this question a system was designed with greatly improved azimuthal symmetry. It consists of five eight-turn coils, each fed by a separate capacitor bank. In order to achieve initial values of dB/dt comparable to the former experiment the coil diameter was reduced, so that the present system is reduced to 6 in. from the 18-in. injection end.

Both the light monitor and the electrostatic probes indicate considerable wall bombardment in the 6-inch chamber at the time of injection. This was reduced to some extent by increasing the field in the injection region to 1000 gauss. However, the amount of bombardment is still apparently higher than in the 9-inch system.

The performance of the 6-inch system as judged from neutron output is quite sensitive to timing and field conditions. This sensitivity is due in part to the short trapping length and perhaps in part to a competition between heating and charge exchange. When the system is optimized the maximum neutron output is 3×10^5 n/pulse, which is about an order of magnitude greater than obtained previously.

At this production level the neutron signal in the fast counter provides a histogram for each operation. These histograms have been very useful in evaluating the effect of various modifications of the system. Typically the neutron production starts between 30 and 40 μsec after the sources are fired, and persists to 150 to 200 μsec. Therefore production times of 150 μsec are common. This is to be compared with typical production times of 50 μsec in the 9-inch system.

Two types of decay of the neutron production have been tentatively identified. In the first type (mode I decay) there is a sudden drop in the neutron production, occurring most frequently in the time interval between 100 and 200 μsec. Both large light signals and large probe signals are obtained at the time of the sharp decrease in neutron production. Indeed, the phenomenon is much the same as that observed in the 9-inch system at the time the plasma struck the chamber wall. In the 6-inch system the mode I decay is also associated with a loss to the walls of a large fraction, perhaps all, of the hot plasma ions. In the second type of decay (mode II) the decay of the neutron-production rate is slower and on the average the production lasts to slightly later times. However, the compression process continues to 270 μsec, so it is apparent that there is a loss of hot plasma ions due either to a plasma loss or to a cooling process. There is an early plasma loss (as detected by probes) associated with some mode II decays and perhaps indicating a density effect. However, in controlled-density experiments the ratio of mode II decay to mode I decay was not affected. It is possible to postulate for the mode II decays a loss of plasma involving a cascade process due to charge exchange and slow neutral production at the walls by the fast neutrals. So far, we have not been able to check this hypothesis, and it may well be that the question will not be resolved until the 6-inch system is replaced by a larger system.

Attempts to stabilize the plasma by means of weak "Ioffe type" fields and by end conduction have yielded no positive results. With the stabilizing fields there is a large plasma loss. Consequently the total neutron production is lower. However, the lower neutron production may in part be due to the added production of neutrals by the escaping plasma. Added neutral production and slower pumping speed prevented any large effect due to the introduction of a conducting end plate. There was, however, weak evidence that the neutron-production time was slightly extended.

Summary and Conclusions

There are rather large end losses of plasma throughout the time of neutron production, but the loss of plasma through the mirror does not seem to extend much beyond the neutron-production time. As the density and ion-energy distributions are unknown, the end-loss rate cannot be compared with theory. Neither the energy or e/m has been measured for the plasma lost out of the end.

We suspect that neutrals produced at the walls at the time of injection play a large role in the operation of this device. Preliminary designs of clean and hot wall systems are in progress. Such systems require larger volumes, and their construction may await the installation of larger facilities.

Certainly in some instances a flute-like instability develops. Its velocity is apparently low, about 2×10^5 cm/sec. Within the limits of our observations, the development of the flute (perhaps, in some instances, m = 1) in the 6-inch system is random in time and in azimuthal position. In the 6-inch system the curvature of the field is too sharp to expect the full effect of "stabilization by finite larmor orbits." Also, because of the presence of sharply curved field lines and small mirrorlike regions (rather rippled field lines) within the containment region, conditions for other instabilities may be enhanced, leading to the development of flutes as a secondary process.

We conclude that operation with the 6-inch system has definitely shown that factors other than azimuthal field symmetry are important for control of transverse plasma transport in mirror containment geometries.

The study of the reaction history has been an invaluable aid in evaluating the operation of this device. In particular, neutron production large enough to provide that history with each operation is essential for a device which has large fluctuations in its operation from one shot to the next. For example, distinct modes of decay of the neutron production can now be distinguished. These modes would be completely unobservable if the histogram were constructed from several operations.

3. TABLE TOP III

New Results in Experimental Studies of an Instability

Walton A. Perkins, Richard F. Post, and Norris W. Carlson

Previous results of experiments on Table Top II indicated a velocity-space instability, and this instability was thought to be the "mirror" instability.[1] Recent calibration of the scintillation detectors with an electron source has shown that the experimental critical β (associated with the high-energy electron component) is less than the theoretical β_c by some two or

[1] R. F. Post and W. A. Perkins, Phys. Rev. Letters 6, 85 (1961).

more orders of magnitude (deduced from approximate measurements of the velocity-space anisotropy of the energetic electrons). Also one qualitative disagreement has been discovered; in a few cases the instability was observed to start after the peak density and, presumably, the largest anisotropy had passed. Both these observations seem incompatible with an explanation based on "mirror" instability induced by the high-energy electrons. With these facts in mind we initiated new studies of this instability in Table Top III under conditions as similar as possible to those formerly used in Table Top II.

A diagram of the experimental arrangement was shown in the preceding report.[2] Unlike Table Top II the vacuum chamber walls are stainless steel in the plasma-trapping region.[3] The principal diagnostic detectors were a 4.5-in.-diameter scintillator monitoring the end-escaping electron flux, a 0.25-in.-diameter scintillator 3.5 in. from axis in the midplane detecting the radially escaping flux, and an electrostatic pickup probe also in the midplane.

For the results reported here the initial midplane magnetic field was about 10 gauss and the pulsed mirror field rose to 17 kilogauss (at the midplane) in 7.5 msec; the decay time constant was 200 msec. One hydrogen-loaded titanium source was used.

Figure I-1 shows the different phases through which the instability passes as the base pressure is changed for a given source voltage (chosen to enhance the likelihood of instability; see remarks in next paragraph). The presence of the instability, which results in a rapid transport of plasma across the field lines, is indicated by the radial probe signal. Note that at a pressure of 2×10^{-7} mm Hg the end probe signal sharply decreases and the radial probe signal appears at the same time, both evidencing the rapid loss of plasma radially. The main characteristics of the three regimes are:

(a) At high vacuum the plasma becomes unstable very early and most of the plasma is lost to the instability; note the pulse heights (volts) of the end probe signals.

(b) At medium vacuum, the plasma seems to be quasi-stable. The instability starts at from 1 to 9 msec with a sharp rise. It usually occurs right at the crowbar time of the pulsed mirror coils. The crowbarring of the field triggers the instability, as is discussed below;

(c) At high pressure, the plasma appears to be stable.

Different phases of the instability are also encountered, as the source voltage is varied at a base pressure of 5×10^{-9} mm Hg. These are shown in Fig. I-2. The main characteristics of the four regions are:

(a) At very low injected plasma density (0.5 kv on source) the plasma is observed to be stable. Here the Debye length is presumably greater than the dimensions of the containment region.

---

[2] Walton A. Perkins and Richard F. Post, in Controlled Thermonuclear Research Quarterly Report, UCRL-9777, August 1961, p. 5.

[3] Whether the walls are metallic or not seems to have an effect on the instability. See Walton A. Perkins, in Controlled Thermonuclear Research Quarterly Report, UCRL-9598, March 1961, p. 9.

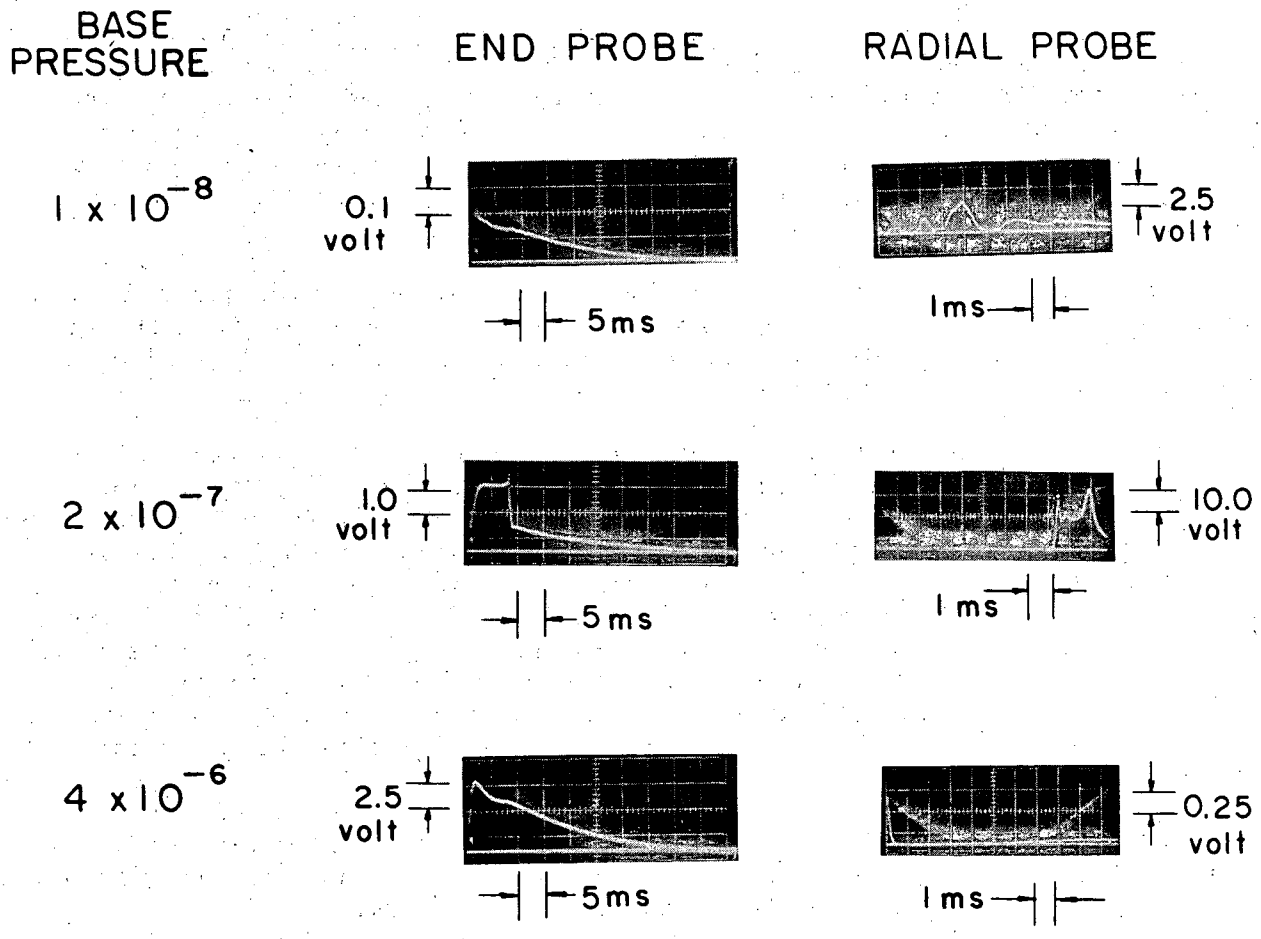

Fig. I-1. End and radial scintillation probe signals, showing the effect of chamber pressure on the instability.

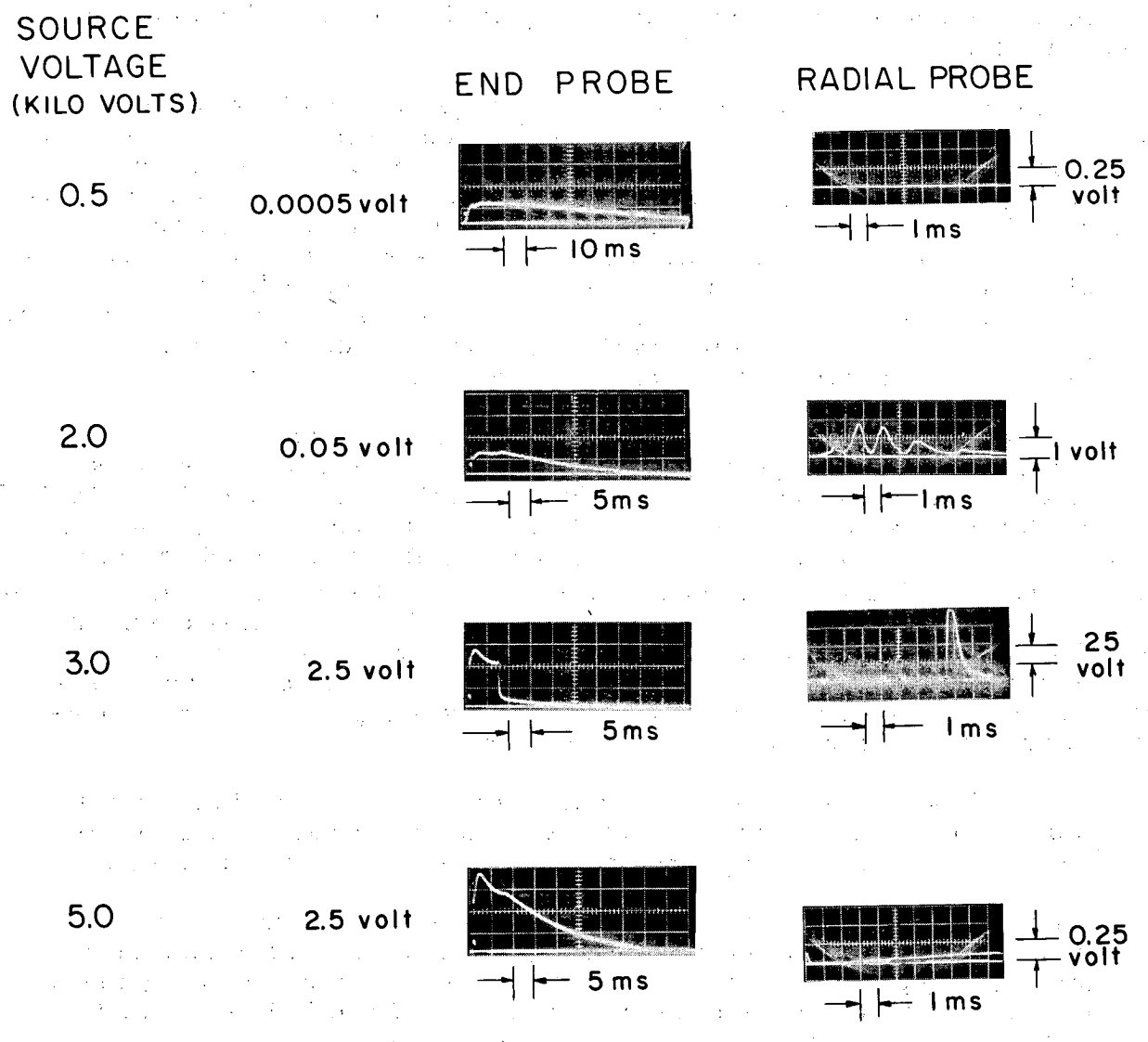

Fig. I-2. End and radial scintillation probe signals showing the effect of source voltage on the instability at a base pressure of 5×10^{-9} mm Hg.

(b) At moderately low injected density (2.0 kv on source) the plasma is observed to be very unstable.
(c) At medium injected density (3.0 kv on source) the plasma is "quasi-stable," only occasionally exhibiting unstable behavior.
(d) At high injected density (5.0 kv on source) the plasma appears to be stable. It should be noted that when the source fires, a gas burst occurs whose magnitude varies with source voltage. However, the effects of this gas burst are greatly reduced by the fast pumping speed of the molybdenum-coated walls.

The fine structure of the end and radial probe signals was observed in detail. When examined with a fast scope and nonintegrating tube base, the end probe signal is seen to be composed of random 0.01-μsec pulses--typical of pulses from a plastic scintillator. However, the instability signal of the radial probe is composed of regular, periodic pips, as is shown in Fig. I-3A and B. The half width of the pips is usually about 0.1 μsec, but is occasionally as long as 2 μsec. By use of two radial scintillation probes (one of which was movable along the circumference of the circular chamber) at opposite sides of the chamber in the midplane, we discovered that the periodicity is associated with a rotation of the unstable plasma.

To study the rotation further, we inserted an electrostatic probe in the midplane, which samples the changing electric field. The probe is essentially an antenna consisting of a short length of insulated wire. Typical electrostatic probe signals are shown in Fig. I-3 C and D. By (a) pulling the electrostatic probe back out of the region accessible to charged particles, and (b) using a similar probe enclosed in a glass tube, we have demonstrated that the signal received is not caused by collected charged particles. The positive part of the signal is caused by the presence near by of a predominance of positive charges, whereas the negative part is caused by a predominance of electrons. This means that the unstable rotating plasma form is electrically polarized, i. e., some charge separation is present.

Occasionally, two or more plasma forms rotate around the chamber at the same time with different angular velocities. A case in which this occurs is shown in Fig. I-3 E; the two periods are 4.0 μsec and 7.4 μsec.

Three possible models for the simple cases of rotating plasma are shown in Fig. I-4: (a) a rotating column, (b) a rotating wave on a disk, and (c) a spinning arm. These models are meant only to indicate general shapes. The $\vec{E}$ field should actually point almost directly inward, as the rotational velocity is in fact about 100 times the outward radial velocity.

There is some experimental evidence for the simple outer configuration, but almost none for inner structure. The evidence for the outer shape is as follows:
1. The direction of rotation relative to the direction of the magnetic field was determined by the time sequence of signals from a fixed and a movable probe.
2. The electrostatic probe signals showed that the electrons pass by first, the ions second. The polarization would have to be in this direction in order to produce an azimuthal $\vec{E}$ field that would drive the plasma outward across the field lines (with a velocity $v_r = E_\theta / B$).

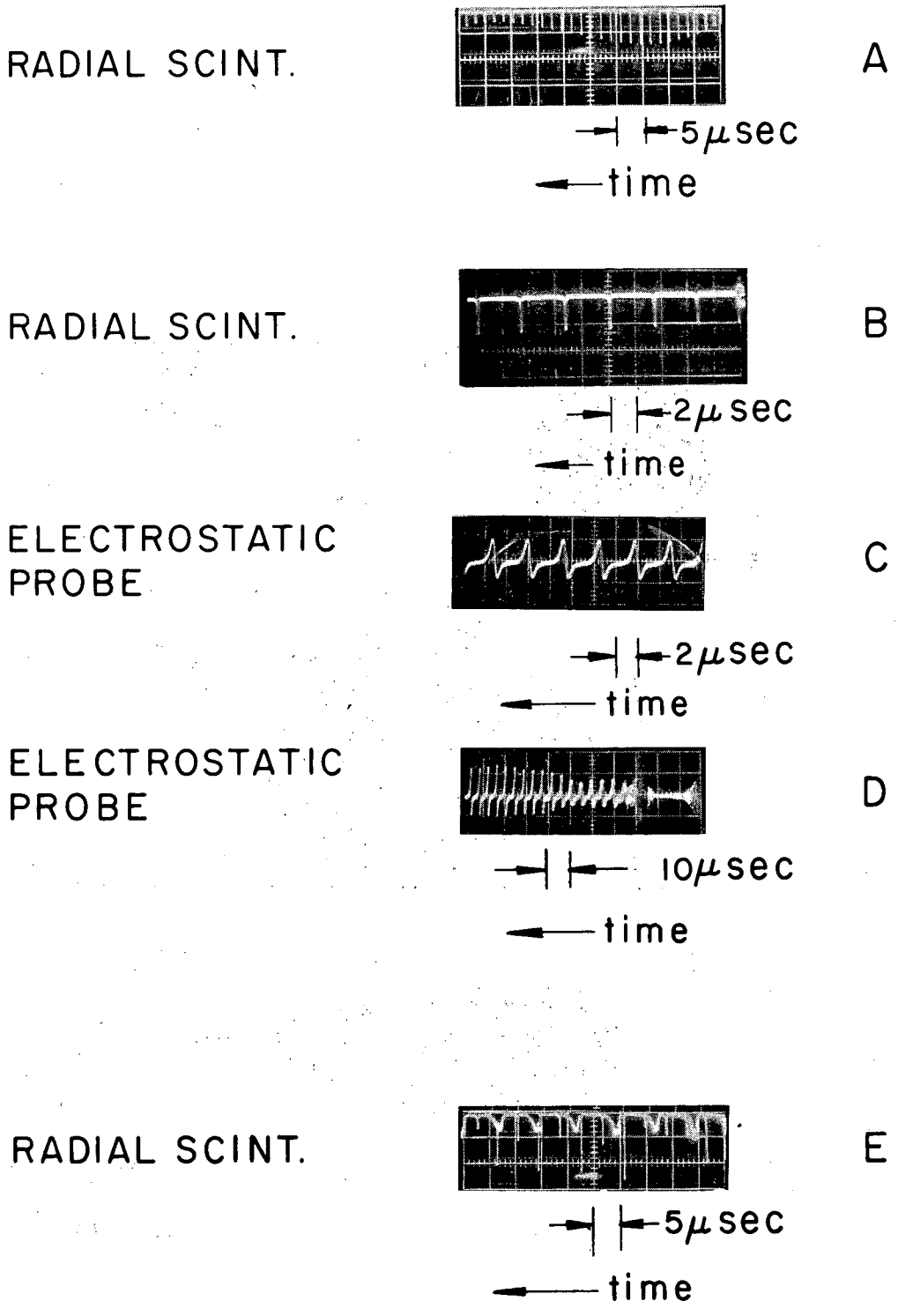

MUB-930

Fig. I-3. These traces were all taken with a delayed trigger on the scope. A and B are radial scintillation probe signals. C and D are electrostatic probe signals. B and C are for the same pulse and the scopes were triggered at the same time, but the probes were at different locations in the chamber. E shows a case in which two plasma forms rotate with different angular velocities. The periods are 4.0 μsec and 7.4 μsec. (Time goes from right to left.)

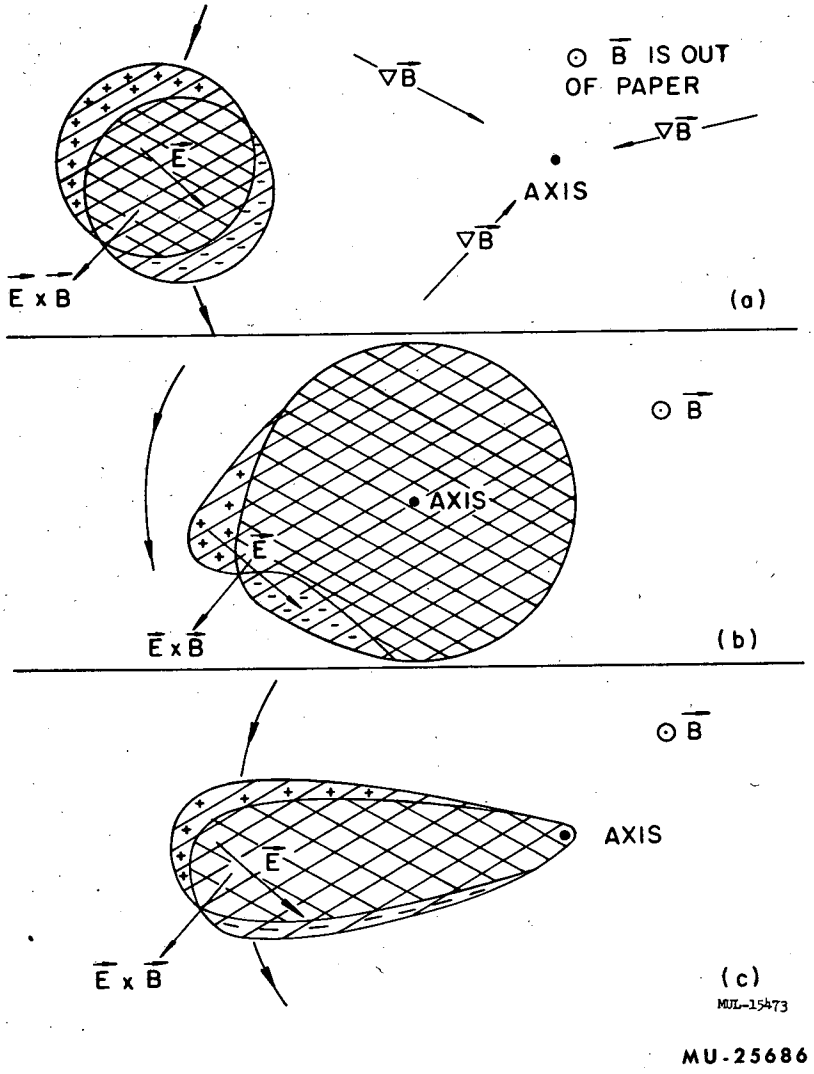

Fig. I-4. Three models for the rotating plasma: (a) rotating column, (b) rotating wave on a disk, and (c) spinning arm.

3. The relative pulse heights of the positive and negative electrostatic probe signals indicate that relative to the negative region, the positive region is closer to the probe, i. e., farther from the axis. This is supported by the fact that the scintillation probe is observed to be struck by particles just at the time when the predominantly positive part goes by it. Also, the observed direction of rotation would require inward radial $\vec{E}$ fields.

In cases in which the plasma is quasi-stable, the instability can be triggered. Many methods were found to trigger the instability anytime from 3 to 50 msec after injection. Three of the best methods were (a) firing a second plasma source in the midplane, (b) crowbarring the pulsed mirror field (see Fig. I-5 a), and (c) pulsing an axial magnetic coil nearby (see Fig. I-5 b). In Fig. I-5 a the fast-scope traces were initiated with the triggering of the crowbar ignitrons and in Fig. I-5 b with the triggering of the ignitrons for the coils. The instability could even be triggered with no voltage on the coil' s capacitor bank. The electrostatic probe picks up the ignitron "hash" at the beginning of the trace.

The period of the rotation of the instability varies from shot to shot, but is usually from 1 to 10 μsec. The period for a single shot was measured with a raster scope over the whole instability time and found to be quite constant. It usually increases slowly with time (much slower than B changes), but there are exceptions. These data are occasionally complicated by one plasma form, rotating with one period, dying out while another one, with a different period, takes over. The instability has been observed sometimes to start as early as 130 μsec (when the magnetic field is only 450 gauss).

These results reported suggest the presence of an interchange instability with a single, rotating flute. Since the start of experiments on Table Top III in September the results on the instability have been very informative, but these results have in turn raised many new questions. A few of these are: (1) What does the inner shape of the rotating plasma look like? (2) Why does the rotation occur at all? (3) What is the stabilizing mechanism in the high-pressure and high-density cases? (4) What actually happens when the instability is triggered?

Discussion and Calculation of Some Possible Stabilizing Effects

Richard F. Post

The questions raised by the experiments reported show that instability phenomena in magnetic-mirror geometry may be more complex than previously suspected. That the plasma can exist in a state in which instability appears only when triggered by an electrostatic perturbation signals strongly suggests that there are stabilizing forces present of an effectiveness which depends on the plasma parameters. The fact that instability and anisotropy seem to go hand in hand suggests that one should look for both destabilizing and stabilizing effects which are anisotropy-dependent. The further observations that we apparently cannot appeal to the "mirror" instability to explain our results, and that the nature of the instability (when fully developed) seems most nearly to resemble the "flute" instability, suggest that this instability be considered. Although no definitive theoretical treatment of the flute instability in a realistic model of the mirror

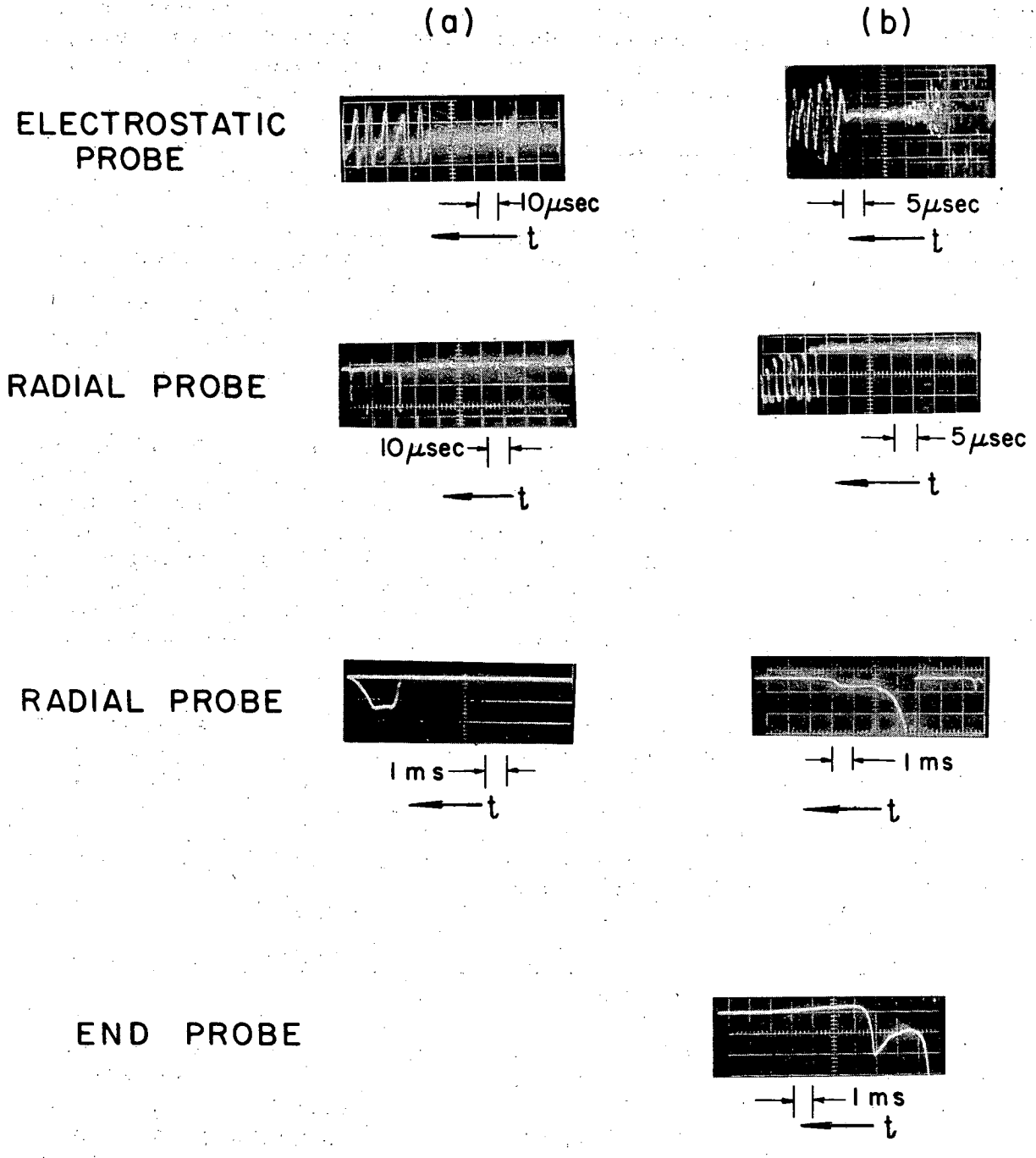

Fig. I-5. The instability is triggered by (a) crowbarring the pulsed mirror field, (b) pulsing an axial magnetic-field coil near by to 2 kilogauss. Time goes from right to left.

machine has yet been made, some informative leads can be derived from partial treatments.

That plasma velocity space anisotropy can lead to a destabilizing effect can be shown from the energy principle.[4] A treatment, more general than previous ones, of interchange instabilities in the mirror machine has been given by Newcomb.[5] In the limit of infinitesimal orbits (where finite-orbit induced drifts are negligible), and for $\beta \ll 1$, Newcomb finds the expression

$$\oint \frac{d\ell}{r^2 B^2 R^2} \left\{ \frac{\nabla p^*}{\nabla B} \Big|_{\parallel} - \frac{\nabla p^*}{\Delta B} \Big|_{\perp} \right\} > 0, \text{ stable,}$$

(I) (II)

where $p^* = p_\perp + p_\parallel$ and the gradients are taken in the directions indicated, i.e., either parallel or perpendicular to the local field direction. The line integral is to be taken along any axi-symmetric flux tube, the instability characteristics of which are to be evaluated. The quantities r, B, and R refer to the radius of the flux tubes, the local magnetic field strength, and its local radius of curvature, respectively.

Examining Newcomb's expression, one can see that the "parallel" term (labeled I) is always destabilizing, for any realistic plasma distribution, and is the more so the more anisotropic the distribution. This is because p^* always decreases with position in going away from the midplane, and at a more rapid rate as the distribution becomes more anisotropic. Similarly term II, the "perpendicular" term, has stabilizing contributions only near the mirrors (where $\nabla B/B$ changes sign), and is still always on the whole unstable for realistic distributions, the more so the higher the degree of anisotropy.

Consistent with the general trends predicted by Newcomb's expression, we do observe a tendency for greater instability for the more anisotropic distributions. In disagreement with his expression, however, we observe stable cases where none are predicted. This suggests that the observed stability may be traced to one or more stabilizing terms, not included in his formulation, and which may also be anisotropy-dependent. One such term is the effect of "line tying," i.e., the relative effectiveness with which electrical contact is established to some conducting surface external to the ends of the confining region. However, other than to say that the degree of electrical conductivity along the magnetic lines and through the mirrors is presumably less if the plasma is concentrated at the midplane and does not reach the mirrors, nothing quantitative can presently be said about this mechanism. There exists, however, another stabilizing effect which can be evaluated quantitatively, at least as far as its time scale relative to that of the observed instability growth times is concerned. This is the mechanism of the statistical smearing of a flute, arising from the

[4] I. B. Bernstein et al., Proc. Roy. Soc. (London) A, 244, 17 (1958).

[5] W. Newcomb, Annals of Physics (to be published).

azimuthal ∇B drift velocities (traceable to the finite size of the particle orbits) of the particles of the plasma.[6] A spread in these drift velocities arises from the distribution of energies of the particles about the mean. This spread will result, in the absence of compensatory effects, in the eventual "smearing out" of any azimuthally varying charge separations. It is easy to see that in first order the magnitude of the ∇B drifts are independent of the existence of such charge separations, since the resultant motions are at right angles to each other, so that the rate of smearing is also independent of charge separation, to this order. A brief summary of the calculations that have been made follows.

Considering the guiding center motion of the individual particles of the plasma, we can distinguish two independent kinds of drifts, (a) the usual $E \times B$ drift velocity of magnitude $v_0 = c(E_\perp/B)$, and (b) the ∇B induced drifts which for $\beta << 1$ are given by the expression $v_d = (1/\omega_c R)(v_\parallel^2 + \frac{1}{2} v_\perp^2)$. Here ω_c is the gyromagnetic angular frequency of the particle, and R the local radius of curvature of the magnetic lines. Drift (a) is in the same direction for both electrons and ions, and is independent of particle energy. When it arises from axi-symmetric charge separations (such as in the equilibrium state) it may be formally eliminated by transforming to a rotating frame of reference where $E_\perp = 0$. Drift (b) is in opposite directions for electrons and ions and varies linearly with energy; this drift gives rise to the smearing effects which we wish to evaluate. The results will be given for a simple Maxwellian distribution; they can readily be generalized to include more realistic distributions.

We consider an initial azimuthally varying infinitesimal charge separation of "flute" form (in the mth mode) and ask for its rate of decay due to smearing. Take the charge-separation distributions to be of the form

$$\rho_+ = \rho_0(r)[\,1 + \delta \cos m\,(\theta - \omega_+ t)],$$

$$\rho_- = \rho_0(r)\,[\,1 - \delta \cos m\,(\theta - \omega_- t)]\,,$$

where $\delta << 1$, and ω_+ and ω_- are the magnitudes of the angular precession frequencies (owing to ∇B drift) of ions and electrons, respectively.

For the case $\omega_+ = \omega_-$ the net charge separation is then simply

$$(\rho_+ - \rho_-) = 2\rho_0\, \delta \cos\,(m\theta) \cos\,(m\,\omega\, t).$$

If the energy distribution is taken to be Maxwellian, we then find, upon Fourier analysis in θ, for the rate of decay of the mth mode,

---

[6] Rosenbluth et al. have also considered stabilizing effects arising from finite orbit size, but their calculation considers another aspect of the problem, related to the difference in orbit size between electrons and ions, a difference which clearly persists even at very small orbit sizes. (M. N. Rosenbluth, N. A. Krall, and N. Rostoker, Paper CN-10/170, presented at the Conference on Plasma Physics and Controlled Nuclear Fusion Research, Salzburg, Austria, September, 1961.

$$A_m = A_{m0} \frac{1}{[1 + (m\omega_0 t)^2]} .$$

Here ω_0 is the mean angular velocity of ∇B precession of the particles, and A_{m0} is the initial Fourier amplitude of the mth mode. The characteristic time for the mode to decay to half amplitude is thus $t_{1/2} = 1/m\omega_0$. The significance of this time resides in comparing it with the observed or calculated growth times of the instability. If $t_{1/2}$ is comparable to these latter times, it should result in a stabilizing effect. At the mean energies believed to exist, ω_0^{-1} is calculated to be of the same order as the observed growth rates.

Some remarks can be made concerning the above expression. First, the rate of decay is more rapid for high-order modes (as is intuitively obvious). Since the theoretical growth rate of flutes is independent of m, for $m >> 1$, this should result in inhibiting the growth of high-order modes. Second, it can readily be seen from the form of the expression for the ∇B drifts that ω_0 is anisotropy-dependent, so that $t_{1/2}$ tends to be longer for more anisotropic distributions, and vice versa. Thus the competition between smearing and unstable growth is a function of anisotropy. Qualitatively, it can also be seen that this competition is also a function of the amplitude of the flute, since when the flute is of finite amplitude its effect on the azimuthal plasma drifts is no longer negligible.

The last remark hints at what may be one of the most significant features of the instability now being studied. That it can be "latent" and then be triggered by an electrostatic perturbation of sufficient amplitude suggests that amplitude-dependent--i. e., nonlinear--effects are important in determining the actual stability or instability of the confined plasma.

In summary, although no adequate theoretical treatment is available, many of the observed features of the plasma instability in Table Top suggest that in its finally developed form it is a rotating hydromagnetic flute. The evidence further indicates that the plasma exhibits the instability only when the anisotropy is large or when a triggering electrostatic perturbation is available to start the instability. Anisotropy-dependent destabilizing and stabilizing effects have been suggested to arise from the particle drift motions. These same effects may also play a role in the fact that in its latent regimes the instability does not start from statistical fluctuations, but requires a triggering perturbation of finite amplitude.

4. ALICE ION SOURCE AND FAST ATOM BEAM STUDIES

Charles C. Damm and Frank Gordon

Ion-source parameters have now been standardized, although improvements can undoubtedly be made. Too few runs have been made to pinpoint the large number of physical parameters exactly. For instance, the experiment to determine the shape of the entrance end of the magnetic shield has been limited to three possibilities. An attempt to vary this shape in small steps failed because of vacuum difficulties with the assembly.

Two important parameters that have been fairly well bracketed are the exit-slit shape and the beam path in the magnetic field. The exit slit is now 3 in. long, 0.102 in. wide, and curved on a 19.0-in. radius, while the beam is allowed to bend 107.5 degrees before entering the magnetic shield.

The accelerating voltage power supply is now regulated to better than 0.1%. A flip of a switch converts from unregulated to regulated operation, with a resultant gain in beam on a remote target (34 ft) of about 10%.

The ion source can now be depended upon to operate smoothly at a total drain on the accelerating voltage power supply of about 1 amp with target currents as reported below.

The ALICE beam tube, including the neutralizer, all differential vacuum pumps, and the beam-disposal pump, has been assembled. A bridge tube was inserted in place of the mirror machine to complete the vacuum system. Base pressures in all sections of the assembly were adequate, after evaporation of the getter materials, except for the molybdenum pump on the input side of the tube. A large leak was located in a weld at this pump, and will be repaired during the next shutdown. Meanwhile, varnish was used to seal this leak; the base pressure achieved, however, was only 3×10^{-8} mm Hg, whereas a value in the range of 10^{-9} mm Hg is desired.

Two retractable beam targets are located along the tube; the first is just before the neutralizer and the second is 7.5 ft from the first. In addition, the quick-acting plug valve beyond the second target was operated for rapid on-off gating of the beam. The terminal target in the beam-disposal chamber was arranged to give both electrical and calorimetric measurement of the beam, as were the two retractable targets. A magnetic "sweep" coil was installed beyond the neutralizer to remove the residual charged particles from the beam.

During steady operation at 20 kev, typical (and reproducible) beam currents were 320 ma total at the first target, 95 ma total at the second target, and 77 total at the terminal target. With the sweep magnet on, the beam on the second target dropped from 95 to 75 and on the terminal target from 77 to 64 ma equivalent. The latter figure appears to determine a hydrogen atom flux of about 1.8×10^{16} atoms/cm^2 sec available for injection.

The vacuum system was prepared for gated operation of the beam by evaporation in all getter pumps. When the best base pressures were achieved, the beam was gated through the system by opening in order the first target, the second target, and the quick plug valve. After approximately 5 sec all three beam stoppers were reclosed. During the "beam-on" period, the electrical beam reading on the terminal target was observed to climb slowly from about 80% of its steady value. It is not clear whether this is a true change in transmitted beam or a change in the secondary electron emission from the target. The calorimetric response was too slow to be of use during this period. Additional measurements will be needed to settle this point.

The pressures along the tube were noted during the beam pulse. The disposal-chamber gauge reading increased from about 5×10^{-8} mm Hg to 2×10^{-7} mm Hg, which is adequate. The other pumps also indicated suitably

low pressures, again except for the molybdenum pump on the input side of the bridge tube. The pressure at this pump rose to 3×10^{-7} mm Hg, indicating a loss of about 10 to 15 ma of beams at this point. This is excessive, and is probably due to scattering in the neutralizer (which used water vapor for these experiments).

A slight decrease in beam collimator area will be tried, in order to reduce the beam loss in the critical regions near the trapping chamber. The effect of a slightly smaller beam on the buildup process is negligible according to the numerical solutions of the buildup equations obtained by Futch et al. [1]

During the next shutdown of the beam tube, the vacuum leak will be repaired, the beam size will be reduced slightly, and the mirror machine will be inserted to complete the system.

5. BEAM NEUTRALIZATION

Archer H. Futch and Charles C. Damm

The measurements of proton and deuteron neutralization by water vapor have been concluded. The equilibrium fractions of charged and neutral beam components were measured in the energy range of 6 kev to 20 kev. In addition, data were obtained which enable determination of the ionization cross section σ_{01}, and the neutralizing cross section, σ_{10}, in this energy range. The data are currently being analyzed.

6. ALICE DIAGNOSTICS

James H. Foote, Archer H. Futch, and Charles C. Damm

Ion Beam

The "Diagnostic Development and Testing" ion-beam apparatus is now assembled and the facility is in operation. We expect to continue debugging and improving the beam, intermittently, for some time. The utility of this experimental area has been increased by allowing for two simultaneous experimental setups rather than just one as originally planned. To accomplish this, we employ an analyzing magnet that can deflect the particles leaving the ion source by 30° to either the right or the left. This increased flexibility will allow us to perform not only experiments associated directly with the ALICE diagnostic program but also related investigations.

---

[1] A. H. Futch, W. Heckrotte, C. C. Damm, J. Killeen, and L. Mish, Plasma Production by Neutral Atom Injection: Equations and Numerical Solutions, UCRL-6728 (to be submitted to Phys. Fluids).

Our ion source is of the von Ardenne type and was purchased from the High Voltage Engineering Corporation. The maximum ion energy expected is about 50 kev, although at present we have operated the source only up to 30 kev. We have obtained a proton beam (20 kev) of about 1-ma intensity at a distance of 84 cm from the source anode. After the beam is analyzed and focused, and after it is passed through two collimation holes, 0.6 cm and 0.3 cm in diameter and separated by 50 cm, the beam intensity is approximately 1 μa. About two-thirds of these ions can be changed to neutral atoms by allowing water vapor to enter the neutralizer section of the beam apparatus. We will soon use the neutral beam to check and calibrate the ALICE fast-atom detector.

Probes

Two movable probes have been designed for the ALICE diagnostic work. A long bellows arrangement in each permits the necessary motion. The first probe fits into the top diagnostic port on the ALICE trapping chamber, and consists of two separate parts: a nude ionization gauge and a water-cooled copper target. We can move each of these individually along the radial direction into the center of the trapping chamber. The target can be used to measure the beam intensity at the chamber center. By setting the target at intermediate radial positions, we can use its inner edge to limit the radial extent of the volume of trapped particles.

The second probe will move along the axial direction and is designed to measure the radial variation of intensity of the charged particles escaping through the magnetic mirrors. A series of 17 small collector plates, extending radially and preceded by biased screening, will be used to determine this radial profile. We will be able to move this probe to positions inside the mirror point. Its inner edge can then be used to limit the axial extent of the trapped particles.

Scintillation Counter for Low-Energy Particles

A scintillation counter for the detection of low-energy particles has been installed in the east arm of the "diagnostic Development and Testing" apparatus. A counter of this type would be useful for detection of energetic neutral atoms produced by charge-exchange collisions in the confinement region of ALICE. A counter for low-energy particles is also needed as a detector in the Lorentz-dissociation experiment.

The present counter consists of a thallium-activated CsI crystal mounted directly on the face of an RCA-6810 photomultiplier tube with Dow-Corning high-viscosity silicone oil. A light-collection cone similar to that described by Sweetman surrounds the crystal and photocathode of the tube.[1] The present system has detected 30-kev protons, but with poor resolution from the noise pulses. At present a number of photomultiplier tubes are being checked for low noise in pulse counting. A selected tube should improve the resolution considerably and enable lower-energy particles to be counted.

[1] A. E. Souch and D. R. Sweetman, Rev. Sci. Instr. 29, 794 (1958).

7. TRAPPING WITH COLD PLASMA

James F. Steinhaus and Charles C. Damm

The application of a cold plasma to the ALICE experiment for additional trapping of atoms has been described earlier. [1, 2]

Experiments have been conducted to study the effect on high vacuum of the pulsed cold plasma source. [3] Other related data, including source operation and a brief spectrographic analysis of the plasma, were obtained. These results are reported in more detail in a separate paper. [4]

The experimental arrangement for pressure measurements is shown in Fig. I-6. The occluded-gas cold plasma source was located on axis at one of the magnetic mirrors. The source was fired in a region surrounded by a liquid-nitrogen-cooled liner through the opposing mirror and into a pumping region at room temperature. Both regions contained molybdenum evaporators and nude Bayard-Alpert-type ionization gauges. Total volume of the apparatus was 230 liters. The source was operated in magnetic fields ranging from 0 to 30.4 kilogauss.

All pressure measurements were, of course, dependent on the energy delivered to the source, i. e., pulse-line voltage and pulse length. The pulse line was operated up to 15 kv with a maximum pulse length of 200 μsec. These maximum values delivered 30 joules to the source. Besides the conventional single titanium hydride washer in the source, a loaded trigger washer was used for obtaining the data presented here. Peak pressures are only from 1/4 to 1/8 as large without the loaded trigger washer.

The pressure rise due to the firing of the source with no pumping (before installation of the evaporators) ranged from 5.6×10^{-7} to 5.5×10^{-5} mm Hg.

After molybdenum evaporation the peak pressures, with the same conditions as above, ranged from 9×10^{-8} to 6.4×10^{-6} mm Hg, as shown in Fig. I-7. It is possible to obtain even smaller peak pressures with reduced source energies, but plasma densities may be correspondingly smaller. The observed pressure range represents charge-exchange times ranging from about 3 msec to 0.1 msec. Note that these pressures were read on gauge No. 2 outside the cold liner. Peak pressure values were difficult to obtain on gauge No. 1 because of plasma interference. Peak pressure values

---

[1] R. F. Post, Fast Neutral Particle Injection into a Mirror Machine, Riso Report No. 18, Presented at the Plasma Physics Summer School, Roskilde, Denmark, August 1-13, 1960, p. 529.

[2] C. C. Damm, J. F. Steinhaus, and N. L. Oleson, in Controlled Thermonuclear Research Quarterly Report, UCRL-9777, August 1961, p. 21.

[3] C. C. Damm, J. F. Steinhaus, and N. L. Oleson, Paper C11, presented at the APS Division of Plasma Physics Meeting, Colorado Springs, Colorado, November, 1961 (UCRL-6614-T-Abstract-Rev.).

[4] J. F. Steinhaus, Pressure Measurements Associated with the Occluded Gas Source and Cold Plasma Injection, UCID-4416 (in preparation).

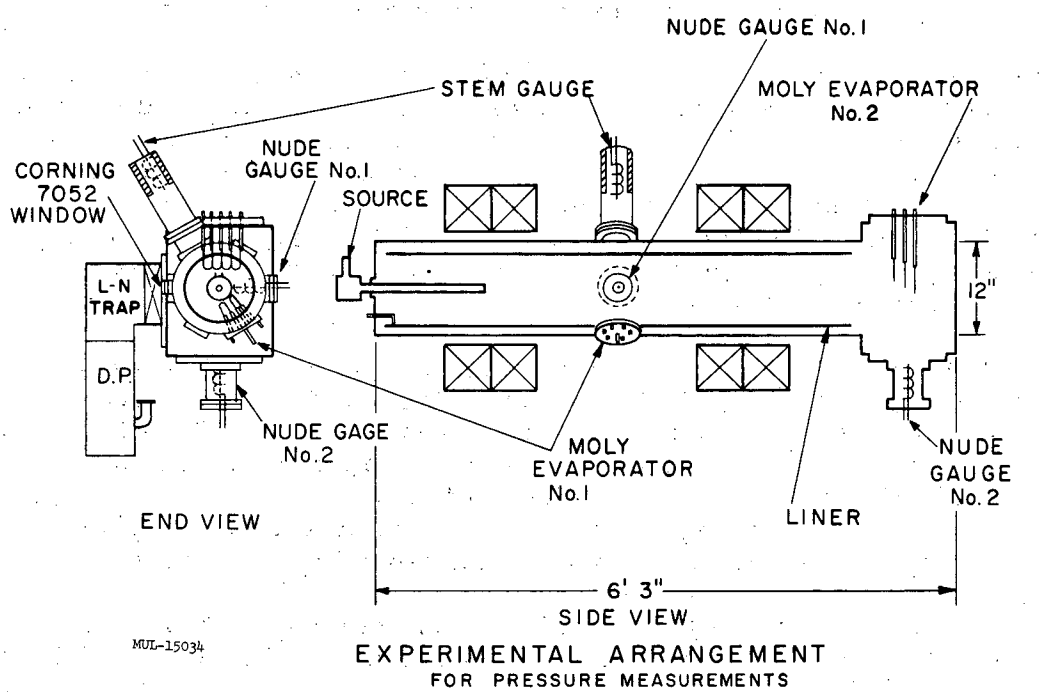

Fig. I-6. Experimental arrangement for pressure measurements.

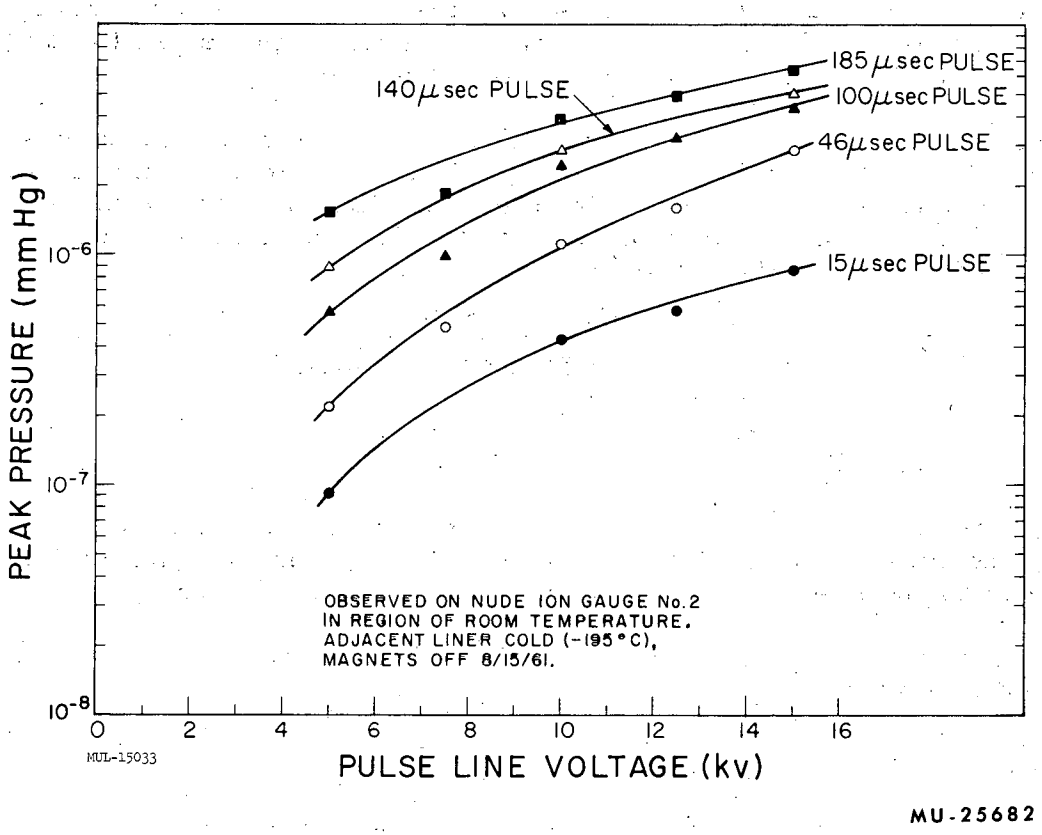

Fig. I-7. Peak pressure as related to pulse-line voltage and pulse length.

in the midplane region of ALICE may also be lessened with additional cold surfaces and a recently conceived scheme by which those particles outside the plasma column (approximately 3/4-in. diameter) are reflected back into a molybdenum pump, while the column itself is allowed to leave the confinement region through a 1-in. -diameter hole into another pump.

One of the main parameters of interest in these measurements is the characteristic time τ required for the pressure to decay 1/e of its original value. This was measured on gauge No. 2 and found to be 0.7 msec. The liner was cold (-195°C) and both molybdenum evaporators had been used. A limited number of corresponding measurements on gauge No. 1, in the liner region, gave a value for τ of about 0.3 msec. The pressure decay rate was found to be independent of the magnetic field, pulse length, and pulse-line voltage within the accuracy of the experiment.

Spectrographic observations were made by William L. Barr, observing the cold plasma column perpendicularly at the mirror midplane. Adequate exposure was a problem with the high-dispersion spectrographs; however, 403 firings of the source at 15 kv and 200 μsec did provide positive identification of the following lines:

1 line - H_α (6562A)
11 lines - TiII (3300 to 4500A)
1 line - TiIV (3541A)
2 lines - TiII or TiIV.

By using a spectrograph of lower dispersion it was possible to photograph approximately 200 lines, and though identification was uncertain, nearly all of these appeared to be TiII with possibly one H_β line.

Further spectrographic work is expected following the source-output profile studies currently under way.

8. VACUUM AND SURFACE STUDIES

Angus L. Hunt, Charles C. Damm, and Earl C. Popp

Relative Pumping Speeds of Hydrogen on Molybdenum Films at Room Temperature and at Liquid Nitrogen Temperatures

The study of the relative hydrogen adsorption rates on evaporated molybdenum films at room temperature and at liquid nitrogen temperature was formulated in terms of the difference between the pumping speeds at these two temperatures. The molybdenum film is deposited on the walls of a large experimental volume. Hydrogen is admitted from a gas-introduction chamber at one end of the experimental volume through an orifice of calculated conductance, C. The pumping speed of the molybdenum deposit is obtained from the equality of the rates of hydrogen admission and the rates of hydrogen adsorption on the molybdenum deposit by $C(P_1 - P_2) = S P_2$,

where P_1 is the pressure in the hydrogen-introduction chamber and P_2 is the pressure over the molybdenum deposit.

The study was designed to determine if the hydrogen pumping speed or the sticking probability for hydrogen on the cold molybdenum surface was relatively less than, equal to, or greater than the pumping speed or sticking probability at room temperature. No design effort was expended on maintaining a cold molybdenum surface of known geometrical area or in eliminating the warm or room-temperature molybdenum surface at the ends of the chamber. For this reason, no absolute values of the sticking probability can be quoted, for the sticking probability is related to the area available to adsorption and the pumping speed by $S/Ak = p$, where A is the area, S is the pumping speed, p is the sticking probability, and k is the maximum conductance per unit area for the hydrogen.

The inability to determine absolute sticking probabilities in this geometry does not interfere with the determinations relative pumping speed.

The schematic of the apparatus is shown in Fig. I-8. To make it possible to evacuate the hydrogen introduction chamber, the chamber was constructed with an orifice which could be retracted from the closed position shown in Fig. I-8 with a bellows-protected screw mechanism. Under bake-out, the same low pressure could be obtained on each side of the orifice. Hydrogen was diffused into the introduction chamber through a palladium thimble to assure the purity of the hydrogen. The complete introduction system, including the palladium diffusion thimble, was enclosed in the bakable region. After the system was heated to 220°C for several days to remove at least the water vapor from all portions of the system and allowed to cool, the hydrogen-introduction system was baked with auxiliary heaters to about 400°C to maintain the purity of the hydrogen. Because the pressure rise in the molybdenum-gettered volume was small even at high hydrogen admission rates, the ion current from the ionization gauge in the large chamber was read with an auxiliary high-gain dc amplifier which would allow suppression of the background current and full-scale indication of only the small pressure changes. By this technique ionization current changes corresponding to 10^{-12} mm Hg could be easily measured in the presence of a background current corresponding to 10^{-9} mm Hg. As hydrogen was diffused into the introduction chamber, the pressures on the high-pressure side of the orifice (P_1) and on the low-pressure or molybdenum-gettered side (P_2) were recorded as functions of time. The pumping speeds were then computed as a function of the amount of hydrogen adsorbed by the molybdenum deposit, which was accurately equal to the amount of hydrogen introduced through the orifice.

Before any molybdenum films were deposited the pumping speed of the ionic pump with the connecting tubulation was determined as 170 liter/sec for hydrogen. Molybdenum was then evaporated to reduce the residual pressure in the chamber. The subsequent procedure and the pumping speeds obtained with the films at room temperature and at liquid nitrogen temperature are summarized in Table I.

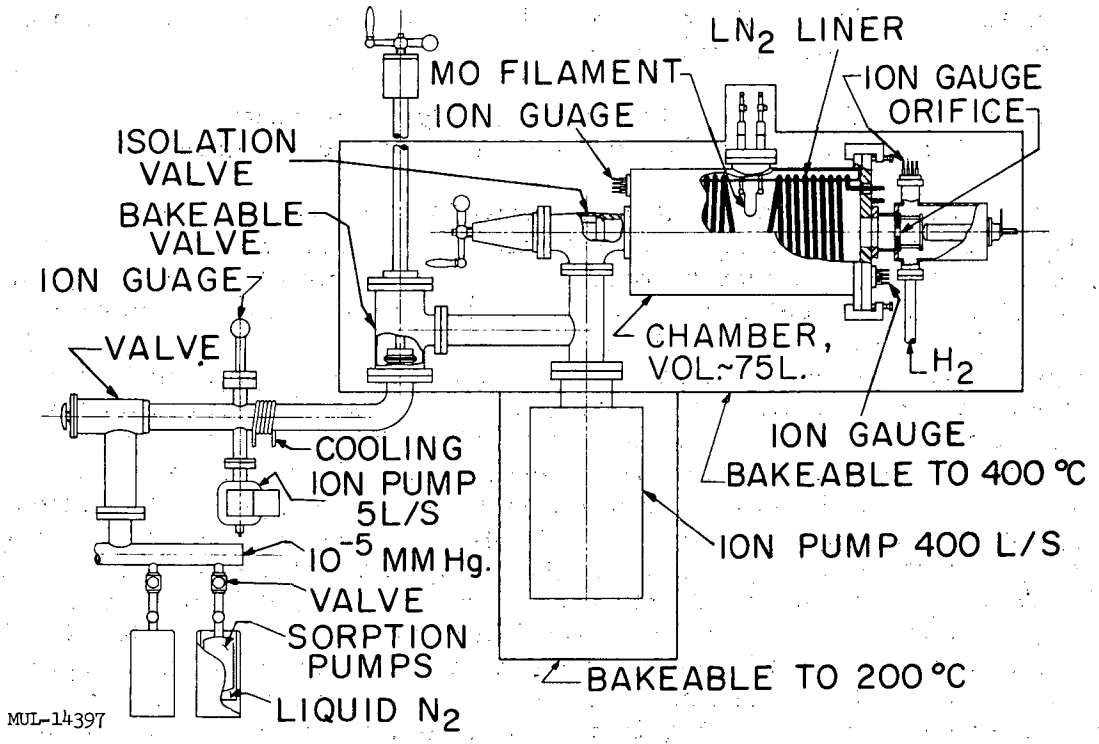

Fig. I-8. The pumping system and molybdenum gettering chamber with the hydrogen introduction system.

Table I. Summary of pumping data

Experimental procedure	Maximum pumping speed for H_2 (liters/sec)	
	Substrate at room temperature	Substrate at liquid N_2 temperatures
Initial Mo deposit	3.5×10^4	
After 8 Mo deposits	6.8×10^4	
After 16 Mo deposits		3.5×10^5
After 27 Mo deposits	1×10^5	
Deposit aged 18 hr		1.6×10^5
Deposit aged 43 hr	4.5×10^3	1.2×10^4
Deposit warmed and recooled		1.6×10^4
Deposit aged 211 hr	2.8×10^3	9.1×10^3
Five fresh Mo deposits		$5.\times10^5$
Deposit aged 22 hr	5.3×10^3	8.3×10^4

Figures I-9 and I-10 are illustrative of the variability in shape in the curves of the pumping speed plotted as a function of the amount of hydrogen adsorbed. Figure I-9 shows two curves for the molybdenum film after it had been aged 211 hours. The room-temperature measurement was made first, and indicated that an old previously saturated molybdenum film still had appreciable pumping speed at room temperature and that the pumping speed had both a minimum and a maximum with amount of hydrogen adsorbed. Immediately after this measurement was made the molybdenum deposit was cooled to liquid nitrogen temperatures and the upper curve obtained. The aged but cold molybdenum film, even with all the hydrogen previously adsorbed at room temperature, showed a large increase in sticking probability as well as a complete change in the shape of the curve. Figure I-10 shows the shape of the curve for a fresh molybdenum deposit as a function of the amount of hydrogen adsorbed at liquid nitrogen temperatures. The general shape of the curve, starting at a low pumping speed and increasing to a maximum just before saturation, is very much like that for the aged molybdenum film at liquid nitrogen temperatures shown in Fig. I-9. It appears that the shape of the curve may be a function of the temperature of the molybdenum film. D. Alpert and his students at the University of Illinois, during experiments on nitrogen adsorption on molybdenum, previously have observed similar changes in the rates of adsorption with the degree of coverage.

An argument can be advanced to show that the shape of the curves of pumping speed plotted against the quantity of hydrogen adsorbed cannot be due to impurities in the gases, and that a gradually increasing pumping speed or sticking probability attaining a maximum before saturation is a real characteristic of the rate of adsorption of hydrogen on these molybdenum films. The changes in pumping-speed measurements due to impurities can range only over a factor of thirty even under the most adverse composition changes. In terms of the probable contamination of a system such as that used in these experiments the maximum range possible would appear to be less than this. We observe, however, as illustrated in Fig. I-10, that the pumping speed increases by a factor of about 75, which is about twice that expected on the basis of possible impurity content influencing the pressure as obtained from the gauge readings. We conclude that some effect other than impurities is causing the observed increase in pumping speed with the amount of hydrogen adsorbed. A possible mechanism which could account for the result is nucleated growth of the adsorbed hydrogen on the molybdenum surface.

In summary, the results indicate that there is an increase in pumping speed and sticking probability for hydrogen on molybdenum films as hydrogen is adsorbed and as the temperature of the molybdenum film is decreased to liquid nitrogen temperatures.

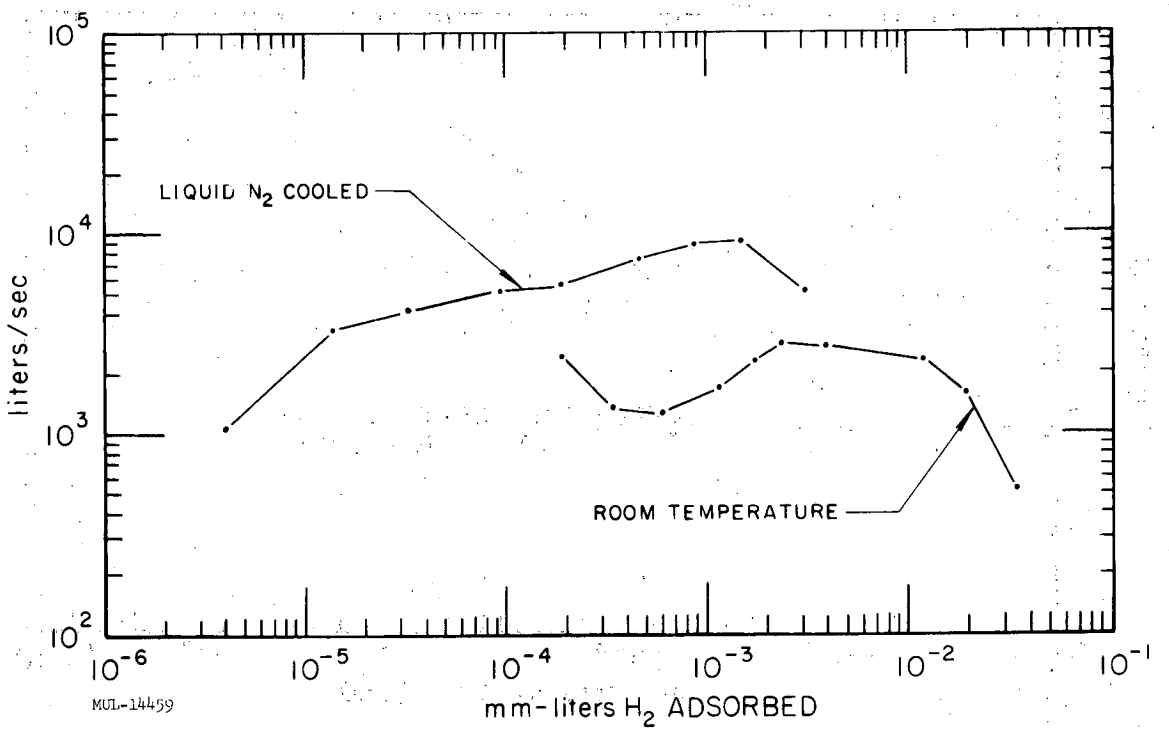

Fig. I-9. Pumping speed as a function of the quantity of hydrogen adsorbed for an aged Mo deposit. The hydrogen pumping speed was first measured at room temperature, then the molybdenum deposit was cooled to liquid nitrogen temperatures and the pumping speed measurement continued.

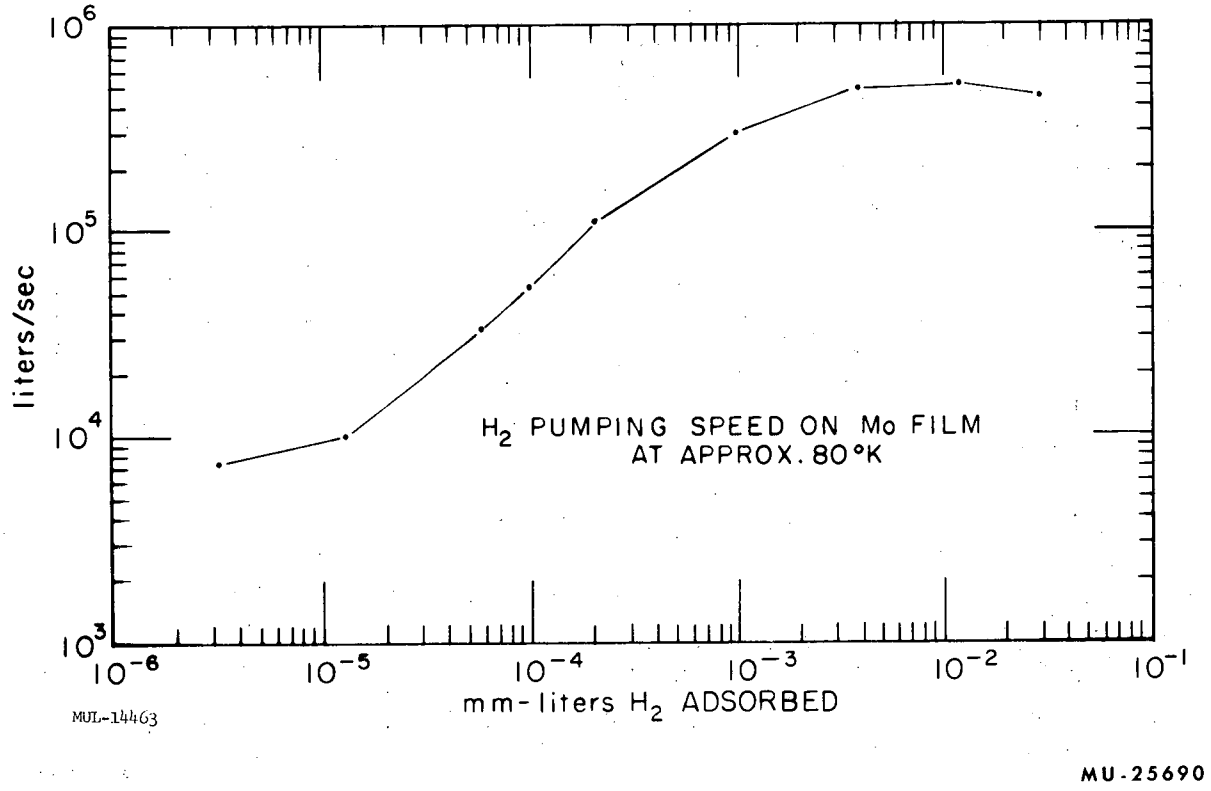

Fig. I-10. Pumping speed as a function of the quantity of hydrogen adsorbed for a fresh Mo deposit.

Rates of Hydrogen Adsorption on Solidified-Gas Films

In an experimental study with Clyde E. Taylor and John E. Omohundro on the rates of adsorption of hydrogen at about 11 °K on solidified-gas films of A, N_2, O_2, H_2O, N_2O, and CO_2, it has been found that the hydrogen adsorption rates are comparable to those previously found for molybdenum films.[1] The fresh solidified gas surfaces were formed by admitting gas into a high-vacuum system containing a copper substrate which had been refrigerated to about 11 °K. The vapor pressure of the solidified film was not measurable, for at temperatures below 18 °K the solid-vapor equilibrium pressures for all gases except H_2, Ne, and He are less than 10^{-13} mm Hg.[2] Although it is well known that the solid-vapor equilibrium pressure for hydrogen near 11 °K is about 10 mm Hg,[2] it was found that when the amount of hydrogen in the gas phase is limited and no bulk solid hydrogen is present, surface adsorption reduces the partial pressure of hydrogen in the gas phase to less than 10^{-8} mm Hg. Adsorption proceeds at a very high rate until quantities sufficient to form about a monolayer have been adsorbed on the solidified gas.

As shown in Fig. I-11, sticking probabilities for hydrogen on solidified carbon dioxide films ranged from 0.25 to 0.5 for the lowest measurable coverages, but remained almost constant until monolayer coverage was approached. The monolayer of hydrogen could be desorbed after each measurement by increasing the temperature of the solidified-gas substrate from 11 °K to 15 to 20 °K. After desorption of the hydrogen and recooling of the substrate to 11 °K, the sticking probability would return to approximately the original value. In some cases the sticking probabilities on subsequent adsorption of hydrogen were higher than those obtained with the fresh solidified-gas film. A sequence of adsorption-desorption measurements on the same carbon dioxide film gave sticking-probability curves within the two curves shown in Fig. I-11. The reversibility of the adsorption and desorption with temperature changes of about 5 °K was also found for hydrogen on solidified nitrogen films, and is thought to be characteristic of all the solidified-gas films investigated. With carbon dioxide the perturbation of the solidified-gas surface due to the 9 °K temperature increase was probably small, as the vapor pressure of carbon dioxide does not exceed 10^{-13} mm Hg at temperatures as high as 59 °K.[2]

The rate of hydrogen adsorption on a solidified film of nitrous oxide was similar to that on carbon dioxide with a low-coverage sticking probability of 0.3, but the surface density of hydrogen required to saturate the nitrous oxide film exceeded 10^{13} per cm^2.

---

[1] A. L. Hunt, C. C. Damm, and E. C. Popp, J. Appl. Phys. 32, 1937 (1961)

[2] R. E. Honig and A. O. Hook, RCA Review 21, 360 (1960).

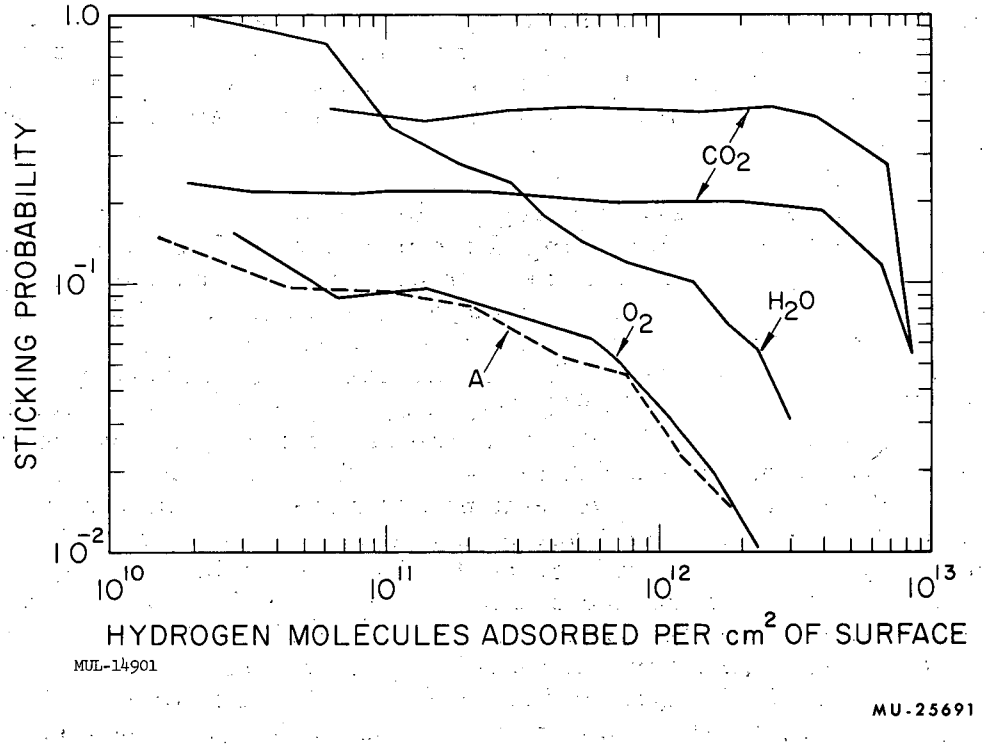

Fig. I-11. The experimental sticking probabilities for H_2 on solidified-gas films of A, O_2, H_2O, and CO_2 at 11°K.

For a water substrate at 11 °K, the hydrogen sticking probability approached unity for low surface coverages, but decreased monotonically to 3×10^{-2} as the substrate adsorbed 0.3 mm liter of hydrogen or sufficient hydrogen to form a surface density of about 10^{12} molecules per cm^2. In our apparatus, in which the effective surface area was only 3×10^3 cm^2, the initial hydrogen pumping speed on water at 11 °K was 1.2×10^5 liters/sec. With this same water substrate a helium pumping speed of 60 liters/sec was found, which was the speed expected with only an auxiliary diffusion pump.

Solidified-gas films of argon, oxygen, and nitrogen had hydrogen sticking probabilities, for low coverages, of about 0.1. The sticking-probability curves were very similar to the curves for argon and oxygen shown in Fig. I-8. The vapor pressures of the monatomic and diatomic gases are relatively high compared with the triatomic gases such as water, carbon dioxide, and nitrous oxide, so the surface disorder might be responsible for the similar and generally lower sticking probabilities on the monatomic and diatomic solidified gases.

Although there apparently have been no comparable measurements on the kinetics of hydrogen adsorption at low temperatures, two recent observations lead one to expect adsorption of hydrogen with low vapor pressure on solidified-gas surfaces at temperatures below the normal hydrogen boiling temperature. The concurrent trapping of nitrogen in condensing carbon dioxide and water vapor at liquid nitrogen temperatures has been observed at pressures in the micron range,[3] and the vapor pressure of adsorbed helium over Pyrex (Corning 7740) in coverages of less than a monolayer has been found to be less than 10^{-9} mm Hg at 4.2 °K.[4]

---

[3] E. S. J. Wang, J. A. Collins, Jr., and J. D. Haygood, General Cryopumping Study, presented at the Cryogenic Engineering Conference, August 15-17, 1961, Ann Arbor, Michigan.

[4] J. P. Hobson, Can. J. Phys. 37, 300 (1959).

9. P-4 (STEADY-STATE PLASMA) SYSTEM

William L. Barr, Andrew L. Gardner, and Norman L. Oleson*

Electron Beam Interaction with the Plasma

Effort during this period has been devoted principally to a study of the plasma and a pulsed beam of energetic electrons that is injected longitudinally into the open end of the plasma system.

By redesigning coils and optimizing the magnetic focusing fields in the vicinity of the electron gun, the injected current has been increased (more than three fold) to 0.8 amp. The focusing-field configuration is rather critical, because the electrons must traverse the magnetic mirrors on their way into the plasma column. Modifications of the modulator have permitted pulse lengths up to 40 μsec. Other modifications of the modulator are planned in order to increase the accelerator voltage over its present maximum of 17 kv--this will also provide a higher electron current.

A microwave horn (which looks radially at the plasma column in the central portion of the system) and a superheterodyne receiver have been used to detect radiation which is emitted near the plasma frequency (approx 35 kMc) when the electron beam is passing through the plasma. The presence of the rotating probe has been found to enhance this radiation (presumably by providing better coupling to the horn) and this permits, to a degree, a localization of the region from which the radiation emanates.[1] This technique has indicated that typical probes at the center of the P-4 plasma cause a reduction in the density of about 10 to 20%, depending on probe size and potential.

The detected radiation typically occurs in bursts 1 or 2 μsec long at random times during the current pulse and throughout a frequency band 1 or 2 kMc wide. At first it was thought that the short duration of the signal might be resulting artificially because of the narrow band width of the receiver (2 to 5 Mc with 30 Mc i. f.). This would occur if a continuous radiation were emitted at a frequency (or narrow frequency band) which fluctuated so as to cross a sideband of the receiver in times like 1 or 2 μsec. However, this is not the case. The broad-band character of the radiation has been established by viewing the signal simultaneously on two superheterodyne receivers separated in frequency by as much as 600 Mc.

The x rays that are emitted when the electron beam strikes the rotating probe show large amplitude fluctuations, particularly at the higher electron currents. The fluctuations are sometimes rather periodic, with a period of about 10 μsec, and they have no time correlation with the observed microwave radiation. This suggests that the electron beam may be wiggling about in the plasma so that more or less of it hits the probe (or the probe stem insulator). Apparently there is no marked correlation between this x-ray

---

*U. S. Naval Postgraduate School, Monterey, California.

[1] A. L. Gardner, Paper H7 presented at the APS Division of Plasma Physics Meeting, Colorado Springs, Colorado, November 1961 (UCRL-6620-T-Abstract).

fluctuation and the voltage variations across the discharge chamber, which have a similar period.

In order to avoid both the perturbation caused by the probe and its sensitivity to the position of the electron beam, a small aluminum-foil-covered scintillator, in a water-cooled housing, was recently installed inside the anode section but outside the plasma near the output end of the discharge chamber. It was oriented to detect x rays emitted from the cathode and the anode when they are struck by the electron beam which then will have traversed the entire P-4 system (about 5 meters). The resulting x-ray signals were found to have no severe fluctuations. Furthermore, the first measurements of the decrease in x-ray intensity when the plasma is present corresponds to an energy loss of less than 20% (less than 7 ev/cm average energy loss).

Beam Interaction with a Self-Created Plasma

Brief observations were made of the type of strong interaction studied at MIT and reported by Smullin.[2] In the P-4 system this was seen when the electron beam was injected with the discharge off but with gas being introduced and with the magnetic field present. In a few microseconds the beam built up its own plasma in the discharge chamber and for a short time the beam current to the end electrode (cathode) was severely curtailed while it appeared, instead, at the cylindrical anode section. After the electron beam terminated, the net negative charge subsequently collected by the end electrode was of the same order of magnitude as the entire charge of the electron beam pulse.

Spectroscopy

When P-4 was operated on hydrogen gas it was observed that the first three Balmer lines were all broadened by about 0.45 A. This is in contrast to experience with He, in which the neutral lines are sharp. Zeeman effect should be negligible. The nearly constant width, independent of wave length, appears to rule out the Doppler effect as the main broadening mechanism. Present theory (Kolb et al.[3] and Baranger[4]) is not applicable for the low density (approx 10^{13} cm^{-3}) and high electron and ion temperatures (approx 20 and 10 ev, respectively) of P-4. To get some measure of the relative abundance of molecular and atomic hydrogen in the background gas, a spectrum analysis was performed. During June and July, Lt. Fred Kinley and Lt. Robert O' Malia of the U. S. Naval Postgraduate School, Monterey, California, obtained spectrograms under nearly identical conditions at ports

---

[2] W. D. Getty and L. D. Smullin, Paper L5 presented at the APS Division of Plasma Physics Meeting, Colorado Springs, Colorado, November 1961.

[3] H. R. Griem, A. C. Kolb, and K. Y. Shen, Phys. Rev. 116, 4 (1959).

[4] M. Baranger, Phys. Rev. 111, 494 (1958).

6, 5, 4, 2, and 1 and at the discharge chamber. At port 1, where the background pressure is 2×10^{-4} mm Hg, more than 1300 lines of H_2 were identified in the spectral range 2800 to 5450 A. Six members of the Balmer series were definitely observed, as well as the same impurities (C, N, O) as are present in He operation. Comparison of the spectrograms taken at the various ports shows that the number of H_2 lines decreases rapidly with decrease of background pressure. At port 6, where the pressure is 2×10^{-5} mm Hg, no H_2 lines could be detected in a similar exposure.

II. ASTRON PROGRAM

1. INTRODUCTION

N. Christofilos

During the last six months the major effort of the Astron group was the construction of the electron accelerator. The development and detail design of all the components has been completed, and orders have been placed for the hydrogen thyratron switch chassis and associated electronic gear. Installation of the pulse-forming networks is proceeding. The assembly of the electron gun is almost completed. Delivery of all the components is expected to be completed by Spring 1962. Since it is expected that after the completion of the accelerator some time will be required for debugging and achievement of reliable operation, the emphasis during the last six months was toward expediting the construction of the accelerator.

Most of the activities in the theoretical field have been reported in the Salzburg meeting, thus there is no need of detailed discussion in this report. Some additional work was recently done by Kelvin Neil on the stability of the E layer; see Section V-1 of this report. The engineering and construction activities are discussed in more detail in Sections VI-3 and VI-2, respectively.

2. ASTRON PLASMA CONDUCTIVITY MEASUREMENT

Thomas M. Comella, Joseph E. Katz, Daryl D. Reagan, and Charles B. Wharton

An attempt is being made to reconcile optical and microwave measurements with the results of the "pulsed loop" skin-effect conductivity measurements.[1] It appears that after a few microseconds the outer layers of plasma become cooler than the interior, so that a simple comparison is not possible. The microwave noise measurements and optical measurements show electron temperatures decreasing from about 10 ev just after the discharge pulse to 4 or 5 ev a hundred microseconds later. The skin-effect measurements, made 10 μsec after the discharge pulse, indicate about 2 ev temperature, assuming uniform electron temperature throughout the vessel. These results would be consistent if the hot plasma were about 1/3 the diameter of the vessel.

[1] D. D. Reagan, Astron Gas Target Electric Conductivity Measurement, Lawrence Radiation Laboratory (Informal) Rept. CVL-60-28, Oct. 1960.

3. TESTING OF Al_2O_3 FOILS

Ross E. Hester and William A. Sherwood

During this period construction and testing of beam windows required in the Astron beam research program have continued. For some of the anticipated experiments it will be required that the foils transmit a 200-amp 4-Mev beam while withstanding a pressure differential of several mm Hg. Consequently the foils have been tested in a similar environment.

The foils chosen for the final tests were 1-in. -diameter 1600-A-thick Al_2O_3 foils on which 400 A of carbon had been evaporated. It was found that initially these foils would burst with a static pressure greater than 1.5 mm Hg, therefore testing began with a 1.0-mm Hg pressure differential and a 1-amp 10-kev electron beam with a 0.3-μsec pulse width at 300 pps. As the test continued it was possible to increase the pressure differential to a range of 8 to 10 mm Hg. Some foils were bombarded under these conditions for as long as 19 hr with no apparent deterioration. The apparent increased strength of the foils which have been tested can be explained as a gradual stretching of the foil allowing it to assume a partially spherical shape. The foils once "cured" can be subjected to high pressures immediately in further tests.

The Bethe formula for energy loss by electrons in matter is expected to be good at 4 Mev, but there is a question of its validity at low energies. Therefore an experiment was performed to measure the energy loss of a 1-amp 10-kev electron beam incident on the foils. The transmitted beam was collected in a Faraday cup which could be biased from 0 to 10 kev. In this way the energy spectrum of the transmitted beam was measured and the energy loss in the foil determined. The energy loss appeared to be about 5 times that predicted by the Bethe formula. Therefore the tests are considered adequate.

III. LIVERMORE PINCH PROGRAM

C. K. Birdsall, Dale H. Birdsall, Stirling A. Colgate, Harold P. Furth, Fred O. Halliday, Charles W. Hartman, Charles E. Kuivinen, Ross L. Spoerlein, and Alvin W. Trivelpiece

1. SUMMARY

The main aim of the pinch research effort continues to be towards the understanding and elimination of the small-scale instabilities. During the past half year much progress has been made along these lines. Evidence is accumulating that the small-scale instabilities are not of the velocity-space type, but are hydromagnetic modes, due to finite conductivity. A recent theoretical development provides a general description of the finite-conductivity modes in a current layer. Current-driven flute instabilities are being studied in particular, since experiment suggests that these may be of greatest importance. The linear-pinch experimental setups for studying finite-conductivity modes include diagnostics by multiple probes, by electron beams, and by Kerr-cell photography through screen electrodes or walls. On completion of its present upgrading process, the levitron will permit extension of these studies to better conductivity conditions, under which the achievement of effective stability appears theoretically plausible.

Theoretical and experimental studies on the interaction of interpenetrating plasma streams are being continued. A new velocity-space instability of relativistic sheet pinches is being studied. A high-powered laser setup for plasma diagnostics is being developed.

2. ELECTRON-BEAM EXPERIMENT

Experiments with a pulsed beam of approx 0.1 μsec duration have previously shown that magnetic turbulence in the pinch will lead to erratic electron-beam traces covering large total distances.[1] Various indirect arguments led to the conclusion that the beam traces were not due to beam motion in time, but instead were instantaneous mappings of an extremely distorted and widely spreading flux bundle emanating from the point of introduction of the beam into the tube.

A recent modification of the beam injection permits the pulse to be left on for a few tenths of a μsec or to be cut off after a few hundredths of a μsec. Exposures made with a "stabilized pinch" under these two conditions yield the typical traces shown in Fig. III-1, which demonstrate directly that the beam spreading is indeed an instantaneous phenomenon. For these exposures the beam was injected at a radius of about 3 cm, and the photographic aperture was adjusted to give comparable intensities in the two cases.

---

[1] D. H. Birdsall et al., in Controlled Thermonuclear Research Quarterly Report, UCRL-9777, June 1961.

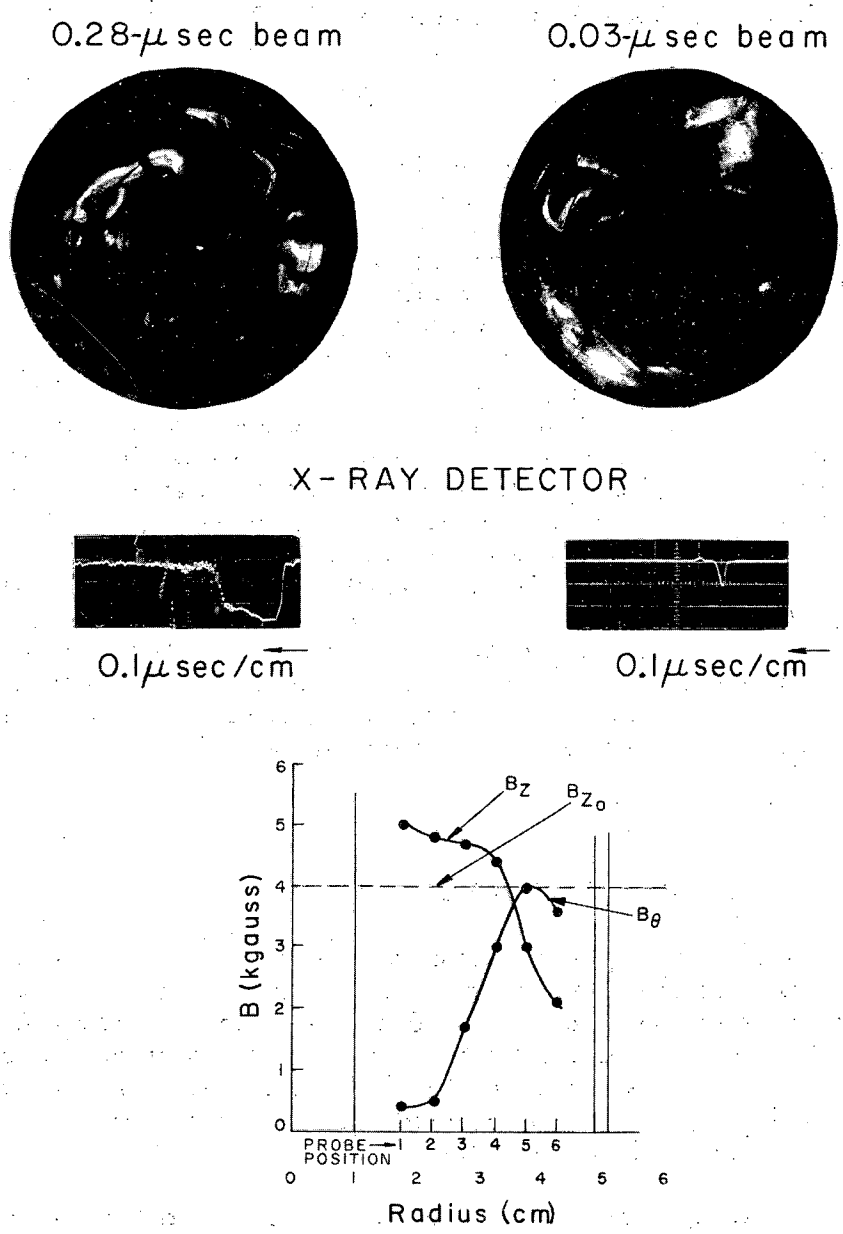

Fig. III-1. Electron beam traces with 0.28-μsec and 0.03-μsec pulse lengths.

A comprehensive report on electron-beam experiments has recently been issued.[2]

3. CUSP-PINCH EXPERIMENT

In pinch devices there is a natural tendency for pressure-driven flute instabilities to occur, because the absolute field strength decreases at larger radii. When the plasma has finite conductivity, these flutes are only imperfectly inhibited by shear (see Section 8). In order to test the importance of this phenomenon, a 4-inch hard-core pinch was built which has a series of cusps on the outside in place of the usual B_z field. The absolute strength of the cusp field increases by a factor of two from the axis to the tube wall. Experiments have been conducted at about 5-kilogauss field in 100-μ gases.

If no initial B_θ is used, the plasma expands dynamically towards the outer wall during "unpinching." There is essentially no difference in this behavior whether the cusp field is on or off. Both photographic and probe measurements have been made.

If an initial B_θ of either sign is used, there is appreciable coupling to the cusp field, which is swept out of the small-radius region and kept out during passage of the unpinching current (approx 10 μsec). The plasma now cannot flow directly to the wall, but only by following the spiral field lines due to the superposition of the B_θ field and the B_r component of the cusp field.

In spite of the theoretical improvement of the rigidity of the magnetic field structure relative to the ordinary hard-core pinches, very pronounced hydromagnetic disturbances are still detected by magnetic probes. The measurements are suggestive of small-scale finite conductive modes, which depend only on properties of the current layer and are unaffected by the absolute magnetic field gradient. Further studies are needed to determine the extent of plasma contact with the wall, and the effect of rotary motions set up by the unpinch current and the radial component of the cusp field.

4. RESISTIVE SHEET PINCH EXPERIMENT

Extensive theoretical work has been done[1] on the tearing instability of the ordinary sheet pinch. This phenomenon is believed to occur in reverse-field theta pinches, but can be studied under more controlled conditions in the tubular dynamic pinch geometry. O. Anderson has kindly lent to us a 12-inch tubular pinch device with screen sides and electrodes specifically suited for photography. In this tube slow, low-temperature discharges will be studied and the growth rates of tearing modes compared with theory.

---

[2]S. A. Colgate et al., Particle Motion on Magnetic Flux Surfaces in "Stabilized" and Hard-Core Pinches, IAEA Conference on Plasma Physics and Controlled Nuclear Fusion Research, Salzburg, Austria, September 1961, UCRL-6385.

5. LEVITRON PROGRESS

The levitron experimental program had progressed to the point at which an improvement in the base pressure of the machine became of prime importance. A 10-kc rf generator was used to inductively heat the liner to a bakeout temperature of 450°C.

Although the liner-heating method proved quite satisfactory, serious trouble developed in the high-temperature-epoxy insulation which had been applied to the inside of the stabilizing shell. This coating was, of necessity, quite thick in some areas. Heat transfer to the water-cooled shell was inadequate at the thick sections and the epoxy failed. One case in point was the shell minor parting line which was insulated and sealed with epoxy. An irreparable leak occurred along this line.

The base pressure of the machine was too high to permit further experiments, so dismantling began on August 23. Inspection revealed that not only had the epoxy failed but also the Inconel-x liner had developed a number of hairline cracks which accounted for a high communication rate between the annular space and the liner. These cracks were not detectable during assembly but were apparently initiated by heliarcing the flanges between liner sections. Extensive tests indicated that the metallurgy of Inconel-x is such that repairs were impossible.

A new liner of 321 stainless steel was ordered. This material has about 50% the resistivity of Inconel-x, but is considerably more workable and is considered a satisfactory compromise. The liner sections have been received and are being assembled.

A number of seals had been made in the levitron with RTV 731 silicone rubber. This material proved most satisfactory and remained essentially unchanged even in areas where it was adjacent to charred epoxy.

Several major changes have been made in the levitron which should result in a major improvement, particularly with regard to the vacuum system. These are summarized below.

1. A phenolic coating is being used on the inside of the copper shell. This material appears to be a superior high-temperature coating, although some trouble is being experienced in its application. Test samples and one half of the shell have been satisfactorily coated to date.

2. Alumina insulators are being fabricated to provide feed-throughs for the ports. This was a troublesome area for high-temperature epoxy.

3. All joints in both the ring and the liner are to be heliarced or made with B-T solder. This change will eliminate high-vapor-pressure metals, which were used in the previous assembly. This requirement is imposed by the desirability of initiating the pinch with the liner hot.

4. A retractable cryogenic pump has been fabricated and is being tested. Should it prove satisfactory a substantial improvement will be made in the pumping speed from the liner.

5. Silicone rubber will be used to replace epoxy for the minor parting-line seal. In the final assembly no epoxy will be exposed to the hot liner.

6. COLLISIONLESS PLASMA SHOCK (EXPERIMENTAL)

In the preceding report it was conjectured that the observed absence of growing transverse magnetic fields in interpenetrating plasma streams was due to small-angle Coulomb collisions. A more likely effect leading to suppression of the magnetic two-stream instability appears to be due to the highly mobile electron background. Coupling of the electrons to the ion motion through induction electric fields can lead to complete stabilization at zero electron temperature without collisions (see Section 9). Although transverse wave growth persists at finite electron temperature, or when collisions are included, growth rates are considerably reduced. In addition, the presence of a weak axial magnetic field which makes the electron Larmor radii less than the shortest growing wave length can lead to stabilization. Most of the experiments reported earlier were conducted with axial fields.

Initial investigation of the firehose instability has begun in the more generalized configuration of contrastreaming plasmas carrying a net current. This is accomplished by passing the moving plasma through a stabilized pinch. Use of the stabilized pinch permits an arbitrary reduction of stability to hydrodynamic disturbances to be attained as conditions are approached which lead to the familiar pinch turbulence effects. In addition turbulence may be used to provide strong initial excitation of hydrodynamic modes which are predicted to grow during subsequent contrastreaming.

Strong coupling between pinch and moving plasma is observed, as illustrated by the magnetic probe traces shown in Fig. III-2. The traces for B_θ (2 kgauss/cm) were taken 10 cm from the plasma gun. Peak pinch current is 40 kiloamperes, axial magnetic field is 3 kgauss, pinch and moving plasma density are both 5×10^{15} D^+/cm^3, and the mean kinetic energy of the moving plasma is about 300 ev. In the absence of moving plasma, the typical characteristics shown are observed. When plasma is injected during the initial quiescent phase, turbulence is progressively excited and driven by the pinch current in the wake of the moving plasma. The moving plasma undergoes a decrease in kinetic energy corresponding to friction observed with neutral gas. As ionization becomes complete, friction approaches the low value corresponding to motion through plasma.

If the plasma is injected after the onset of pinch turbulence, an interaction occurs consisting primarily of a gross deflection corresponding to the distorted flux tubes. Little radial dispersion is observed and dynamic friction is again small.

Stimulation of turbulence may have two possible causes. Passage of the plasma through the pinch in effect represents a pulse of ion and electron current of about 10^4 amp/cm^2 so far as electron collision and ionization processes are concerned. This may rapidly bring the pinch to the turbulence onset conditions which would have been reached later by the pinch current

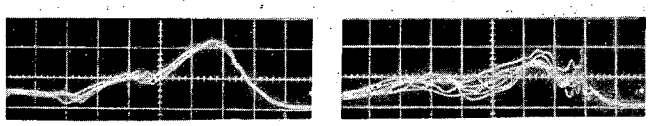

2 kgauss/cm

← 2 μsec/cm

ZN-3006

Fig. III-2. Pinch with plasma injected at 3.6 μsec.

alone. Alternatively, if turbulence arises from strong nonlinear coupling, the large disturbances produced may be sufficient to pass rapidly through the initial small-amplitude growth phase.

7. OPTICAL PUMPING OF A RUBY LASER BY A DYNAMIC PINCH

The optical pumping of a laser by a dynamic pinch was attempted in order to achieve sufficient laser light output so that plasma diagnostics could be performed. Initial operation was hampered by the breakage of the central quartz tube at pinch voltages considerably below optimum for maximum pump power. However, it was found that this breakage occurred only for argon gas, presumably because of the dynamic force in a strong shock wave. Other gases left the quartz minor tube intact but no laser operation was observed. We have since found that the crystal used was faulty, and therefore a commerical laser unit, built by Raytheon Company, has been purchased to facilitate investigations of various materials and to allow study of the optical properties of various rubies, reflecting coating, etc. We have modified this unit slightly, and we have observed the so-called hair-trigger mode of operation in which the ruby is "primed" by pumping to a level just below threshold, and then triggered from a separate energy source which supplies the necessary additional light.

The Raytheon unit is undergoing further modification to allow it to operate with the addition of a small dynamic pinch trigger light source built into the optical reflecting housing.

By the pinch technique the instantaneous output power of the laser may be raised by a factor of 10^3, which will facilitate its use for plasma diagnostics.

8. COLLISIONLESS PLASMA SHOCK (THEORETICAL)

Several features of electrostatic shock formation with mass ratio 10 have become apparent following more detailed analysis after interpenetration of 10 ion periods (total length of shocked plasma ≈ 10 ion plasma wave lengths). At the shock front a potential wave that is nearly static (in the shock frame) is generated with wave length about

$$\sqrt{\lambda_{pe}\,\lambda_{pi}}\,, \text{ where } \lambda_{pe,i} = v_0/f_{pe,i},$$

and v_0 = streaming velocity in the shocked fluid frame,

and amplitude comparable to the incoming electron kinetic energy observed in the shock frame. The potential wave remains nearly static for several wave lengths into the shocked region, giving way to oscillating modes which develop larger potentials comparable to the ion streaming energy. When fluctuating fields begin to dominate, the electron velocity distribution is nearly thermalized. The ion velocity distribution, which is double peaked

near the shock front, relaxes to a thermal distribution 10 λ_{pi} within the shocked plasma, with roughly one-third of the initial kinetic energy given to the electron background.

In the shocked plasma, potentials fluctuate at nearly the electron plasma frequency. The modes spectrum appears to be thermalized, with the largest potential developed by the longest possible wave length mode ($\lambda = 40\ \lambda_{pi}$), which oscillates at ω_{pe} with a peak amplitude of several times the ion streaming energy.

Similar shock characteristics are observed with mass ratios of 1 and 100. For mass ratio 1 similar oscillating potentials are observed with thermalization of the particle and mode distributions about 5 plasma wave lengths from the front. The mass-ratio-100 shock has not been carried to ion thermalization, although saturation of the mode potentials appears to have been approached. Based on this tentative conclusion, the ratio of maximum field potential to ion kinetic energy decreases as the square root of the mass ratio.

9. INSTABILITY THEORY

Previous work on a magnetic instability of thermally anistropic plasmas in null magnetic field[1] has been generalized to allow for the presence of both ions and electrons. For an anisotropic particle distribution

$$f_0 = \frac{n_0}{(2\pi)^{3/2} a^2 v^2} \exp\left[- \frac{1}{2v^2} \left(\frac{v_x^2 + v_z^2}{a^2} + v_y^2 \right) \right] \qquad (1)$$

with isotropic neutralizing particles, one obtains the dispersion relation

$$\frac{4\pi n_0 r_c}{k^2} \left[\frac{1}{a^2} - 1 - \frac{1}{a^2} F(\Lambda) - \frac{m}{m_n} F(\Lambda_n) \right] = 1, \qquad (2)$$

where

$$r_c = \frac{e^2}{mc^2},$$

$$F(\Lambda) = \Lambda e^{\Lambda^2} \left(\sqrt{\pi} - 2 \int_0^{\Lambda} e^{-\Lambda_1^2} \, d\Lambda_1 \right), \qquad (3)$$

$$\Lambda = \omega / \sqrt{2}\, k\, v\, a,$$

and where m_n and $\Lambda_n = \omega / \sqrt{2}\, k\, v_n$ refer to the neutralizing population.

For $v_n > 0$ the marginal stability condition is the same as when the neutralizing particles are neglected (i.e., when $m/m_n \to \infty$). If the neutralizing particles are the electrons, the growth rate of the instability is, however, held down to a mean thermal transit time of the electrons over a distance of the order of one instability wave length. If, on the other hand, we have $v_n = 0$, then

$$m/m_n > \frac{1}{a^2} - 1 \tag{4}$$

becomes sufficient for stability.

In the presence of a uniform magnetic field B_y in the direction of maximum thermal velocity, the instability tends to be inhibited. Equation (4) is not always sufficient for stability. The marginal stability condition is

$$\frac{4\pi n_0 r_c}{k^2} \left\{ \frac{1}{a^2} \left[1 - e^{-\epsilon} I_0(\epsilon) \right] - 1 - \frac{m}{m_n} e^{-\epsilon_n} I_0(\epsilon_n) \right\} < 1, \tag{5}$$

where $\epsilon = (k r_g)^2$, $r_g = mavc/e B_y$, and I_0 is the zero-order imaginary Bessel function. If the neutralizing population is assumed to be relatively massive, then one can write Eq. (5) in terms of

$$\beta \equiv \frac{8\pi n_0 v^2 a^2}{B_y^2} = 8\pi n_0 r_c r_g^2 \tag{6}$$

as

$$\frac{\beta}{2} \left(\frac{1}{a^2} - 1 \right) G(\epsilon) < 1, \tag{7}$$

where

$$G(\epsilon) = \frac{1}{\epsilon} \left[1 - \frac{e^{-\epsilon} I_0(\epsilon)}{1 - a^2} \right] . \tag{8}$$

For a high degree of anisotropy ($a^2 \ll 1$), we have $G(\epsilon) < 1$, and the minimum β at which the instability can occur equals $2a^2$. This is exactly the same stability condition as for the conventional fire-hose mode. Equations (6) through (8) serve to correct a numerical error in the definition of β in an earlier report.[1]

The instability of the E layer against spontaneous generation of B_θ field[1] has been shown to become somewhat greater at finite wave length along the axis of Astron. The marginal stability criterion is found to be

$$\bar{v}_\theta^2 > \bar{v}_z^2 \left[1 + \frac{3}{2} \left(\frac{k \bar{v}_z}{n v} \right) \right]^2 , \tag{9}$$

where a beam of mean velocity components $\bar{v}_\theta$, $\bar{v}_z$ and beam spread v is injected. The analysis was carried out in the plane approximation, for

$k^2/h^2 \ll 1$, where 2/h is the E-layer thickness. An estimate has been made for the stabilizing effects of cylindrical geometry. These are found insufficient to permit the condition

$$v_z^2 > 3\, v_\theta^2 \tag{10}$$

to be met (as required to achieve field reversal in Astron under the present plan) without running into the B_θ-generation phenomenon. What effect the B_θ generation will have on the realization of the E layer remains uncertain.

The familiar plasma-pressure-driven flute instability has been studied in a sheared magnetic field with finite plasma conductivity.[3] Using the methods of the infinite-conductivity analysis by Rosenbluth and Longmire,[4] one finds the dispersion relation

$$\omega^2 = \frac{1}{\tau_A^2} - \frac{2\omega}{\tau_c} , \tag{11}$$

where τ_A is the growth time in a shear-free field B of radius of curvature R,

$$\tau_A = \frac{1}{v_t} \left(\frac{2R}{k}\right)^{1/2} , \tag{12}$$

v_t being the ion thermal velocity, and where

$$\tau_c = \frac{\eta \epsilon}{\pi^2} (k\ell)^2 , \tag{13}$$

$$\epsilon = \frac{4\pi n Mc^2}{B^2} , \tag{14}$$

M being the ion mass and η the resistivity, which for simplicity is assumed isotropic. The quantity ℓ is the distance along magnetic field over which the shear in the field does not significantly distort the interchange motion. Using as the basic time unit the resistive plasma diffusion time over a wave length,

$$\tau_r = \frac{\pi^2}{k^2 \eta c^2 \beta} , \tag{15}$$

$$\beta = \epsilon \frac{v_t^2}{c^2} , \tag{16}$$

---

[3] H. P. Furth, Finite-Conductivity Flute Instabilities, UCID-4374, Oct. 1961.

[4] M. N. Rosenbluth and C. L. Longmire, Ann. Phys. 1, 120 (1957).

we obtain in the limit of interest ($\tau_c \ll \tau_A$) the instability growth time

$$\tau_u = \frac{R}{k\ell^2} \tau_r, \tag{17}$$

which shows that the plasma diffusion rate across magnetic field is enhanced by the geometrical factor $k\ell^2/R$.

The resistive pressure-driven flute may be the mechanism whereby the plasma in Zeta moves out through the vacuum field near the tube wall, where there is little current to drive it via the other resistive flute that has been discussed in this section.

In a pinch of higher temperature, one will expect the pressure-driven flute to become weak, since the ion gyroradius limits k, while the ion drifts combined with a slow growth rate at improved conductivity will tend to wash out the fluting motion.

An investigation has been made of a class of resistive instabilities which may appear in weakly ionized plasmas with anisotropic velocity distributions. An example is the interaction of an electron stream with plasma generated by the beam from a high-pressure background gas. This instability was investigated and verified earlier in resistive wall traveling-wave amplification.

Initially, the stability of contrastreaming electrons in a resistive background has been investigated. By use of simple collision-frequency approximations for the background, it is found that as ν_c exceeds ω_{ps} (ω_{ps} = stream electron plasma frequency), the usual electrostatic two-stream mechanism gives way to a slightly lower-growth-rate resistive instability, which extends over a much broader wave-length spectrum. Dissipative effects in the background therefore do not suppress collective interaction as might be expected, but instead give rise to new modes. Collisions of streaming electrons, however, would introduce damping.

10. THE DYNAMICS OF A SUPERNOVA EXPLOSION

Stirling A. Colgate, William H. Grasberger, and Richard H. White

Previously we have calculated the dynamical implosion of a supernova star 10 solar masses using an equation of state that includes the thermal decomposition of iron to helium and of helium to neutrons and protons. Starting from an initial equilibrium star of polytropic index 3, a mock quasistatic evolution evolves the star by 2.5 % total change in energy until a dynamical collapse takes place. The validity of the calculation is limited to $\rho \lesssim 3\times10^{11}$ g/cc, corresponding to a compression of the central zones of 10^4, at which point the transformation to a neutron star by inverse beta decay occurs within the dynamic time of the implosion.

We have programmed the solid neutron star equation of state of Salpeter[1] into the same Lagrangian hydrodynamic code used previously, and included an inverse β-decay neutrino energy sink. The inverse β decay proceeds rapidly, both because the density is so high--10^{10} to 10^{11} g/cc--and also because the electron Fermi level at 50 mc^2 gives a considerably larger cross section. The calculations have proceeded through the conversion to the solid neutron star phase (the inverse β decay occurred predictably at 3×10^{10} g/cc density) and have demonstrated a "bounce" at the predicted 2×10^{15} g/cc density. Fortunately, the gravitational potential is less than 1/3 mc^2, so that general relativity need not be included. The reflected shock wave appears strong enough to eject a major fraction of the star, but the calculations are not yet complete. If this ejected fraction proves to have traversed the solid neutron phase, it gives credence to the hypothesis that Cf^{254} is produced in major abundance.

[1] E. E. Salpeter, Ann. Phys. 11, 393 (1960).

IV. BERKELEY PLASMA RESEARCH

1. HOMOPOLAR PROGRAM

Klaus Halbach, G. Donald Paxson, and Didier Veron*

We continued the spectroscopic analysis of the light that is emitted along a line that intersects the outer electrode of Homopolar IV under 45°. So far we have failed to find a spectral line that showed mirror symmetry of the two line shapes for the two polarities of the magnetic field. In the preceding report (UCRL-9777) we expressed the opinion that the failure of our line shapes to show the proper symmetry upon magnetic field reversal was caused by the fact that we are always looking at line shapes resulting from a superposition of at least two spectral lines. A detailed analysis of two line shapes [around 4267 A (C^{+}) and 4070 A (C^{++})] showed that this was indeed true in both cases.

Some experiments were performed to obtain information about the back-voltage-producing breakdown of the machine. Homopolar IV is equipped with two pairs of mirrors; one is in a fixed position at the end of the machine (not disconnectable from the main coil), the other two coils can be moved into any position along the axis and can be disconnected. Experiments showed that energizing only one coil of the movable pair still gave a back-voltage-producing breakdown, whereas disconnecting both movable coils caused a very late breakdown that did not show a back voltage. These facts, together with the delay time between the gas release and the breakdown, show that the gas must have reached the mirrors by the time the breakdown occurs and imply that the sloping of the magnetic field lines in the mirror region is important for the breakdown. Under these circumstances, some gas will always spill over the mirror peaks and, after ionization, will be driven into the insulator region. In order to obtain some control over the time of the breakdown and therefore the spreading of the gas, we studied the effects of an improvised PIG discharge (Fig. IV-1), used as a firing mechanism in Homopolar IV. Experiments showed that the PIG discharge indeed reduced the delay between the gas release and the breakdown, particularly when the delay time without PIG was large. To quote some typical numbers: For a total gas release of 15 μliters and a machine voltage of 20 kv, the delay time was without PIG 1.8 msec, with PIG 0.6 msec. On October 25 we abandoned Homopolar IV, and we hope that the changeover to Homopolar V will be completed early in January 1962.

*Visitor from Centre d' Etudes Nucléaires de Fontenay-aux-Roses, France.

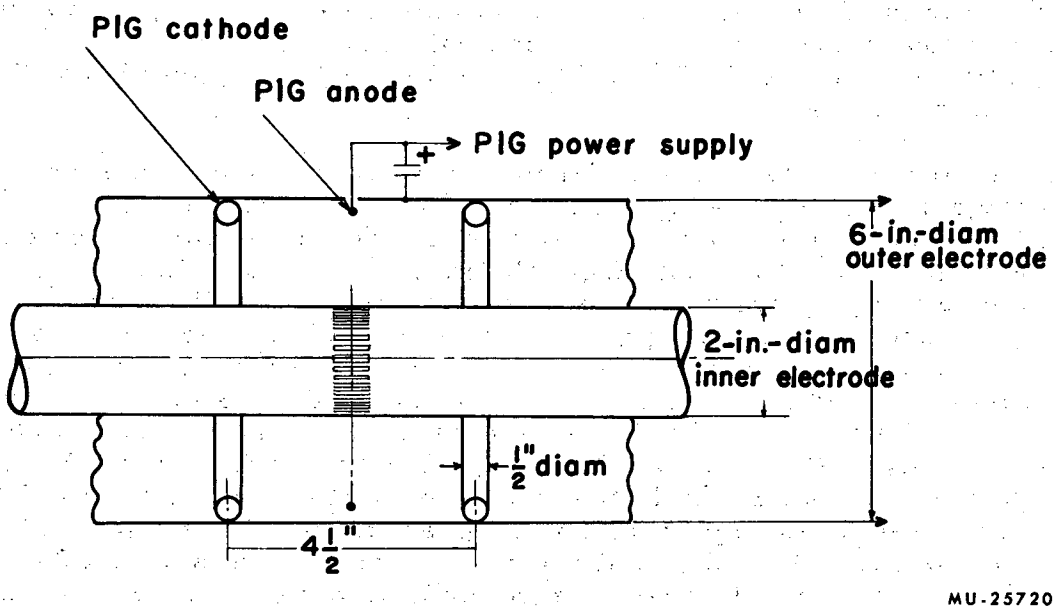

Fig. IV-1. PIG electrodes in Homopolar IV.

2. HYDROMAGNETIC WAVES AND CYCLOTRON HEATING

A Preionizer

George R. Spillman,* Forrest I. Boley, and William S. Cooper III

The ionizing technique used in Hothouse I[1] has been adapted to a geometry similar to that employed in Scylla compression experiments.[2] The adapted device is shown in Fig. IV-2. An initial discharge occurs within the coaxial electrode structure located at one end and an ionizing front propagates at 2 to 3 cm/μsec down the tube through the glass portion to the opposite end. When the front reaches the Pyrex end plate the electrodes are short-circuited (crowbarred), thus stopping the plasma rotation. Kerr-cell photographs were made which show the progress of the front down the tube. These photographs show the front to be rather nonuniform with occasional luminous regions extending well beyond the front.

Time-dependent ion-density measurements were made by using the polychromator[3] to observe the Stark-broadened H_β and H_γ line profiles. Although a variety of experimental conditions was investigated, only that using a 6-kgauss magnetic field and 8600-amp discharge current, and producing ion densities approximating the initial neutral hydrogen atom density of 7×10^{15} cm^{-3} is discussed in detail here. At 4 kgauss magnetic field and a discharge current of 4300 amp a maximum ion density of 3×10^{15} ions/cm^3 was observed. Doubling the current increases the ion density less than 15%. The original neutral atom density in this case was 7×10^{15} per cm^3. A qualitative explanation of this effect has been given by Kunkel.[4]

Density measurements were made both parallel and perpendicular to the tube axis at three viewing positions in each direction. Figure IV-3 shows the time-dependent density measurements made parallel to the axis together with the corresponding viewing areas. Times are measured after initial breakdown. All three viewing positions yield ion densities of the order of 7×10^{15} per cm^3 shortly after crowbar, which occurs at 23 μsec.

Special care must be taken in evaluating the data from the darker central "core" region. A similar core was observed in framing-camera photographs of Hothouse I. Light intensity as observed by the polychromator is low, about 1/6 peak intensity, at about 60 μsec and then rises slowly to peak intensity at about 135 μsec. A small "precursor" appears at the center of the spectral line, reaching its maximum intensity shortly before crowbar. Early in time the data fit theoretical line profiles poorly, but seem to indicate

---

*1st Lt. U. S. Air Force. The opinions expressed by the Air Force author are his own and do not necessarily reflect those of the United States Air Force or of the Department of Defense.

[1] J. M. Wilcox, A. W. DeSilva, W. S. Cooper, P. Pellisier, and W. R. Baker, A Device for Generating a Highly Ionized Hydrogen Plasma, UCRL-9528, Jan. 1961.

[2] E. M. Little, W. E. Quinn, and F. L. Ribe, Phys. Fluids 4, 711 (1961).

[3] G. R. Spillman, W. S. Cooper, and J. M. Wilcox, Nine-Channel Polychromator for Observation of Time-Dependent Spectral Line Profiles, UCRL-9843, Sept. 1961.

[4] W. B. Kunkel and R. A. Gross, Hydromagnetic Ionizing Waves, UCRL-9612, May 1961.

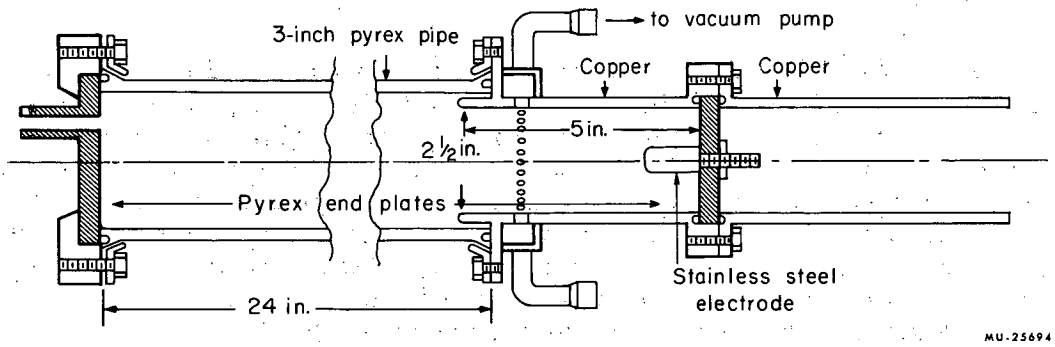

Fig. IV-2. Modification of Hothouse I design to a geometry similar to that employed in Scylla.

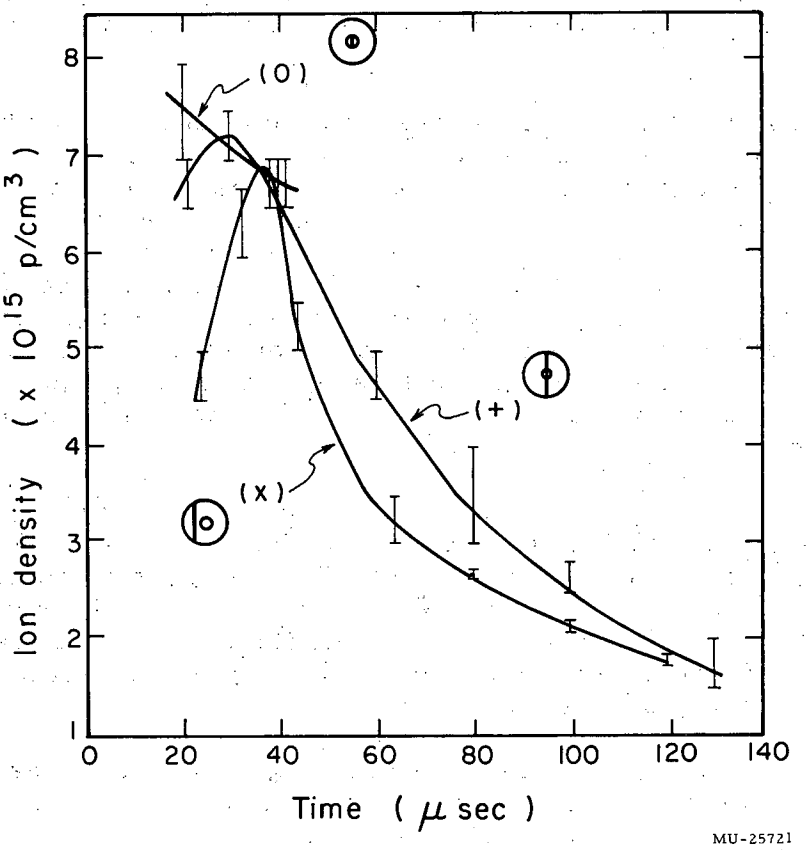

Fig. IV-3. Ion-density measurements made parallel to the tube axis in the viewing areas shown. The upper and lower bars indicate estimates of maximum and minimum densities, respectively.

the light is coming from a region of high ionization. Density measurement at 135 μsec corresponds to the density measurement elsewhere in the plasma at that time. It is believed that these measurements should be interpreted as follows:

(a) Except for the "precursor" in the center of the line the light observed early in time is due to reflections into the core region.

(b) The "precursor" may be due to ionization in the core region by fast electrons and photons.

(c) The peak at 135 μsec is due to diffusion of matter into the core region in a manner similar to that shown in the Hothouse I framing-camera pictures. [5]

Figure IV-4 shows density measurements made perpendicular to the axis along a tube diameter at three longitudinal positions. From these data one notes that the maximum ion densities do exceed the initial neutral gas density. For the magnetic field used the density falls after passage of the front and is not, in general, uniform along the tube. Thus measurements made parallel to the tube axis represent an intensity-weighted composite of the longitudinally variable density. At crowbar time (23 μsec) the ion density at the passive end is still rising while at the other positions it is falling slowly. However, the ion density at this time is nearly equal to the initial neutral density throughout the entire tube, with the possible exception of the center electrode region.

Carbon and oxygen impurities were determined by intensity comparison of the 4649-A O^+ and 4267-A C^+ lines from the plasma with those obtained by introducing known amounts of CO_2 gas into the system before ionization. The impurity levels of carbon and oxygen observed in this manner are approximately 0.04% and 0.7%, respectively. The ion density and impurity levels indicate that a device of the type discussed has possible application as a preionizer in compression devices.

Recently the diameter of the Pyrex pipe has been increased from 3 in. to 6 in. so that the effects of launching the ionizing front into a region relatively free of wall influence can be studied.

Ion Cyclotron Resonance Experiment

Peter R. Forman, Gordon W. Hamilton, Alan W. DeSilva, and Forrest I. Boley

Considerable evidence was cited in the preceding quarterly report for the existence of an ion cyclotron resonance condition for high-intensity torsional Alfvén waves in a magnetic mirror geometry. The wave magnetic-field amplitude and relative phase measurements reported at that time depended for their interpretation upon shot-to-shot reproducibility, and wave amplitudes were determined by averaging over a substantial portion of the 3-msec radio-frequency wave driving pulse. To allow simultaneous observation of the wave fields at several positions, a seven-coil magnetic

[5] In Controlled Thermonuclear Research Quarterly Report, UCRL-9777, August 1961, p. 68.

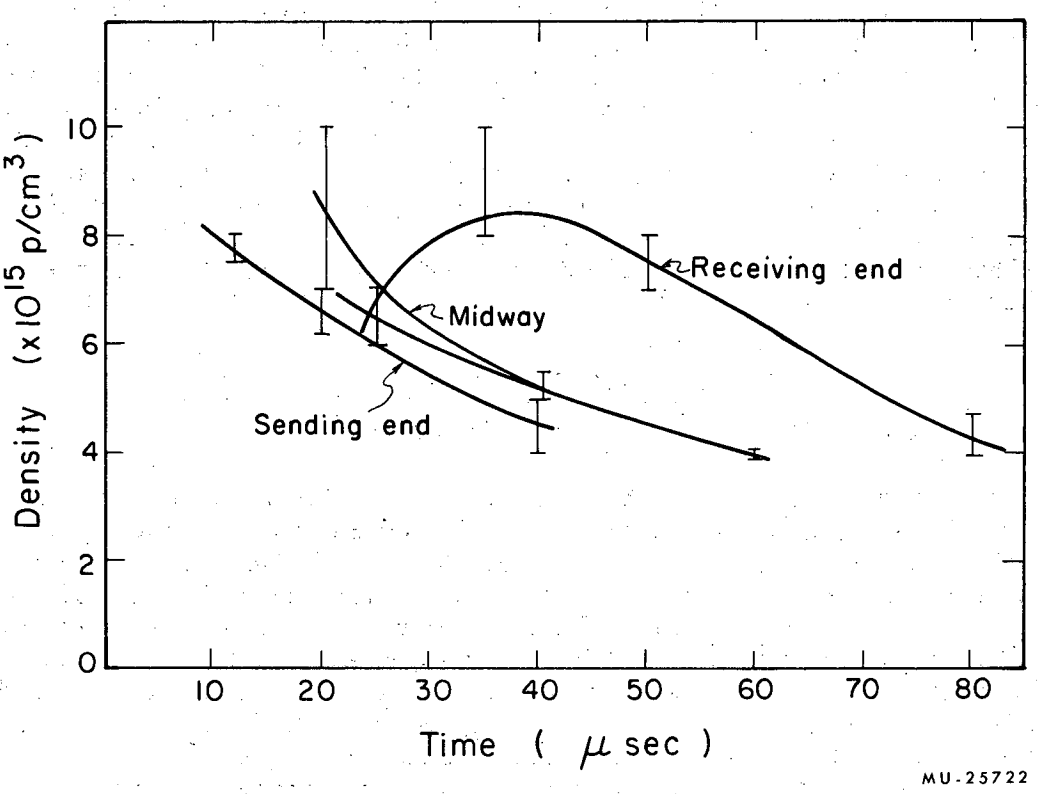

Fig. IV-4. Ion-density measurements made perpendicular to the tube axis along a diameter at the launching end, the midpoint, and the receiving end of the Pyrex pipe. The upper and lower bars indicate estimates of maximum and minimum densities, respectively.

probe has been constructed. By use of this probe the averaged wave-amplitude results reported earlier have been confirmed and the over-all evidence of ion cyclotron resonance substantiated. In addition, the seven-coil probe should allow more detailed measurements of the b_θ wave field phases and amplitudes as functions of time and longitudinal position z than has heretofore been possible. Measurements of the detailed behavior of b_θ amplitude as a function of radius, axial position, and time are not yet complete, but have already yielded some interesting results. It has been found that the wave field has large azimuthal asymmetries, which, however, are fairly reproducible in their general appearance from shot to shot. The wave field shows large variations with z position, including some striking and quite reproducible minima which suggest the presence of standing waves. These minima appear about 100 μsec after the rf is switched on, and persist for at least the next 100 μsec. The b_θ amplitude in the earlier part of the rf pulse is very different from shot to shot. The rf oscillators which supply the plasma heating energy were tested under resistive dummy loads applied at the same point as the plasma load. By comparing the oscillator input power with plasma loads to the input power with dummy loads, it was estimated that the plasma impedance is initially equal to about 0.8 ohm, and that the plasma impedance increases to about 1.5 ohm during a pulse of 1 msec. This change in plasma impedance is another indication of the "pump-out" process.

Alfvén Wave Reionizer

George R. Spillman* and Forrest I. Boley

For some time it has been thought desirable to have a means of measuring the density of neutral hydrogen atoms in the Hothouse I plasma to study the effect of the neutrals on Alfvén-wave propagation. One method of making this density measurement is being studied; it involves reionization of the decaying plasma and measurement of the resulting ion density by means of the polychromator.[3, 5] The method is to propagate a large-amplitude Alfvén wave in the plasma at the time a neutral-density measurement is desired. The experiment is to be repeated using progressively higher amplitudes until a plateau in the resulting ion density is observed. Of course, if there has been no pumping action on the neutrals this measured ion density should be that measured immediately after crowbar.

Some preliminary experiments were carried out to aid in the choice of parameters in the system. Between 90 and 100% reionization was achieved in a plasma which had decayed from approx 3.3×10^{15} ions/cm^3 to 2.3×10^{15} ions/cm^3 (initial H_2 pressure of 50 μ Hg). In a plasma which had decayed from 6.6×10^{15} ions/cm^3 to 4.7×10^{15} ions/cm^3, reionization resulted in more than 5.5×10^{15} ions/cm^3. An estimated 110 joules was delivered to the plasma in reionization. In each case the wave frequency was about 125 kc.

---

*1st Lt. U. S. Air Force. The opinions expressed by the Air Force author are his own and do not necessarily reflect those of the United States Air Force or of the Department of Defense.

Temperature Measurements in Hothouse I

William S. Cooper III and Forrest I. Boley

Since the preceding quarterly report, considerable effort has been devoted to developing spectroscopic methods of measuring the time dependence of the electron temperature in the decaying hydrogen plasma produced in the Hothouse I experiment. The first method investigated depended on the fact that the frequency dependence of the Balmer recombination continuum (due to the capture of free electrons by hydrogen ions to form excited neutrals with principal quantum number 2) is proportional to $N_i N_e e^{-h\nu/kT}$, where T is the electron temperature, N_i is the ion density, and N_e is the electron density. If only relative intensity measurements are made, the electron temperature at a given time may be determined from a plot of the continuum intensity as a function of ν, without knowledge of N_i or N_e. This $e^{-h\nu/kT}$ dependence of the continuum intensity is the result of assuming a Maxwellian velocity distribution for the electrons, probably a very good assumption for the Hothouse I plasma; if the electrons have a non-Maxwellian velocity distribution, the distribution could presumably be measured by this method.

The measurements were made with a single Jarrell-Ash Model 82-000 monochromator looking end wise into the Hothouse I tube midway between the center electrode and the tube wall. The average time dependence of the light intensity, averaged over nine shots, was measured at five wave lengths in the region between 3500 and 2500 A, using a bandpass of 1.5 A. Cross-plots then gave the relative continuum intensity versus frequency for different times. The use of a carbon arc as a radiation standard allowed the combined transmission of the optics and response of the 1P28 photomultiplier used as a detector to be determined at these wave lengths. Figure IV-5 shows a typical plot of continuum intensity per unit frequency interval vs frequency, at 100 μsec after breakdown, or 87 μsec after the plasma was crowbarred and began to decay.

The expected $e^{-h\nu/kT}$ dependence is observed; the slope indicates an electron temperature at this time of about 24,000 ± 7000°K. One point is about 10% high; another is about 10% low. These discrepancies are probably due to the presence of faint spectral lines in the band of continuum observed from the plasma and from the arc respectively, although considerable pains were taken to discover these faint lines and avoid them. Similar observations at different times indicated an electron temperature of more than 50,000°K shortly after crowbar, which then dropped rapidly to about 25,000°K at about 50 μsec, and remained roughly constant to as late as 180 μsec, at which time the light intensity from the plasma had dropped to a level too low to permit measurements. These measurements are not in good agreement with temperature measurements previously made by observing damping of Alfvén waves induced in the plasma and also by direct measurements of the electrical conductivity of the plasma; the earlier measurements had indicated electron temperatures lower than spectroscopically determined values by a factor of about 3.

This method of measuring electron temperatures suffers a serious disadvantage in measuring electron temperatures above about 20,000°K. The reason is a practical one: at high temperatures, the continuum in the

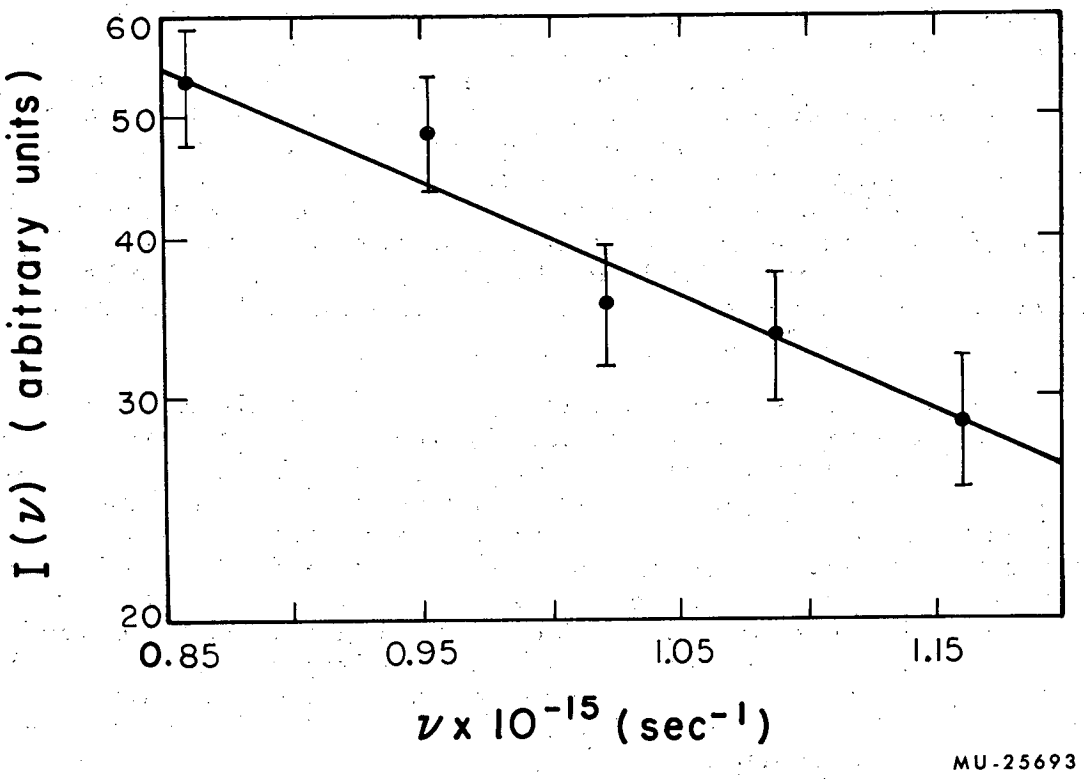

Fig. IV-5. Continuum intensity per unit frequency interval (arbitrary units) vs frequency, at 100 μsec. Crowbar was at 13 μsec. The slope of the solid line corresponds to a temperature of 24,000°K. The vertical lines show experimental errors.

region of the spectrum between 3500 and 2500 A becomes more and more nearly flat, and measurements of the slope become more difficult. Extending the range of observation either way is impractical; the Balmer series limit is at 3646 A, and the carbon arc, although probably the most suitable radiation standard for this region, does not emit enough light to be of use in calibration below 2500 A.

In view of these limitations, a second method of measuring electron temperatures spectroscopically is being investigated. The ratio of the intensity of a hydrogen emission line (H_β, for instance) to that of an adjacent band of the continuum is a sensitive function of the temperature in the range 10^4 to 10^5 °K, and is also practically independent of the ion and electron densities. This method is expected to yield electron temperatures accurate to 10%.

3. HYDROMAGNETIC IONIZING FRONTS

Arthur R. Sherwood and Wulf B. Kunkel

During the time covered by this report, construction has begun on an apparatus intended to be used for the experimental investigation of some of the properties of hydromagnetic ionizing fronts. The device will initially be used to produce and study "switch-on" waves, particularly in conjunction with the previously reported theoretical work on ionizing fronts. [1]

The geometry of the apparatus, Fig. IV-6, is similar in general to that used by Patrick. [2] The annular region between two concentric cylinders will be used for the experimental region as an approximation to the one-dimensional plane geometry of the theoretical work. [1] The outer cylinder is approximately 6 in. in diameter and consists of a 1/16-in.-thick welded stainless steel tube. The inner cylinder consists of a Pyrex tube of approximately 4 in. o.d. At the driving end there is an annular ceramic insulator, and at the receiving end there is an annular pyrex window. The total axial length of the experimental region is about 4 ft. These dimensions have, to a great extent, been dictated by the axial magnetic field coils, which have been inherited from the Homopolar IV experiment.

The device is to be mounted vertically, i.e., the axis of the cylinders will be vertical. The driving end will be at the top and the receiving end at the bottom. The axial magnetic field coils will be pulsed by the new electrolytic bank, described elsewhere in this report.

The fabrication of the major components is nearly complete, with the exception of the annular ceramic insulator. The initial assembly awaits this last part. The driving-current source, a pulse line, has been constructed, but dummy load tests have yet to be conducted.

---

[1] Wulf B. Kunkel, in Controlled Thermonuclear Research Quarterly Report UCRL-9777, June 1961, p. 75.

[2] R. M. Patrick, Phys. Fluids 2, 589 (1959).

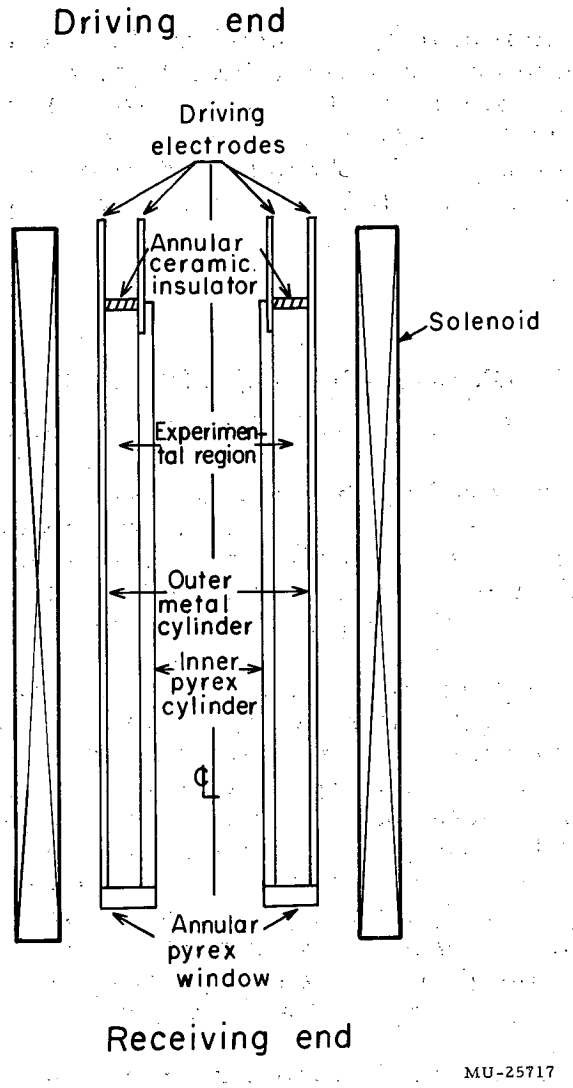

Fig. IV-6. Geometry of apparatus being constructed for study of hydromagnetic ionizing fronts.

4. CROSSED-FIELD BREAKDOWN STUDIES

Melvin J. Berstein and Wulf B. Kunkel

The experiments preliminary to a study of breakdown in a transverse magnetic field have been concluded. A detailed description of the apparatus and results for the ionization coefficient, drift velocity, and diffusion experiments are given elsewhere.[1]

A. Diffusion of Electrons in Hydrogen in a Transverse Magnetic Field

This experiment measured the diffusion of a small number of electrons (about $10^4/cm^3$) colliding only with neutral molecules (about $10^{16}/cm^3$). The apparatus used the coaxial cylindrical geometry previously described in general for the ionization and drift-velocity measurements.[2]

The anode consisted of five rings stacked vertically (magnetic field is vertical) with dimensions shown in Fig. IV-7. The electrode gap (1 cm) was small compared with the anode radius (8.25 cm). Electron emission from the cathode of about 10^{-11} amp was provided by a hot tungsten filament behind a slit perpendicular to the magnetic field. The experiment measured the ratio of the current collected by the middle ring to the sum of currents collected by the two adjacent rings as shown in Fig. IV-7. By use of the drift-velocity results (shown in Fig. IV-8) obtained in the previously described drift-velocity experiment, the parallel diffusion coefficients were computed. According to theory a plot of the pressure times the diffusion coefficient as a function of E/B should give smooth curves for the different gases; results for hydrogen and deuterium gave good agreement, with a scatter of less than 10%. The range of parameters was: E from 6 to 270 v/cm; p from 1.7 to 4.0 mm Hg; B from 0.8 to 7 kgauss. The ratio of electron-cyclotron to elastic-collision frequencies $\omega_b \tau$ ranged from about 3 to 8. Good results could not be obtained for helium because apparently the tank of helium was quite contaminated, and copious numbers of negative ions were formed which swamped the electron current at strong magnetic fields. For hydrogen and deuterium an analysis of the drift-velocity and diffusion results, using an IBM 709 computer and assuming a Maxwellian distribution, yielded the elastic-collision cross section as a function of electron velocity and the average energy of the electrons as a function of E/B (Figs. IV-9 and IV-10). The cross section around 2 to 4 ev is a little high because transverse diffusion caused the measured ratio of perpendicular to transverse drift to be smaller than it really is. The error is not enough to explain the discrepancy with other authors. In the strong-magnetic-field limit, deviations from the assumed Maxwellian distribution produce only small deviations in the cross section and average energy.

---

[1] Melvin J. Bernstein, Electron Drift, Diffusion, and Ionization Measurements in Hydrogen with Crossed Electric and Crossed Magnetic Fields (Thesis), UCRL-9865, Sept. 1961.

[2] Melvin J. Bernstein and Wulf B. Kunkel, in Controlled Thermonuclear Research Quarterly Report, UCRL-9243, June 1960, p. 26; in Controlled Thermonuclear Research Quarterly Report, UCRL-9393, Sept. 1960, p. 56.

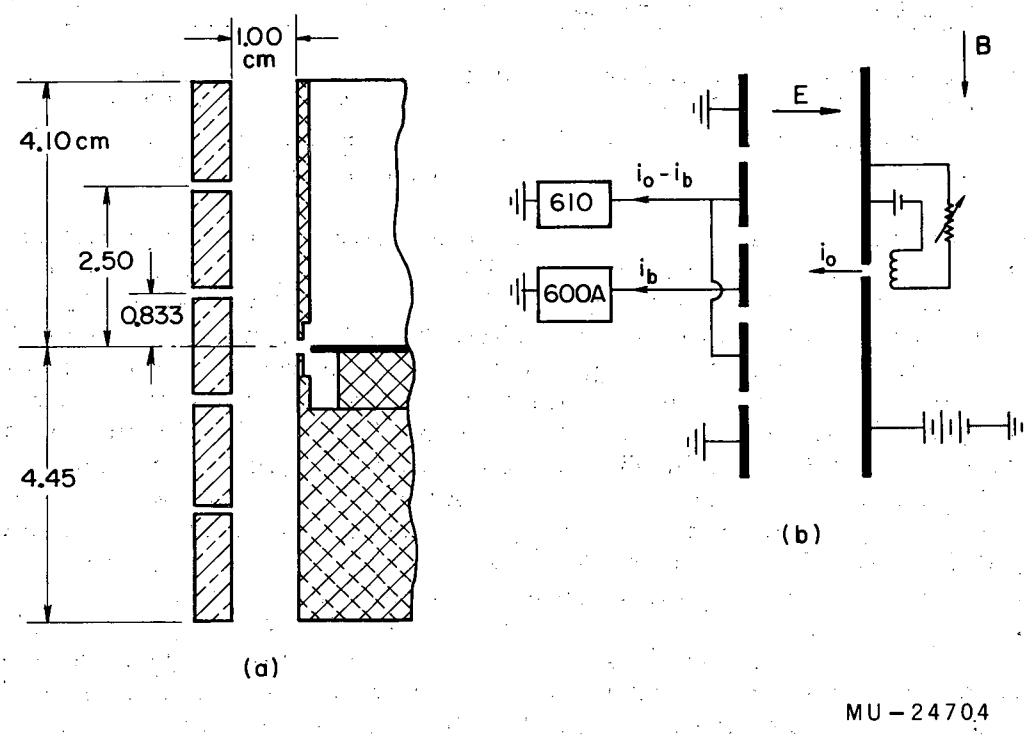

Fig. IV-7. Experimental details for measuring the parallel diffusion coefficient.
(a) Electrode detail. The cathode was an aluminum cylinder and the anode a stack of copper rings. The filament was parallel to the slit in the cathode (normal to the view shown and perpendicular to B).
(b) Electrical schematic for measuring ratio of currents to the middle rings. At a given pressure and electric field, the magnetic field was adjusted until a predetermined ratio of currents ($i_b/i_0 = 0.70$) was obtained.

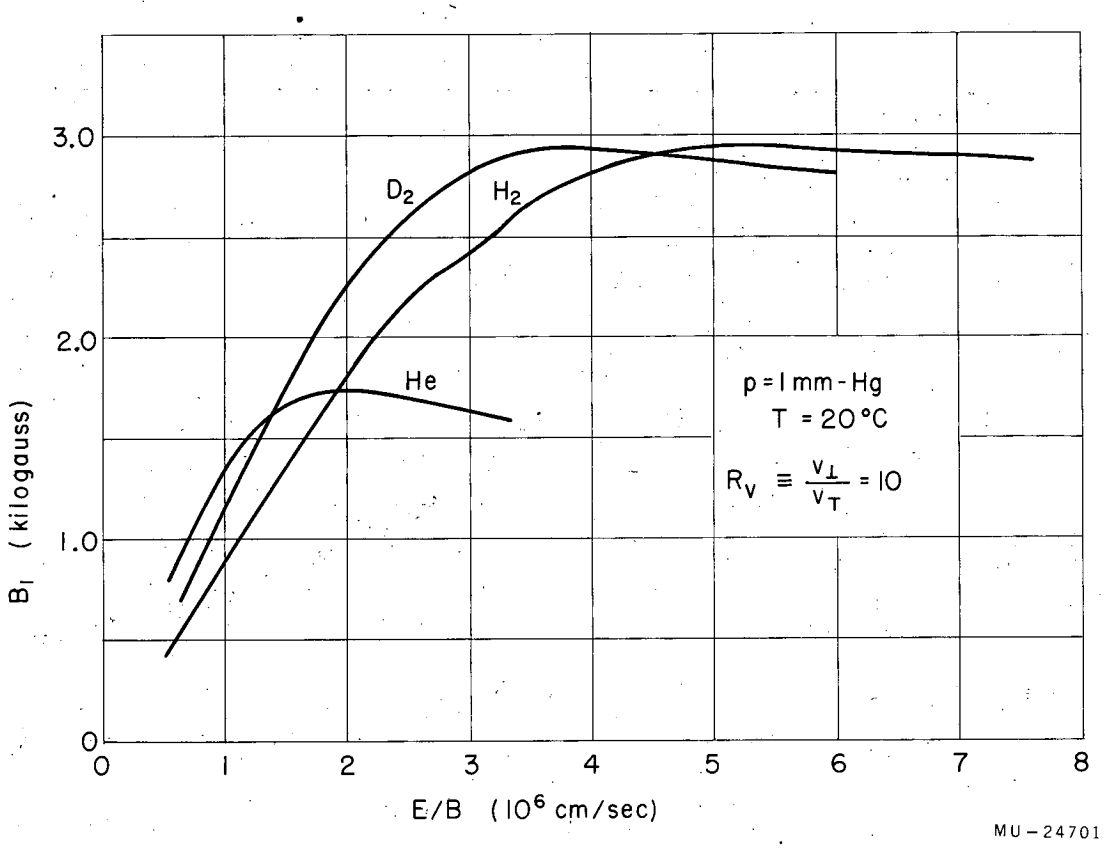

Fig. IV-8. Magnetic field B_1 needed to produce a drift-velocity ratio $R_v = 10$ as a function of the perpendicular drift velocity E/B when the pressure is 1 mm Hg at T = 20°C. The transverse drift velocity is given in cm/sec by $v_T = 10^4 B_1(p/B)(E/B)$ for the units of p in mm Hg, E in v/cm, and B in kgauss.

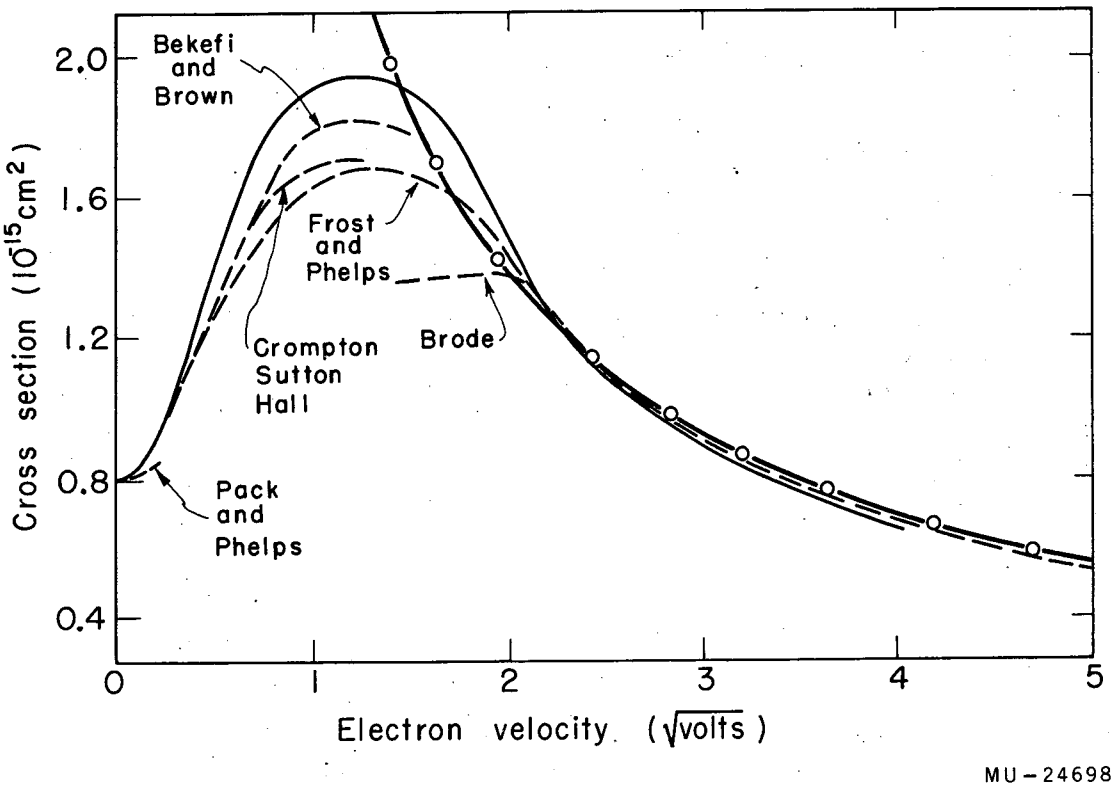

Fig. IV-9. Elastic cross section in hydrogen. Present results are shown as a solid line, and a cross section corresponding to a constant collision frequency is shown as a circled line.

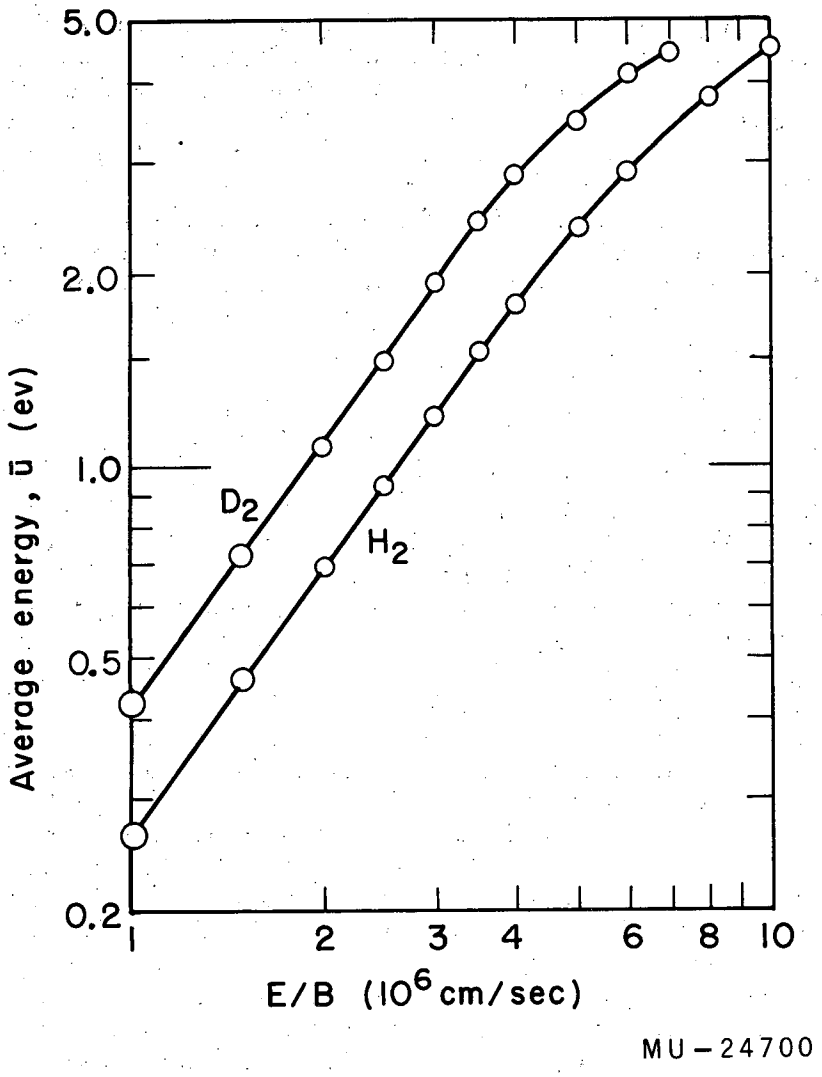

Fig. IV-10. Average energy of electrons (in ev) as a function of E/B.

B. Breakdown Threshold in Crossed Fields

Measurements have been made of Paschen curves (minimum breakdown voltage vs pd) for different magnetic fields in the crossed-field geometry. The experimental setup was exactly as used for the α/p measurements shown in Fig. IV-11. An electrode gap of 0.5 cm was used with hydrogen as the gas. The cathode voltage was slowly raised until the anode current indicated breakdown was almost reached. Results (see Fig. IV-12) show that a moderate magnetic field greatly decreased the breakdown threshold (with Al cathode) from about 230 volts for zero magnetic field to as low as 185 volts at about 400 gauss. This is caused by the magnetic field trapping the electrons. Much higher fields raised the breakdown voltages to well over 300 volts minimum at 2000 gauss. The range of pressures was 0.3 to 3.0 mm Hg. If the pd corresponding to minimum threshold at a given field is denoted by $pd(B)_{min}$, then $pd(B)_{min}$ attained a minimum itself at about 400 gauss and increased at higher magnetic fields.

C. Formative Time Lag

An experiment has been set up to measure the formative time lag for breakdown across a strong magnetic field. The electrode structure is exactly the same as that described for the breakdown threshold measurements. A fast-rising pulse (rise time of about 0.2 μsec) is provided with a 1-μf capacitor and a hydrogen thyratron. Measurements in hydrogen with Al cathodes show formative time lags of 1 to 100 μsec for pressures of 0.05 to 1.0 mm Hg, electrode gaps of 0.3 to 1.0 cm, electrode potentials of 0.8 to 3 kv, and magnetic fields of 4 to 10 kgauss. The range of $\omega_b \tau$ was 20 to 400. A theory on the rate of ionization in hydrogen can be used to compute a formative time lag when the breakdown is initiated by essentially a single avalanche.[3] The theory predicts that the product of the gas density n_g and the formative time lag T_B is a function only of E/B, the ratio of electric to magnetic fields. To convert the theoretical ionization rate to a formative time lag, we have assumed that the electron number increases by a factor of 10^8 to 10^{11} during the time lag. The results, Fig. IV-13, are shown as a range of the measured values because of the large number of parameters used; the theoretical values are shown by vertical bars. The measured values were reproducible to within less than 15%. It was observed that at a given E/B the product $n_g T_B$ decreased as either the magnetic field or the pressure was increased. A lower limit to the values seemed to be reached at high pressures, as indicated by lower edge of shaded area. Longer time lags are the result of multiple avalanche crossings in which secondary emission needs to be taken into account. It was found that any component of electric field parallel to the magnetic field, such as found at the edge of the cathode, enhanced ionization rate. This problem was solved by enclosing both ends of the electrode gap with insulators.

---

[3] Gary A. Pearson, this report, Section IV. 5.

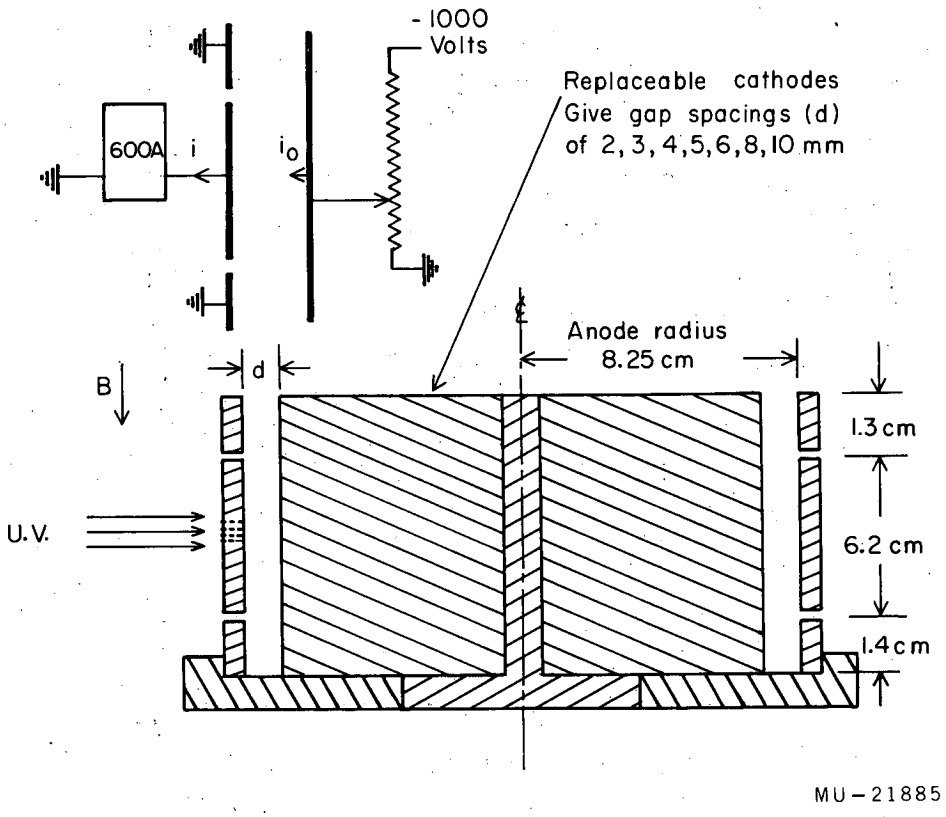

Fig. IV-11. Experimental setup for measuring α/p and breakdown threshold. For measurements of the breakdown threshold only an electrode gap of 5 mm was used.

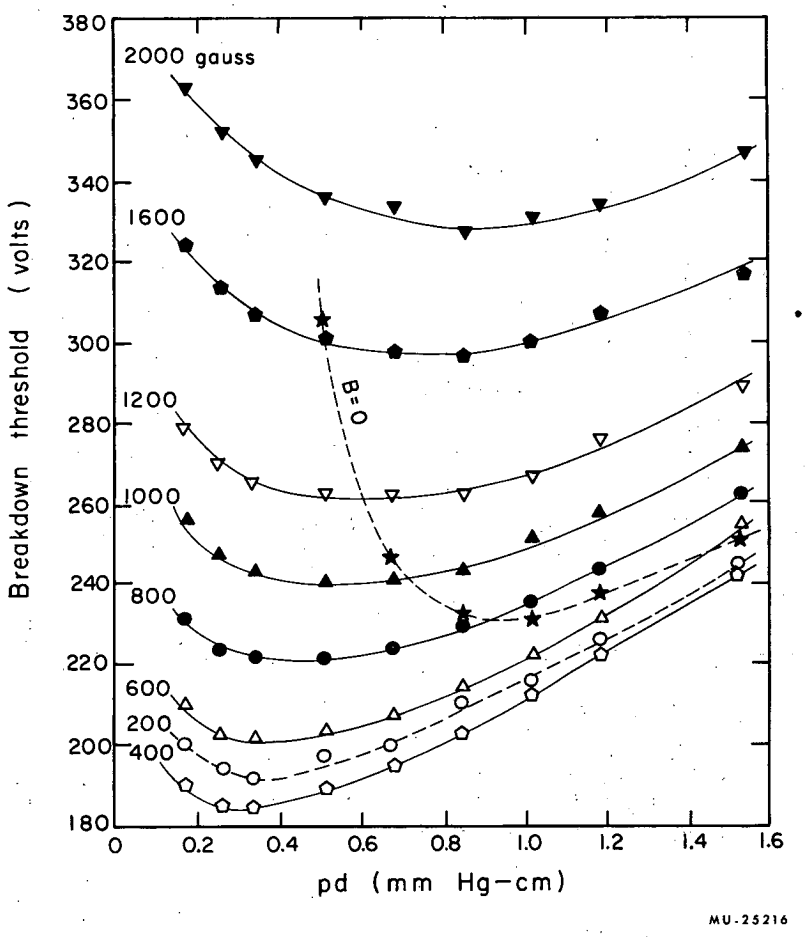

Fig. IV-12. Breakdown threshold as a function of pd (product of pressure and gap) in hydrogen with an Al cathode. Note that the curve for B = 200 gauss lies above the curve for B = 400 gauss.

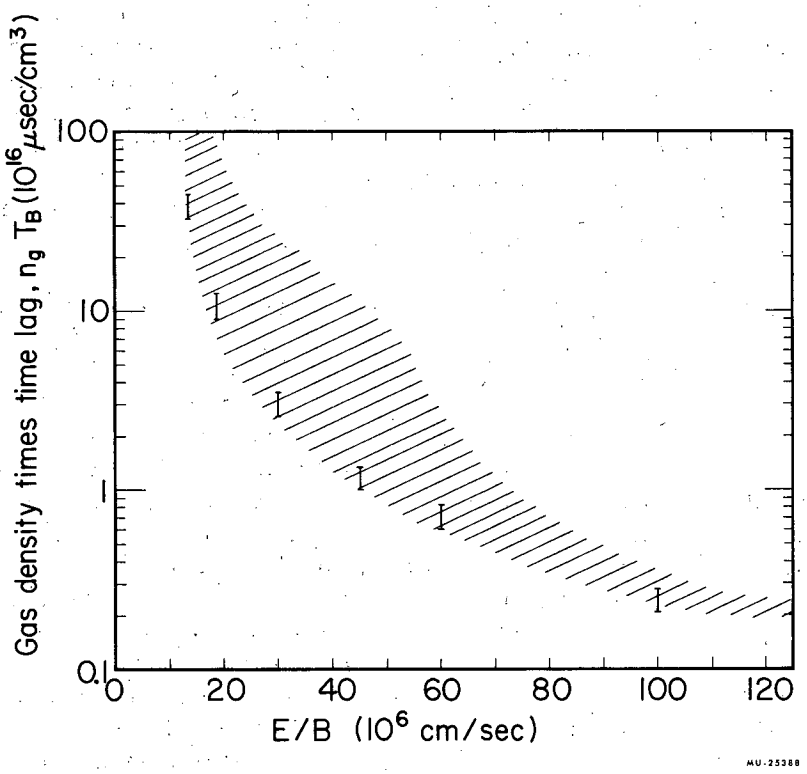

Fig. IV-13. Product of gas densities and formative-time lags in hydrogen as a function of the perpendicular drift velocity E/B. Measured values are shown by the shaded area. Broad range of values arises as the pressure and magnetic field are varied. Theoretical values are shown by vertical bars.

5. NUMERICAL CALCULATION OF THE ELECTRON ENERGY DISTRIBUTION IN H_2 AND D_2 IN CROSSED FIELDS FOR LARGE $\omega\tau$

Gary A. Pearson

An equation analogous to the Boltzmann equation has been derived to give the time development of the energy distribution of nonrelativistic electrons in a cold gas and under the influence of uniform and mutually perpendicular electric and magnetic fields. The electron cyclotron frequency ω is assumed to be large compared with the electron collision frequency $1/\tau$, and the degree of ionization is assumed to be small enough that the electron energy distribution is affected only by collisions with slow molecules. Although this energy distribution applies whenever both it and the electron density are spatially uniform, it may also be interpreted as the spatial integral over any volume that has no electrons passing through its surface. The analysis includes elastic collisions, which cause the electrons to drift in the direction of the electric field and gain kinetic energy; ionization, which increases the number of electrons; and other inelastic collision, which remove kinetic energy from the electrons.

This equation is being solved numerically for solutions of the form

$$f(\epsilon, t) = e^{\beta t} f_0(\epsilon),$$

where ϵ is the electron energy as observed from the $\vec{E}\times\vec{B}$ drift reference frame, $f_0(\epsilon)$ is a normalized energy distribution, and β is a positive quantity which accounts for the buildup from ionization. At present $\vec{E}\times\vec{B}$ drift velocities from 3×10^6 cm/sec to 6×10^7 cm/sec in H_2 and D_2 are being considered. Under these conditions rotational excitation of the molecules may be neglected, but vibrational excitation, electronic excitation, dissociation, and ionization are important. Several of these cross sections are not yet well established. In particular, the cross section for electronic excitation can only be inferred from swarm data, and the vibrational excitation energy loss in D_2 has not been investigated; thus a variable parameter has been introduced into each of these two cross sections.

Knowledge of $f_0(\epsilon)$ allows one to compute most things of interest. Some of the parameters that can be compared with experiment are the mean electron energy, the drift velocity in the direction of the electric field, the first Townsend coefficient α, and the mean energy loss per collision η. One can also predict the formative time lag in experiments in which single avalanche breakdown occurs. Preliminary comparison with the experimental results of Bernstein[1, 2] shows excellent agreement.

---

[1] Melvin J. Bernstein, Electron Drift, Diffusion, and Ionization Measurements in Hydrogen with Crossed Electric and Strong Magnetic Fields (Thesis), UCRL-9865, Oct. 1961.

[2] Melvin J. Bernstein and Wulf B. Kunkel, this report, Section IV-4.

6. SHEET PINCH STUDIES

Oscar A. Anderson

6×10 Triax

The flare effect in the Triax discharge, described in a previous report,[1] has been observed steroscopically. Almost all flares were found to be located near the lower electrode or the insulating walls. There is little doubt now that flares develop from particles that crumble off the ceramic wall, as conjectured earlier.[2]

Stereoscopic streak photography has also been used to study the sheet pinch itself. It was found that after the first plasma-compression period, most of the visible light comes from the ends of the plasma sheet (near the electrodes), as would be expected if the central region were almost completely ionized.

At pressures above 0.5 mm Hg, impurity lines studied with the monochromator tend to appear gradually rather than as flares. It remains to be determined whether or not this gradual contamination is uniform throughout the plasma. Color films exposed in the streak camera show the plasma changing from pinkish to blue-white after about 2 μsec, confirming the monochromator observations. These films were made before the stereoscopic system was ready. Combining the two techniques should locate the contaminants. If it turns out that they are confined to the region of the electrodes, then the gradual type of contamination is less serious than previously assumed.

In any case, the flare effect itself must be detrimental to pinch confinement. The rate at which flares are observed through the 1/16-inch streak slit implies that over the whole tube, hundreds of flares occur on each shot. Those near the bottom electrode are observed to badly perturb that region of the plasma, although it is hard to tell how far the disturbance propagates. Flares near the wall are probably even more serious.

It is true that the flare rate is reduced after the tube is disassembled and cleaned, but this is time-consuming and only a temporary cure, since the wall soon starts to decompose again. Wulf B. Kunkel has suggested that this might be avoided if helium rather than deuterium were used for most of the diagnostic work, for deuterium is suspected of chemically attacking the ceramic wall. Experiments are under way to determine whether the use of helium is advantageous.

---

[1] Oscar A. Anderson, in Controlled Thermonuclear Research Quarterly Report UCRL-9598, March 1961, p. 42.

[2] Oscar A. Anderson, in Controlled Thermonuclear Research Quarterly Report UCRL-9777, Aug. 1961, p. 63.

Flat Sheet Pinch

The tubular pinch (Triax) exhibits long confinement times when the high density is considered. A time of 5 μsec at 10^{18} density corresponds to 5 msec at 10^{15}, according to Lawson's criterion.[3] However, it is technically difficult to reach very high temperatures because the Triax shape and size make large condenser banks necessary. Furthermore, the effect on stability of the (slight) plasma curvature has been questioned. Thus there was interest in an experiment that would utilize the sheet stability in a different configuration.

A sheet pinch tube was designed which was similar to the Triax in almost every respect except that the sheet was to be flat instead of cylindrical. The electrodes and insulating walls were made of the same materials, and the spacing between electrodes and between the main walls was the same. The difference was that the walls were flat and were joined at the ends to form a rectangular ceramic box. The tube is shown in Fig. IV-14. It will be noted that the inner perimeter is about 40 cm, compared with 120 cm (total) for the Triax. A given current in the early stages of compression will then produce a field three times as strong, exerting nine times the force of the Triax pinch. At later times the edges of the sheet will be forced toward the center, giving a further increase in the field-to-current ratio. Of course, as the edges come together, the central region can no longer be considered as an isolated flat sheet. (This will be discussed further on.)

The design of this first tube emphasized ease of assembly and versatility rather than freedom from sources of organic contaminants. The top electrode was removable and could be quickly interchanged with a fine-meshed screen for purposes of observation. Initially the tube was connected to a small 33-μf condenser bank to check the low-energy behavior. Strong impurity lines, especially carbon, were detected with a monochromator, as expected. Kerr-cell photographs taken through the screen electrode showed the usual sheet pinch behavior in the shorter dimension. (See Fig. IV-15.) There were several bounces, with strong light emission starting at the first bounce. Meanwhile the edges contracted somewhat but did not interfere with the other behavior. In general, at a condenser voltage of 10 to 15 kv the reproducibility was reminiscent of the low-energy mode of the 4-inch Triax previously reported.[4]

When the bank voltage was raised to 22 kv the fine screen could not withstand the plasma bombardment, and the solid electrode had to be installed. A plastic scintillator, which had been designed and calibrated by Robert V. Pyle, was placed near the tube. Neutrons were found to appear 1.5 μsec after the start of the discharge and to disappear at around 2 μsec. The number produced was about 10^4, varying less than ±25% from shot to shot, compared with variations over several powers of ten in the ordinary unstabilized pinch.[5] The large voltage spikes characteristic of pinch instability were also absent.

---

[3] J. D. Lawson, Proc. Phys. Soc. (London) B70, 6 (1957).

[4] Wulf B. Kunkel, in Controlled Thermonuclear Research Quarterly Report UCRL-8682, March 1959, p. 39.

[5] Conference on Controlled Thermonuclear Reactions, held at Princeton University, Oct. 17-20, 1955, TID-7503, Feb. 1956, pp. 211-212.

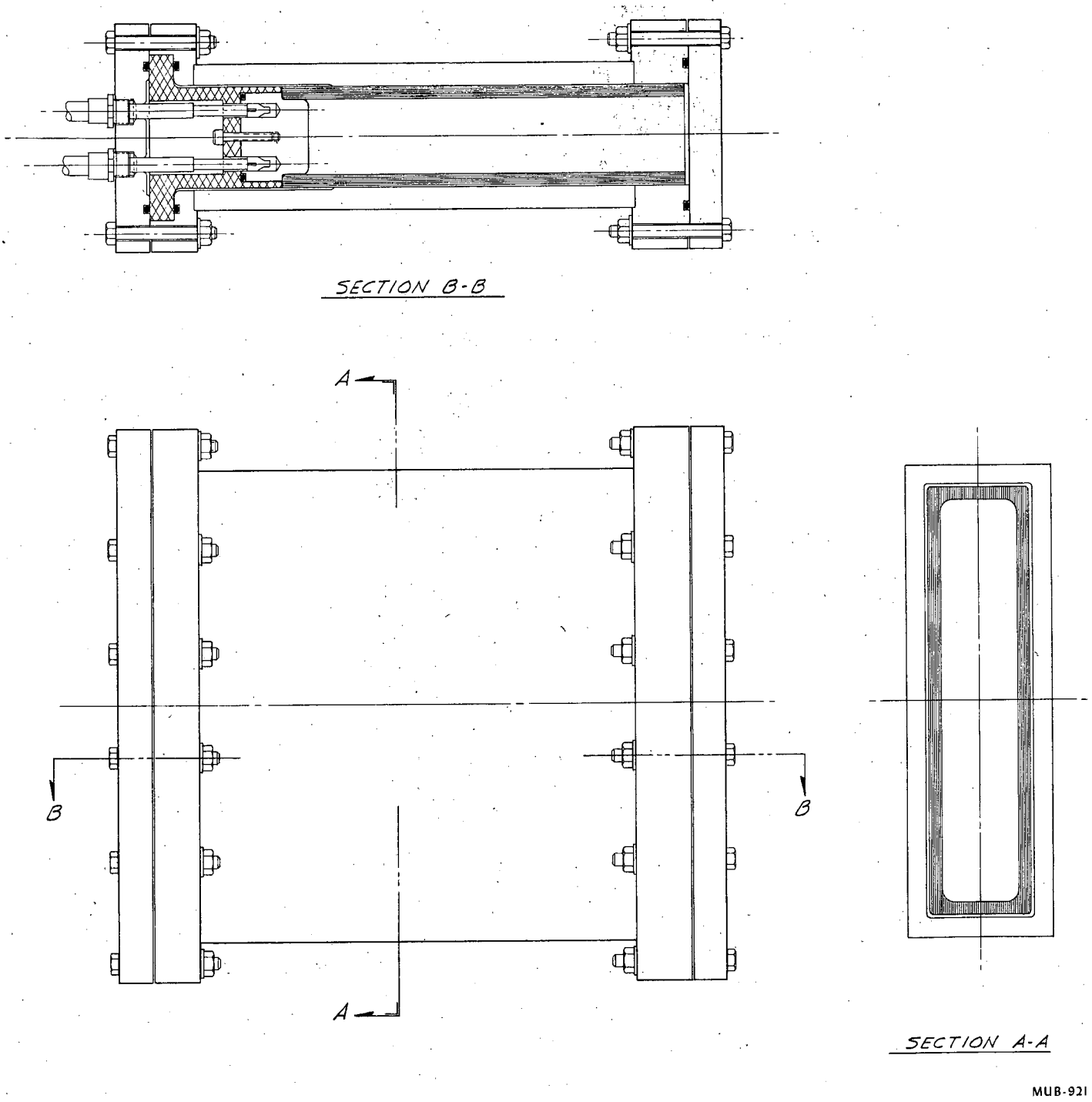

Fig. IV-14. Assembly drawing of ribbon pinch tube.

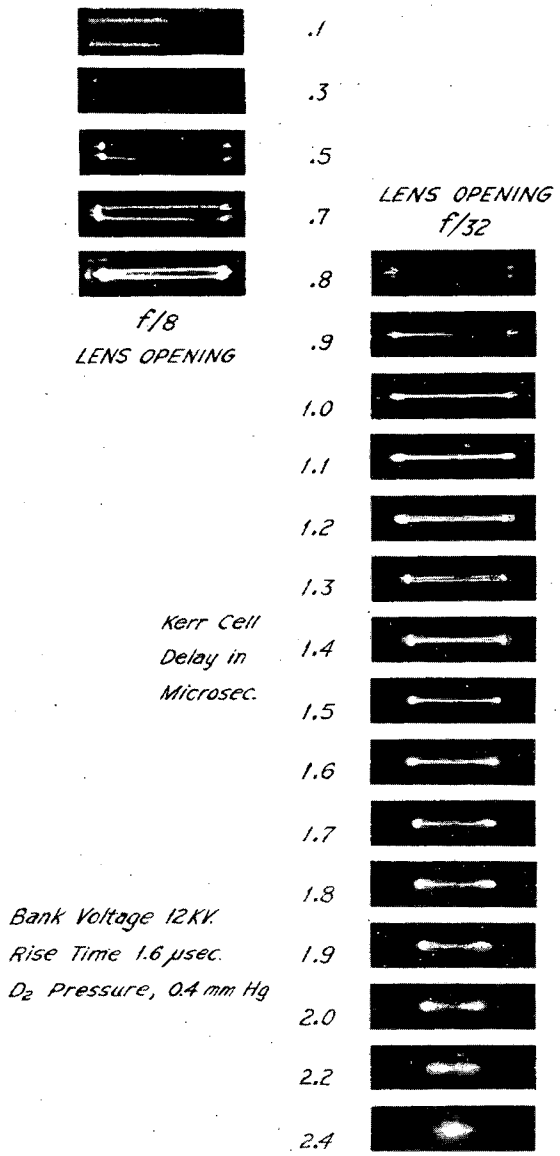

Fig. IV-15. Ribbon pinch dynamics at low energy.

Since the period of plasma confinement seemed to be limited by the discharge time of the condenser bank, the tube was moved to a larger bank of 100 μf capacity. To reduce electrode and insulator damage, a damping-type crowbar was built which diverted part of the bank energy after the current peak. This made the screen electrode usable at higher plasma temperatures than before, but not at neutron-producing levels. Because it was considered important to observe the pinch at these high powers, other viewing methods were tried.

The simplest method, suggested by William R. Baker, was merely to omit the screen--the cover glass then became the central part of the anode. A good view was obtained at early times but slight irregularities were induced in the plasma shape. As the current rose there was the further difficulty that sparking occurred between the edge of the glass and its metal boundary, obscuring the view. When the pyrex window was replaced by quartz the sparking started at lower currents, presumably because of the higher resistivity under the operating conditions. With some design changes and experimentation these problems could probably be solved. The idea of a transparent anode would then appear to be useful in other applications as well.

A second method of viewing was through a pair of crossed slits in the anode. Of course, less information was obtained and, furthermore, sparking occurred across the slits at high power levels. This may have been caused by slight asymmetries in the current distribution. (In the Triax, the current never becomes so concentrated, and no sparking has been observed in the streak slit used there.)

The best compromise proved to be a 1/32-in. -thick copper electrode in which 0.025-in. holes were drilled, forming a grid with 2.5-mm spacing. There was no sparking problem, and a reasonably good measure of the plasma dynamics was obtained at neutron-producing levels.

It was determined that neutrons first appear when the edges of the plasma sheet collide. Meanwhile there have been several bounces in the thin direction, and the plasma has been preheated to perhaps 50 ev. (The central region is comparatively dark; only the edges appear in the photographs.) The relative velocity of the edges was 2×10^7 cm/sec for a bank voltage of 15 kv and initial pressure of 0.2 mm Hg. Their relative energy is 400 ev, which suggests the possibility that the neutrons may be thermonuclear in origin.

The neutron burst, as expected, was indeed longer in duration than with the small bank. Reactions started 1.5 μsec after the beginning of the discharge and the rate remained roughly constant until around the 3.0-μsec point. The fall-off was not caused by the current passing its peak, and might occur later in a tube of cleaner design. Still, the confinement time seems promising for a deuteron density in the range 10^{17} to 10^{18} per cm^3.

Discussion

Originally, the ribbon pinch tube was intended to provide a means for studying a completely flat sheet plasma. This would allow comparison with some of the theoretical work that has been done for the one-dimensional case.[6,7,8] The time available for measurements would depend on the motion of the edges and would be roughly proportional to the width of the tube. Although it was not possible to obtain a ceramic box as wide as would have been liked, at least the size obtained (1.5×7.5 in.) made high magnetic fields easy to produce.

Early in the course of the experiments, interest turned from the central region to the edges of the sheet. Part of this new interest arose from the discovery by Harold P. Furth of what he called the rip instability.[9] Since the edges of the sheet pinch resemble a fully developed rip, the study of their behavior is useful when considering any applications of such rips, for example, Furth's proposed method of plasma acceleration.[10]

As indicated by the Kerr-cell photographs and the neutron studies, the ribbon pinch with colliding edges is also of intrinsic interest. Its advantage over an ordinary unstabilized pinch is that high velocities and compression ratios are easily obtained on the first edge-compression cycle before any instabilities have developed. The flat shape apparently stabilizes not only the central region, but also the edges because the magnetic lines have to go around the long way. Yet the magnetic field at the edges is much higher than the average, and this accounts for the high velocities observed.

Because of its reasonably reproducible behavior and the ease of attaining high temperature, the ribbon pinch ought to be useful as a plasma-generating device. For example, if a suitable opening were provided in the top electrode, hot plasma would be ejected. This might be captured in another system, or sent through a MHD power generator or allowed to produce thrust. The time of good behavior indicated by the length of the neutron burst is long enough to allow a good fraction of the plasma to be expelled. This would be facilitated if the edge walls were suitably tilted. The parallel main walls would stabilize the plasma while the tilted edge walls induced axial motion in the manner of the conical pinch.[11] It seems reasonable, at least, that the advantages of the ribbon-pinch principle would carry over into this type of operation.

---

[6] O. Buneman, in Proceedings of the Symposium on Electrodynamics and Fluid Mechanics of Gaseous Plasma (Polytechnic Press, New York, 1961).

[7] Nicholas N. Krall and M. N. Rosenbluth, Stability of a Slightly Inhomogeneous Plasma, GA-1417, July 1960.

[8] H. Grad, The Boundary Layer between a Plasma and a Magnetic Field, NYO-9491, December 1960.

[9] Harold P. Furth and John Killeen, in Controlled Thermonuclear Research Quarterly Report, UCRL-9777, August 1961, p. 91.

[10] H. P. Furth, An Instability-Type Plasma Accelerator, UCRL-6118-T, August 1960.

[11] Stirling A. Colgate, in Controlled Thermonuclear Research Quarterly Report, UCRL-9002, December 1959, p. 64.

7. DISSOCIATION BY MAGNETIC FIELDS

Selig N. Kaplan, George A. Paulikas, Robert V. Pyle,
Henry F. Rugge, and J. Warren Stearns

Dissociation of H_2^+

Work has continued on the dissociation of H_2^+ ions in a magnetic field. The percentage dissociation depends on the populations of the various vibrational states, the strength of the magnetic field, and the time that the ion spends in the magnetic field. The populations of the vibrational levels vary with the manner of production, e.g., the H_2^+ ions that emerge from the Hilac high-voltage PIG ion source are not appreciably dissociated in our experiments at equivalent electric fields up to about 10^6 v/cm. The development of a possible injection technique for thermonuclear diffusion devices will therefore require considerable experimentation with kinds of sources and source parameters. We have been interested in investigating the dissociation of a reproducible population distribution by very high equivalent electric fields, and work with a H_2^+ beam obtained by passing a H_3^+ beam through a Hg vapor stripper in the Berkeley heavy-ion linear accelerator. The resulting H_2^+ current is about 1/10 as large as the H_2^+ beam obtained directly from the ion source. The reaction $H_2^+ \rightarrow H^+ + H^0$ is measured.

Some results obtained with constant magnetic fields up to about 18 kilogauss have been reported previously[1] (at the maximum Hilac energy of 10 Mev/nucleon, a magnetic field of 10 kgauss is equivalent to an electric field of 4.4×10^5 v/cm). Higher magnetic fields were obtained with a pulsed magnet[2] powered by an electrolytic condenser bank capable of giving a maximum field of 100 kgauss. The coil was potted in epoxy resin and mounted in a vacuum chamber. The magnetic field was crowbarred at its maximum value (quarter-cycle time = 500 μsec) and the beam was introduced in a 50-μsec-wide pulse.

Data were recorded with nuclear emulsions and are still being reduced; at 75 kgauss the percentage dissociation is 2.0 ± 0.2%. The dissociation mechanism is a barrier-penetration problem, the threshold field changing by a factor of less than 2 for a 10^6 change in decay time.[3] In Fig. IV-16 are shown the data that have been reduced to date and the threshold fields obtained from Ref. 3. The thresholds shown are for J = 0; different rotational states have different thresholds. As the unreduced data are filled in it should be possible to examine the populations of the various vibrational and rotational levels. Further measurements with the magnet in its present modified form should allow us to reach the $v = 14$ ($B \approx 150$ kgauss), $J = 0$ state.

---

[1] S. N. Kaplan, G. A. Paulikas, and R. V. Pyle, Phys. Rev. Letters 7, 511 (1961).

[2] We are grateful to Harold P. Furth for lending us the basic coil assembly.

[3] John R. Hiskes, Electric and Magnetic Dissociation of Molecular Ions and Neutral Atoms, UCRL-6372, June 1961.

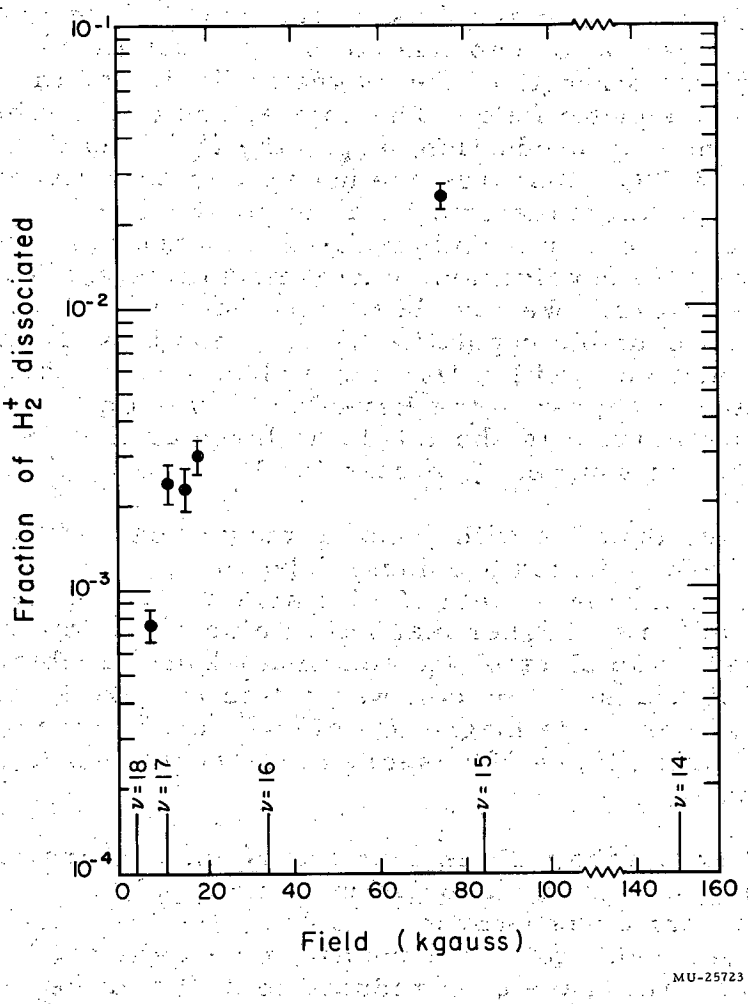

Fig. IV-16. Fraction of H_2^+ dissociated in ~ 10^{-9} sec vs the magnetic field.

Dissociation of D^-

Because so many possible excited states can be involved in the dissociation of D_2^+, we are investigating the magnetic dissociation of D^- as a check on both the experimental technique and the threshold calculations. The negative hydrogen ion has a single fairly sharply defined threshold that should allow an unambiguous measurement. This problem has been of interest to accelerator designers concerned with the acceleration and transfer of beams to storage rings, and the threshold for the reaction $H \rightarrow H^0 + e^-$ due to $e\vec{v} \times \vec{B}$ forces was estimated by Khuri in 1956.[4] First estimates of the equivalent electric field necessary to produce ionization in our experimental time of about 10^{-9} sec were extrapolated from Khuri and gave about 7×10^5 v/cm. We therefore looked for this process with the steady-state magnetic field apparatus described in Ref. 1, and 20 Mev D^- from the Hilac. No dissociation was observed and the experiment was repeated with the pulsed magnet at fields up to 75 kg. ($E_{max} \approx 3.3 \times 10^6$ v/cm). Again no dissociation was observed.

Recently, Hiskes has recalculated the threshold for our particular case, using somewhat different approximations, and is in the process of making an exact calculation.[5] Present theoretical estimates are that the threshold is somewhat greater than 3×10^6 v/cm. We have partially analyzed emulsion data up to equivalent fields of 4.5×10^6 v/cm and will repeat the experiment at higher magnetic fields if necessary.

8. ION-DENSITY MEASUREMENTS IN A HOLLOW-CATHODE DISCHARGE

Robert V. Pyle, Henry F. Rugge, and J. Warren Stearns

As was mentioned in the preceding report (UCRL-9777), we are attempting to obtain measurements of the ion-density distribution in a highly ionized gas by the attenuation of visible, nearly resonant radiation. This work is done in cooperation with members of the UC Physics Department Optical Pumping Group. We have been able to obtain absorption curves with good signal-to-noise ratio (including complete absorption) and are attempting to unfold the ion-temperature distribution. Satisfactory ion temperature measurements have not yet been made, but density and electron temperature measurements made with Langmuir probes are rather interesting in themselves.

---

[4] N. N. Khuri, Dissociation of H^- ions by the $e\vec{v} \times \vec{B}$ Force, Palmer Physical Laboratory Report KNK-1, June 1956.

[5] John R. Hiskes (Lawrence Radiation Laboratory), private communication.

The apparatus is shown schematically in Fig. IV-17. Strontium is used to make the highly ionized plasma, chiefly for reasons concerned with the optical absorption measurements, but it also has the advantage of being rapidly pumped at the walls. The strontium oven is shown in Fig. IV-18. To establish the strontium plasma a longitudinal field of a kilogauss or so is established and argon is introduced through the oven. An arc of about 20 amp is struck through the hollow cathode, raising the snout to about 2100 °C. The oven is then heated to about 800 °C by electron bombardment to provide a suitable strontium vapor pressure; following this, the argon flow can be turned off if desired.

To provide a known geometry for density-distribution measurements, the central arc passes through 1-cm-radius holes in aluminum baffles 30 cm apart, the baffles being intimately connected to the 20-cm-diam aluminum vacuum chamber, except for pumping apertures near the wall. The plasma column usually runs within a volt or so of anode potential, consequently when the anode and the vacuum tank are tied together the diffusion region is approximately free of externally generated electric fields. The central core of fast electrons (about 40 ev) is 3 mm in diameter. A cylindrical, quartz-shielded Langmuir probe is introduced radically at the midplane.

Typical electron temperature measurements are shown in Fig. IV-19 for argon gas at 2 μ pressure. The apparent temperature drops rapidly outside the core and rises near the wall, sometimes more dramatically and at a smaller radius than is shown in Fig. IV-19. Ecker has obtained qualitatively similar results for the case of diffusion of a fully ionized, infinitely long column, with plasma production along the axis.[1] It is not obvious whether a similar phenomenon could occur in these moderately ionized cases. The probe curves are clean, but some 2 to 100 kc small-amplitude ripple can be detected on the probes.

Densities obtained from saturated ion currents are given in Fig. IV-20. The theoretical curves are for "Simon diffusion,"[2] and are normalized to the experimental curves at a radius of 2.8 cm. The slopes of the curves at intermediate radii agree with $1/B^2$ classical diffusion.

When Sr is introduced at a rate that is sufficient to give optical absorption and a reduction in the discharge voltage, curves very similar to those shown in Figs. IV-19 and IV-20 are obtained. If the argon is turned off, the voltage rises by a factor of 3 or 4 and very-large-amplitude rf is often generated. This is true even when the flow of strontium through the hollow cathode is large, suggesting that some production of plasma along the discharge axis (i.e., external to the hollow cathode) is necessary for quiet operation. The same effect is observed for pure argon at low pressures.

Density and temperature measurements for pure Sr are not complete. With B = 3200 gauss and a neutral density of 5×10^{11}/cc, the radial density distribution is similar to that shown in Fig. IV-20, i.e., falls off with radius much more rapidly than would be true for a long, fully ionized column. Further measurements, including axial distributions, are in progress.

---

[1] Günter Ecker, Theory of a Fully Ionized Column with External Particle Production, UCRL-9988 (in preparation).

[2] A. Simon, An Introduction to Thermonuclear Research (Pergamon Press, New York, 1959), Chapt IX.

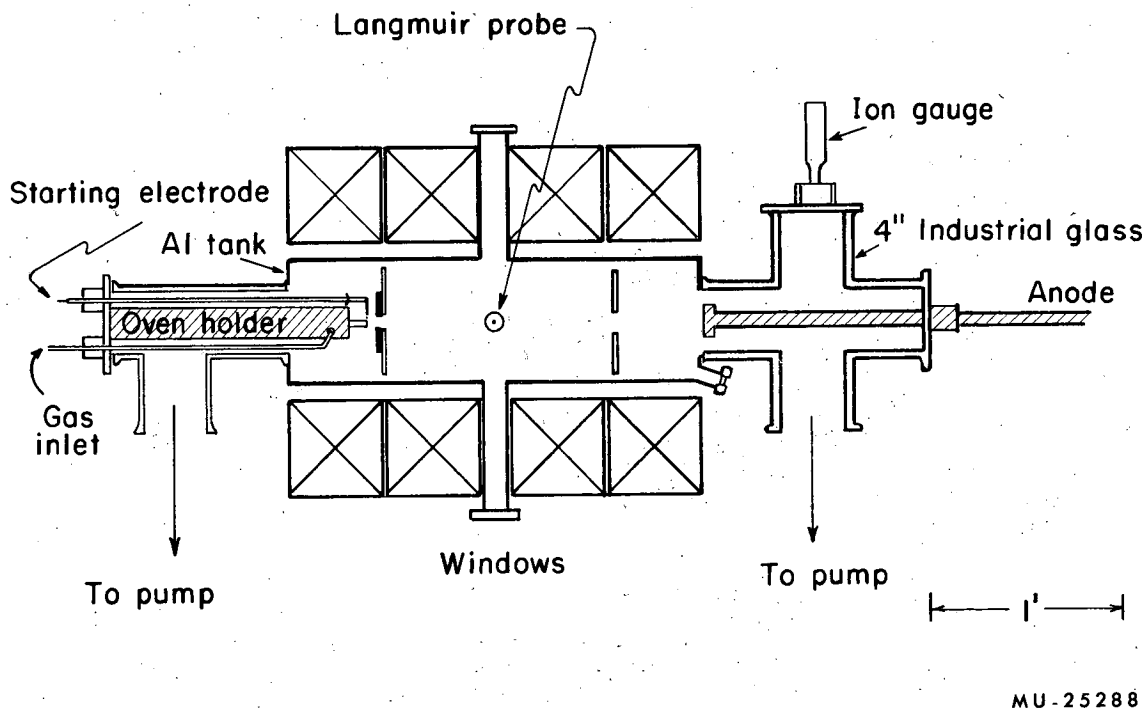

Fig. IV-17. Schematic of the hollow-cathode strontium plasma device.

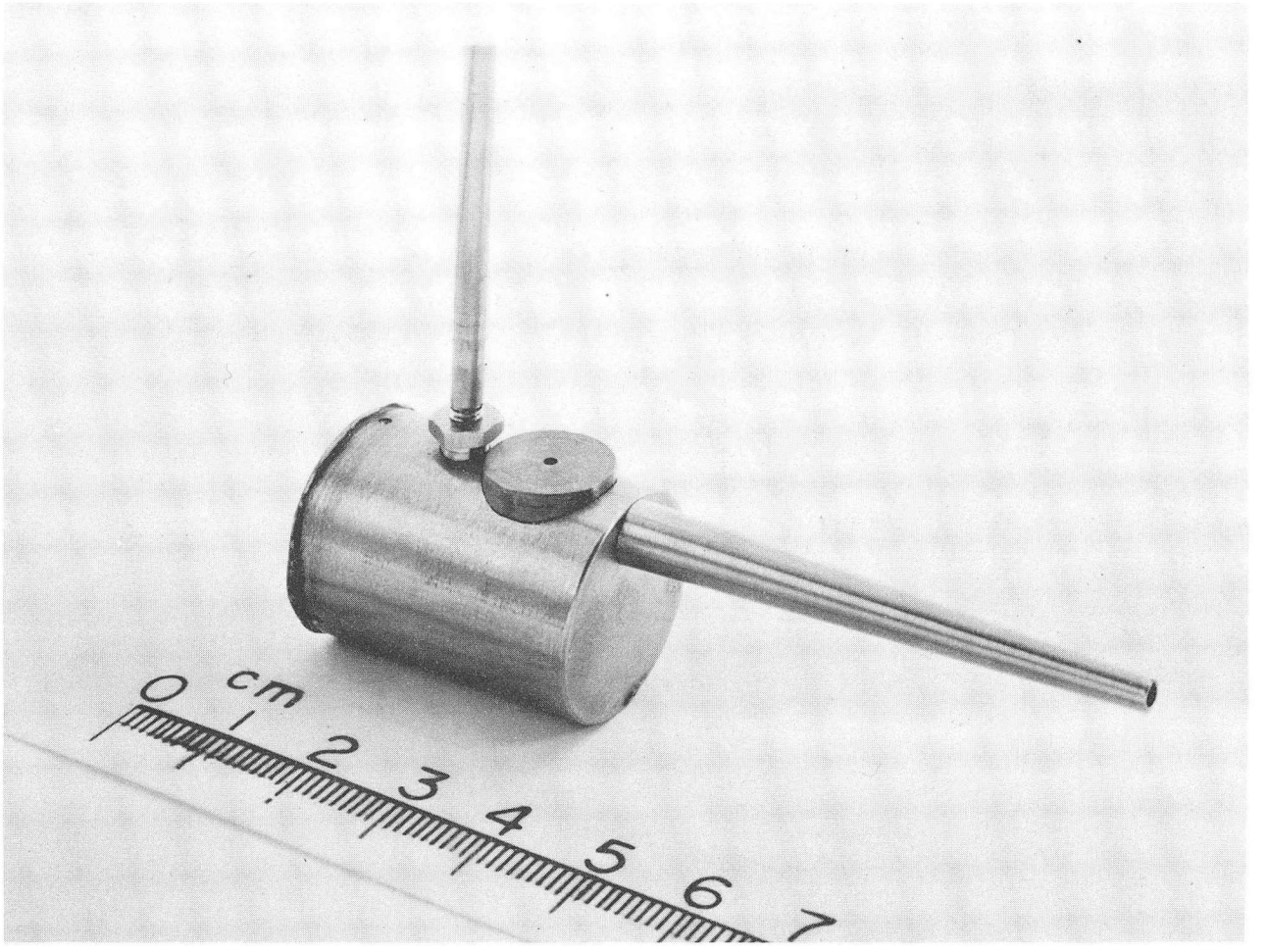

ZN-3013

Fig. IV-18. Stainless steel strontium oven. Gas inlet at top. Tantalum hollow cathode at right.

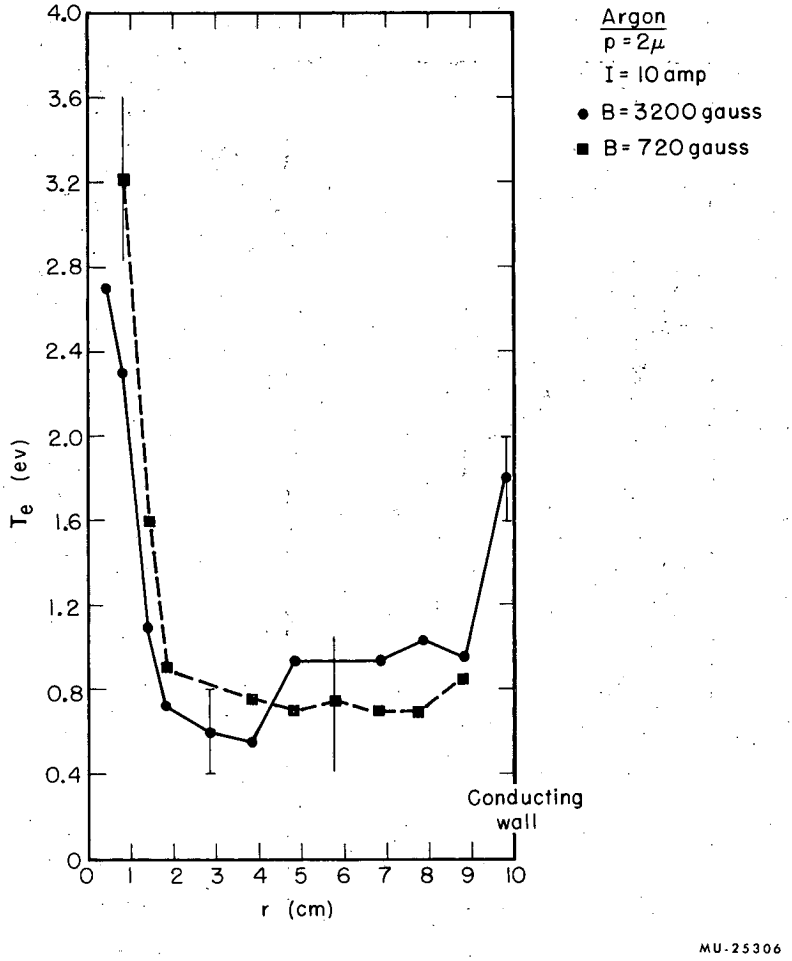

Fig. IV-19. Apparent electron temperature vs radius for argon at 2 μ pressure. I = 10 amp, B = 3200 gauss, B = 720 gauss.

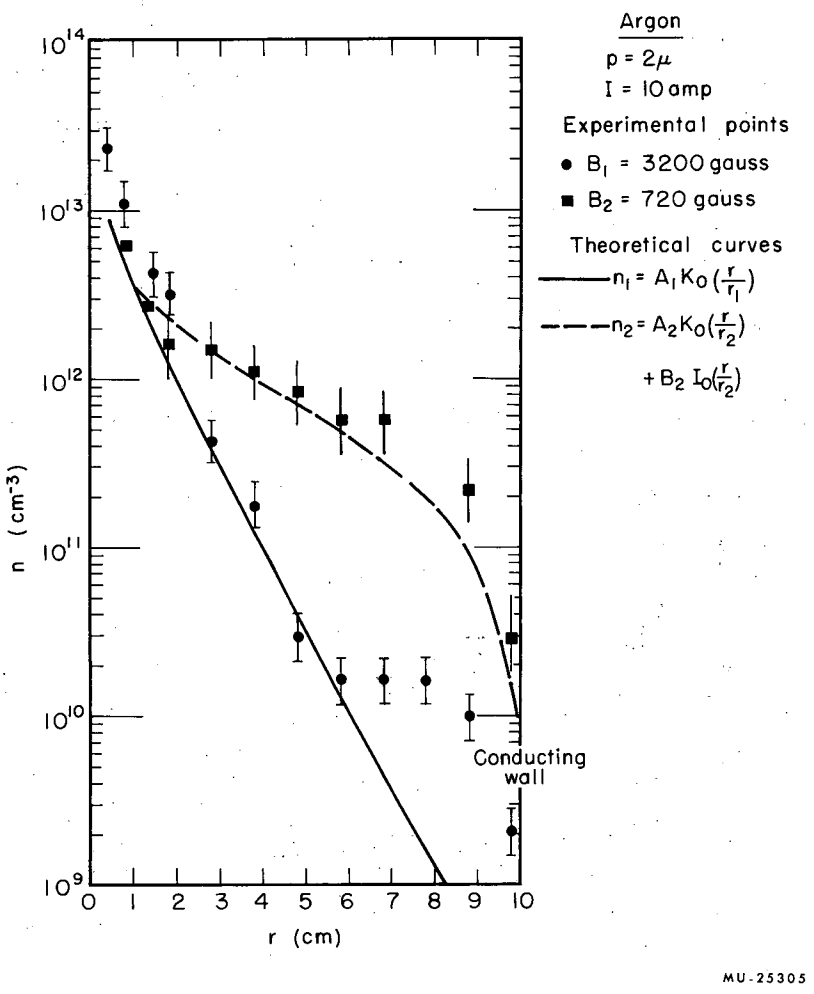

Fig. IV-20. Ion density vs radius for argon at 2 μ pressure. I = 10 amp, B = 3200 gauss, B = 720 gauss. The theoretical curves are $n = AK_0(r/r_1) + BI_0(r/r_1)$, normalized at 2.8 cm radius.

9. INSTABILITY OF AN ALTERNATING-CURRENT POSITIVE COLUMN IN A MAGNETIC FIELD

Robert V. Pyle, Henry F. Rugge, and J. Warren Stearns

We previously have argued in a qualitative way that the macroscopic instability of a positive-column discharge in a longitudinal magnetic field (e-folding times of the order of 10^{-4} sec) should be reduced or suppressed if the discharge current alternates at a sufficiently high frequency. The experimental technique for demonstrating this is the same as in the original positive-column measurements: The rms current through a long discharge tube is held constant as the axial magnetic field is varied. The axial electric field (measured with probes near the wall) is then a measure of the wall losses and should decrease with increasing magnetic field until an instability occurs, at which point the losses to the wall increase.

The apparatus is shown in Fig. IV-21. Hot filaments at each end of the 5.5-cm-diam discharge tube serve alternately as cathodes and anodes. (If one electrode is cold, the instability occurs in much the same way as in the dc case.) Alternating currents up to 500 ma peak and up to 55 kc are supplied from a large audio oscillator. The variation of axial electric field with axial magnetic field is obtained with an x-y recorder.

Experimental E_z-vs-B_z curves for discharges in He at frequencies of 0, 12, and 50 kc are given in Figs. IV-22 and IV-23. The pressure in Fig. IV-22, 0.12 mm Hg, is below the Simon limit for ambipolar diffusion for magnetic fields less than approx 1000 gauss.

According to the Simon criterion, the diffusion at a pressure of 0.50 mm Hg (Fig. IV-23) should be ambipolar for magnetic fields less than about 4000 gauss. Both figures demonstrate that the growth of instabilities is indeed reduced by raising the frequency of the discharge current. In Fig. IV-24 we show the dependence of B_c, the critical magnetic field at which losses increase, on the pressure for three discharge frequencies.

Further measurements, including streak-camera photographs and noise spectra, are being made; the theoretical aspects of the problem are being investigated by Günter Ecker.

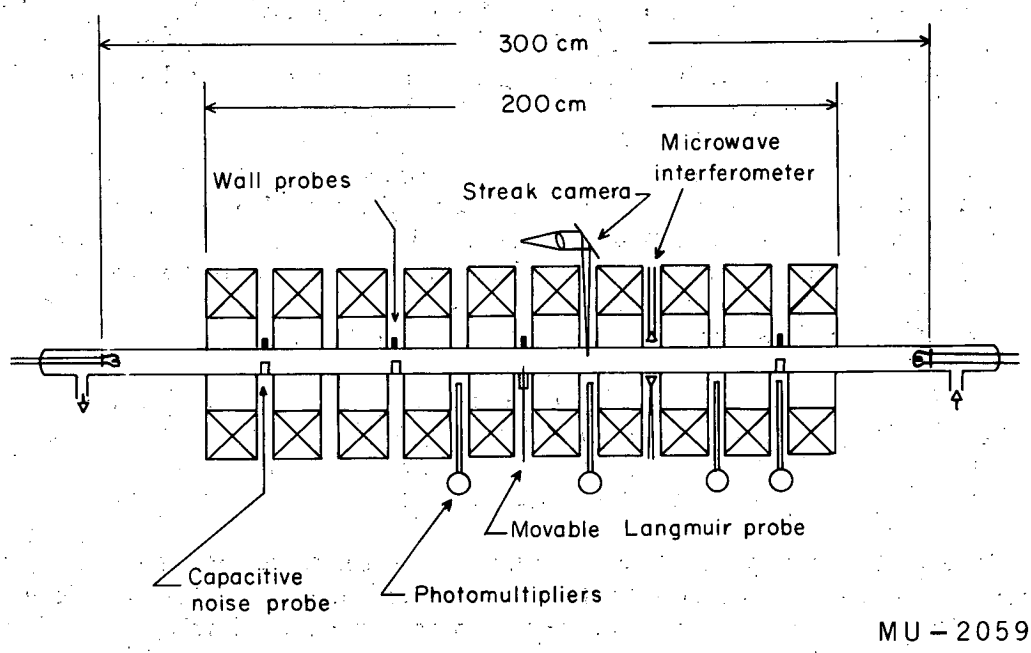

Fig. IV-21. The experimental arrangement.

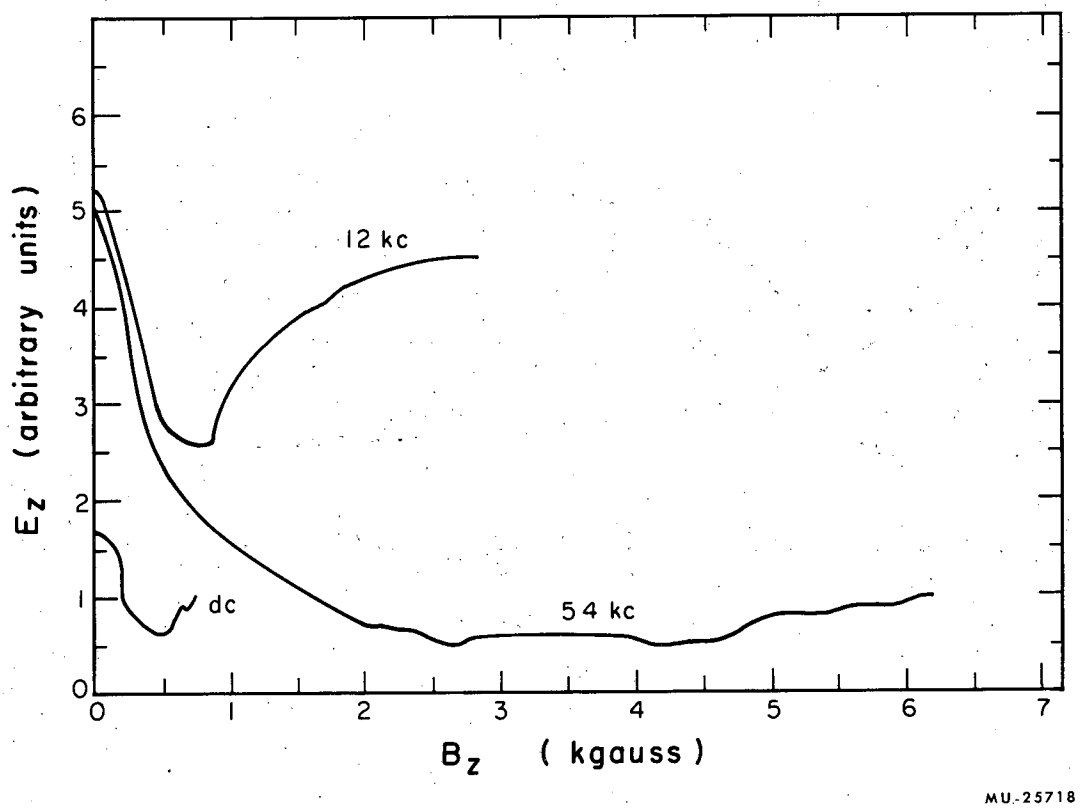

Fig. IV-22. E_z vs B_z in He at p = 0.12 mm Hg.

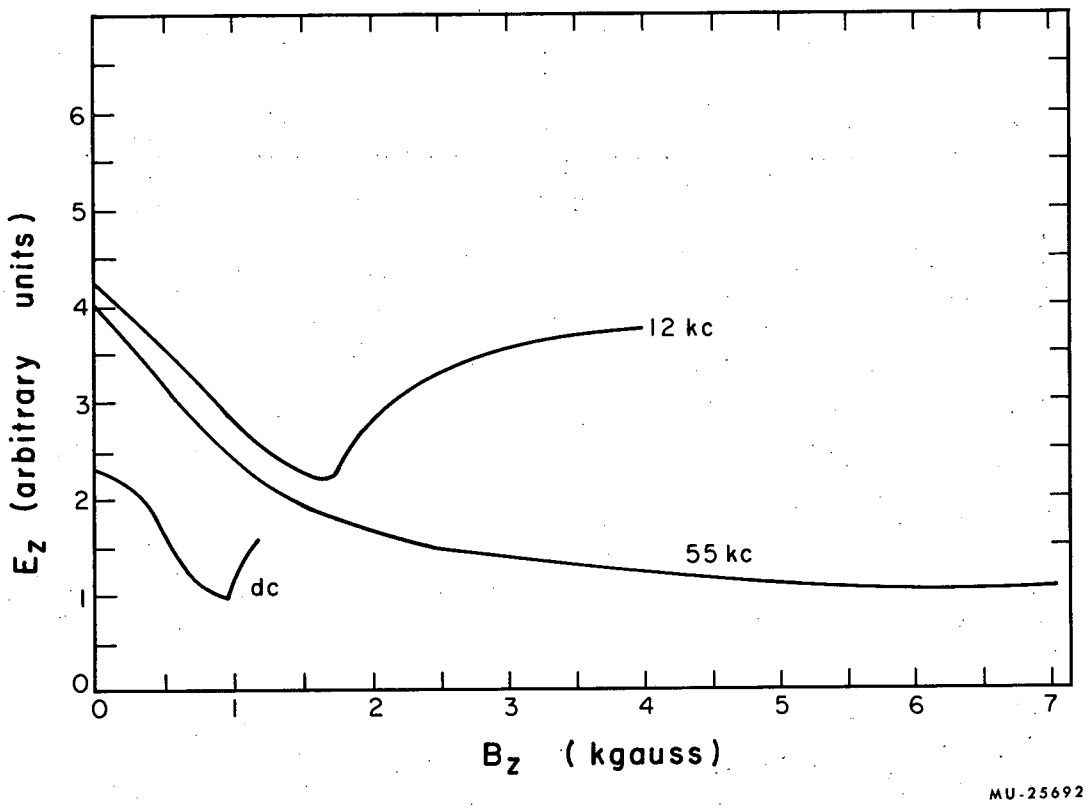

Fig. IV-23. E_z vs B_z in He at p = 0.50 mm Hg.

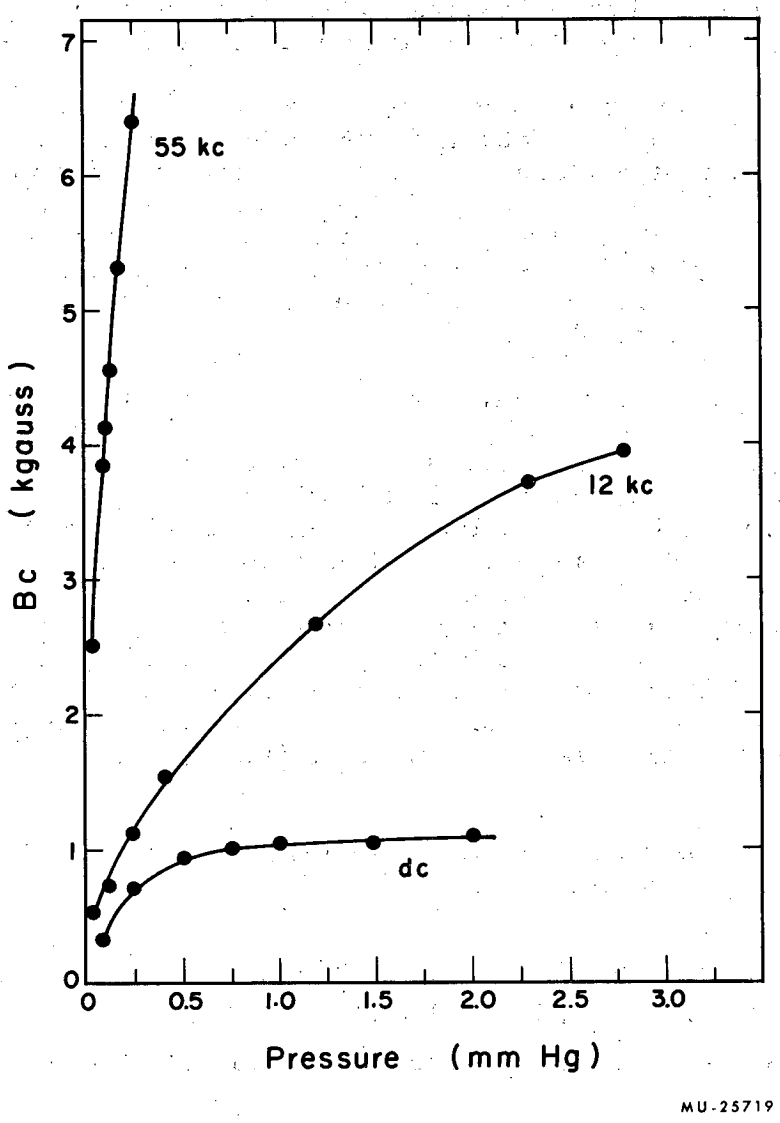

Fig. IV-24. B_c vs pressure of He at 0, 12, and 55 kc/sec. The solid lines are not theoretical curves.

10. THEORY OF THE FULLY IONIZED PLASMA COLUMN WITH EXTERNAL PARTICLE PRODUCTION. I

Günter Ecker

The mechanism of the self-sustained positive column[1, 2] with internal particle production in the plasma volume inherently requires high electron temperatures and with them an external electric field. The difficulties introduced by such an external field have been discussed elsewhere.[3, 4]

In the recent past, therefore, experiments have been proposed and carried out which produce the charge carriers outside the actual plasma column. This can be done, e.g., by contact ionization of atoms at a metal surface (Cs at W),[5, 6, 7] or by ionization in a hollow cathode.[8, 9] The carriers are introduced axially into the center of a column which lies in a longitudinal magnetic field. Here they form an electron ion ensemble of given temperature and density, and diffuse across the magnetic field towards the wall, where they recombine.

To describe this process we consider theoretically the following model.

The plasma volume is limited by two infinite coaxial cylinders of radius r_0 and R respectively, lying in a longitudinal magnetic field, B. Within the smaller cylinder of radius r_0 we have an electron ion ensemble of temperature T_0. This is the external particle source. It provides a radial electron ion current of density. The electrons and ions entering from the core move across the magnetic field under the influence of mutual collisions and the radial electric field. As we neglect volume recombination all particles recombine at the insulated wall, R. We assume that the effective mean free path of the electrons and ions is much smaller than the extension of the discharge vessel, 2R, and that the concept of quasi-neutrality is applicable.

In the second part (II) the calculations will be extended to include end effects and volume recombination.

---

[1] W. Schottky, Physik. Z. 25, 342, 625 (1924).

[2] E. Spenke, Z. Physik. 127, 221 (1950).

[3] B. B. Kadomtsev and A. V. Nedospasov, J. Nuclear Energy, Part C, 1, 230 (1961).

[4] F. C. Hoh and B. Lehnert, Phys. Rev. Letters 7, 3 (1961).

[5] R. C. Knechtli and J. Y. Wada, in Proceedings Fifth International Conference on Ionization Phenomena in Gases, Munich, 1961.

[6] N. Ryn and N. D'Angelo, Rev. Sci. Instr. 31, 1326 (1960).

[7] R. B. Hall and G. Bekefi, Research Laboratory of Electronics, M.I.T., Quarterly Progress Report 55, 16 (1959); 56, 20 (1960).

[8] C. Michelson and D. J. Rose, Bull. Am. Phys. Soc. II, 6, 385 (1961).

[9] S. D. Rothleder and D. J. Rose, 14th Annual Gaseous Electronics Conference, Oct. 1961, E-5.

The Basic Equations

It was first attempted to solve this problem by calculating from the Boltzmann fundamental equation the complete distribution function in phase space. The attempt used an expansion in special Laguerre polynomials. One arrives at an infinite set of linear equations for the expansion coefficients. An approximate solution of these equations gives the coefficients in the form of determinants which include heavy integral expressions. This general solution therefore has the disadvantage of being practically unintelligible. Consequently we found the magnetohydrodynamic approach more appropriate.

These transport equations for the mass, momentum, and energy read

$$\frac{\partial n_\pm}{\partial t} + \vec{\nabla} \cdot (\vec{v}_{d_\pm} n_\pm) = \alpha_n, \tag{1}$$

$$\pm \vec{B} \times \vec{\Gamma}_\pm + \frac{\Gamma_\pm}{\mu_\pm} + e \eta n_\pm (\vec{\Gamma}_\pm - \vec{\Gamma}_\mp) = \pm n_\pm \vec{X} - \vec{\nabla} \left(\frac{\overleftrightarrow{P}_\pm}{e} \right) \tag{2}$$

$$\vec{\nabla} \left\langle n \vec{v} v^2 \right\rangle_\pm \mp \frac{2 n_\pm \cdot e \cdot v_{d_\pm}}{m_\pm} X =$$

$$\sum_i \frac{2 n_\pm \nu_{\pm i}}{m_i + m_\pm} (m_i v_i^2 - m_\pm v_\pm^2) - \sum_{i,x} \frac{2 e n_\pm \nu_{\pm x} V_{ix}}{m_\pm}, \tag{3}$$

where we have used the following notations:
X = electric field, n = particle density, $\vec{\Gamma}$ = particle current density, $\vec{v}_d$ = drift velocity, μ = mobility due to neutral particle collisions, $\overleftrightarrow{P}$ = pressure tensor, $\vec{v}$ = velocity, $\vec{B}$ = magnetic field, e = elementary charge, m = particle mass, α_n = net particle production per second and unit volume, η = electron-ion interaction parameter. The hexagonal brackets indicate averages over the velocity space. The indexes +, - refer to ions and electrons respectively.

Equations (1) - (3) are simplified considerably by the lack of a neutral gas component and the concept of quasi-neutrality, which means

$$\mu_+, \mu_- \to \infty, \tag{4}$$

$$n_+ \approx n_- = n. \tag{5}$$

But even with Eqs. (4) and (5) the general problem is still complex, mainly owing to the radial temperature variation. Under the assumption that the energy loss due to ion excitation and ionization is small, only the sum of the electron and ion temperature across the discharge is constant ($T_- + T_+ = 2T_0$). This follows readily from Eqs. (1) - (3).

From Eqs. (1) - (3) we derive the following two simultaneous differential equations:

$$\frac{d}{dx}\, z^2 = -C_1\, \frac{(1 - y/z)^{3/2}}{x}\,, \tag{6}$$

$$C_2(1-y) = \frac{1}{2}\, \frac{dz}{dx} \left\{ -\frac{dy}{dx} + 2g(y)\, \frac{1}{2}\, \frac{dz}{dx} \right\}, \tag{7}$$

where we have used the abbreviations

$$z = n/n(0), \quad y = T_+/T_0, \quad x = r/R, \tag{8}$$

$$\mathcal{A} = \frac{\mu_+(T_0)}{\mu_-(T_0)}\,, \quad g(y) = y\, \frac{1 - \mathcal{A}\left(\frac{2-y}{y}\right)^{3/2}}{1 + \mathcal{A}\left(\frac{2-y}{y}\right)^{1/2}}\,, \tag{9}$$

and where the constants C_1 and C_2 are defined by

$$C_1 = \frac{2^{3/2}\, \Gamma_0\, r_0\, B^2}{k\, T_0\, \eta_0\, n_0^2}\,; \qquad C_2 = \frac{6\, e^2\, B^2\, R^2}{k T_0\, (m_+ + m_-)}\,. \tag{10}$$

In addition to these differential equations the boundary conditions[10]

$$\begin{aligned} &x = x_0 \rightarrow y = 1\,; \quad z = 1, \\ &y = 1 \rightarrow z = \frac{4 x_0 \Gamma_0}{n_0} \left(\frac{m_+}{3\, k\, T_0\, y}\right)^{1/2} \end{aligned} \tag{11}$$

must be satisfied.

Similarity Law

Obviously the coefficients of the differential equations (6), (7) and the boundary conditions (11) include the experimental parameters of our problem only in the combinations

$$\frac{\Gamma_0 r_0}{T_0^{5/2}}\,; \quad \frac{B^2}{T_0} \cdot \frac{R^2}{m_+}\,; \quad \frac{n_0}{T_0^2}\, \frac{R}{\sqrt{m_+}}\,. \tag{12}$$

[10] G. Ecker, Proc. Phys. Soc. (London) B 67, 485 (1954).

Similar discharges are defined to have identical relative parameter values--density, temperature, etc. --at homolog points. This is true if the quantities (12) have the same values. It follows that we have similar discharges for

$$R \propto \sqrt{m_+} \; ; \qquad \Gamma_0 \propto 1/r_0 \, . \tag{13}$$

If discharges are to be similar then the variation of one of the experimental parameters prescribes the variations of all the other parameters, as shown in the following scheme.

	T_0	B	$R/\sqrt{m_+}$	$\Gamma_0 r_0$
$T_0 \rightarrow$	$\propto T_0$	$\propto T_0^{-3/2}$	$\propto T_0^{2}$	$\propto T_0^{5/2}$
$B \rightarrow$	$\propto B^{-2/3}$	$\propto B$	$\propto B^{-4/3}$	$\propto B^{-5/3}$
$R/\sqrt{m_+} \rightarrow$	$\propto (R/\sqrt{m_+})^{1/2}$	$\propto (R/\sqrt{m_+})^{-3/4}$	$\propto (R/\sqrt{m_+})$	$\propto (R/\sqrt{m_+})^{5/4}$
$\Gamma_0 r_0 \rightarrow$	$\propto (\Gamma_0 r_0)^{2/5}$	$\propto (\Gamma_0 r_0)^{-3/5}$	$\propto (\Gamma_0 r_0)^{-4/5}$	$\propto \Gamma_0 r_0$

Results

Equations (6) and (7) do not allow an analytic solution. Machine solutions are complicated by the fact that we are dealing with a boundary value problem. However, this difficulty can be evaded by transforming the problem into an initial-value problem, making use of the variability of the expermental parameters.

The solutions use the parameters

$$p_1 = \frac{\Gamma_0 r_0}{T_0^{5/2}} \; ; \qquad p_2 = \frac{(BR)^2}{T_0} \, . \tag{14}$$

Figures IV-25 and IV-26 show some typical results obtained for the distributions of radial density z and temperature y.

Discussion

The features shown in Fig. IV-25 may be qualitatively understood simply from the mass-conservation law, which requires that the radial particle current should be constant across the plasma volume, and from the fact that the effective diffusion coefficient varies in proportion to the particle density in this situation.

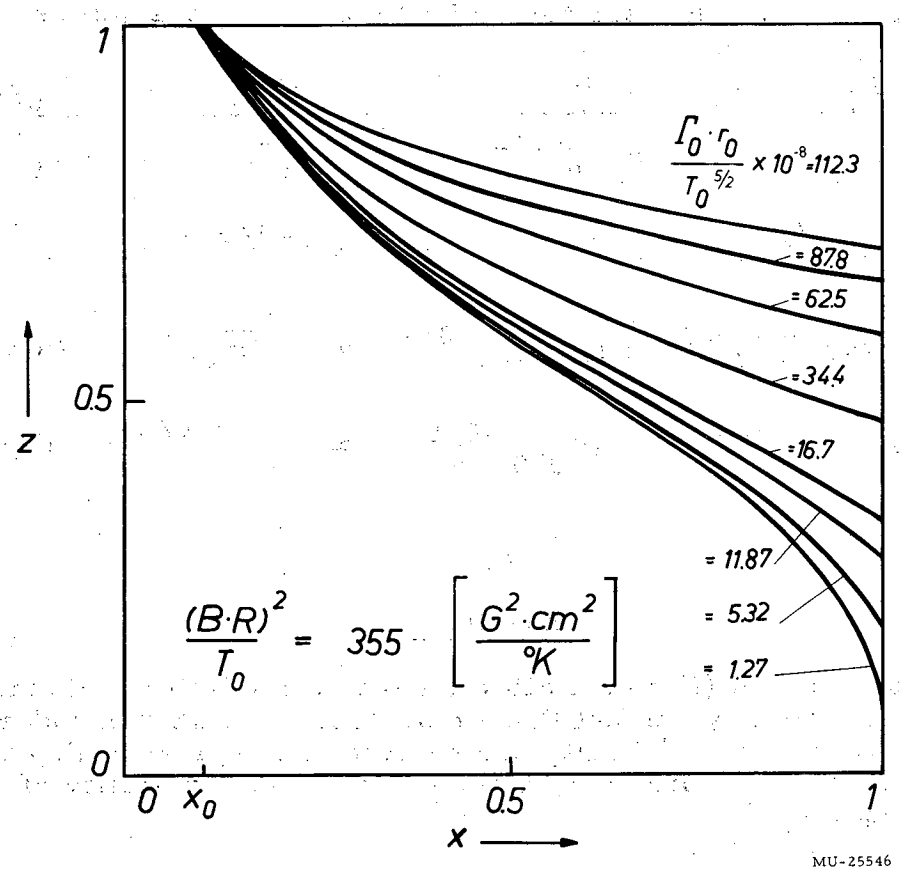

Fig. IV-25. Radial density distributions (z) for a constant parameter value p_2 and various values of p_1.

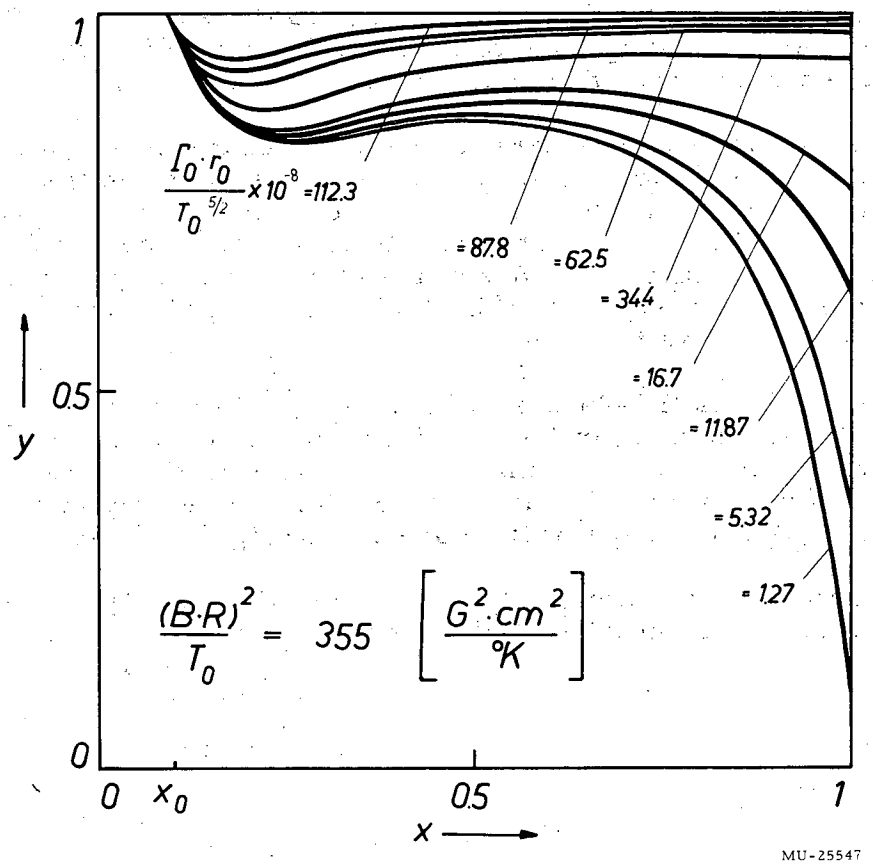

Fig. IV-26. Radial temperature distributions (y) for a constant parameter value p_2 and various values of p_1. (See Eqs. 11 and 14.) Remembering $T_-/T_0 = (2 - y)$, one may take the electron temperature variation from this figure.

For a constant diffusion coefficient we would expect a decrease of $|dz/dx|$ towards the wall proportional to $1/r$. However, owing to the decrease in the particle density near the wall, an increase in $|dz/dx|$ is to be expected.

The temperature variation shown in Fig. IV-26 can be qualitatively understood by remembering that two processes govern the change in temperature. There is the collective interaction of the particles of the fully ionized column via the space and wall charge (ambipolar field). This interaction takes energy from the ions and gives it to the electrons. The other process--the energy exchange due to individual particle interactions--tends to decrease the temperature difference between ions and electrons.

At the edge of the core where the two temperatures are identical only the ambipolar field is in action, which causes a decrease in the ion temperature. This increase in the temperature difference brings the individual energy exchange of the unlike particles into play. It causes an increase in dy/dx. Remembering that this individual exchange varies in proportion to the particle density, we expect dy/dx to decrease again in the regions of low particle density close to the wall.

Figures IV-25 and IV-26 are to be considered only as an example. They do not demonstrate the influence of the magnetic field. Information about this can be taken from calculations for different parameter values p_2. The solution of Eqs. (6) and (7) further provides the density value $n_0(R, B, r_0, \Gamma_0, T_0)$ at the edge of the core as the eigenvalue of the problem.

This eigenvalue n_0 and the dependence of the density and temperature distributions on the parameter p_2 will be communicated in the final report.

11. ION MAGNETRON

Robert W. Layman

Although this report is primarily concerned with an experiment designed to test the practicability of cutting off neutral flux entering the circulating-ion region from the outside, a preliminary discussion of anode alignment and porous anodes is necessary. Any system that reduces or cuts off the inward neutral flux requires a method of neutral injection inside the sheath. [1] In the experiment described herein, neutral particles are injected through a porous anode. Further, because of inherent problems with porous anodes, anode alignment becomes increasingly important. Therefore this report consists of three parts: anode alignment, porous anodes, and finally the neutral-cutoff experiment.

Anode Alignment

Absolute anode alignment--that is, coincidence of the anode axis and the magnetic field axis--is not possible with the present apparatus because of the ratio of its length to diameter combined with the fact that it is horizontal. Since the sheath lies in the center 30% of the machine length, and it is in the sheath region where alignment is important, reasonably good alignment can be obtained by bending the anode up in the center to counteract the sag due to gravity and then adjusting the vertical position of the anode axis to the proper height. Aside from the physical problem of anode alignment there is a second problem, that of determining the degree of alignment. This is solved through visual observations of the discharge under different conditions of magnetic field and anode voltage. Methods of alignment and of determining alignment have been continually improved, and it is believed the best possible alignment for a horizontal machine of the present dimensions has been obtained.

The final alignment brought about an unexpected change in the neutron-producing characteristics of the machine. All previous experience had shown neutron output to increase monotonically with high voltage, with neutrons first appearing in easily countable quantities at around 10 kv. Figure IV-27, a comparison of neutron output with the new optimum alignment and with alignment that was previously considered the best possible, demonstrates this change. With better alignment neutrons appear in larger quantities at lower voltages, increasing with voltage up to 10 or 11 kv, where there is a sudden drop in counting rate. After the drop, the counting rate again increases with increasing high voltage, only now the increase in counting rate with voltage is not as fast as below 10 kv.

As unexpected as the effects described above are, an equally surprising effect (considering past experience) of increased magnetic-mirror ratio on neutron production was found. Maximum counting rates versus magnetic-mirror ratio have always been found at a ratio of 1.02; however, with improved alignment the counting rate increases with increased mirror ratio as shown on Fig. IV-28.

---

[1] J. D. Gow, L. Smith, and J. M. Wilcox, The Ion Magnetron, UCRL-8579, Feb. 1959.

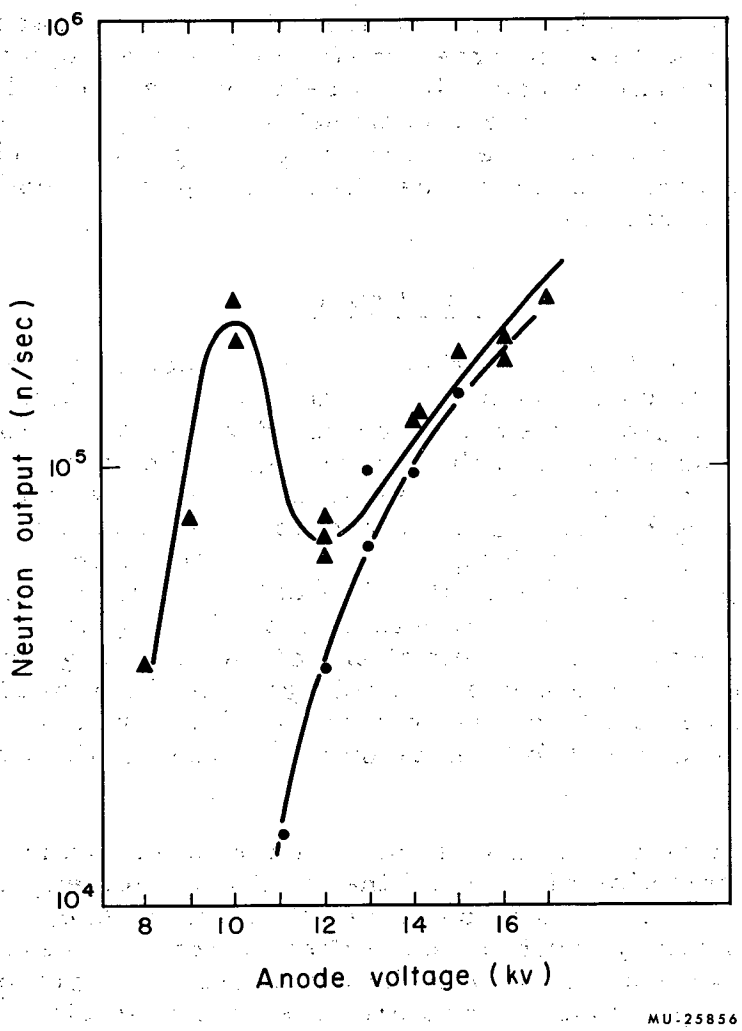

Fig. IV-27. Effect of anode alignment on neutron output. ●=before alignment, ▲=after alignment. P = 0.09 μ(gauge), H = $\frac{1100}{1000}$.

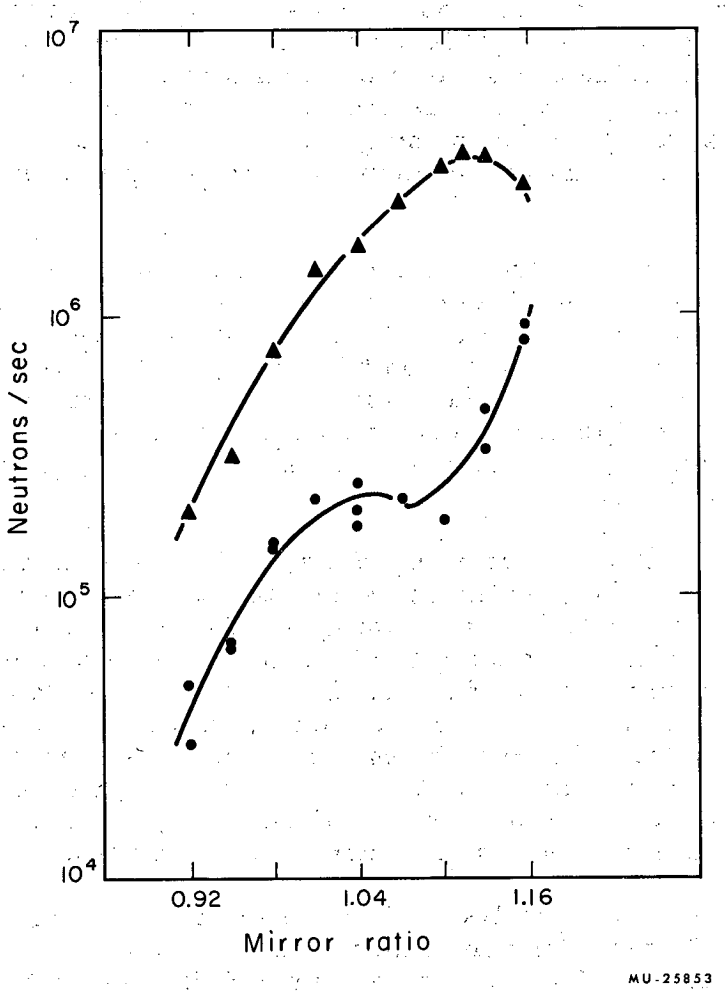

Fig. IV-28. Neutrons vs mirror ratio for well-aligned anode. ● = 0.1 μ D_2, ▲ = 0.2 μ D_2; B ≈ 10 kgauss at center.

A mode shift was observed in the current trace and visually in the discharge. This mode shift, which appeared in the current trace as a step, is coherent with the change in counting rate. Figure IV-29 shows how the mode shift appeared on the current trace and the effect of the mode change on the counting rate. The upper curves are the machine current and the 200-msec square wave is the scaler on gate. Referring to the counting rates, the modes are called fast and slow. Pictures 1, 2, and 3 in Fig. IV-29 show how the shift from slow to fast mode varies in time from the initial on pulse as a function of high voltage. This variation in time delay in mode shift with high voltage explains the drop in neutron output with increasing voltage. (Fig. IV-27) As the high voltage is increased the time delay of the mode shift progresses through the counting gate. The time delay of the mode shift is also sensitive to starting gas pressure, increasing with increasing pressure.

The magnetic field influenced the mode shift in two ways. First, the time delay of the shift is decreased with increased magnetic field; secondly, the height of the current step is usually reduced by increased magnetic field. It can be reduced to the point that, on the current trace, the mode shift is recognizable only by the slight increase in the slope of the tail of the current trace. In these cases the perturbation in current is so slight that it would not normally be noticed, yet there still exists a mode shift that sharply influences the counting rate.

The magnetic-mirror ratio appeared to affect the mode shift only because of the change in field strength associated with a change in mirror ratio. Increasing the mirror ratio by increasing mirror peaks reduces the time delay of the mode shift; increasing the mirror ratio by decreasing the center field increases the time delay of the shift. If the gas pressure and high voltage are set so the mode shift occurs early in the pulse, a slight increase in pressure or reduction in high voltage can cause the discharge to oscillate between the fast and slow mode. The frequency of oscillation can vary from a single flip to 50 kc. Although not explaining the reason this explains the source of the low-frequency hash frequently seen in the discharge.

The mode shift is visually discernible in the discharge provided the on time is about 600 msec and the mode shift is delayed 200 to 300 msec. In the slow mode there appears to be a faint longitudinal discharge running outside and extending into the circulating-ion region. When the mode shifts from slow to fast the faint discharge goes out. The circulating-ion region becomes brighter and better defined on the outer edge. If the shift is seen the appearance of each mode is quite distinct from the other; however, in the absence of a shift one cannot be sure of the mode of operation.

In summary it can be said there are at least two distinct running modes. Counting rates are sensitive to mode, being higher by an order of magnitude in the fast mode. The discharge either starts in the slow mode or shifts into it within microseconds of the high-voltage on pulse. A shift to the fast mode, if it occurs, is usually delayed for several milliseconds after there has been a considerable pressure drop. The mode of operation, after the initial pulse, is determined by a combination of anode voltage, starting pressure, magnetic field strength, and anode alignment. The slow mode is favored by higher voltage, higher pressure, lower magnetic field, and poor anode alignment.

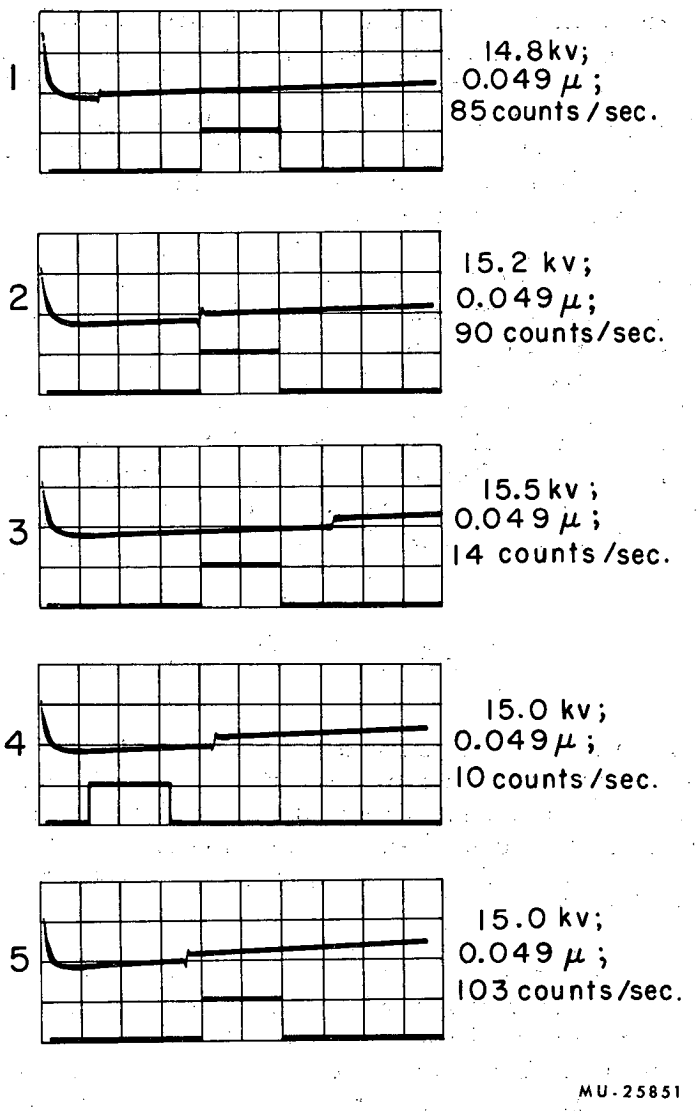

Fig. IV-29. Influence of running mode on neutron counting rate. Vertical scale = 100 ma/div; horizontal scale = 100 msec/div.

Conclusion

Previous experiments have shown that the anode sheath is the principal source of ionization in the ion magnetron;[2] however, considering the geometry of the machine, another though secondary source of ionization can be reasonably expected, namely a hollow cylindrical Penning discharge surrounding and extending into the circulating-ion region. The existence of this discharge depends on the energy of the secondaries and photoelectrons from the regions of the cathode threaded by the magnetic field. It is postulated that the so-called slow mode is due to competition between the anode sheath and a cathode sheath resulting from a Penning or PIG discharge running between opposite ends of the machine.

To visualize how the PIG discharge might start and affect the operation of the machine, consider the machine running in the fast mode, e. g., the PIG is not running. The thickness of anode sheath is determined by the incident neutral-particle flux, the outer surface of the sheath being the surface at which the negative space charge is neutralized by a radially increasing positive space charge due to the low-energy ions produced in the outer regions of the sheath. If the neutral flux to sheath is now increased, sheath ionization increases. The sheath electron density is determined by the ionization rate and cross-field mobility of the sheath electrons. The cross-field mobility is given by[3]

$$\frac{4}{\pi}\,\frac{mc^3 E}{e\pi B^3 \lambda}\ ,$$

where λ is the mean free path for electrons and E is the average sheath gradient. Therefore sheath electron density does not increase in proportion to the increased ionization rate, whereas the positive space charge due to the low-energy ions in the outer radii of the sheath does. Consequently the plasma moves in on the sheath, reducing the sheath thickness. This effect has been observed.[4]

Decreased sheath dimensions without a proportionate increase in gradient reduce the sheath voltage with a consequent increase in voltage drop between the plasma region and the cathode. The energy and number of secondaries from the cathode are increased. If the increase in energy and number of secondaries is sufficient the PIG can be initiated.

The above hypothesis is well supported by experimental observation. Initially the pressure is relatively high; as the discharge continues the pressure drops. If a PIG were to start while the pressure was still high it would be cut off if the pressure drop was sufficiently large, the time of cutoff being a function of starting pressure. This is in agreement with observation--increased initial pressure increases the time delay of the mode shift or PIG

---

[2] J. Donald Gow and Robert W. Layman, in Controlled Thermonuclear Research Quarterly Report, UCRL-8775, June 1959, p. 55.

[3] A. Simon, Thermonuclear Research (Pergamon Press, New York, 1959).

[4] James Donald Gow, John M. Wilcox, and Robert W. Layman (Lawrence Radiation Laboratory), unpublished work with Plus-Four Machine.

cutoff. The required pressure for a PIG discharge is a function of voltage. Higher voltages permit operation at lower pressures. Higher voltage would increase the time delay for PIG cutoff, which is consistent with experiment. An increase in magnetic field would be expected to reduce the time delay for mode shift. This is found to be the case.

Finally, the effect of anode alignment must be considered, since the observation of the mode shift was a result of improved alignment. With better anode alignment the sheath electron density will be higher owing to closer proximity of the sheath to the anode. The critical pressure for the PIG shutoff will therefore be higher, bringing the mode shift within the normal pulse length.

Porous Anode

The porous anode is constructed with the center 25 inches made of porous stainless steel tube with an outer diameter of 1.5 in. The rest of the anode is made of water-cooled aluminum. Lack of water cooling in the porous section required good alignment of the anode to prevent excessive heating anywhere on the porous tube.

The circulating-ion current gain possible with a porous anode is a function of pumping speed and sheath efficiency and can be calculated. With a measured pumping speed of 500 liters per sec for D_2 and 20% sheath efficiency, the circulating-current gain would be 4% higher than with a solid anode. The neutron output should be increased by a factor of 1.1. Counting rates were essentially the same for anode and liner neutral injection. Although there was no observed increase in neutron output with this anode, it proved to provide a practical system for neutral injection through the anode sheath.

Neutral Cutoff Experiment

Figure IV-30 is a cross-section drawing of the filament assembly installed in the magnetron liner. The filament, filament holder, and reflector are insulated from one another and from the liner for better than 2 kv. The accelerator and reflector shields are at liner potential. The gap in the accelerator and the accelerator-to-filament spacing are large to allow for changes in mirror ratio and filament warpage due to motor forces on the filament. The filament is a 0.040-in.-diameter tungsten wire. The accelerating electrode and reflector shield are made of tantalum. The reflector and filament holder are of water-cooled copper.

With this assembly, a hollow cylindrical hot cathode PIG is produced running outside the circulating ion region cutting off neutral flux entering the discharge from the walls. The total surface area of the PIG (inside and out) is 1.1×10^4 cm^2. A normal running pressure in the region of the PIG is 5×10^{-5} mm, meaning the total neutral flux entering the PIG discharge 1.1×10^{20} neutrals/sec. For total ionization the current would be 18 amp. The required electron current for 1-kv electrons would be 0.6 amp, assuming 30 ionizations per electron. The filament bias supply (1 kv, 24 kw) is able to provide sufficient power, but the electron emission is limited by the large

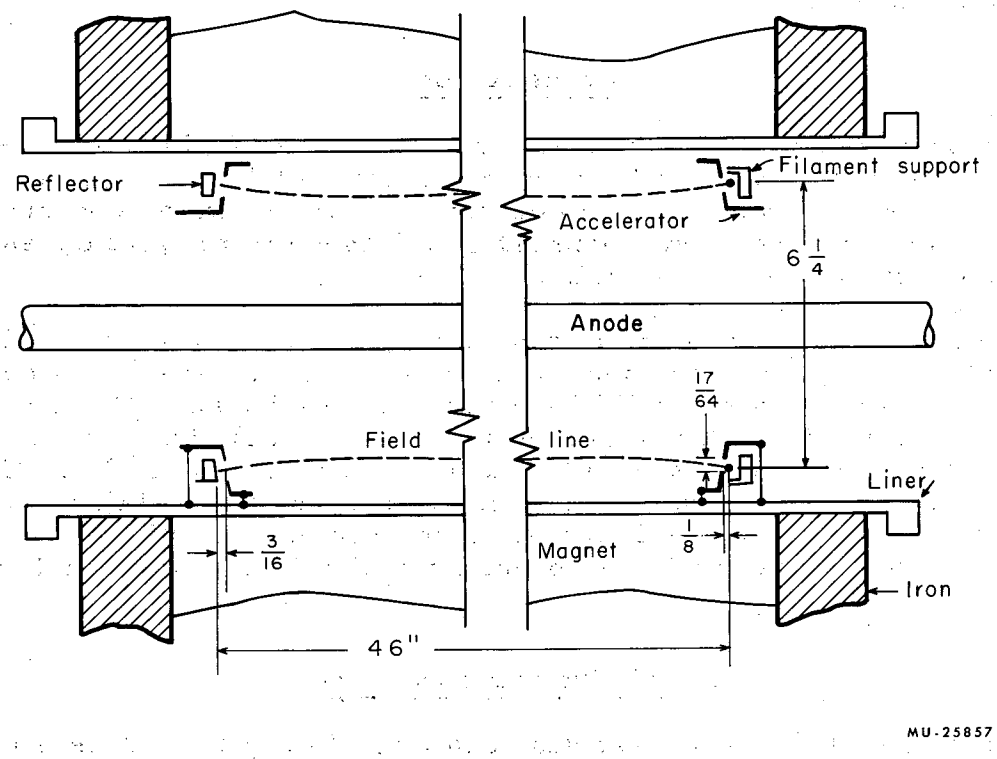

Fig. IV-30. Filament assembly installed in magnetron liner.

electrode spacing, so that the total running current at allowable operating pressures is a few amperes. This should provide a reduction of 10 to 20% in the neutral flux from the liner walls.

That the assembly is in proper alignment with the magnetic field is shown in Fig. IV-31. The reflector is tied to liner potential, indicating the emission current is primarily to the reflector.

Figure IV-32 shows reflector and total bias current with reflector tied to the negative side of the filament. The assembly is clearly operating in the proper manner. The effect of 1 kv filament bias on the pressure with no anode voltage is shown on Fig. IV-33. The pressure reacts to filament bias in the same manner as it does to high voltage on the anode, indicating pumping by the assembly. Under the conditions shown on Fig. IV-33, after 1 second the pressure will rise very rapidly if the filament assembly is left on. Pulsing the bias voltage with high voltage on the anode produces no effect on the pressure as seen by the ion gauges, the running current is reduced, however, as is shown on Fig. IV-34, pictures 1B, 2B, and 3B. (Figure IV-34 will be referred to again.) There is good evidence that the assembly is cutting off neutrals from the main discharge. The neutral reduction is of the order of 10 to 20%, which should increase the counting rate measurably (by a factor of 1.5 to 2).

The effect of the filament assembly on neutron production was first tested by running the assembly continuously and pulsing the anode high voltage. A run consisted of starting with the filament and bias voltage off and measuring initial (i. e., peak) and minimum (i. e., valley) currents and taking a count; this was repeated with the filament on, and then several more times with increasing bias voltage. After one of the early runs the bias and filament were turned off to repeat the sequence; the step appeared in the current trace as shown in Fig. IV-35, picture 1. Turning the filament on moved the step out in time, as shown in picture 2. Picture 2 also shows evidence of gas cutoff to the sheath by the filament alone. This is inferred from the larger initial current drop in picture 2. Therefore in spite of some screening by the filament the fast mode is not favored. The effect of the filament with 100 volts bias is seen in picture 3. The discharge is now oscillating between modes.

Analysis of the effect of the filament assembly was complicated by influence on the mode by the assembly. It was attempted to keep the discharge in one or the other of the two modes during a complete run. This was possible for the slow mode but not the fast. With a pumping speed greater by a factor of 2 or 3 there would not have been this complication.

Figure IV-36 shows counting rate as a function of bias voltage with the filament and bias on continuously while the high voltage is pulsed. There are at least ten high-voltage pulses at each point. The bias voltage was limited to 300 volts when run continuously because of runaway current.

Before any comment on the increased neutron output, reference must be made to Figs. IV-37 and IV-38. Figure IV-37 shows initial and valley current and pressure (gauge) as a function of bias voltage. Of interest here is the increase in running current with bias voltage. The filament assembly

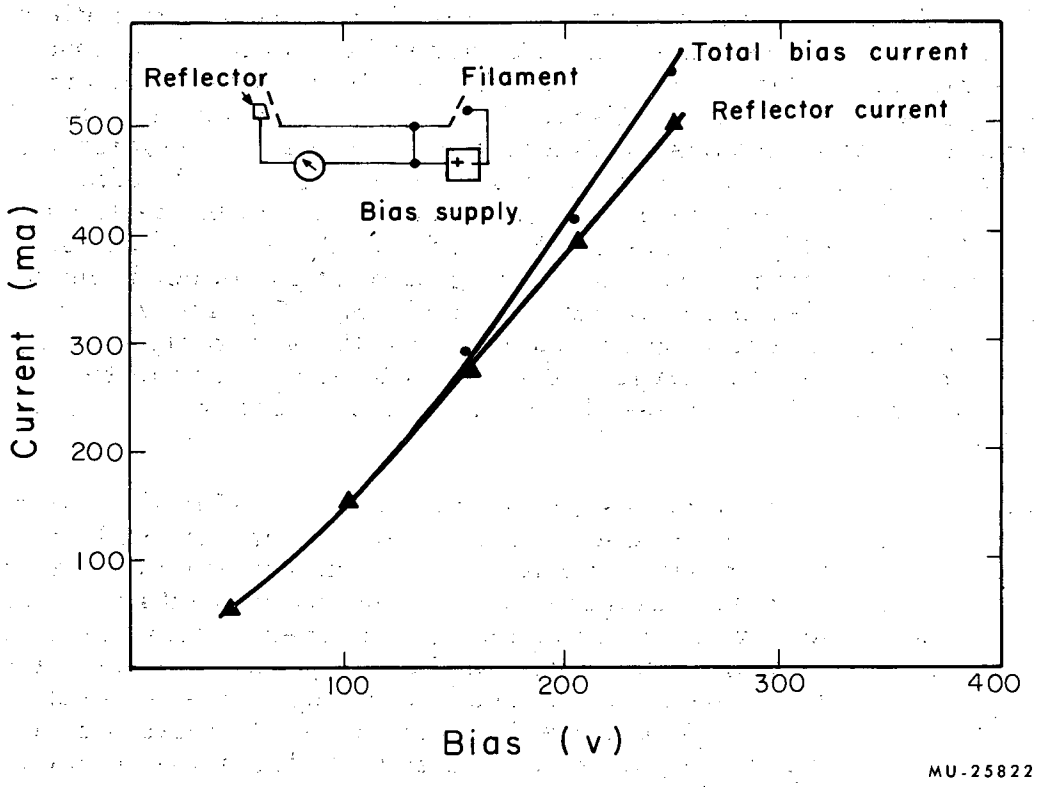

Fig. IV-31. Total bias current and reflector current as a function of bias voltage with reflector at liner potential. $P \approx 6 \times 10^{-6}$ mm. Filament at 22.5 v, 50 amp. (Data p. 19, 12/16/60 log.)

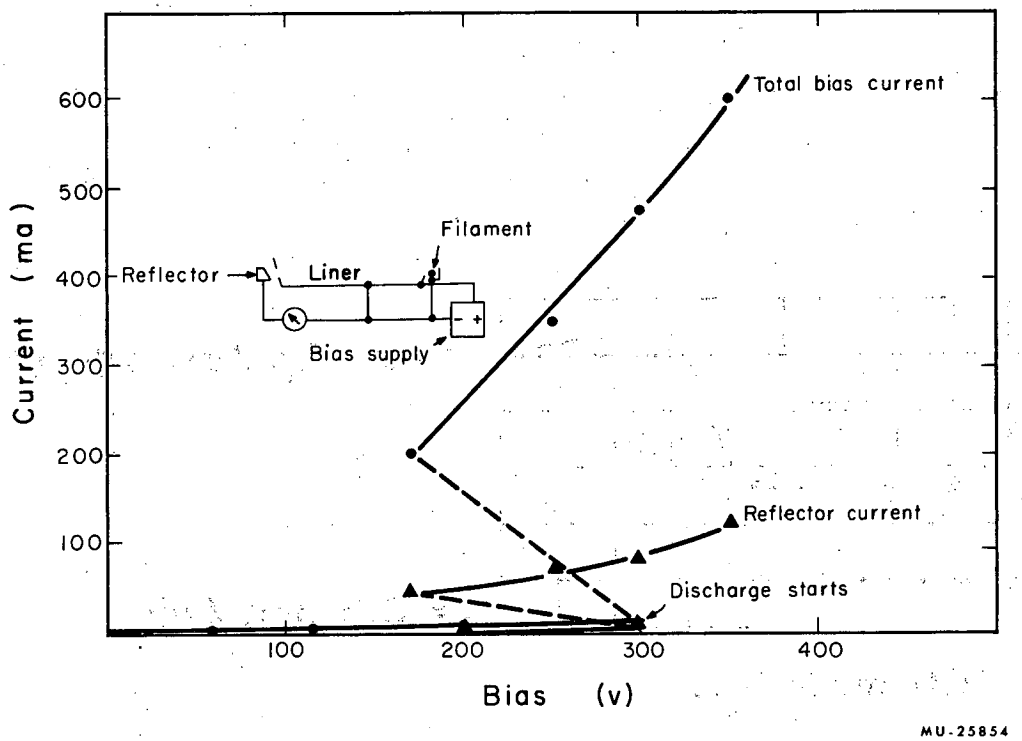

Fig. IV-32. Total bias current and reflector current as a function of bias voltage with reflector at filament potential. Filament 22.5 v, 50 amp. $P \approx 3.7 \times 10^{-6}$ mm up to discharge, $\approx 2.5 \times 10^{-6}$ after discharge. (Data p. 19, 12/16/60 log.)

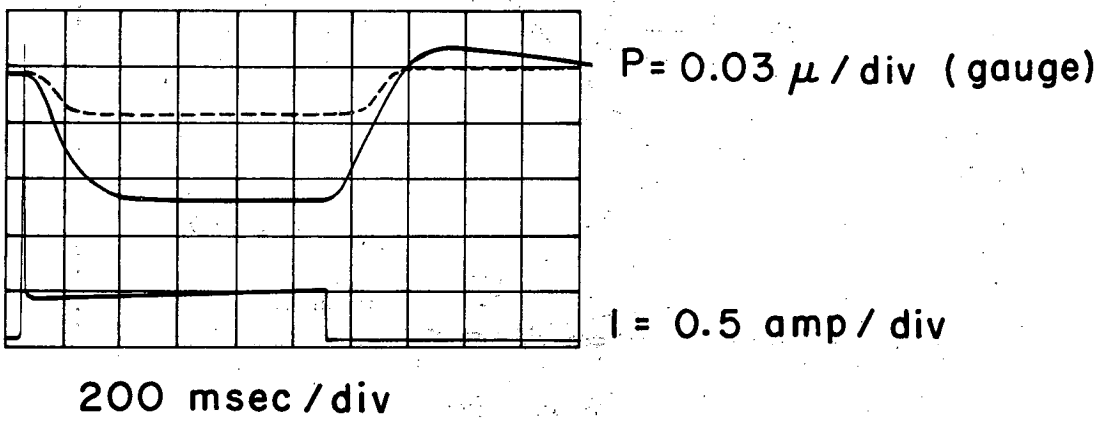

Fig. IV-33. Comparative pressure drop due to pumping of filament assembly and main discharge. Starting pressure 0.1 μ; starting current 0 amp.
--- Pressure drop due to 1 kv filament bias, no anode voltage.
—— Pressure drop due to anode voltage (filament and filament bias on or off).

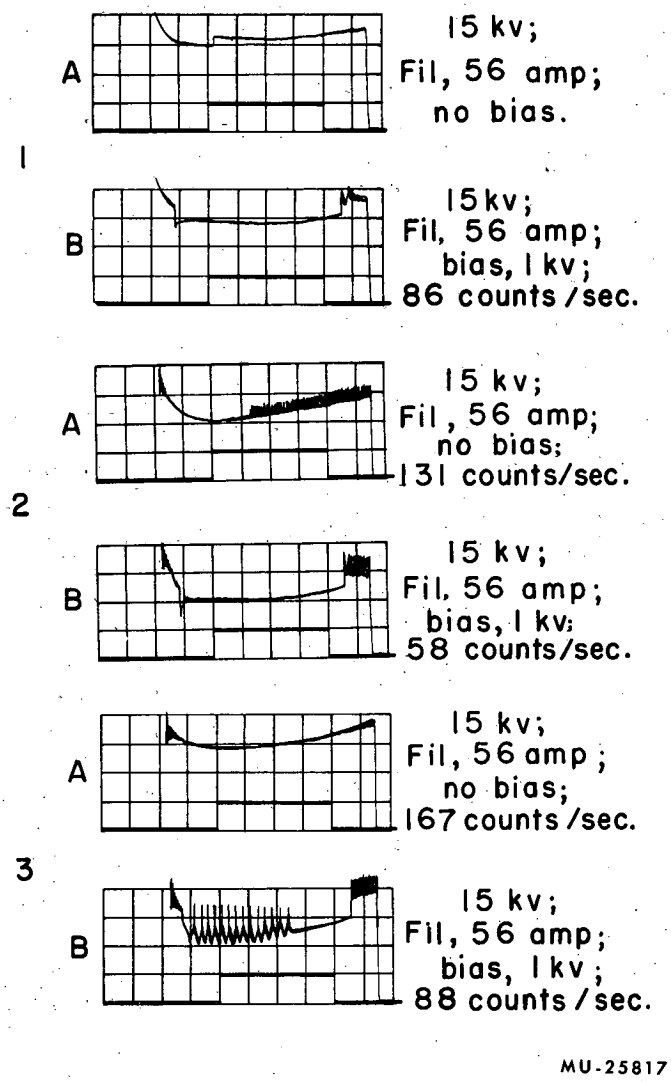

Fig. IV-34. Machine current trace with and without filament bias. Vertical scale = 0.2 amp/div; horizontal scale = 50 msec/div.

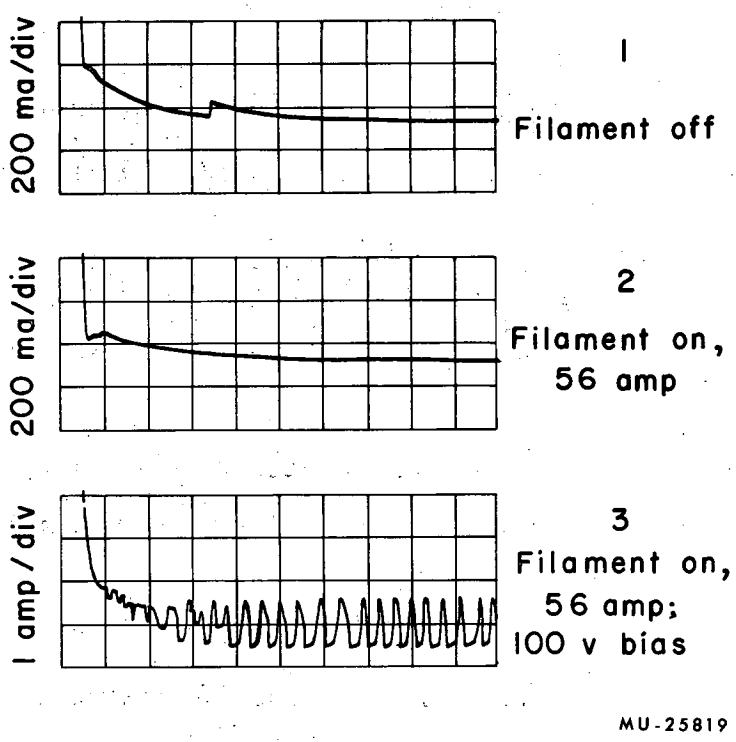

Fig. IV-35. Effect of filament and bias voltage on current step. Horizontal scale = 10 msec/div.

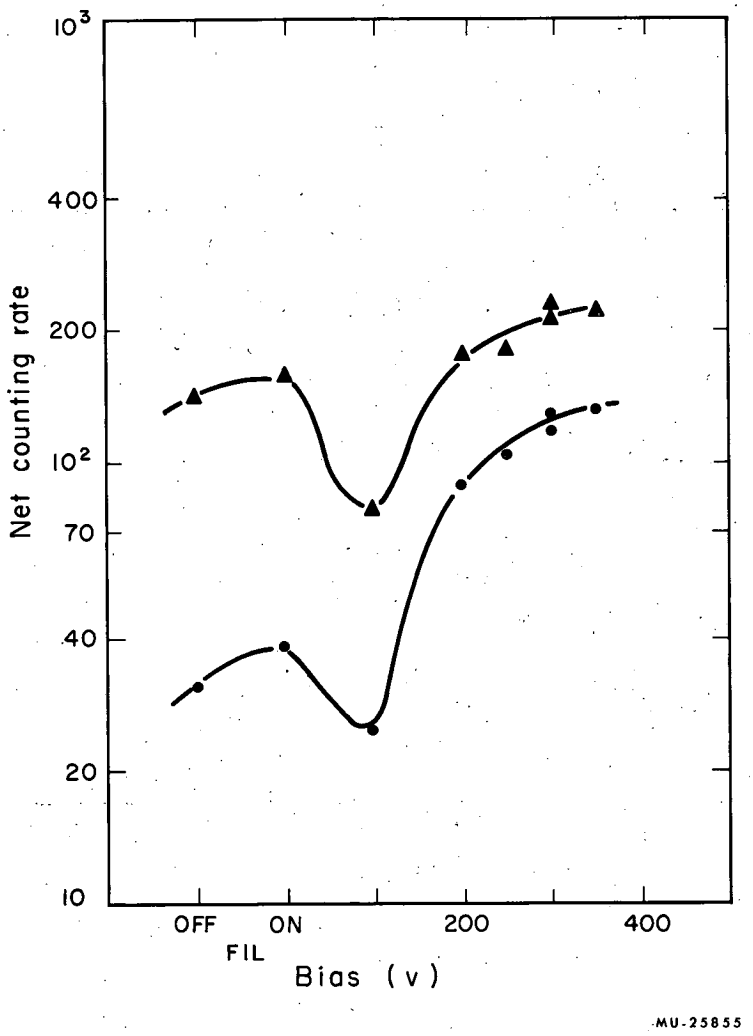

Fig. IV-36. Counting rate vs filament bias with bias on continuously; hv = 12 kv, H = $\frac{1200}{1090}$.
●=counts/sec, ▲=counts/amp sec.
Counter calibration 2.3×10^3.

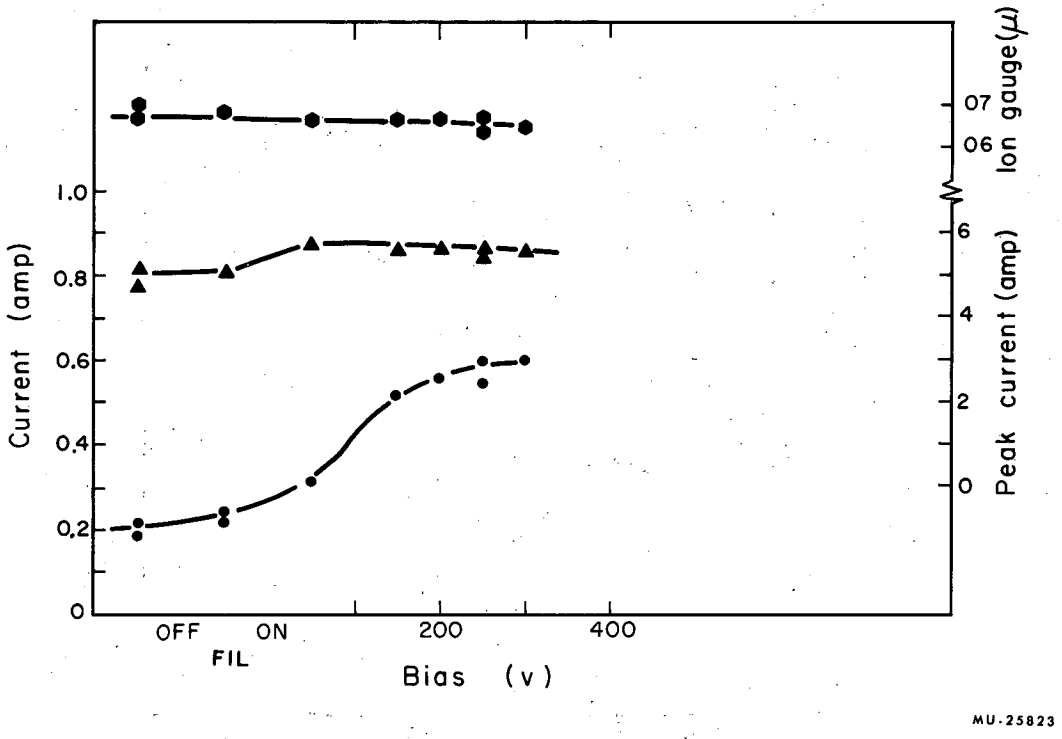

Fig. IV-37. Peak and valley currents vs filament bias; hv = 12 kv, $H = \frac{1200}{1090}$. ● = valley current; ▲ = peak current; ○ = ion gauge.

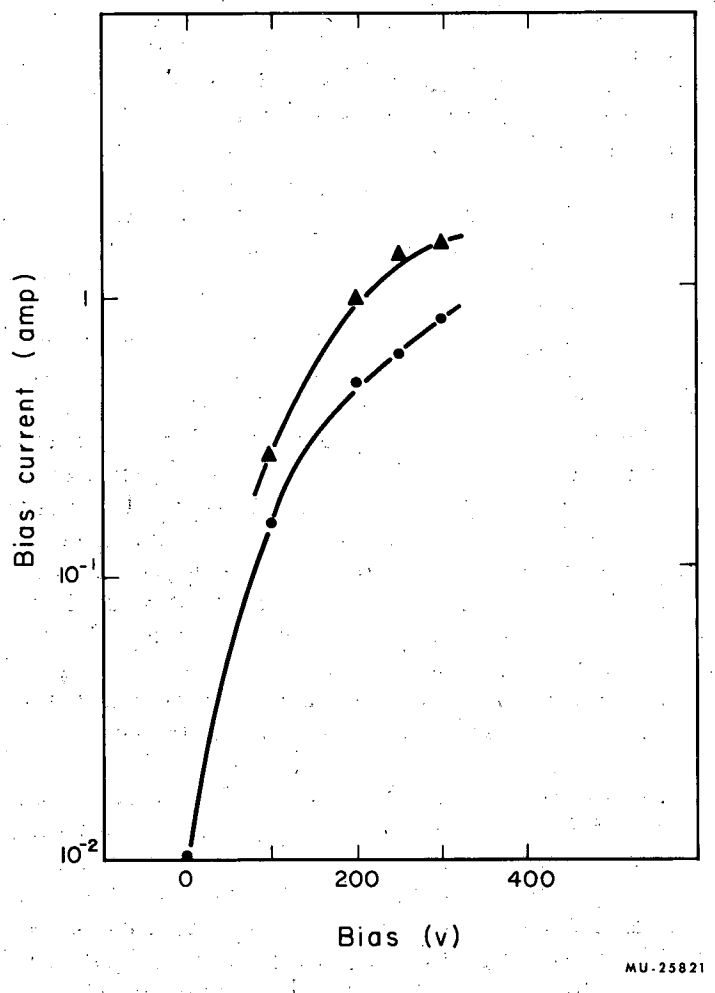

Fig. IV-38. Filament bias current vs bias voltage with anode high voltage on and off; hv = 12 kv, H = 1200/1090.

appears to be operating as a gas valve triggered by the main discharge. Figure IV-38 shows a reduction in bias current with anode voltage. It should be pointed out that normal pressure drop of 60 to 70% is reduced to 45 to 50% with the continuously running filament assembly.

It is reasonable to conclude the increased counting rate shown in Fig. IV-36 is the result of additional gas being fed to the sheath. The source of this gas can be explained. The pressure reduction due to the high-voltage pulse reduces the ionization rate in the cylindrical discharge, consequently increasing the space-charge limiting of the electron emission from the filament and reflector. The pumping by the filament assembly is thus reduced, increasing the gas flow to the main discharge. To test this, with the filament and bias off, the gas flow was increased to bring the valley current to the same points as it was with various values of bias voltages. The counting rates were the same at the same running current. A similar result could be obtained by shutting off the bias voltage concurrently with the high voltage on pulse.

A logical experiment to test for any fast ion buildup due to neutral cutoff would be to pulse the bias voltage after the anode voltage. The bias voltage was pulsed for 300 msec, starting 50 msec after the high-voltage pulse and 50 msec before the scaler-on gate. The results are shown on Fig. IV-34. It is clearly indicated by the drop in current that neutrals are being cut off from the main discharge. It is also clear that the counting rate is reduced. If the sheath were really 20% efficient it should then be possible to increase the ratio of fast ions to neutral background for a given running current by increasing the gas flow so the current with the bias on is the same as a previous value with the bias off. The increased ratio should be reflected in increased counting rates. Comparison of Fig. IV-34 picture 2A with 2B and 3A with 1B, shows that rather than an increase in counting rate there is a decrease. This was found to always be the case.

This performance can be explained as follows. If at some running current I the filament bias is turned on, I will drop owing to the reduced neutral flux from the outside. If the flow rate is now increased to bring I back up to its original value, the required increase will be about 12%. This, assuming a 20% sheath efficiency, would give an increase of 2.4% in the ionization of neutrals entering the sheath directly from the anode. The consequent increase in counting rate should be between 10 and 20%. The filament assembly, however, cuts off neutrals that are mostly entering the discharge radially; therefore, when the flow rate is increased to bring the current up the neutral flux from the ends of the machine is increased. Since the mean free path for collisions between neutrals is around 100 cm, the neutral flux parallel to the anode is increased. The natural result is of course a reduction of fast-ion density.

Although the reduction of charge-exchange losses in these experiments did not increase the fast-ion density, it is reasonably certain that such an increase would have resulted if the sheath efficiency had been higher and if the pressure had been lower. At lower pressures the cutoff efficiency of the filament assembly could be increased by running at higher voltages. At 10^{-6} mm an emission current of a few milliamperes would be sufficient to get complete cutoff. There is some evidence that sheath efficiency is influenced by pressure, efficiency dropping with pressure. If this were true it could also be a contributing factor in the above behavior.

12. THE EFFECT OF RADIATION REACTION ON GUIDING-CENTER MOTION

David Sachs

An expansion similar to that of Kruskal[1] was obtained for the non-relativistic motion of a charged particle in slowly varying electric and magnetic fields with the classical radiation reaction force on the particle included. The smallness parameter of the expansion is r_0/L, where r_0 is the Larmor radius of the particle and L is a characteristic length of the fields, e.g., $|B/\vec{\nabla} B|_{min}$.

It was shown that the force of radiation reaction leads to a modification of the usual drift expression. The modification of the drift velocity is, however, smaller than the rate of decay of the Larmor orbit due to the particle's radiation. Therefore radiation reaction is unimportant in the guiding-center approximation of the particle's motion.

A quantity was obtained which is an adiabatic invariant in the special case in which $\vec{E}$ and $\vec{B}\cdot(\vec{\nabla}\times\vec{B})$ are small (that is, proportional to r_0/L, the smallness parameter). This adiabatic invariant is given, in the limit of small radiation effects, by

$$M = \mu\left[1 + \frac{2a_0^3\left|\vec{B}\left(\vec{R}_0(t)\right)\right|^2}{mc^2}\right]\exp\left[\frac{4a_0^2}{3mc}\int_0^t\left|\vec{B}\left(\vec{R}_0(t')\right)\right|^2 dt'\right]$$

where μ is the magnetic moment of the particle, $a_0 = e^2/mc^2$ = the classical radius of the particle (not the Larmor radius), and $\vec{B}(\vec{R}_0(t))$ is the magnetic field at the position $\vec{R}_0$ of the guiding center at time t.

The radiation effects go to zero with a_0 and the expression goes to the magnetic moment of the particle, which is the adiabatic invariant when radiative effects are neglected.

---

[1] Martin Krushkal, The Gyration of a Charged Particle, PM – S – 33 (NYO - 7903), March 1958.

13. STABILITY OF STEADY HYDROMAGNETIC FLOWS

Alan B. Macmahon

R. W. Bussard has recently discussed the stability of steady hydromagnetic flows.[1] His double variational principle $\alpha_{minimax} > 0$ for stability (< 0 for instability), has been found to fail for the hydrodynamic Helmholtz instability of two compressible fluids of equal density. A brief outline of Bussard's derivation of the variational principle is given here to clarify the

---

[1] R. W. Bussard, An Energy Principle for the Stability of Hydromagnetic Plasmas in Equilibrium Motion, LAMS-2534, May 23, 1961.

reason for its failure in this case, and the relation of the condition $a_{minimax} > 0$ to the sufficient conditions of Frieman and Rotenberg[2] is discussed.

The hydromagnetic equations, when linearized about a condition of steady flow, may be written in the form[2]

$$\mathcal{L}(\xi) \equiv -\omega^2 \xi + 2\omega i\rho v \cdot \nabla\xi - F(\xi) = 0. \qquad (1)$$

Here $\xi(\sim e^{i\omega t})$ is the displacement of a fluid element from its equilibrium position with the equilibrium position taken as independent variable. Equation (1) is supplemented by boundary conditions of the usual form. The differential operator $F(\xi)$ is self-adjoint, and $i\rho v \cdot \nabla$ is Hermitian because of the equilibrium conditions of steady flow and the boundary conditions.

To obtain the double variational principle observe that for real ω the operator $\mathcal{L}(\xi)$ is Hermitian and hence the solutions of the equation

$$\mathcal{L}(\xi) = \rho a \xi \qquad (2)$$

form a complete orthogonal set ξ_n with real eigenvalues $a_n(\omega)$. Both the ξ_n and $a_n(\omega)$ depend on the real parameter ω. If ξ belongs to an N-dimensional function space there will be N eigenvalues $a_n(\omega)$. These have the limiting behavior $a_n(\omega) \to -\omega$ as $\omega \to \pm\omega$. The character of the a_n as a function of ω is indicated in Fig. IV-39. It is assumed that there is no degeneracy so that the curves do not cross.

Every intersection of an $a_n(\omega)$ curve with the ω axis gives a stable solution to Eq. (1), and there are exactly 2N values of ω that satisfy Eq. (1). It follows that (1) has no unstable solutions if and only if the set of $a_n(\omega)$ curves makes 2N intersections with the ω axis. This is the case if the lowest curve becomes positive at any point. Similar arguments can be applied if N is countably infinite.

The lowest $a_n(\omega)$ curve has a single maximum. This value, $a_{minimax}$, can be found by minimizing the functional

$$a(\xi^*, \xi) = (\xi^*, \mathcal{L}(\xi))/(\xi^*, \rho\xi)$$

with respect to all ξ that satisfy the boundary conditions and then maximizing with respect to the real parameter ω. Thus $a_{minimax} > 0$ is a sufficient condition for stability. The argument does not prove necessity, however, since higher $a(\omega)$ curves may cross the ω axis more than twice, and even the lowest eigenvalue may be degenerate for some values of ω.

Bussard suggests that the condition $a_{minimax} > 0$ may be strictly necessary for stability and, in any event, that changes in sign of $a_{minimax}$ as system parameters are varied should correspond to transitions between stability and instability.

Consider the hydrodynamic Helmholtz instability of two uniform compressible fluids of equal density ρ, flowing with equal and opposite

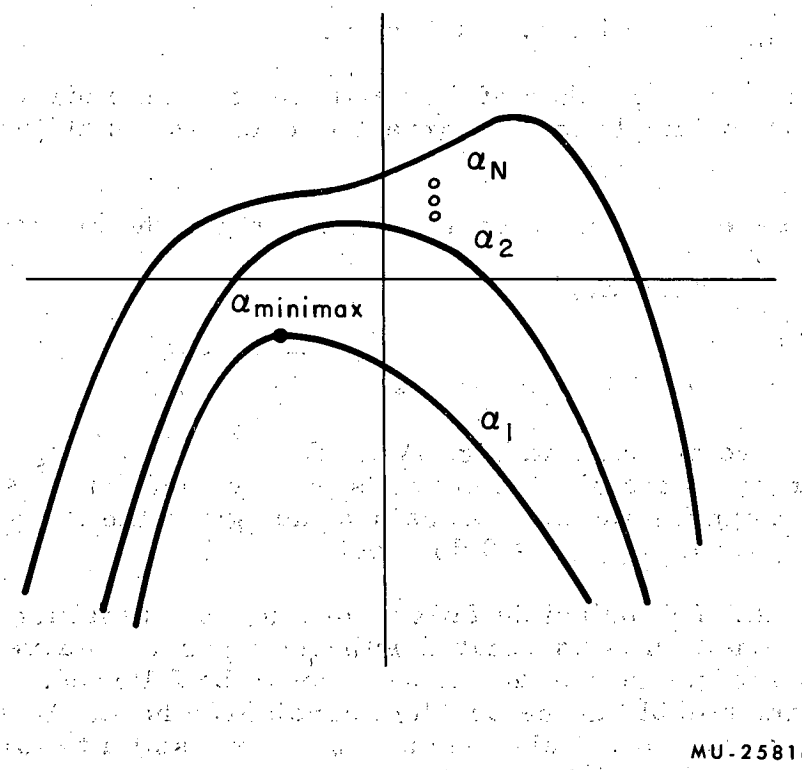

Fig. IV-39. Illustrating the general nature of the eigenvalues α as a function of ω.

velocities v, and separated by a plane interface. The normal mode analysis for this case is simple and yields the well-known result that the flow is stable for $v^2 > 2a^2$, where a is the sound speed. (Only perturbations uniform in the direction perpendicular to the flow velocity and parallel to the interface are considered.)

Minimizing the functional α for this configuration with respect to ξ yields

$$\alpha_{\min\xi} = -(|\omega| + kv)^2 < 0 \text{ for all } \omega, v,$$

where k is the wave number of the perturbation in the direction of flow. The variational principle thus incorrectly indicates instability for all flow velocities.

In this case Eq. (2) can be solved directly. The eigenvalues are found to be

$$\alpha(\omega) = \begin{cases} (-\omega \pm kv)^2 \\ \omega^2 + k^2 \left[a^2 - v^2 \pm \sqrt{a^4 + 4a^2v^2}\right]. \end{cases}$$

These curves are sketched in Fig. IV-40 for $v^2 > 2a^2$. For $v^2 < 2a^2$ the central minimum of the highest curve is positive and for $v^2 < 1/2\ a^2$ it disappears. Counting the axis crossings thus gives the correct stability condition although $\alpha_{\text{minimax}} > 0$ does not.

The variational principle fails to predict the transition to stability because the transition is associated with the upper $\alpha(\omega)$ curve. Furthermore, the assumption of no degeneracy is seen not to be followed. Although not the cause of the trouble in the problem considered here, the existence of degeneracies in the lowest eigenvalue $\alpha(\omega)$ allows stability for negative α_{minimax} even if each $\alpha(\omega)$ curve has only a single maximum. Considerable caution should therefore be exercised in interpreting $\alpha_{\text{minimax}} > 0$ as a necessary condition for stability.

The condition $\alpha_{\text{minimax}} > 0$ is closely related to the more general of the two sufficient conditions of Frieman and Rotenberg.[2] This condition is

$$(\xi^*, i\rho v \cdot \nabla \xi)^2 - (\xi^*, \rho\xi)\,(\xi^*, F(\xi)) > 0 \qquad (3)$$

for all admissible ξ. The maximum value of the functional α for fixed ξ is given by Bussard as

$$(\xi^*, \rho\xi)^2\, \alpha_{\max_\omega} = (\xi^*, i\rho v \cdot \nabla \xi)^2 - (\xi^*, \rho\xi)(\xi^*, F(\xi)).$$

---

[2] E. Frieman and Manuel Rotenberg, Revs. Modern Phys. 32, 898 (1960).

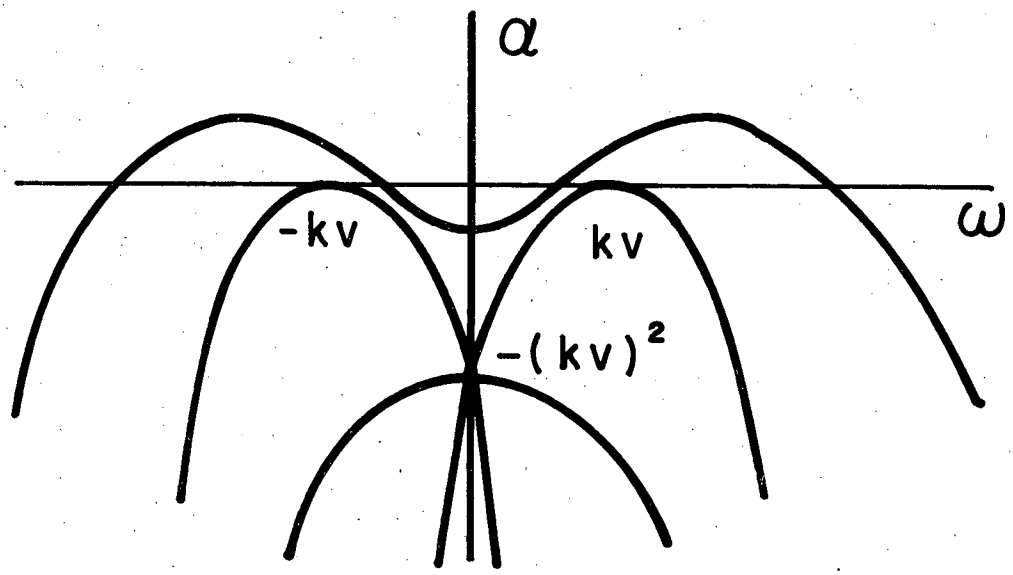

Fig. IV-40. The eigenvalues $\alpha(\omega)$ for the Helmholtz problem with $v^2 > 2a^2$.

Therefore $a_{minimax} > 0$ implies that condition (3) is satisfied, since $a_{max_\omega} \geq a_{minimax}$ for all ξ. Conversely, assuming no degeneracy of the lowest eigenvalue a, condition (3) implies $a_{max_\omega} > 0$ for all ξ, and in particular $a_{minimax} > 0$.

V. THEORETICAL AND BASIC EXPERIMENTAL PLASMA PHYSICS

1. RADIAL MOTION OF ELECTRONS IN THE ASTRON DEVICE

V. Kelvin Neil

In a previous report[1] and in a separate paper,[2] excitation of electromagnetic modes of the Astron vacuum tank was shown to give rise to a serious instability. However, the radial motion of the electrons was not considered properly in that calculation. The radial oscillations provide an additional spread in particle gyrofrequency that has a stabilizing influence on the perturbation. By utilizing the theory of betatron oscillations in particle accelerators, the radial motion may be linearized. If this motion is assumed to be independent of the azimuthal motion, the effect on stability against azimuthal bunching may be calculated. For particle accelerators the assumption is rather good, and the radial motion may have a significant stabilizing influence. If the same assumption is made regarding an electron layer that is infinite in the axial direction, the additional frequency spread may be sufficient to stabilize the layer against the negative mass instability. However, it is not sufficient to stabilize the layer against electromagnetic instabilities. These conclusions are tentative, since it is probably not a good approximation to neglect the coupling between radial and azimuthal motion in this device.

For a very thin layer it is a good approximation to linearize the radial motion. Within this approximation a self-consistent equilibrium configuration, infinite in the axial direction, is easily obtained. This solution agrees quite well with the solution given by Tonks in the limit of high electron density.[3] It is hoped that this approximately self-consistent solution will yield some insight into the problem of formation of the electron layer as well as of its stability under various perturbations.

2. THEORY OF AN ELECTROSTATIC PROBE IN A PLASMA

Laurence S. Hall and Donald P. Geesaman

Work is continuing on the numerical solution of Poisson's equation in an attempt to find self-consistent potential distributions about cylindrical and spherical probes. It has been necessary to devote a great deal of time to increasing the precision, not only in the numerical integrations, but also in the approximations to the differential equation itself and the algebraic approximations to various transcendental functions appearing therein.

---

[1] V. Kelvin Neil, in Controlled Thermonuclear Research Quarterly Report, UCRL-9777, Aug. 1961, p. 101.

[2] V. Kelvin Neil, Electromagnetic Coupling Instabilities in Astron, UCID-4288, June 1961.

[3] Lewi Tonks, The Self-Consistent Field of Single-Type Electrons in a Uniform Magnetic Field, UCRL-5335, Sept. 1958.

A particular difficulty has appeared in that the conventional use for computer applications of Hasting's approximations to the error function[1] is unsuitable for our present calculations. Specifically, an expression for the related function

$$\Upsilon(x) \equiv \frac{2}{\pi^{1/2}} \int_{x^{1/2}}^{\infty} \exp(x - t^2)\, dt \qquad (1)$$

was needed in a form suitable for computer use. A few tables exist (usually with $\pi^{1/2}\Upsilon(x)/2$ tabulated vs $x^{1/2}$), but none were found of sufficient accuracy or of such completeness as to satisfy our requirements, and it was consequently necessary to prepare our own. A computer program has been written for the computation of $\Upsilon(x)$ using the newly available double-precision arithmetic of the IBM 7090. A plot of $\Upsilon(x)$ vs x is shown in Fig. V-1. A short study of the function and a set of tables are currently being prepared for publication as a UCRL report.

[1] C. Hastings, Jr., Approximations for Digital Computers (Princeton University Press, Princeton, N. J., 1955), p 167-169, 185-187.

3. FORMATION OF EXCITED HYDROGEN ATOMS BY CHARGE EXCHANGE IN VARIOUS GASES

John R. Hiskes and Marvin H. Mittleman

Hydrogen atoms excited with principal quantum number of six or more are relatively easy to ionize by Lorentz forces. The production of energetic excited-atom beams by charge exchange and their subsequent Lorentz ionization inside a magnetic field region is of interest as an injection mechanism for fusion machines.[1,2] The possibility of enhancing the populations of the excited states of neutral hydrogen atoms by varying the kind of neutralizing gas has been considered. We report here some calculations, based on a first Born approximation,[3] which give the charge-exchange capture distribution in the range of principal quantum numbers from n = 1 to n = 10. These calculations have been done for s-state transitions in the energy range from 6 to 100 kev, and for a variety of neutralizing gases.

We have considered first an idealized neutralizer consisting either of a gas of H(2s) atoms or H(6s) atoms, since for these systems exact wave functions are available. The calculations have also been done for Li and Cs vapor neutralizers, with approximate wave functions used to describe the outer electron.

[1] John R. Hiskes, Electric and Magnetic Dissociation of Molecular Ions and Neutral Atoms, UCRL-6372, June 1961.

[2] D. R. Sweetman, in Proceedings of the Salzburg Conference on Controlled Nuclear Fusion Research, September 1961, Paper CN-10/74.

[3] Marvin H. Mittleman, Phys. Rev. 122, 499 (1961).

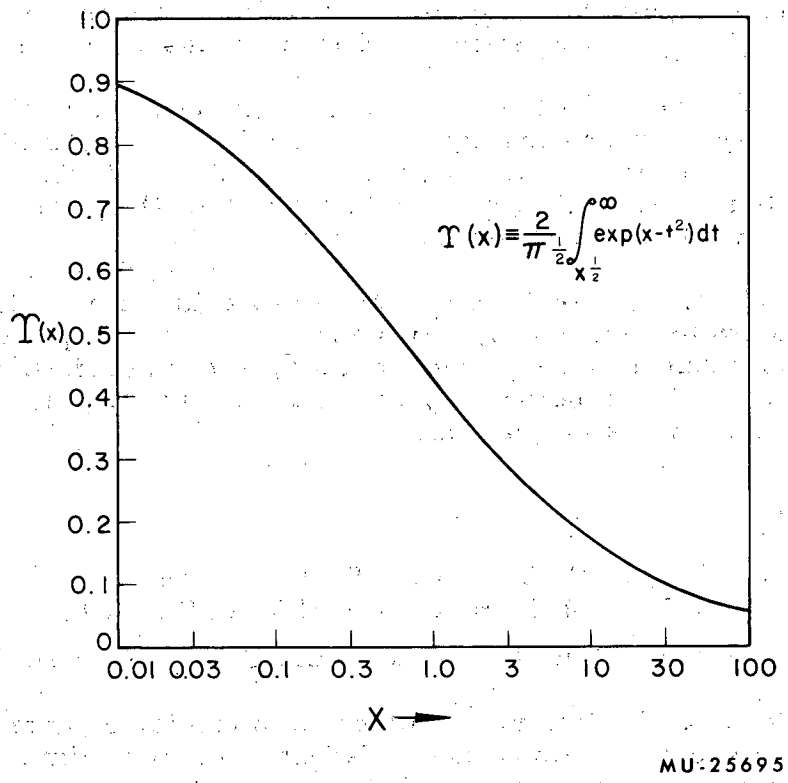

Fig. V-1. The function $\Upsilon(x)$ for $0.01 < x < 100$.

The ratios of the charge-exchange capture cross section for the nth level to that of the ground state for protons moving through a H(6s) neutralizer are plotted in Fig. V-2; the curves labeled V = 1, 2, and 4 are the distributions for different relative velocities, and correspond to laboratory-system proton energies of 6.25, 25, and 100 kev, respectively. In the limit of large velocities it can be shown that these ratios tend to a $1/n^3$ distribution for any neutralizer. The crosses at n = 2, 6, and 10 indicate the ratios for a H (1s) neutralizer and the V = 1 case. We believe that for any energy above 6 kev the ratios of the capture cross sections for a H(1s) neutralizer lie in the region between the crosses and the $1/n^3$ distribution. From the figure we see that at the lower velocities the distribution in the range from n = 6 to n = 10 is enhanced and is greater by approximately an order of magnitude for a H(6s) neutralizer than for a H(1s) neutralizer. The results for a H(2s) neutralizer (not shown) exhibit a similar trend in the sense that capture ratios of the excited states tend to increase at the lower energies.

In Figs. V-3 and V-4 are shown the distribution for lithium and cesium vapor neutralizers. These distributions have been calculated by using hydrogen-like wave functions and choosing an effective Z taken from published variational calculations. These distributions show the same general trends as do those of the H(2s) and H(6s) neutralizers.

The distributions show a pronounced deviation from a $1/n^3$ dependence as the incident proton energy is decreased. The Born approximation, however, becomes suspect at very low energies, and these data must be taken with caution for energies below 25 kev. The calculations are being extended to include other than s-state captures.

4. ELECTRIC DISSOCIATION OF THE HELIUM HYDRIDE MOLECULAR IONS

F. E. Harris, John R. Hiskes, and George A. Paulikas

Calculations to determine the electric dissociation thresholds for the successive vibrational levels of the different isotropic mixtures of the helium hydride molecular ions are continuing. The ground-electronic-state potential function has been calculated over the entire range of internuclear separations by use of a single electronic configuration. With this potential the vibrational-level spectrum has been calculated numerically for the He^4H^+ isotopic mixture. On the basis of this preliminary spectrum, it is evident that the electric dissociation threshold for the uppermost vibrational level is of the order of 10^6 volts/cm or less.

The variational calculation for the potential is being extended to include higher electronic configurations. This more accurate potential and vibrational-level spectrum should permit us to specify the thresholds below 10^6 v/cm.

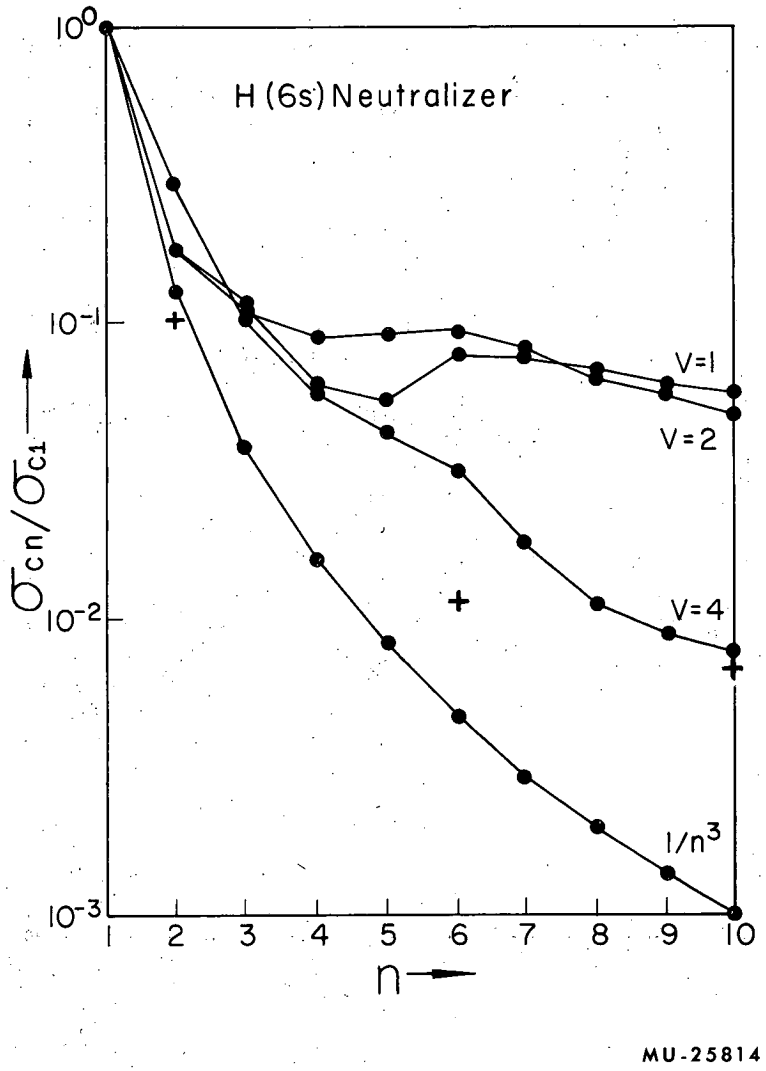

Fig. V-2. Capture distribution for protons in H(6s) neutralizer.

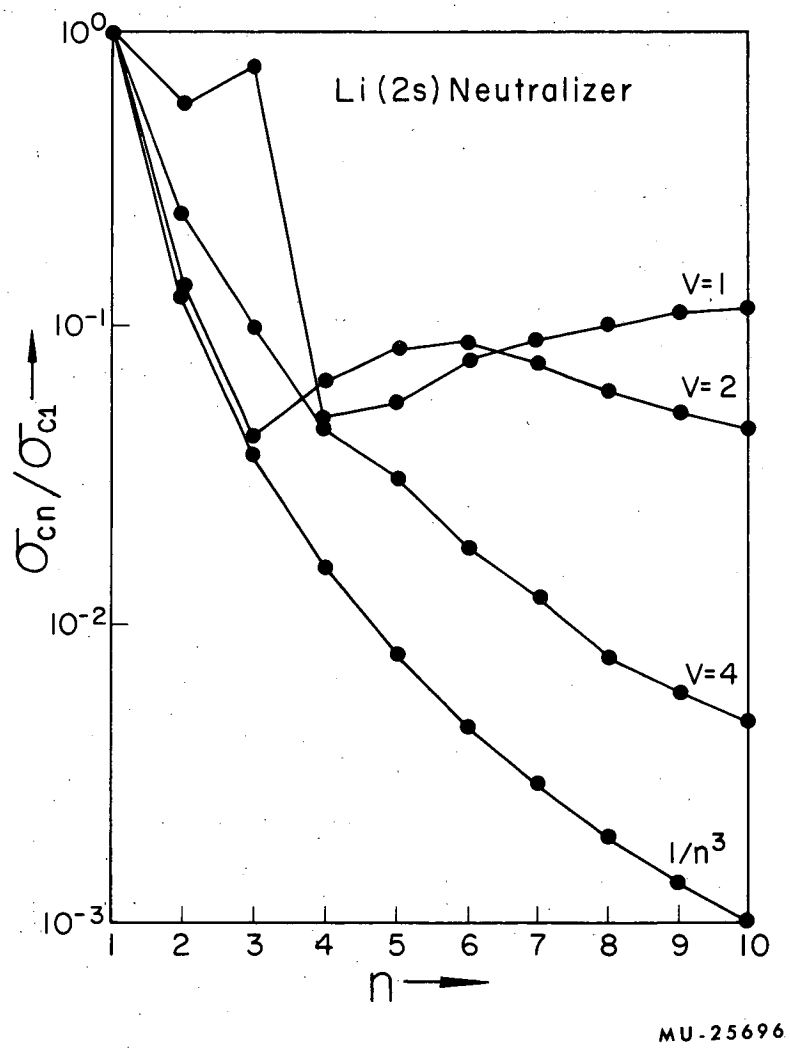

Fig. V-3. Capture distribution for protons in Li(2s) neutralizer.

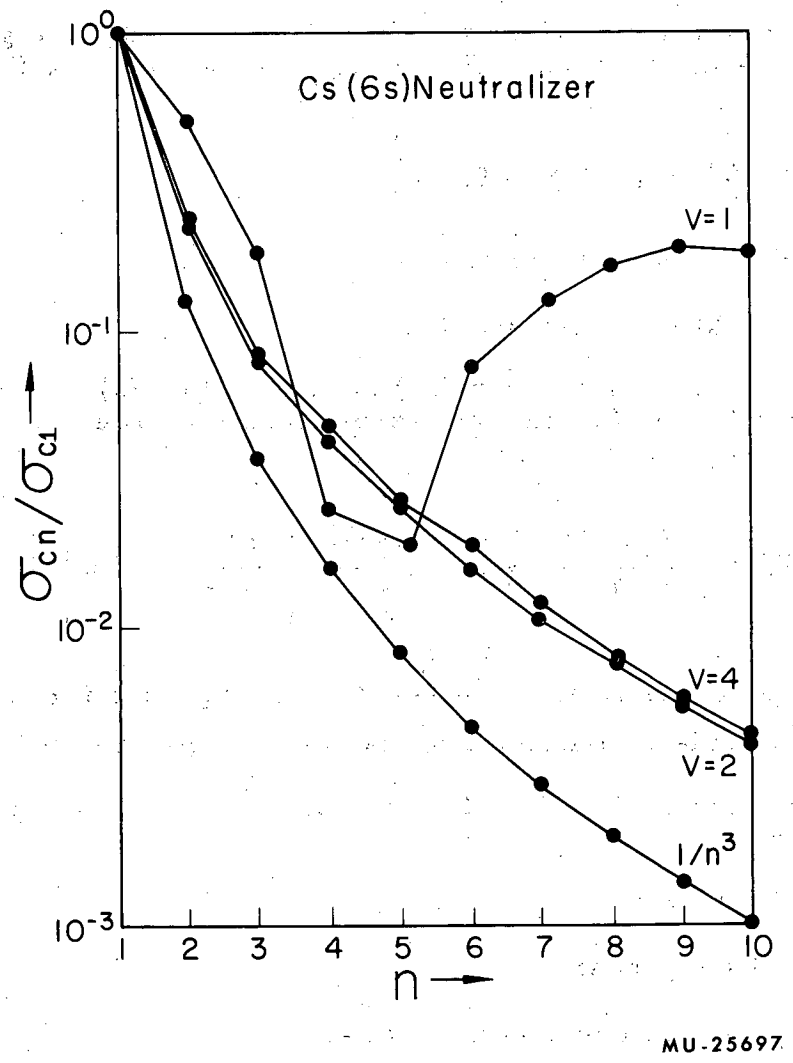

Fig. V-4. Capture distribution for protons in Cs(6s) neutralizer.

5. INSTABILITY OF A RESISTIVE SHEET PINCH

Harold P. Furth and John Killeen

The effect of finite conductivity on the hydromagnetic stability of a sheet pinch has been investigated and reported previously.[1, 2] A description of the mathematical model of the problem is given in the preceding progress report.[1] Some changes in the model have been made and are reported here.

In the older version of the problem the resistivity is a given function of y, and is constant in time. We now let $\eta = \eta(x, y, t)$, satisfying the equation

$$\frac{d\eta}{dt} = \frac{\partial \eta}{\partial t} + (\vec{v} \cdot \nabla)\eta = 0. \qquad (1')$$

We assume that η is of the form

$$\eta = \eta_0(\zeta) + \eta_1(\zeta, t) \cos kx, \qquad (2')$$

where $\zeta = y/a$. If the expression (2') is used in Eq. (1) of the previous report[1] along with Eq. (2) and only zero- and first-order terms are retained, the equation for $\psi(\zeta, t)$ becomes

$$\frac{\partial \psi}{\partial \tau} = -\beta F(\zeta) w + \frac{\eta_1(\zeta, t)}{\eta_\infty} \frac{dF}{d\zeta} + \frac{\eta_0(\zeta)}{\eta_\infty} \left[\frac{\partial^2 \psi}{\partial \zeta^2} - a^2 \psi \right],$$

where η_∞ is a constant, and $\tau = \frac{\eta_\infty}{a^2} t$. The equation for w remains the same and the boundary conditions for both equations are still the same.

The functions $F(\zeta)$ and $\eta_0(\zeta)$ are specified for a particular problem. We are now using

$$F(\zeta) = \tanh \zeta,$$

$$\eta_0(\zeta) = \eta_\infty \cosh^2 \zeta$$

to represent the unperturbed configuration.

The function $\eta_1(\zeta, t)$ is obtained by substituting Eq. (2') into Eq. (1'). Keeping only zero- and first-order terms, we have

$$\frac{\partial \eta_1}{\partial \tau} = -\beta \frac{d\eta_0}{d\zeta} w. \qquad (3')$$

We specify $\eta_1(\zeta, 0)$ and use (3') to solve for $\eta_1(\zeta, \tau)$.

---

[1] Harold P. Furth and John Killeen, in Controlled Thermonuclear Research Quarterly Report, UCRL-9777, Aug. 1961, p. 91.

[2] John Killeen and Harold P. Furth, Bull. Am. Phys. Soc. Ser. II 6, 309 (1961).

The RIPPLE code has been modified for these changes and new results have been obtained which will be presented in a forthcoming report.

A more general theory has been developed for studying current-driven hydromagnetic instabilities due to finite conductivity in a plane current layer. For a current layer specified by

$$B_{x0}(y)\,\hat{x} + B_{z0}(y)\,\hat{z} \qquad (4')$$

and a perturbation

$$B_y = B_0\,\psi(\zeta, t)\,\exp[i(k_x x + k_y z)],$$

one obtains exactly the same equations as before, with the function F now to be interpreted as

$$F = (B_{x0}\,k_x + B_{z0}\,k_z)(B_0 k)^{-1}, \qquad (5')$$

$$k = (k_x^2 + k_z^2)^{1/2}.$$

The time dependence can be eliminated, as before, by substituting

$$\psi(\zeta, t) = \phi(\zeta)\,\exp[p(t/\tau_A)].$$

From this formulation one can derive the tearing instability, as was done earlier.[1] In addition there are short-wave flute-like instability modes in the vicinity of $F = 0$. These flutes occur near the point $F = 0$, where they match the pitch of the field, but they are slightly shifted to one side. Modes of this type are probably responsible for the small-scale flute-like instabilities which drive the plasma from the current layer in experimental pinches. The "magic number" phenomenon in Zeta can also be explained in these terms: the pitch of the current-driven flute must differ slightly from that of the central magnetic field in Zeta if the instability is to grow. Therefore when the central field lines just match up around the torus the flute just fails to match up, and is therefore inhibited. If this interpretation is correct, the points of worst instability in Zeta should occur at currents just below the "magic-number" values.

The computational code developed to handle the tearing instability is readily adaptable to the general type of resistive instability in the current layer, so that a technique now exists for assessing stability against all modes and of studying the modes that are unstable.

6. SPATIAL DISTRIBUTION OF ELECTRONS TRAPPED BY THE GEOMAGNETIC FIELD

John Killeen

The spatial distribution of electrons injected into the geomagnetic field from the beta decay of cosmic-ray-produced neutrons leaking out of the atmosphere has been calculated. There is available an IBM 709 code called APPLE[1] which has been used to calculate the densities of particles trapped by the geomagnetic field for both natural and artificial sources. Two loss processes are considered. Particles can be lost by multiple small-angle Coulomb scattering changing the pitch angle so that particles eventually hit the atmosphere. The other loss mechanism is the slowing down of electrons by near collisions with thermal electrons in the exosphere. For particles with mirror points at high altitudes this is the dominant loss. The results are compared with some observed spatial distributions of electrons and are presented in two papers published recently.[2, 3]

[1] J. Killeen and G. Boer, Bull. Am. Phys. Soc. II, 5, 312 (1960).

[2] W. N. Hess, J. Killeen, C. Y. Fan, P. Meyer, and J. A. Simpson, J. Geophys. Research 66, 2313 (1961).

[3] W. N. Hess and J. Killeen, J. Geophys. Research 66, 3671-3680 (1961).

7. MAGNETIC SHOCKS

Stanley A. Zwick and D. E. Gonzales

Results obtained for the zero-temperature magnetic pulse problem for positive and negative particles of equal mass have been described in previous reports.[1, 2] On the basis of these, one may expect that the counterpart problem--involving the motion of particles of widely differing mass--may lead to similar loop trajectories for the heavy ions. In particular, we may note that in the plasma rest frame, loops correspond simply to the motion of particles at longitudinal speeds in excess of the pulse velocity. Since well-behaved solutions can be obtained for pulse strengths up to an including the critical case, there should be no reason why an increase of the overall stress (electromagnetic plus material) will not cause the ions to travel somewhat faster, at the center of the pulse, than the pulse itself.

To simplify the problem for numerical work, we are considering the motion of the light particles to be purely adiabatic, so that in effect these particles have vanishing mass. They are then constrained to move longitudinally with the magnetic flux lines, and hence cannot display looping

[1] Stanley A. Zwick, in Controlled Thermonuclear Research Quarterly Report, UCRL-9243, p. 103.

[2] Stanley A. Zwick, in Controlled Thermonuclear Research Quarterly Report, UCRL-9777, Aug. 1961, p. 108.

behavior. The equations of motion for the heavy particles (ions) are integrable in closed parametric form in regions where no looping occurs, and the solutions show--as for the equal-mass problem--that the critical pulse speed is Mach 2. Unlike the equal-mass case, a strong longitudinal electric component is present because of the separation of charge. This tends to dominate the interactions outside the loop region, but inside the region it is expected that magnetic effects will become important.

A computer code (IBM 650) for integration through the loop region is now in preparation, and should shortly be put into operation.

8. ATOMIC SCATTERING

Marvin H. Mittleman

The numerical calculations of the elastic and inelastic scattering of protons by atomic hydrogen mentioned in the preceding report[1] have been completed. The results are now being compiled.

The general theory of rearrangement collisions has been developed further[2] to include the effects of excited states and the Pauli principle. The latter effect is probably an important one. The formalism is being applied to the problem of charge exchange of an ion in a heavy gas.

[1] Marvin H. Mittleman, in Controlled Thermonuclear Research Quarterly Report, UCRL-9777, Aug. 1961, p. 103.

[2] M. H. Mittleman, Formal Theory of Rearrangement Collisions, UCRL-6674-T, Oct. 1961.

9. THE EFFECT OF CHARGE SEPARATION ON NONLINEAR WAVES IN A COLLISION-FREE PLASMA

Fred A. Wolf

The problem of a stationary nonlinear wave in a dilute (collisionless) singly ionized plasma immobilized by an applied magnetic field has been investigated by several authors.[1-7] The purpose of these investigations has

[1] J. H. Adlam and J. E. Allen, Phil. Mag. 3, 448 (1958).

[2] L. Davis, R. Lüst, and A. Schlüter, Z. Naturforsch. 13a, 916 (1958).

[3] A. Baños, Jr., and R. Vernon, Nuovo cimento 15, 269 (1960).

[4] Russell Vernon, Large-Amplitude Waves in a Collision-Free Plasma (Ph. D. Dissertation), UCLA, 1960.

[5] M. H. Mittleman (Lawrence Radiation Laboratory), private communication.

[6] R. Z. Sagdeev, Plasma Physics and the Problem of Controlled Thermonuclear Reactions, IV (Pergamon Press, Ltd., New York, 1960) p. 454-460.

[7] H. W. Wyld, Jr., Space Technology Laboratory Report GM-TR-0165-00486 (1958).

been to examine the possibility of the existence of a shock wave in the absence of particle collisions, by studying the structure of nonlinear waves which exist on a characteristic scale that is smaller than the mean free path by several orders of magnitude. The solutions presented in these earlier papers consisted of periodic waves and solitary symmetric pulses propagating perpendicular to the applied field of magnetic induction.

Several assumptions or restrictions were utilized by these authors to obtain solutions. In the first papers to appear in the literature (Adlam and Allen;[1] Davis, Lüst, and Schlüter[2]) two assumptions were employed. The first was that the thermal or random energies of the particles were negligible in comparison with the magnetic field energy and inertial energy (i.e., $\beta = 0$). The second assumption was that the numerical difference between the charge densities of ions and electrons was negligibly small in comparison with either the ion or electron charge density, but that the longitudinal electric field produced by this charge separation was not. This is called quasi charge neutrality.

When these assumptions were employed the solutions obtained consisted of periodic waves[2] and nonlinear pulses[1-2] only so long as the phase velocity did not exceed a certain critical velocity. In terms of the Alfvén Mach number the critical velocity corresponds to Mach 2.

In the next papers to appear (Baños and Vernon,[3] Vernon[4]) the plasma had finite isotropic pressure perpendicular to the magnetic field but still was assumed quasi-charge-neutral. The characteristic behavior of the solution for this case was essentially the same as in the previous solutions for the cold plasma.[1-2] However, the charge-separation electric field was discontinuous when the pulse was propagating at the upper limit of Alfvén Mach number, indicating the presence of a positive charge layer at the pulse center. The discontinuity disappeared as the plasma pressure approached zero.

Employing the assumption of adiabatic electrons (guiding-center electron fluid) and cold ions, the next group of authors[5-7] obtained solutions which appeared discontinuous only for Alfvén Mach numbers in excess of 2, but otherwise quite similar to the previously obtained solutions.[1-4] Quasi charge neutrality was not assumed in these solutions.

To investigate the physical significance of the appearance of an upper bound or critical Mach number and the obvious violation of charge neutrality which occurs at the upper bound when the plasma is "hot," we have considered two plasma models. In the first model we considered a one-dimensional plasma free from magnetic interaction. Here, of course, in the absence of collisions the only forces felt by the particles were the collective charge-separation forces. The solutions found consisted of solitary pulses and periodic waves which are connected to the pulses if dissipation is introduced, in which case a stationary shock is obtained. The upper limit of Mach number in these solutions arises at the onset of "trapped" or restricted ion trajectories. Only so long as the minimum ion energy is greater than the maximum electrostatic potential energy do stationary solutions exist. The upper bound for the Mach number then marks the boundary where these energies are equal (i.e., where the least energetic ions just come to rest at the top of the potential hill at the pulse center).

In the second plasma model we re-examined the solutions obtained previously[1-7] for a plasma in a magnetic field, only we did not neglect the plasma pressure or the charge separation. We found that the solutions with charge separation and plasma pressure differed insignificantly from those previously obtained. The outstanding exception was the behavior of the longitudinal electric field, which we found was well-behaved and continuous for waves propagating at the upper limit of Alfvén Mach number.

The appearance of a discontinuity for solutions at critical Mach number[3] and above[6-7] was attributed to the fact that stationary solutions are possible only if the ions in the wave are energetically capable of climbing the charge-separation-produced electrostatic potential. Maintaining that the solutions are stationary, and allowing ions with energies less than the maximum electrostatic potential energy, produces the discontinuity in the electric field because the ions cannot climb the potential hill and are not allowed to reflect from it. Consequently, they are carried along by the wave at the peak potential as a snowplow carries snow.

Further details are to be found in a forthcoming UCRL report.[8]

10. THE MAGNETIC COMPRESSION OF A FULLY IONIZED GAS

John Fletcher and John Killeen

A new code called PLASMA II has been written for the IBM 7090 which solves the magnetohydrodynamic equations of a fully ionized gas in an axially symmetric magnetic field. The model is a two-fluid model in the sense that the electrons and ions can have different temperatures. Ohmic heating is confined to the electrons; the resistivity is anisotropic and a function of the electron temperature. Shock heating applies to the ions and an artificial viscosity is used. Thermal conductivity is included in both the ion and electron energy equations. Two components of the magnetic field are included, B_z and B_θ. The problem is one-dimensional, i.e., all the dependent variables are functions of r and t only. The differential equations are in Lagrangian form. The solution of the differential equations is accomplished by the solution of a system of implicit difference equations. The code permits a wide range of boundary conditions. We can allow plasma to be emitted from the outer boundary. We can consider either a hollow cylinder or hard-core geometry. A coupling between the plasma equations and the external circuit equations is included. The program is written in Fortran language and is therefore suitable for use on any computer that interprets Fortran and has sufficient storage.

---

[8] Fred A. Wolf, The Effect of Charge Separation on Nonlinear Waves in a Collision-Free Plasma, (Thesis), UCRL-6700 (in preparation).

11. ENERGY TRANSFER BETWEEN ELECTRONS AND IONS IN A PLASMA

John Killeen

The study of energy transfer by means of the numerical solution of the Fokker-Planck equation has continued. In the earlier work reported[1] the ions were hot, as in a high-energy injection scheme, and the energy transfer to cold electrons was calculated by the numerical solution of the F-P equation for the electron distribution function. In the work reported now we start out with the ions and electrons at the same energy--about 1 kev. At this temperature the electrons are heated up by 3.6-Mev α particles from fusion events.[2] We wish to find the energy transfer from the electrons to the ions. We assume that the electrons remain Maxwellian and that their temperature is a given function of time. If the ions are assumed to be Maxwellian then the expression on page 80 of Spitzer[3] is a first-order differential equation for the ion temperature $T_i(t)$, where $T_e(t)$ is given. An IBM 650 code called GAIN has been written and used for obtaining $T_i(t)$ for various functions $T_e(t)$. It is of interest, however, to solve for the energy transfer in the case in which the ion distribution function is not necessarily Maxwellian. In fact it is important to know the ion distribution function. The equation for the ion distribution function is

$$\frac{\partial f_+}{\partial t} = \frac{\partial^2 f_+}{\partial x^2}\left[A(f_+, x, t) + k\,A(f_-, x, t)\right]$$

$$+ \frac{\partial f_+}{\partial x}\left[B(f_+, x, t) + k\,B(f_-, x, t) + k\,\frac{M-m}{m}\,\frac{2}{x^2}\int_0^x f_- y^2\,dy\right]$$

$$+ 2 f_+\left[f_+ + k\,\frac{M}{m}\,f_-\right],$$

where

---

[1] J. Killeen, W. Heckrotte, and G. Boer, Energy Transfer from Hot Ions to Cold Electrons in a Plasma, I. A. E. A. Conference on Plasma Physics and Controlled Nuclear Fusion Research, Salzburg, 1961, Paper 151 (UCRL-6383).

[2] R. E. Kidder, Range and Energy Loss of 3.6-Mev α particles in a Plasma, Lawrence Radiation Laboratory Memorandum, Nov. 2, 1961.

[3] L. Spitzer, Physics of Fully Ionized Gases (Interscience Publishers, Inc., New York, 1956).

$$A = \frac{2}{3}\left[\int_x^\infty f\, y\, dy + \frac{1}{x^3}\int_0^x f\, y^4\, dy\right],$$

$$B = \frac{4}{3x}\left[\int_x^\infty fy\, dy + \frac{3}{2x}\int_0^x f\, y^2\, dy - \frac{1}{2x^3}\int_0^x f\, y^4\, dy\right],$$

and $x = v/v_0$, and k is a constant determined from the initial conditions and depends on the density. If we keep the electrons Maxwellian with temperature $T_e(t)$, a given function of time, then we have

$$f_-(x,t) = a(t)\, e^{-\beta(t)x^2}$$

where $a(t)$, $\beta(t)$ are given. In this case

$$A(f_-, x, t) = \frac{a(t)}{2[\beta(t)]^2\, x^2}\left[-e^{-\beta x^2} + \frac{1}{x}\int_0^x e^{-\beta y^2}\right],$$

$$B(f_-, x, t) = \frac{a(t)}{\beta(t)\, x^2}\left[\frac{1}{2\beta x}\, e^{-\beta x^2} + \left(1 - \frac{1}{2\beta x^2}\right)\int_0^x e^{-\beta y^2}\right].$$

The Fokker-Planck equation code DION[1] can be used to solve for $f_+(x,t)$. We then obtain the energy gain of the ions and the distribution function. Results of these calculations are to be presented in a separate report.

12. THE BUMPY TORUS IN THREE DIMENSIONS

Norris W. Hetherington and C. H. Woods

Investigation of single-particle and plasma behavior in the Bumpy Torus divides quite naturally between two configurations.

(a) If the injection problem is ignored, the first configuration is the N-coil torus comprising N equally spaced coils of radius a, with centers lying on a circle of radius R.

(b) Introducing the injection problem, we have the split-coil torus formed by removing one of the N coils and substituting in its place two somewhat closely spaced coils having specially chosen current, size, location, and orientation.

Eight separate computing programs have been used to study these configurations.[1] For either arrangement the information available is as follows:

1. Particle trajectories are computed from the equations of motion by a program which gives also the guiding-center trajectory, the transverse invariant $p_\perp{}^2/B$, and the (more nearly constant) transver invariant $p_{\perp c}{}^2/B_c$, where the subscript c refers to quantities evaluated at the guiding center.

All particle trajectories have been computed with parameters so chosen that the nominal value of gyro radius is 10% of the coil radius a. For a particle traversing the N-coil torus, or oscillating with large amplitude between two coils, $p_{\perp c}/B_c$ may vary as much as 10% while the particle traverses ten coils or experiences ten reflections.[2]

Particles injected at the appropriate location in the split-coil torus behave qualitatively as originally predicted for this method of injection. Although the parameters originally chosen for the split-coil section turned out not to be optimum, other parameters involving a slightly larger pair of coils are considered to be close to optimum.

2. The vector magnetic potential has been made available for future study of drift velocity and drift-surface diffusion.

3. The stability integral $\int \frac{d\ell}{B}$ has the same general properties for the Bumpy Torus as for the axially symmetric two-coil mirror configuration.

4. The longitudinal invariant $\int p_\parallel \, d\ell$ behaves differently from that of the mirror machine. Whereas surfaces of constant $\int p_\parallel \, d\ell$ for the latter intersect the plane of symmetry along circles, the corresponding intersections in the case of the N-coil torus are approximately circular only for certain values of the transverse invariant. For other values of this invariant the intersections are horseshoe-shaped.[3]

---

[1] IBM 7090 computer program by Elizabeth DeGraw.

[2] Ernest P. Gray and Irvin M. Miller, Numerical Trajectory Analysis of Charged Particle Confinement in a Cusped Geometry, Report CPR-010, Applied Physics Laboratory, The Johns Hopkins University, Dec. 7, 1961.

[3] A. I. Morozov and L. S. Solov'ev, Zhur. Tekh. Fiz. 30, 261 (1960).

For the N-coil torus there are N midplanes each containing the axis of symmetry of the torus and lying midway between adjacent coils. For the particular values N = 64 and R/a = 21.76 the curves of Figs. V-5 through V-8 represent intersections of various surfaces of constant J with any midplane. Here

$$J = \frac{1}{ap} \oint p_{\parallel} \, d\ell = \frac{1}{a} \oint \sqrt{1 - \mu B/B_0} \, d\ell$$

is the dimensionless longitudinal invariant, r and z are cylindrical coordinates (z coincides with the axis of the torus), $\mu = B_0 p_{\perp}^2 / B p^2$ is the dimensionless transverse invariant, B_0 is the nominal magnetic field defined as the field at the ring axis of a smooth torus carrying the same total current as the N-coil torus, p is the momentum of the particle, and the element of length $d\ell$ is taken along a line of force. The particular values chosen for N and R/a yield relative positions of adjacent coils which are similar to the coil positions used in certain of the tilted-coil β-ray experiments. For these same parameters the values of J were already known in the plane of symmetry (S plane), and for z/a = 0 the values given in Figs. V-5-8 correspond to the values previously reported.[4]

In the adiabatic theory, points where the integrand $\sqrt{1 - \mu B/B_0}$ vanishes are said to be turning points for the particle. In calculating J, the integral is performed over only one-quarter cycle--that is, from a midplane to the first turning point, or, if the integrand does not vanish, to the plane of the next coil.

Those curves and portions of curves which cross flux lines that involve turning points have been drawn dashed. Thus, the dashed curves indicate oscillation within one section, and the solid curves indicate traversal of the entire torus. Since both μ and J are supposed to be constants for sufficiently small orbits, the guiding center of a particle can penetrate a midplane only at a point that lies on a J = constant curve. It should be observed that a particle which is initially traversing the torus may not continue to do so even though the guiding center follows the proper curve. For example, for μ = 0.6 and J = 0.67, the particle may initially be traversing the torus near the ring axis, and after drifting some distance along the solid portion of the curve it can reach a dashed portion and become trapped between two coils. Later it may once again start to traverse the torus in either direction. This sort of behavior has been found in the computed trajectories.

Although for the orbit sizes involved in the computed trajectories the value of μ does not remain constant long enough for the particle to drift completely around one of the J = constant curves, the direction of guiding-center drift has been determined for a number of points. The directions observed, and other deductions involving the magnetic field gradient, are consistent with the following hypothesis: For coil currents flowing in the +z direction inside the ring axis, the general direction of guiding-center drift is in the counterclockwise direction. An exception to this rule occurs on the short closed curves in the neighborhood of μ = 0.7, J = 0.6, where the direction of drift is clockwise.

---

[4] G. Gibson, W. C. Jordan, and E. J. Lauer, Lawrence Radiation Laboratory Rept. UCID-4241, Feb. 1961 (unpublished).

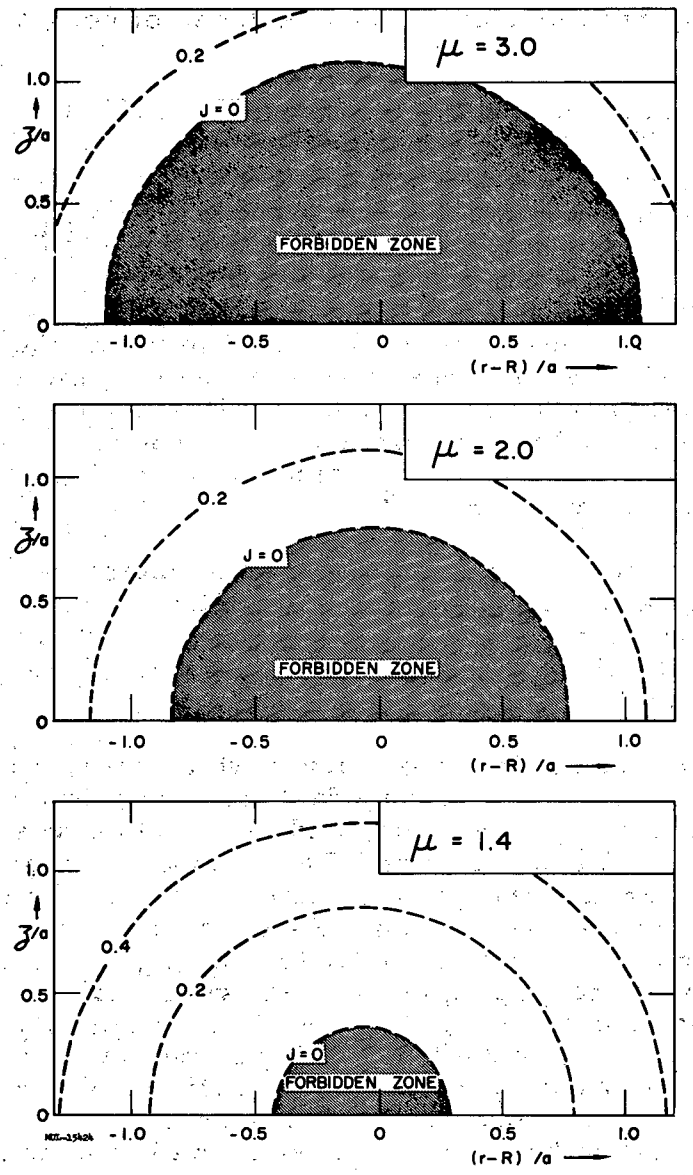

Fig. V-5. Intersections of surfaces of constant J with any mid-plane, drawn for N = 64 and R/a = 21.76; μ = 3.0, 2.0, and 1.4.

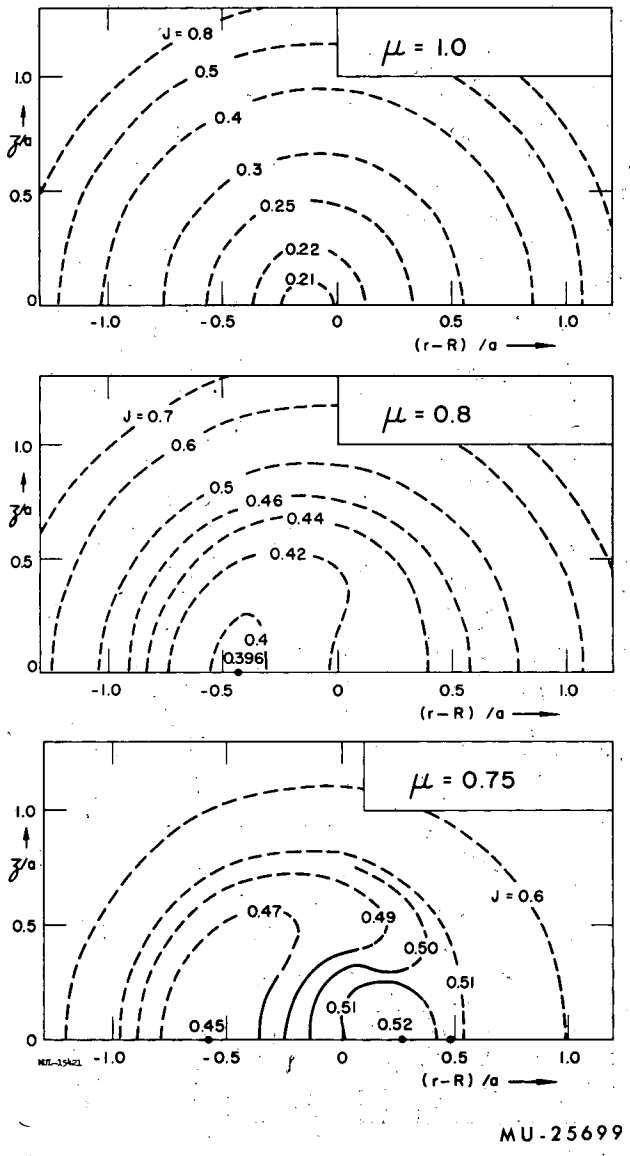

Fig. V-6. Intersections of surfaces of constant J with any mid-plane, drawn for N = 64 and R/a = 21.76; μ = 1.0, 0.8, and 0.75.

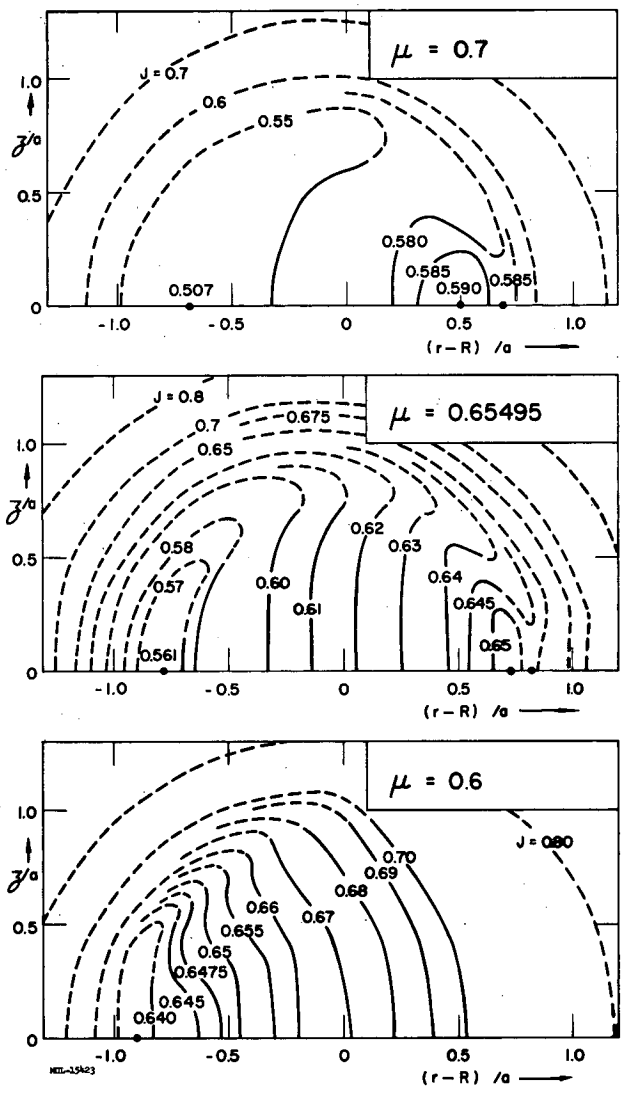

MU-25677

Fig. V-7. Intersections of surfaces of constant J with any mid-plane, drawn for N = 64 and R/a ≈ 21.76; μ = 0.7, 0.65495, and 0.6.

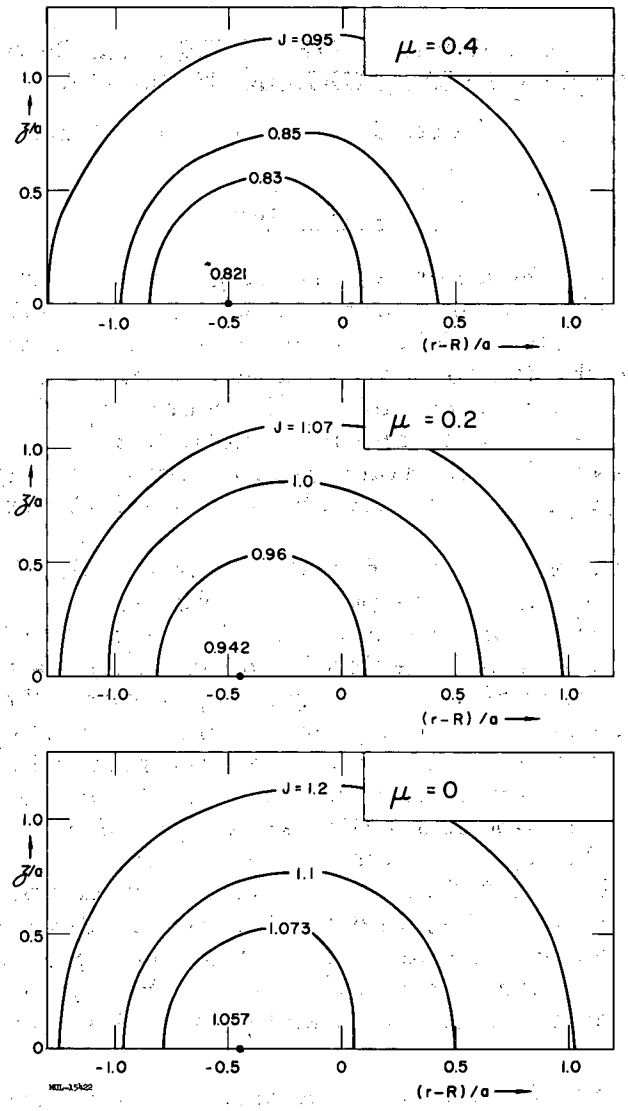

MU-25678

Fig. V-8. Intersections of surfaces of constant J with any mid-plane, drawn for N = 64 and R/a = 21.76; μ = 0.4, 0.2, and 0.

For μ larger than 1.2 there exists a forbidden zone in the figures, and a corresponding forbidden flux tube, in which the value of μ is incompatible with the magnetic field and cannot correspond to real values of J.

13. CONTAINMENT OF POSITRONS IN AN ASYMMETRIC MIRROR GEOMETRY

Gordon Gibson,* Willard C. Jordan,† and Eugene J. Lauer

I. Introduction

In a static axially symmetric mirror geometry the guiding center of a charged particle drifts in the azimuthal direction about the axis as it moves along a line of force. The extension of the guiding center's precessional surface along the line of force may be determined under the adiabatic assumptions from the invariance of $p_\perp^2/B$, where $p_\perp$ is the component of momentum transverse to the magnetic induction, $\vec{B}$. The motion and containment time of energetic positrons from a radioactive gaseous source (Ne^{19}) in a symmetric geometry have been extensively studied.[1,2]

When an asymmetry is introduced, the longitudinal invariant,[3,4,5] $J = \oint p_\parallel \, d\ell$ (where $p_\parallel$ is the component of momentum parallel to the field, $d\ell$ is an element of path length parallel to the field, and the integral is carried out over a longitudinal period of the motion), is also useful in locating the precessional surface of the guiding center. The magnetic-field geometry that results from rotating the two mirror coils through equal angles but in opposite directions from their symmetry locations has been studied theoretically and experimentally similarly to the symmetric geometry. The rotations are about parallel axes each of which lies in the plane of a coil and passes through the center of the coil. This corresponds to one section of a Bumpy Torus.[6] There are two symmetry planes, the S plane, containing the axes of the coils, and the I plane, midway between the coils. Figure V-9 illustrates the geometry for a tilt angle ϕ of $2\pi/64$ (or 5.6°) between the coils. The ring axis is defined as the circle drawn in the S plane through the centers of the coils and centered at the line of intersection

*Westinghouse Electric Corporation, Atomic Power Dept., Pittsburgh, Pa.

†The Bendix Corporation, Research Labs. Div., Southfield, Mich.

[1] G. Gibson, W. C. Jordan, and E. J. Lauer, Phys. Rev. Letters 5, 141 (1960).

[2] G. Gibson, W. C. Jordan, and E. J. Lauer, The Behavior of Positrons in Static Axially Symmetric Magnetic Mirror and Cusp Geometries, UCRL-6771 (in preparation).

[3] M. N. Rosenbluth and C. L. Longmire, Ann. Phys. 1, 120 (1957).

[4] B. B. Kadomtsev, in Plasma Physics and the Problem of Controlled Thermonuclear Reactions (Pergamon Press, Ltd., New York, 1959) Vol. III, page 340.

[5] T. G. Northrop and E. Teller, Phys. Rev. 117, 215 (1960).

[6] G. Gibson, W. C. Jordan, and E. J. Lauer, Phys. Rev. Letters 4, 217 (1960).

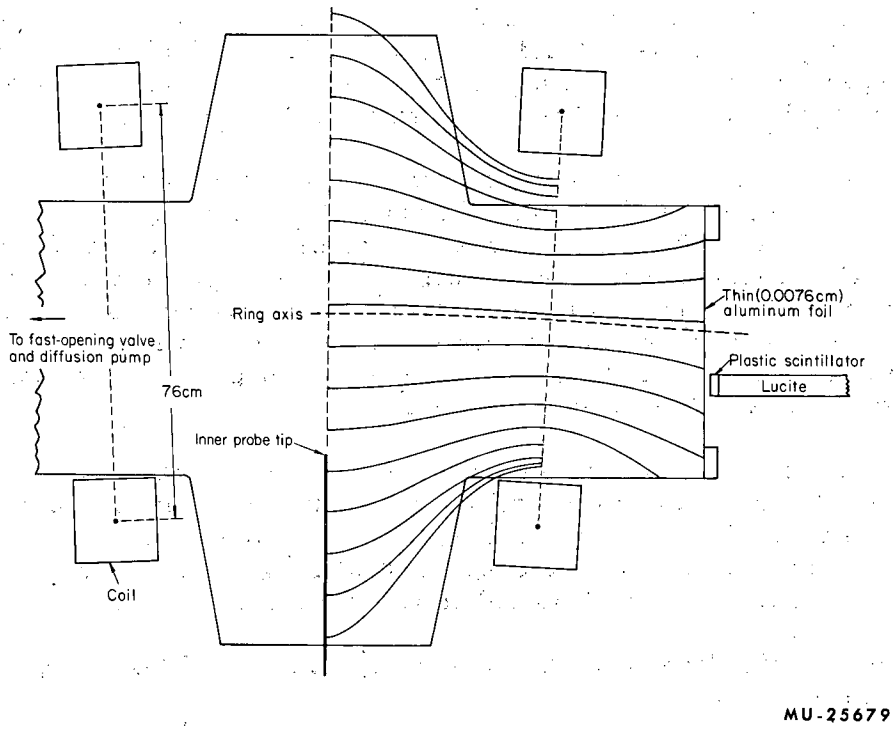

Fig. V-9. Apparatus and magnetic flux lines, 5.6° angle between coils.

of the planes of the coils, i. e., at the major axis. The flux lines in the S plane are shown for the idealized case in which the coils are replaced by circular current loops having radii equal to the mean radius of the coils. The intersections of the precessional surfaces (surfaces of constant J and $p_\perp^2/B$) with the line formed by the intersection of the orthogonal planes S and I may be obtained from Fig. V-10, which gives the calculated values[7] of J along this line. Experimental studies of the motion of charged particles in an asymmetric geometry test the validity of the longitudinal invariant.

An interesting prediction may be made from the calculations of the precessional surfaces, viz. drift-surface diffusion results in a motion of particles across lines of force that does not occur in the degenerate symmetric geometry (see Refs. 6 and 7). This drift-surface diffusion has been observed experimentally[7] by studying the effects of stationary probes on the current of particles escaping through a mirror.

In this paper are presented results of further experiments carried out in the asymmetric geometry. The effects of fast-moving probes on the trapped particles that remain after the source has been removed are observed. In this manner the instantaneous radial distribution of particles may be determined. Furthermore, the transient effects of inserting and withdrawing probes have been observed on the current of escaping particles. As a result, a rather comprehensive picture of the behavior of particles in this particular asymmetric geometry has been obtained.

A model which is consistent with the numerical calculations and the experimental observations (for a tilted coil mirror geometry consisting of one cell of a Bumpy Torus, with approx 0.5-Mev positrons having a mean containment time of a few seconds as limited by gas scattering, and $B \approx 1300$ gauss on the ring axis in the I plane) is the following:

1. The particles behave adiabatically (i. e., $p_\perp^2/B$ and $\oint p_\parallel \, d\ell$ are conserved) between collisions.

2. Drift surfaces with turning points near the mirrors (type E) are displaced inwards toward the major axis; the others having turning points nearer the midplane (type M) are nearly centered just inside of the ring axis (approx 0.1 mean coil radius inside for $\phi = 2\pi/64$).

3. Small-angle scattering steps dominate over large steps.

4. The mean containment time of particles as limited by scattering on E-type drift surfaces is much shorter than for those on M-type surfaces because fewer steps are required for loss starting from the E type than when starting from the M type.

---

[7] G. Gibson, W. C. Jordan, and E. J. Lauer, Containment of Positrons in an Asymmetric Mirror Geometry, UCRL-6380, May 1961, and G. Gibson, W. C. Jordan, and E. J. Lauer, in Proceedings of IAEA Conference on Plasma Physics and Controlled Nuclear Fusion Research, Salzburg, Austria, September 1961, paper CN-10/175.

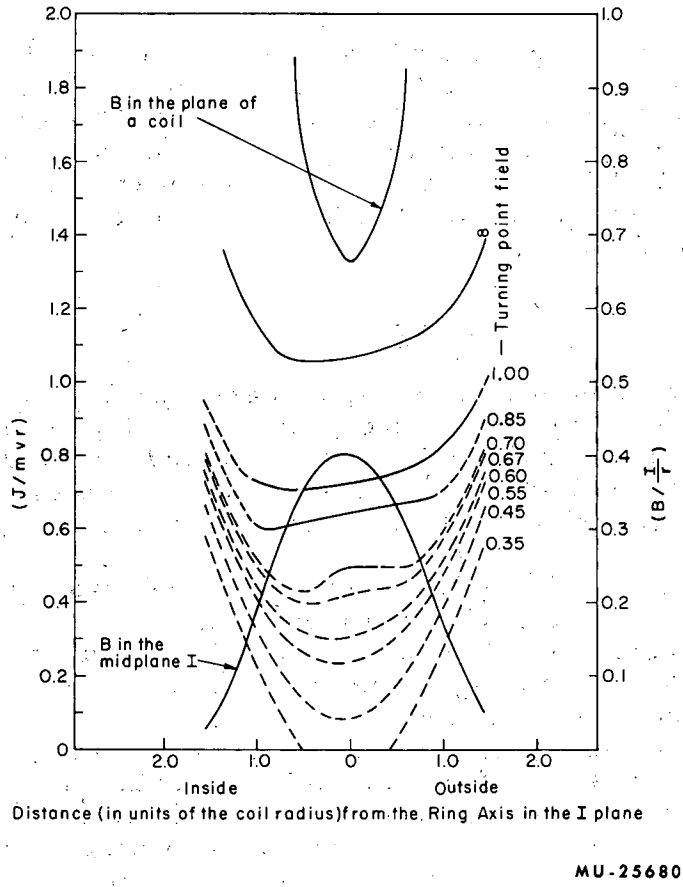

Fig. V-10. Adiabatic invariants and field magnitudes (B) for a tilt angle of 5.6° between coils and a coil spacing of 2.13 MCR. For each of the curves of J versus distance from the ring axis in the I plane, $p_\perp/B$ is a constant; p = mv = momentum, r = coil radius, and I = amperes per coil. The dashed lines indicate that the particle's turning point is inside the mirrors; the solid lines indicate that the particle escapes through a mirror.

5. It follows that if a particle's guiding center is on an M-type surface it remains on M-type surfaces for nearly all of its containment time. It diffuses very little while on the M-type surfaces. However, when the particle's pitch angle changes sufficiently because of scattering so that the particle makes excursions near the mirrors (E-type surfaces) a rapid drift-surface diffusion across field lines occurs and the particle soon penetrates a mirror and escapes.

6. For the isotropic, uniform volume source used in this experiment the steady-state number of particles on the E-type surfaces is much smaller than on the M-type (this is expected because of 4). Therefore the flow of particles inwards towards the major axis is greater than outwards. (It is worth pointing out that in a Bumpy Torus the number of particles on the different types of drift surfaces would be expected to be more nearly equal, since there is no end loss).

II. Apparatus

The apparatus used for these experiments has been described in detail previously.[1, 2, 7] Figure V-9 shows the apparatus schematically. For the data presented a tilt angle of 5.6° was used and the field in the I plane on the ring axis was about 1300 gauss unless otherwise specified. The mean radius of the coils (MCR) was 38 cm. Some general features are repeated here for clarity:

a. A current of Ne^{19} (β^+, $\lesssim 2.2$ Mev) may be fed into the containment region to provide a source of charged particles.

b. A liquid-nitrogen-cooled surface on which Ti is deposited maintains a pressure of $< 1 \times 10^{-7}$ mm Hg in the closed vacuum chamber without pumping on the chemically inert Ne.

c. A fast-opening valve (gate moves 50 cm in 0.04 sec), when closed, isolates the vacuum chamber from an 80-cm oil diffusion pump; if suddenly opened, the source gas is removed with an e-fold pumpout time of 0.5 sec.

d. Stable Ne, which serves as a known background gas, may be introduced at any desired partial pressure in such a manner that the pressure is very nearly independent of the position of the fast-moving valve.

e. A thin (0.076 mm) elongated aluminum foil window (30 cm long measured in the S plane, and 5 cm wide perpendicular to the S plane) is in the end of the vacuum chamber; energetic positrons may pass through this foil and strike a plastic scintillator; a 120-cm lucite light pipe provides an optical connection between the scintillator and a 14-stage photomultiplier tube; electronic circuitry yields the time analysis of the detected positrons, whose energy lies in some selected energy interval. For the data presented positrons at 0.50 ± 0.15 Mev (window width plus counter resolution) were detected if not otherwise specified.

f. Two fast-moving probes (move 45 cm in approx 0.1 sec) may be inserted along the line of intersection of the S and I planes; the "inner" probe lies within and the "outer" probes lies outside the ring axis; the instantaneous position of a probe is determined by means of a slide-wire arrangement; the electronic circuitry can provide for the counting rate to be taken as a function of a given probe's position. Two other stationary probes may be inserted in the I plane at right angles to the fast-moving probes.

Particular features of the apparatus which are unique to each experiment are given along with the description of the experiment.

III. Experimental Results

A. Steady-State Measurement; Stationary Probes, Point Detector

Let us first review the results obtained earlier.[7] It can be predicted that as a trapped positron's velocity vector is altered owing to multiple scattering the particle tends to move in a net inward direction before escaping through a mirror. This is due to the asymmetry of the precessional surfaces. Experiments were carried out under steady-state conditions, i.e., Ne^{19} was allowed to flow into the vacuum chamber (fast valve was kept closed) until a steady-state condition was reached, at which time just as many positrons were being trapped as were escaping. Essentially a point counter (the sensitive area of the scintillator was 3.8 cm in diameter) was used to detect the escaping current of positrons. The procedure was as follows: a valve in the source line was closed after a steady-state condition had been reached; the number of positrons striking the scintillator during a 10-sec time interval was recorded; to normalize the data the field was turned off, and at a fixed time after the initial measurement had been made the number of positrons striking the scintillator during 27 sec was recorded. This count is proportional to the Ne^{19} density. For various counter positions the counting rate was obtained in this manner as a function of the position of each probe. For large distances from the ring axis a probe had no effect on the counting rate. As the probe approached the ring axis some of the trapped particles were removed and the counting rate was reduced. Once the trapped fraction that the counter normally detected was removed, moving the probe to a position nearer the ring axis had no further effect on the counting rate.

The following summarizes the observations and interpretations.

a. The current of escaping particles (all probes out) is greatest inside the ring axis. It approaches zero just outside the ring axis. (The detected particles escaped because of multiple scattering on the background gas.) At the time when the particles escape they are on the shifted E-type precessional surfaces.

b. The fraction of the current representing trapped positrons is intercepted by a probe at a considerable distance from the ring axis (RA). This distance is nearly independent of the counter's position (for counter positions in the range from the ring axis to about 0.4 MCR inside the RA). This is observed for tilt angles as small as 1°. This means that during its containment time a particle's guiding center explores all flux lines (owing to drift-surface diffusion) within a well-defined volume. The cross section of this volume in the I plane is approximately a circle. The diameter is approx 1 MCR for $\phi = 2\pi/64$. These results are independent of scattering gas pressure (over the range 10^{-6} to 10^{-4} mm Hg of Ne).

c. The inner probe removes the trapped fraction at a larger distance from the ring axis than the outer probe, and this inward shift increases with the tilt angle.

B. Fast-Empty Experiment

The remaining data presented were obtained from the fast-empty experiment. The procedure for this experiment is as follows.

a. With the fast valve closed and the field on, Ne^{19} flows into the containment region until the steady-state condition is reached.

b. A valve in the source line is closed, and the fast valve is opened.

c. Opening the fast valve triggers an analyzer which records the number of positrons within a selected energy interval that strike the scintillator as a function of the time.

d. To normalize the data the number of positrons striking the scintillator is recorded during a fixed time interval (10 sec) which occurs between the time the flow of Ne^{19} into the system is stopped and the fast valve is opened.

The counting rate drops suddenly upon the opening of the fast valve because of removal of the source gas. There follows a slower decrease due to the escape of the trapped component. Within the experimental uncertainty, this slower decay of the counting rate as a function of time may be fitted with a straight line on a semilog plot. The intercept of this straight line at zero time (time of opening the fast valve) is a measure of the trapped fraction. Mean containment times (taken from the slope of the straight line) of the order of seconds are observed when about 10^{-6} mm Hg of Neon is present as a scattering gas.

1. Stationary probes, point detector

Data were obtained previously from the fast-empty experiment also.[7] During a "run" each probe was held at a fixed position, and the effect on the escaping current of positrons as detected by the point counter was noted.

The slope (measure of containment time) was not appreciably affected by the probes, but the intercepts (measure of the remaining trapped fraction) did decrease as a probe's position penetrated the well-defined "containment" volume found from the steady-state experiment.

2. Fast-moving probes, point detector

This experiment was similar to 1 above, except that a probe was not left at a given position throughout the run; rather, the inner or outer probe was plunged in to a prescribed distance from the ring axis at some time during the run and then withdrawn at a later time. It should be pointed out that the time for a particle to precess once around a drift surface is short (order of magnitude of 10^{-6} sec) compared to the time (approx 0.1 sec) for probe motion. Figure V-11 gives the results for the case in which the inner probe plunges to various distances from the ring axis 4.5 sec after the fast valve has opened, and is withdrawn 7.5 sec later. The counter is located 0.27 MCR inside the ring axis. At least five runs were added for each curve. The 0.58-MCR data were plotted as recorded. The other curves were normalized to match the 0.58-MCR curve at zero time. The remaining data have not been normalized, but the rate of producing Ne during the time while a set of data was taken was held quite constant. The counting rate decreases suddenly as the probe is inserted and remains low during the time the probe remains in. When the probe is withdrawn the counting rate instantaneously

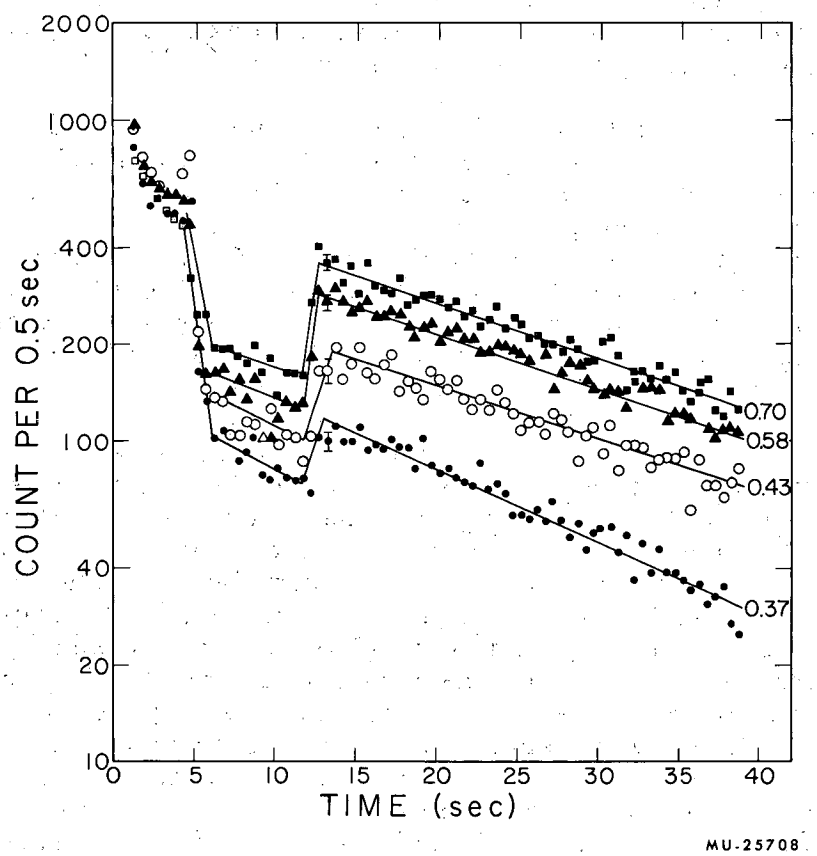

Fig. V-11. Effect of the inner probe on the escaping current of positrons detected with the scintillator located at 0.27 MCR inside the ring axis; 4.5 sec after the fast valve is opened (zero time) the probe moves in to various distances (0.70, 0.58, 0.43, and 0.37 MCR) from the ring axis, and is withdrawn 7.5 sec later.

(within the experimental resolution) increases, then decreases with the usual e-fold decay time characterizing the mean containment time as set by scattering. As the probe plunges closer to the ring axis the initial decrease in counting rate is greater; also, the remaining trapped fraction after the probe is removed is smaller. Figure V-12 shows the effect of varying the time interval during which the probe remains inserted.

Figure V-13 is a plot of the data obtained with the counter at 0.40 MCR inside the ring axis and the inner probe plunging to 0.37 MCR and 0.29 MCR from the ring axis. When the probe is inserted the counting rate increases and remains high. With the probe inserted the counting rate remains high because the probe is "in front of" the detector. That is, some positrons may scatter through a large angle in the probe and follow field lines that pass through the scintillator. When the probe is withdrawn the counting rate for the 0.37-MCR case decreases instantly and the remaining trapped positrons escape with the characteristic scattering-out time.

The data for the case in which the probe plunges to 0.29 MCR from the ring axis is especially interesting. In this case the tip of the probe is intercepting field lines closer to the ring axis than those passing through the scintillator. While the probe is in, the current of escaping positrons is primarily due to scattering from the probe tip. (Note that the counting rate is reduced relative to the 0.37 MCR case, as would be expected.) The important characteristic of this case, which should be emphasized, is the behavior just after the probe is retracted. The counting rate drops momentarily to a value near zero, then builds up over a detectable time interval (approx 1.5 sec) before decaying away in the usual manner. This particular behavior is observed with the inner probe and only when the probe is inserted to field lines closer to the ring axis than the counter. The buildup in counting rate is interpreted as a diffusion across field lines. This is probably drift-surface diffusion, but ordinary diffusion can not be ruled out. In principle this could be decided by measuring the dependence upon orbit diameter of the time to diffuse a fixed distance--the time for ordinary diffusion is proportional to $1/(\text{orbit diameter})^2$, whereas the time for drift-surface diffusion is less sensitive to orbit diameter. Summarizing:

a. When the inside probe tip is plunged to positions that are farther from the ring axis than the flux lines intercepted by the detector, the probe acts like a prompt shutter on part of the current of escaping particles--switching it promptly off when the probe goes in and promptly on when the probe is retracted. The particles that were intercepted by the probe would normally have hit the detector in less than 0.5 sec (analyzer width). These correspond to particles on E-type surfaces.

b. When the inside probe tip is plunged to a position that is closer to the ring axis than the flux lines intercepted by the detector a resolvable diffusion time is observed upon retracting it.

Figures V-14 to V-17 show the effect of inserting and withdrawing the outer probe. When the probe is plunged to 0.15 MCR from the ring axis most of the trapped fraction is removed and the counting rate drops instantly to a low value. For a given counter position, as the probe plunges to greater distances from the ring axis the decrease in counting rate is less. In fact (see Fig. V-17), the probe has little effect on the counting rate when it plunges to 0.58 MCR from the ring axis when the counter is on the ring axis or

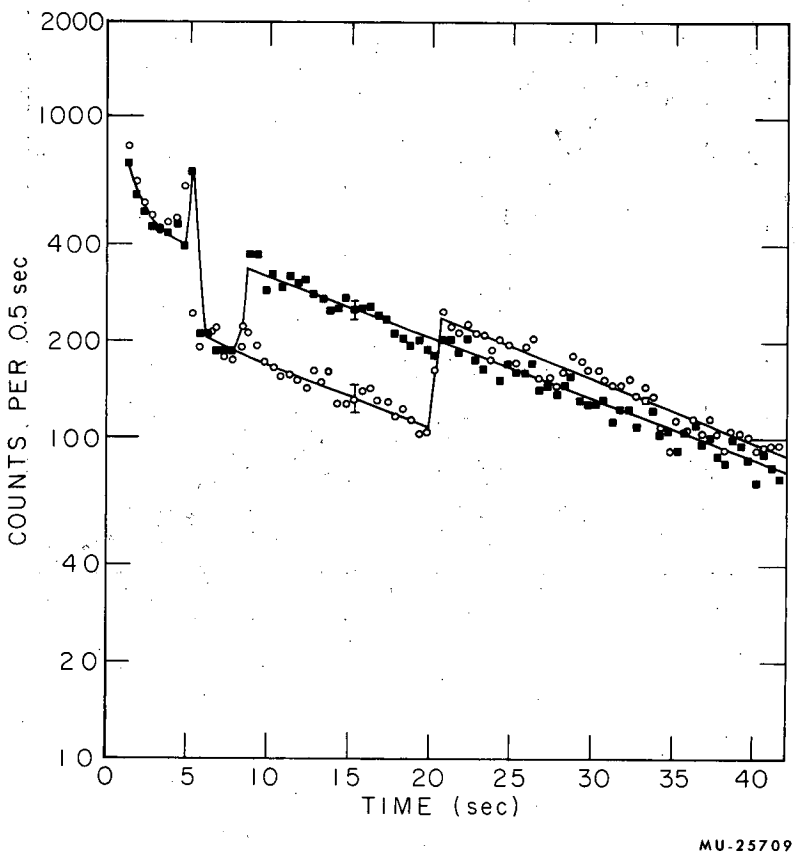

Fig. V-12. Inner probe plunging to 0.70 MCR from the ring axis 4.5 sec after opening the fast valve and withdrawn Δt sec later. The scintillator is located at 0.27 MCR inside of the ring axis. ■ Δt = 3.5 sec; O Δt = 15 sec.

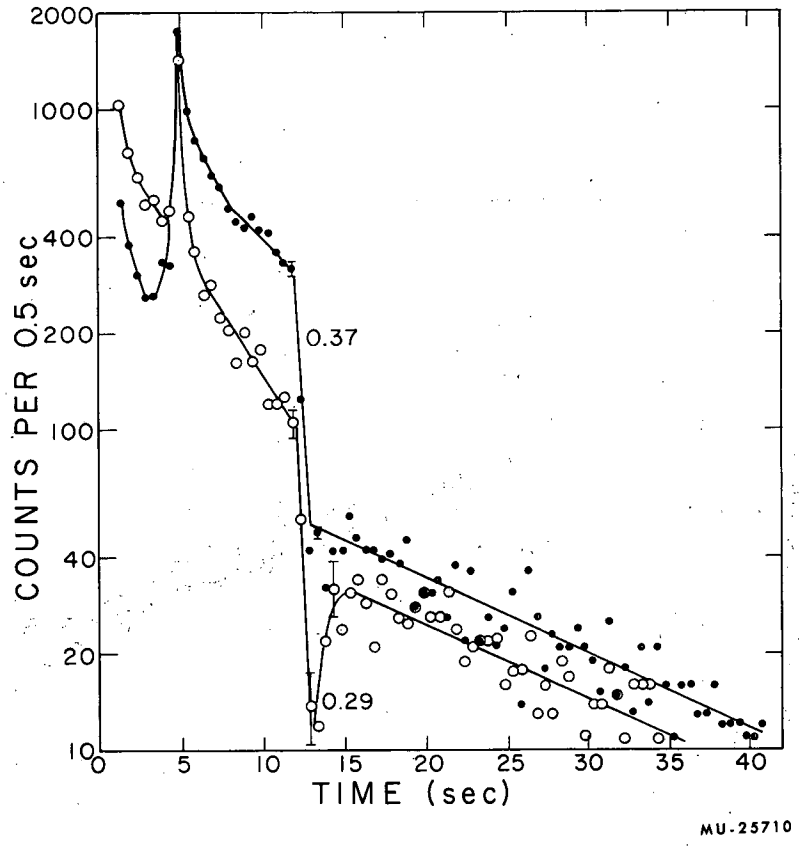

Fig. V-13. Effect of the inner probe on the escaping current of positrons detected with the scintillator located at 0.40 MCR inside the ring axis; 4.5 sec after the fast valve is opened (zero time), the probe moves in to various distances (0.37 and 0.29 MCR) from the ring axis, and is withdrawn 7.5 sec later.

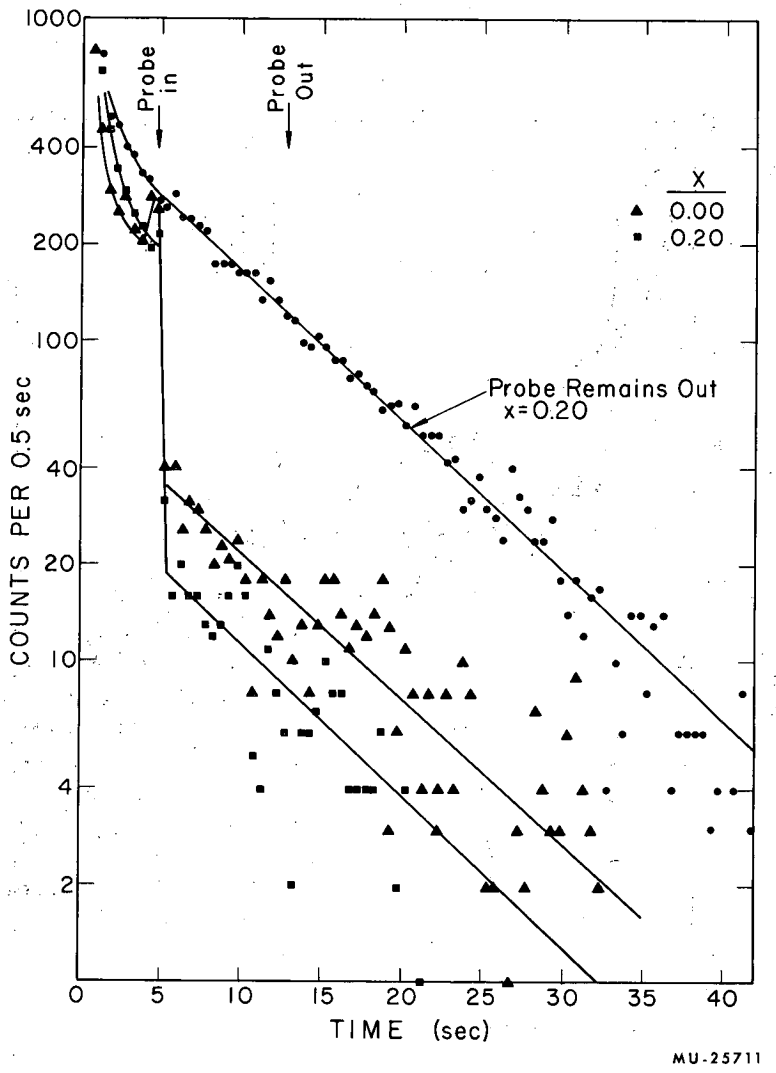

Fig. V-14. Outer probe plunging to 0.15 MCR at 5 sec and withdrawn 8 sec later. Counter x MCR inside ring axis.

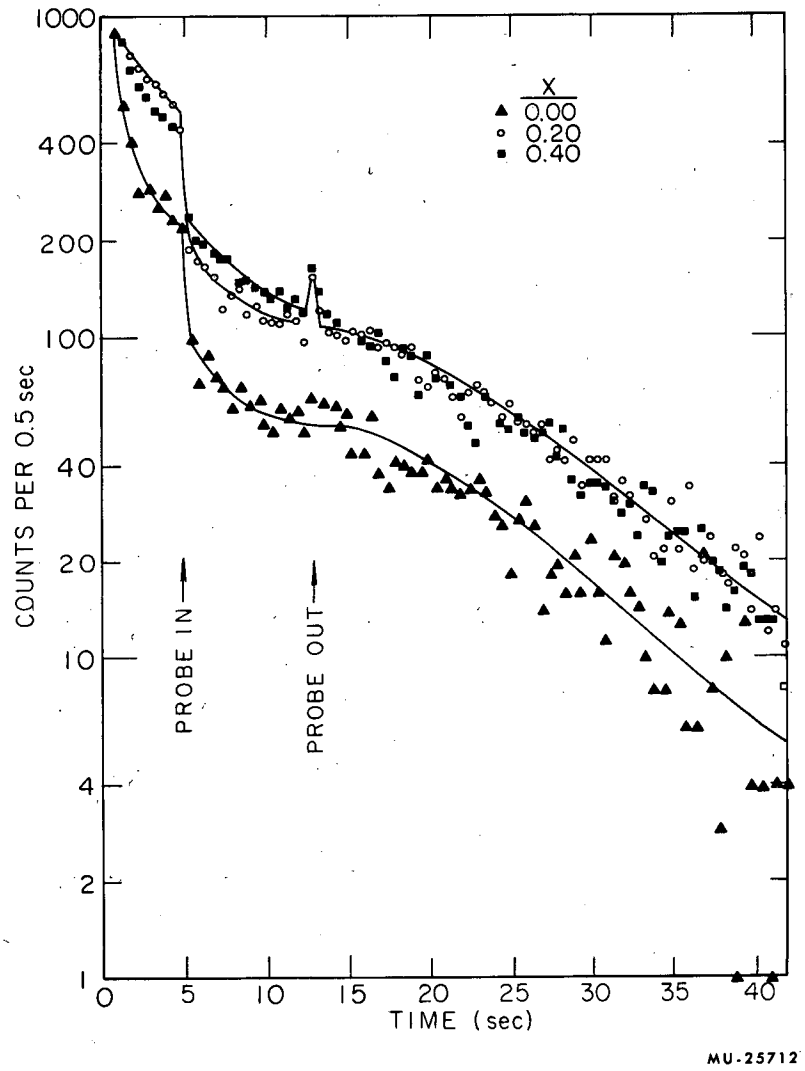

Fig. V-15. Outer probe plunging to 0.35 MCR at 5 sec and withdrawn 8 sec later. Counter x MCR inside ring axis.

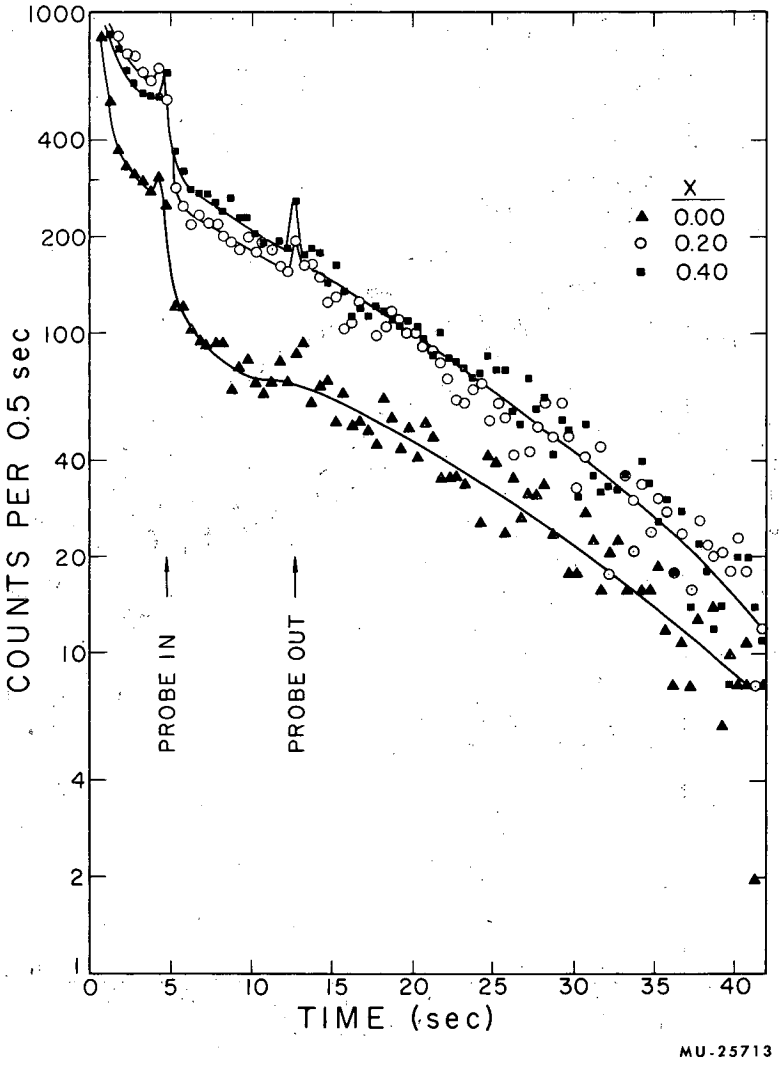

Fig. V-16. Outer probe plunging to 0.43 MCR at 5 sec and withdrawn 8 sec later. Counter x MCR inside ring axis.

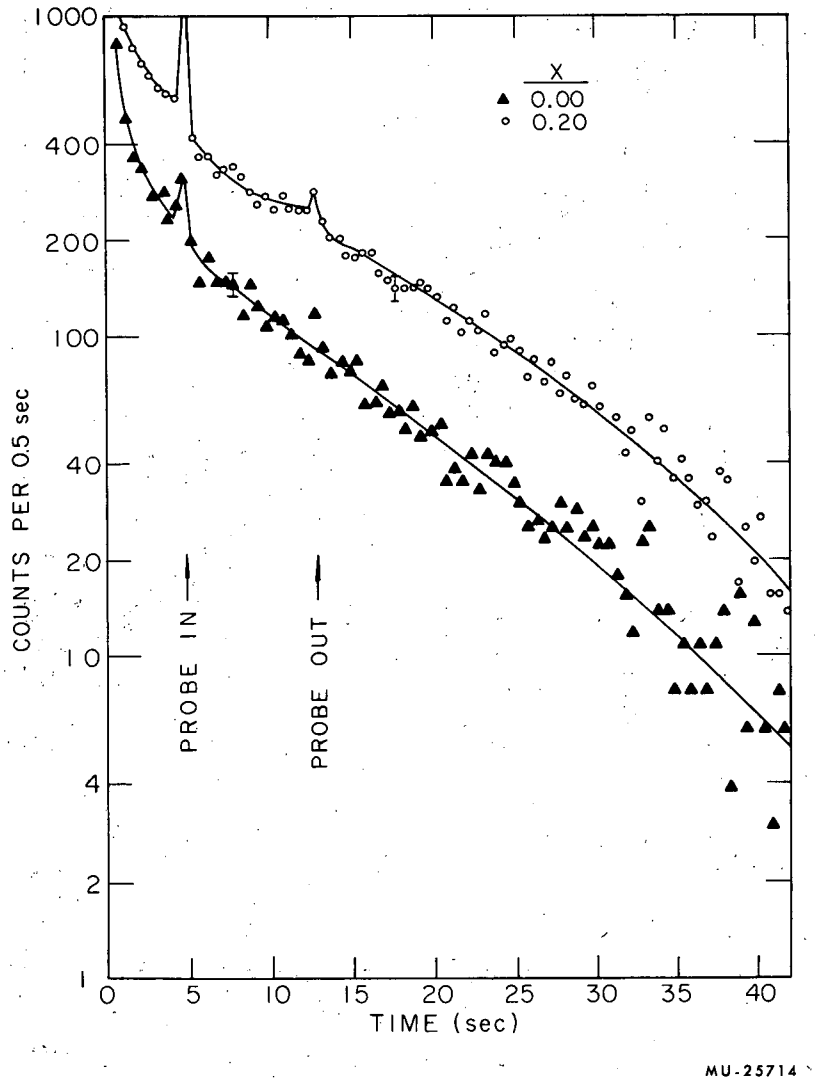

Fig. V-17. Outer probe plunging to 0.52 MCR at 5 sec and withdrawn 8 sec later. Counter x MCR inside ring axis.

0.20 MCR inside the ring axis. Removing the probe has no significant effect on the counting rate for any of these curves. The bumps that occur on some of the curves when the probe moves in or out are due to a small burst of gas entering the vacuum chamber. This problem was more troublesome for the outer probe than the inner.

3. Fast-empty experiment with moving probes and an elongated counter

In order to study the "instantaneous" radial distribution of particles, the point counter was replaced by a long scintillator (approx 50 cm long in the S plane, approx 4 cm wide normal to the S plane) located just outside the plane of one of the coils. This scintillator was optically coupled to the same photomultiplier tube by means of a wedge-shaped lucite light guide. The fast-moving probes were used to scatter the trapped particles into the detector in a time short compared with the gas scattering time. The pulses due to particles with energy greater than about 0.5 Mev were used to gate a variable pulse generator whose output voltage was proportional to the voltage from a slide-wire potentiometer connected to one of the probes. A pulse-height analysis of the output of the pulse generator therefore gives the number of particles scattered into the scintillator per unit of travel of the probe. This procedure can be used to locate the boundaries of the radial distribution.

The procedure used in collecting the data was the following. With a probe tip set at various radial positions as indicated on the curves, fast-empty runs were started in the usual way with no added scattering gas. (When a probe is used in this manner it is referred to as a "scraper.") About 3.5 sec after the fast valve opened the scraper was retracted; after a wait of another 3.5 sec the probe was inserted to its full "in" position. (When used in this manner it is referred to as a "plunger.") The pulse-height analyzer was turned on just before the plunger was inserted.

On Fig. V-18 the scraper and plunger are the same probe. Figure V-18 is a composite of data from both the inside and outside probes. The data have not been normalized; however, the rate of producing Ne was held quite constant for the series of runs. Several things should be noted. The boundary of the positron distribution does not shift significantly during the time the probe is retracted. The center of the distribution lies approx 0.10 MCR inside the ring axis; all the trapped particles have been intercepted by the plunger during the time it takes to reach this point.

The data presented in Fig. V-19 were recorded with both probes on each run, i.e., one as a scraper, the other as a plunger. Some of the runs (open marks) were done similarly to those of Fig. V-18 except that when the scraper was retracted it remained out and the opposite probe was inserted. Also the time delay between retracting the scraper and inserting the plunger was about 9.6 sec instead of 3.5. The curves are labeled according to the initial position of the scraper. The solid points correspond to runs in which the scraper was not retracted, the open points to cases in which the scraper was retracted.

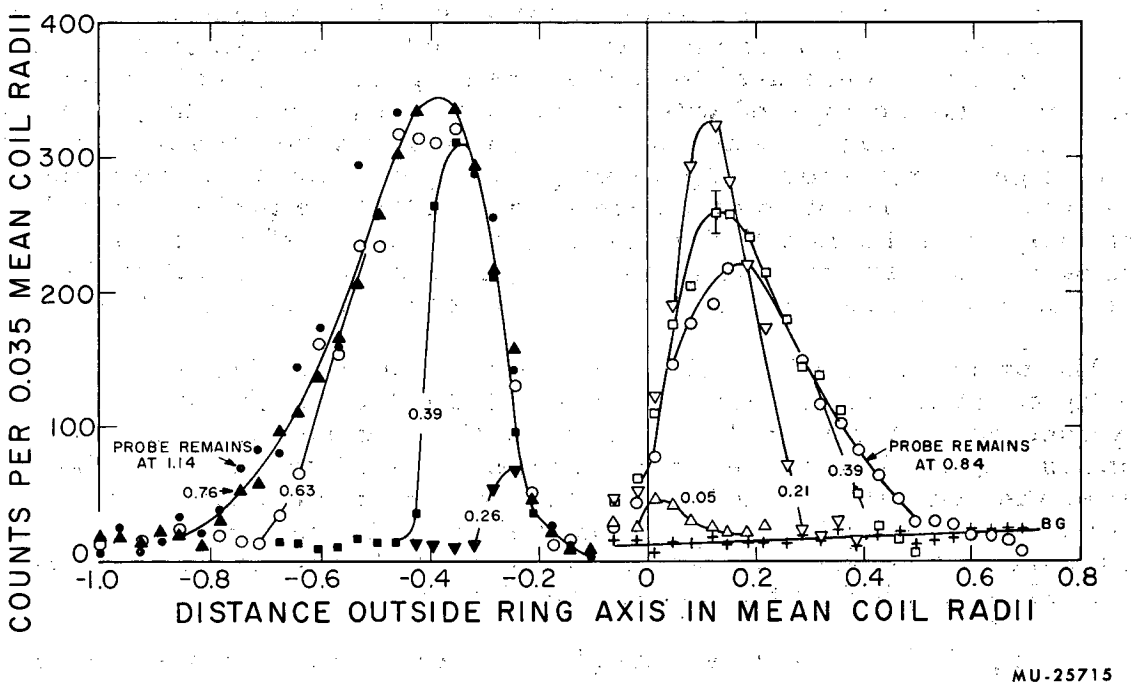

Fig. V-18. Counts per unit of travel as a function of position of the tip of a plunging probe. Scraper and plunger are the same probe. Numbers give initial distance of scraper (in MCR) from ring axis. Scraper retracted 3.5 sec after fast valve opens, plunger in 3.5 sec later.

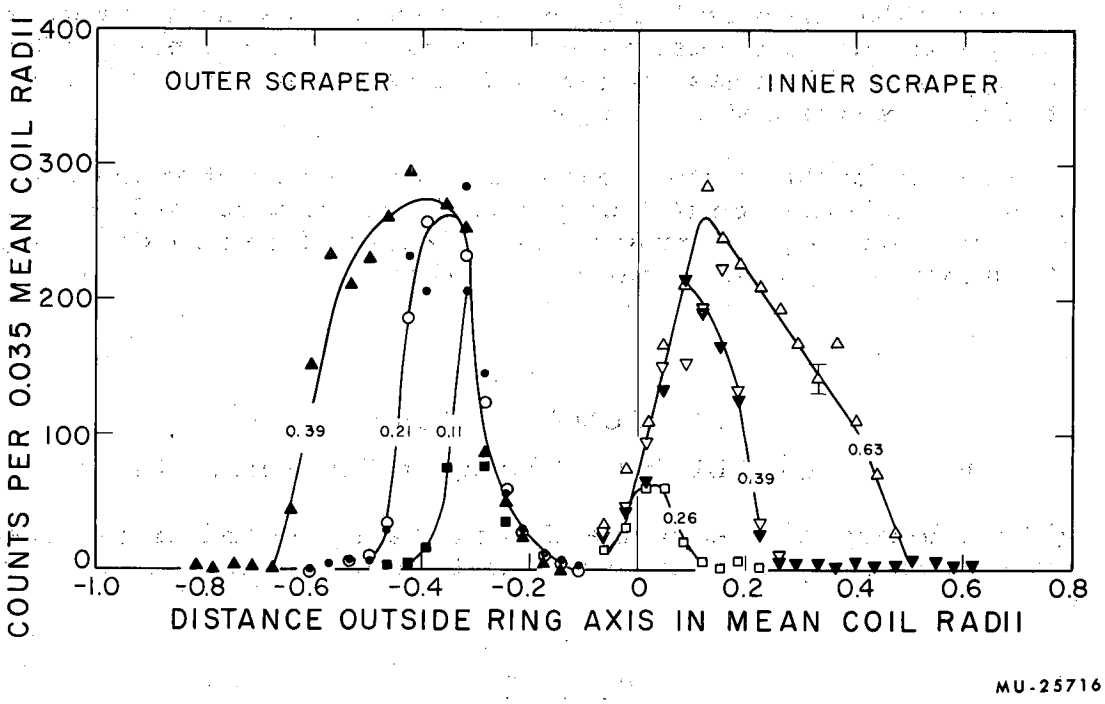

Fig. V-19. Counts per unit of travel as a function of position of the tip of a plunging probe. Scraper and plunger are opposite probes. Numbers give initial distance of scraper (in MCR) from ring axis. Scraper retracted 3 sec after fast valve (open symbols). Scraper not retracted (solid symbols). Plunger goes in 12.6 sec after fast valve.

Note that the results of Fig. V-19 have a symmetry about a point located about 0.1 MCR inside the ring axis. That is, for each combination of scraper and opposite plunger, the initial distance of the scraper on one side of this point is approximately equal to the distance at which the edge of the distribution is subsequently found on the opposite side of this point. Also the distributions are independent of whether the scraper was retracted or left fixed through a run. Thus only a small fraction of the trapped particles remaining in the geometry at any instant have diffused a significant distance across field lines.

The type of experiment described in this section allows one to study the distribution of particles on the M-type drift surfaces, whereas in the other experiments described (gas-scattering dominates), when the particles escape and are detected they are on E-type drift surfaces. In particular it should be noted that the outside plunger scatters just as many particles that are subsequently detected outside the ring axis as the inner plunger does inside the ring axis. When gas scattering dominates, most of the escaping current of positrons is inside the ring axis.

The results of this section lead to the conclusion that at any instant most of the particles are on M-type precessional surfaces, and just a few are "in transit" on E-type surfaces (where drift-surface diffusion is significant) as they tend to escape through a mirror.

14. BUMPY TORUS

Gordon Gibson,* Willard C. Jordan,† and Eugene J. Lauer

(The following is based primarily on the abstract and first two sections of an internal report[1] which proposed a method of injection into a Bumpy Torus.)

Abstract

A method of injecting and trapping all the charged particles of a beam in a magnetic field geometry (the Bumpy Torus) under steady-state conditions is described. A relatively inexpensive experimental test that makes use of an electron beam (1 ma, ~ 150 kev) is analyzed since a lower field, hence lower power, is required than for an ion beam, (e. g. a D^+ beam of energy greater than 10 kev.) However if it is successful, the method is applicable to the injection of an ion beam. A high energy electron plasma is, of course, of interest in itself. If scattering is the dominant loss mechanism, densities approaching $10^{11}/cm^3$ and $\beta \sim 1$ are expected. At this density, the Debye shielding distance is about 1 cm which is small compared to the plasma

*Westinghouse Electric Corporation, Atomic Power Dept., Pittsburgh, Pa.

†The Bendix Corporation, Research Labs. Div., Southfield, Mich.

[1] G. Gibson, W. C. Jordan, and E. J. Lauer, Steady Injection of a Beam of Energetic Charged Particles into the Bumpy Torus - Design of an Electron Experiment, UCID-4241, September 25, 1961. (This report is currently being expanded to include the results of more recent analysis.)

diameter of about 15 cm. Interactions of the charged particles, i. e., scattering and cooperative effects could be studied under steady, controlled conditions.

I. Introduction

The Bumpy Torus has been shown theoretically[2, 3] to be an absolute trap for particles behaving adiabatically, i. e., regions of space can be defined for which there are no loss regions in velocity space. To find the precessional surfaces (in the adiabatic approximation) of the charged-particle guiding centers in the Bumpy Torus, it is assumed that the transverse invarient $\mu = p_\perp^2/2m_0B$, the action integral $J = \oint p_\parallel \, d\ell$, and the total magnitude of momentum p are invariant. There are two special cases, however, for which there is no longitudinal motion, i. e., the velocity vector remains normal to the field direction, and hence the motion can be predicted without recourse to the longitudinal invariant (a) for a particle in the midplane between two coils, and (b) for a particle in the plane of a coil. For case (a) the trajectory of the guiding center obtained from $\mu = p_\perp^2/2m_0B = p^2/2m_0B =$ constant--or B = constant--agrees (as it must) with the precessional surface obtained from the invariance of μ, J, and p in the limit as $p_\perp \to p$. For case (b) they do not agree; but this is not unexpected, for in this case the longitudinal period becomes infinite and the invariance of J is not applicable. It should be emphasized that this is a very special case. The method of trapping described here is to inject a beam of particles in the plane of a coil so that the guiding center follows B = constant in the plane of the coil for a certain distance; the particles then move out of this plane and their guiding centers remain on a μ, J, p surface which does not intersect the point of injection. The calculations presented in the rest of the text are concerned with the details of achieving this type of injection.

The field maximum where the beam is injected must be modified slightly in order to have a particle initially balance on a "mountain top," but once a particle falls off, the probability that it would once again balance on this particular mountain top should be small. To calculate this probability is extremely difficult, since even the phase of the velocity vector is important. In the absence of scattering, the containment time is limited under optimum conditions by Liouville's theorem. It is estimated that the containment time set by this limit is longer than the mean containment time set by scattering.

Modifying one of the field maxima to accomplish the injection compromises the containment; the loss of particles due to scattering into the loss region which is introduced is calculated.

In the Bumpy Torus or a tilted-coil mirror machine a type of precessional-surface diffusion across field lines occurs which does not exist in the cylindrically symmetric systems. This has been described in Ref. 2.

---

[2] G. Gibson, W. C. Jordan, and E. J. Lauer, Phys. Rev. Letters 4, 217 (1960).

[3] A. I. Morozov and L. S. Solovev, Soviet Physics-Technical Physics 5, 241 (1960).

Evidence for the existence of this diffusion has been obtained in the positron experiment, and the boundaries of the region in which it is important have been determined.[4] The electron injection experiment is designed so that these boundaries are several orbit diameters from the vacuum walls of the torus. Thus no rapid loss of particles should result from this diffusion.

The status of stability theory is such that absolute statements cannot be made regarding the stability of the Bumpy Torus. Some numerical calculations pertinent to existing stability criteria have been done for the low β interchange instabilities. An important observation which will be made under controlled conditions during this experiment will be the degree of stability and the effect of the various parameters on stability.

II. Method of Injection

The basic method of injection has already been presented. This section describes one design for accomplishing it. The field of the Bumpy Torus as modified to permit injection is almost identical to that of the ideal Bumpy Torus except in the region of the injection section. The beam is directed perpendicular to the field in the midplane of the injection coil, which is split into halves. The particles make a rapid transition from field-free space into a field of a few kilogauss between iron pole pieces. The injection is done near a corner of the pole pieces, as shown in Fig. V-20.

A model of the corner of the iron pole pieces has been set up and the induction B measured at points near the median plane. From the measurements a plot of lines of constant B was made and trajectories were followed by use of the Livermore differential analyzer (operated by Norris Hetherington). Figure V-21 shows examples of trajectories that appear satisfactory for our purpose. This plot models pole pieces with a narrow gap of 0.64 cm and a wide gap of 1.27 cm. The orbit has a radius of 0.64 cm in the field magnitude labeled 50 on the figure. Two trajectories starting parallel and about 0.32 cm apart are shown. The two guiding centers drift along nearly the same B magnitude line in each case. Variations of the initial direction by 10^{-2} radian and of the momentum by 2% were found to have negligible effects. This demonstrates the feasibility of this step of the injection over a practical range of beam parameters.

Because of the gradient of the field, the guiding center moves across flux lines following a path along which the field magnitude is approximately constant. This motion carries the particle along the edge of the step in the

---

[4] Controlled Thermonuclear Research Quarterly Report, September, October, November 1960, UCRL-9500.

G. Gibson, W. C. Jordan and E. J. Lauer, Containment of Positrons in an Asymmetric Mirror Geometry, UCRL-6380, May 1961.

G. Gibson, W. C. Jordan and E. J. Lauer, CN-10/175 in Proceedings of IAEA Conference on Plasma Physics and Controlled Nuclear Fusion Research, Salzburg, Austria, September 1961.

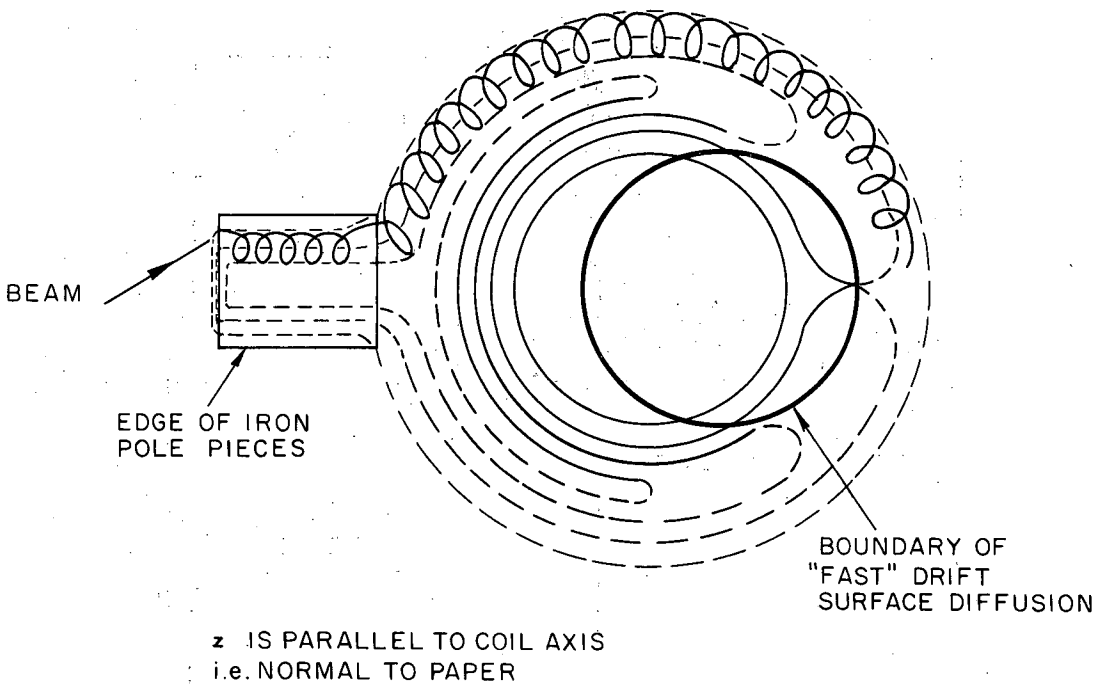

Fig. V-20. Qualitative plot of lines of constant field magnitude in the split injection coil midplane (I Plane). Dashed lines indicate that the z component of motion is stable (i. e., the field increases with motion out of the I plane); solid lines unstable.

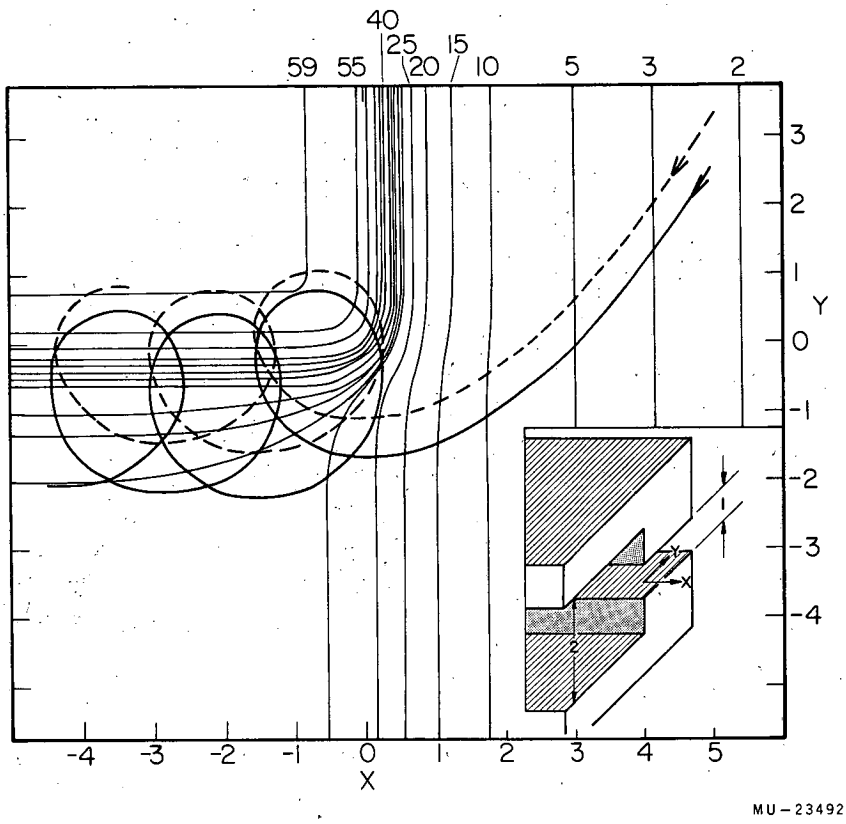

Fig. V-21. Lines of constant field magnitude measured in the median plane of the pole tips. Two particle trajectories are also shown.

iron gap, across a transition region, and into the field resulting from the split injection coil and the other coils of the Bumpy Torus. The separation of the halves of the injection coil is somewhat less than one coil radius so that a shallow minimum* (with respect to displacement $r\theta$ parallel to the ring axis) occurs in the field magnitude at points in the "I" plane that are sufficiently far from the ring axis of the Bumpy Torus. (The field near the ring axis still has a maximum with respect to displacement in the θ direction.) This slight mirror effect keeps the particles near the injection plane as they precess along the curved path (B = constant) shown in Fig. V-20. In other words, the θ motion is stabilized. The separation of the halves of the injection coil is greater on the inside of the torus than on the outside. This results in the "horseshoe" pattern for the lines of constant B shown in Fig. V-20. The tips of the horseshoes correspond to points near which the mirror effect disappears and the θ motion becomes unstable. Particles that enter the unstable region commence moving in the θ direction; hence they move away from the injection plane and into the other sections of the Bumpy Torus. The motion of their guiding center is now determined from the constancy of μ, J, p. The constant μ, J, p surfaces are nearly the same in the Bumpy Torus with the split injection coil as in the ideal Bumpy Torus with all coils identical.

It is planned to set up the electron experiment in the building 157 North Pit, which will afford x-ray protection. The electron gun has been designed and ordered from an outside machine shop. The design of the injection section which contains the iron pole tips and a current-measuring probe is nearly finished. The design of the main part of the torus is partly finished, and one of the 63 main coils has been fabricated and tested.

15. ATOMIC SCATTERING AND CROSS SECTION MEASUREMENTS

Forrest S. Baker, Gilbert O. Brink, Edmund S. Chambers, Robert H. McFarland, and Edward A. Soltysik

Considerable progress has been made during the last six months in the study of atomic scattering phenomena. Both the crossed-beam and gas-scattering programs have begun to turn out data (which are discussed below).

The Crossed-Beam Program

Introduction

The crossed-beam machine has been running consistently during this period and several measurements have been made. The machine has been

*If the ratio of v_θ to the total speed v is $(v_\theta/v) = \phi << 1$ at a point where the field magnitude is B, then the ratio of turning-point field, B_T, to B is $(B_T/B) \approx 1 + \phi^2$. For particles in the beam, $\phi < 0.01$.

described in detail in a separate report.[1] The drifts that were described in the preceding quarterly report have been eliminated and the machine now appears to be very stable. The drifts appear to have been due to charge formation on the electron gun structure.

The Ionization of Argon and Helium

The total cross sections for ionization of argon and helium by electron impact have been measured. Since these measurements have been discussed more fully elsewhere,[2] only a summary is given here. The experimental system is shown in Fig. V-22. The ions formed in the interaction region are collected by a metal plate and the resulting current is measured by an electrometer. Since the atomic beam is chopped at 2 cps, this current consists of two components: a dc component due to the background gas, and an ac component due to the modulated beam. These components are separated by the electrometer and the ac component is fed to a phase-sensitive detector which gets its reference signal from the chopping wheel. The dc output of this phase detector, after suitable filtering, is measured by a 100-mv pen recorder. The dc output voltage is directly proportional to the number of ions formed from the atomic beam.

The results of the measurement of the ionization cross section of argon are shown in Fig. V-23. These results have been normalized to Smith's measurements,[3] some of which are also shown in the figure, at 400 ev. The agreement seems to be quite good except that our results lie below those of Smith in the energy range from 100 to 400 ev.

The ionization cross section for helium is shown in Fig. V-24. It has also been normalized to Smith's data at 400 ev. The agreement here is somewhat better than for argon, although our data lie slightly below Smith's in the vicinity of the maximum.

The Ionization of Potassium

The partial cross sections for ionization of potassium by electron impact have been measured over the energy range from threshold to 500 ev. The experiment was quite similar to that with argon and helium just described, except that a Paul mass spectrometer[1,4] was used to separate the ions formed in the interaction region. These ions were detected by an electron multiplier and the signal treated in the same manner as that from the argon and helium experiment.

The results of this measurement are shown in Fig. V-25. Since the absolute intensity of the atomic beam is not known, the results are only

---

[1] G. O. Brink, A Crossed-Beam Machine for Measuring Atomic Collision Cross Sections, UCRL-6669, Dec. 12, 1961.

[2] G. O. Brink, The Ionization of Argon and Helium by Electron Impact, UCRL-6702, Dec. 11, 1961.

[3] P. T. Smith, Phys. Rev. 36, 1293 (1930).

[4] W. Paul and M. Raether, Z. Physik 140, 262 (1955).

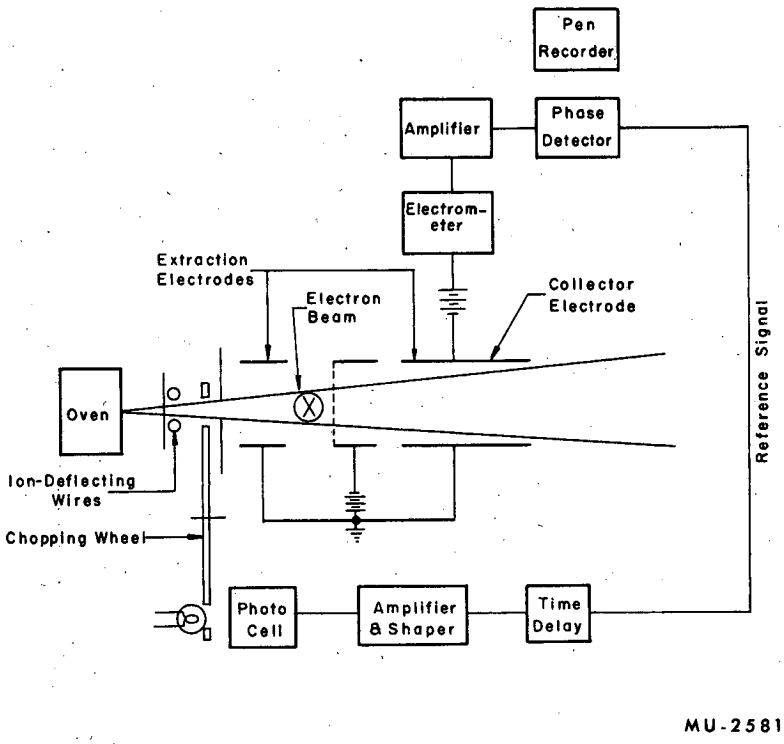

Fig. V-22. Block diagram for argon and helium experiment.

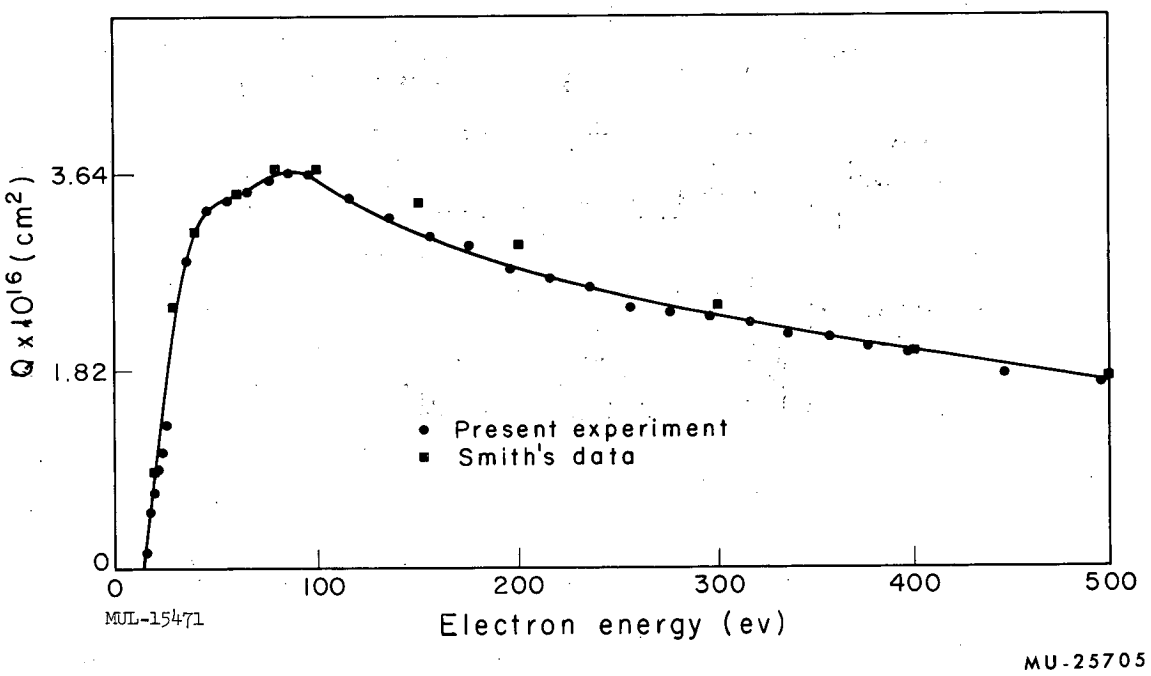

Fig. V-23. Total ionization cross section of argon.

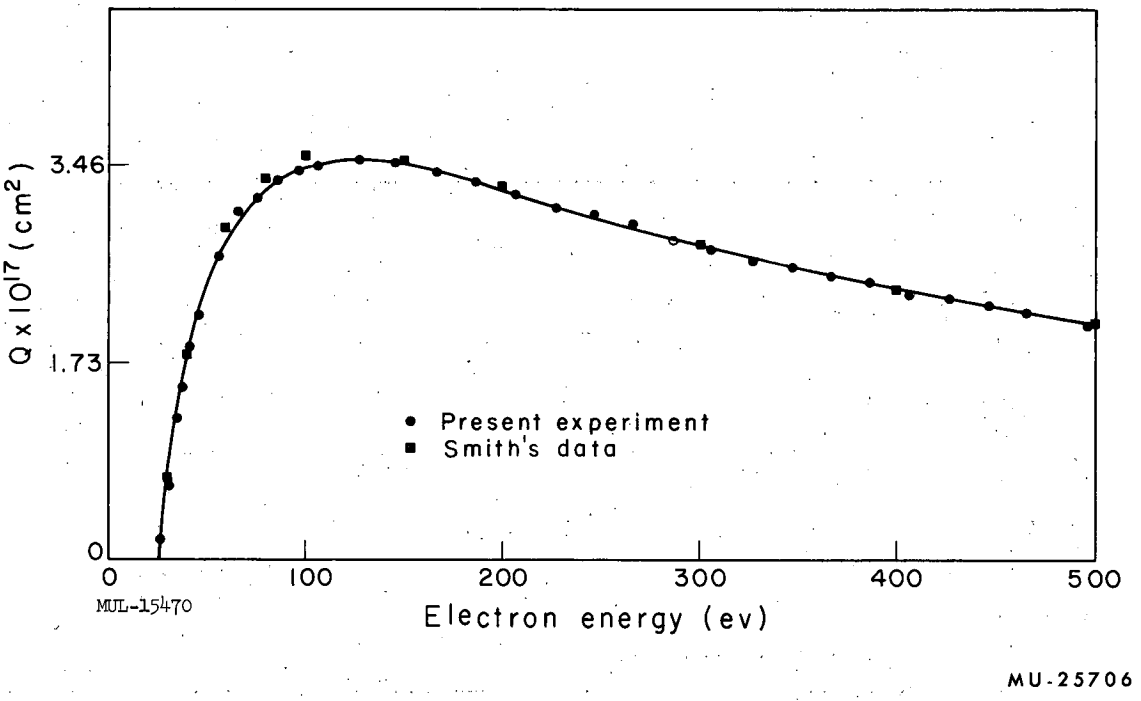

Fig. V-24. Total ionization cross section of helium.

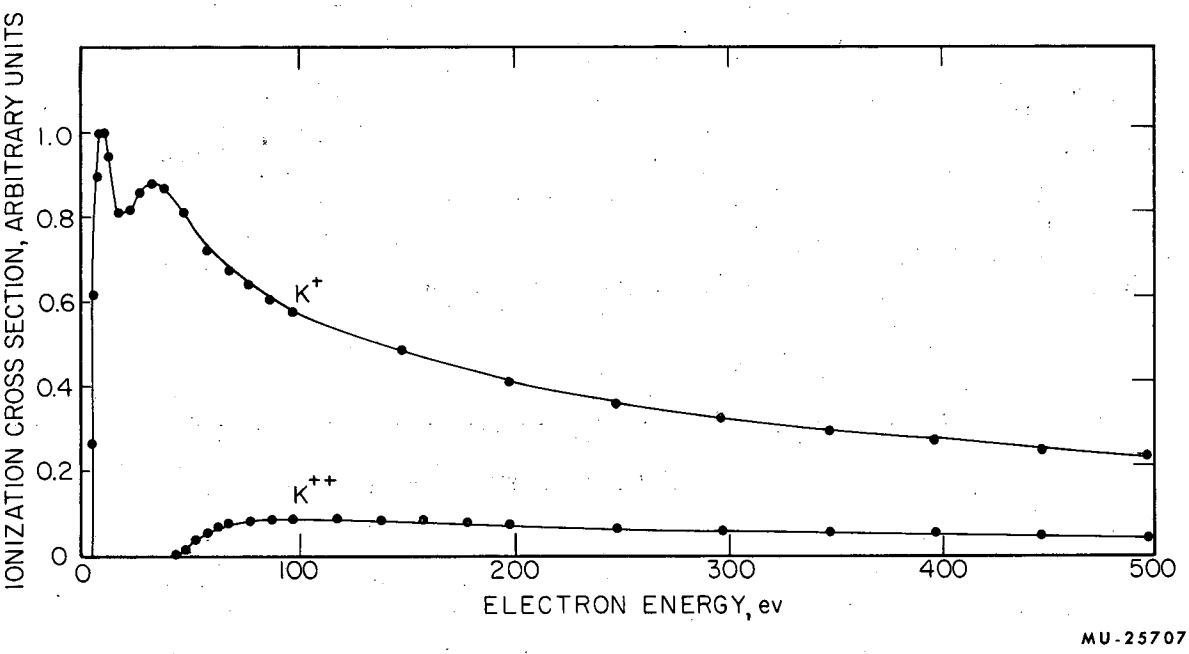

Fig. V-25. Relative ionization cross sections of potassium.

relative. The curve for K^+ shows some structure, while that for K^{++} has the usual shape characteristic of a simple ionization. Results similar to these, obtained by Tate and Smith,[5] lend support to the above data.

It is interesting to speculate on the origin of the structure shown by the K^+ curve. This same structure was observed by Tate and Smith. It is probable that the two peaks shown are due to two independent modes of formation of the K^+ ion. If this were true it should be possible to construct two curves whose sum would be the experimental curve and whose shapes would be characteristic of simple ionization processes. The thresholds of the two processes should be related to the atomic energy-level scheme for potassium.

An attempt to do this is shown in Fig. V-26. The sum of the lower solid curve and the dashed curve is the experimental curve. The threshold of the lowest-energy process is 4.3 ev, corresponding to the first ionization potential of potassium. The threshold for the higher-energy process is about 18 to 19 ev. This threshold will be compared with the known energy levels of the potassium atom, some of which are shown in Fig. V-27. These levels have been calculated from spectroscopic data.[6]

The ground state of potassium has an electronic configuration $3p^6 4S$. The ground state of the K^+ ion, $3p^6$, lies 4.34 ev above the ground state of the neutral atom. The first excited state of the K^+ ion, $3p^5 4S$, lies about 24.7 ev above the ground state of the ion. Above this is shown the ground state of the K^{++} ion, $3p^5$, which lies 36.15 ev above the ground state of the neutral atom. If the second peak in the ionization curve were due to the formation of the K^+ ion in an excited state it should exhibit a threshold of about 25 ev. This threshold seems to be too high to allow the construction of two curves whose sum is the given experimental curve.

There is an excited state of the neutral atom, however, which lies above the first ionization potential. This is shown as $3p^5 4S^2$ in the figure and it lies 18.8 ev above the ground state. If the atom is excited into this state it will become ionized by a process known as autoionization.[7] This will result in a K^+ ion in its ground state and an electron which will carry off the necessary kinetic energy. The threshold for this process agrees very well with the constructed curve threshold to 18 to 19 ev. The ion-detection system would not be able to distinguish between the ions formed by the two different modes. Unfortunately no experiments have been devised up to this time that will allow the further checking of this hypothesis.

Absolute Measurement of the Total Cross Section for Ionization of Potassium by Electrons

All necessary equipment for this experiment is installed. Since July, several runs have been made preliminary to a cross-section measurement attempt. The equipment performs satisfactorily.

---

[5] J. T. Tate and P. T. Smith, Phys. Rev. 46, 773 (1934).

[6] C. E. Moore, Atomic Energy Levels, NBS Circular No. 467, vol. I, June 15, 1949.

[7] H. E. White, Introduction to Atomic Spectra (McGraw-Hill Book Co., New York, 1934) p. 394.

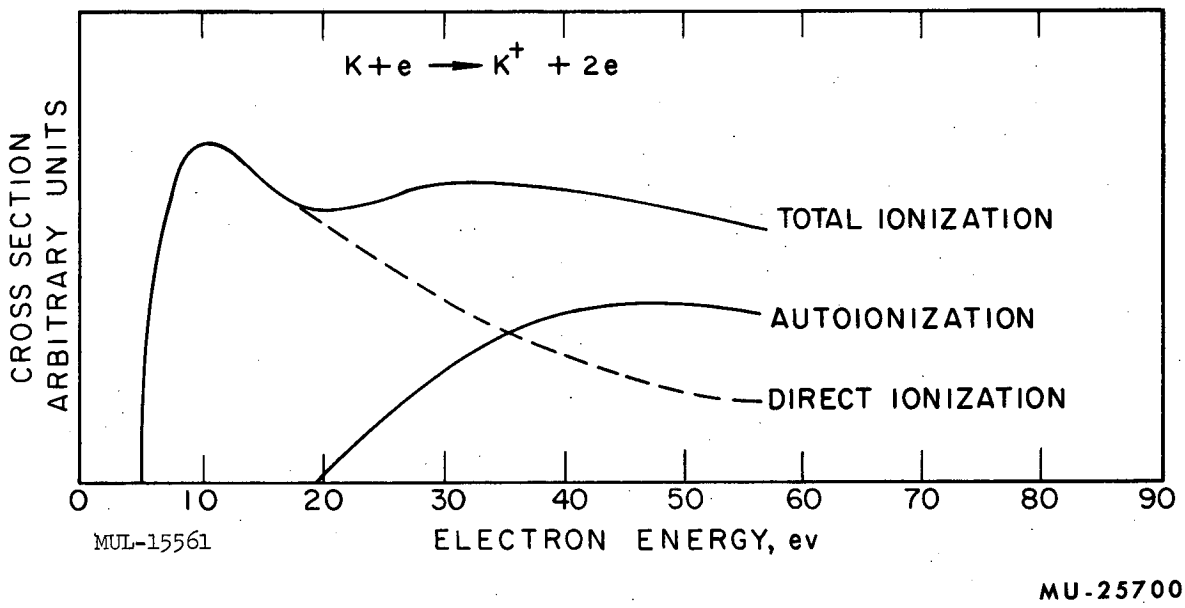

Fig. V-26. Decomposition of K^+ curve.

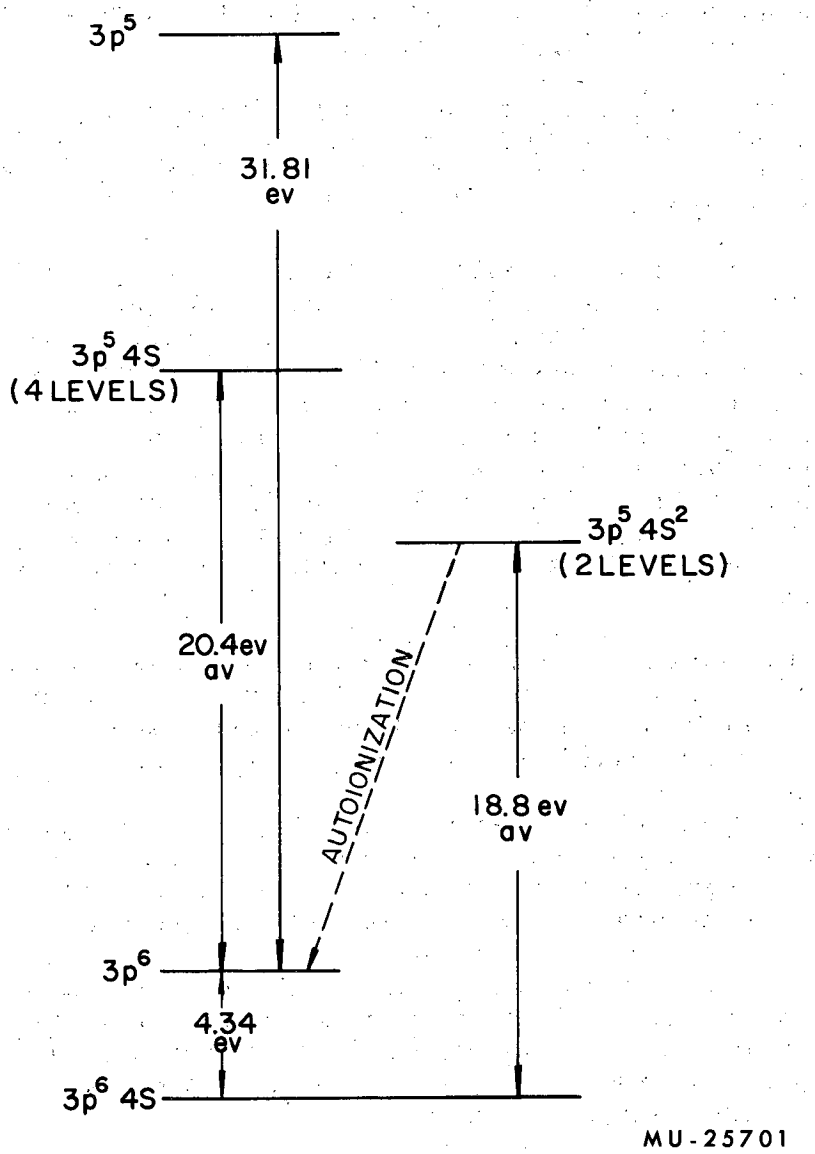

Fig. V-27. Atomic energy levels of potassium.

As described in a previous report,[8] the cross-section measurement depends in part on the detection of extremely weak ion currents. This is to be accomplished by adsorption of the potassium ions, including those of the K^{42} radioisotope, on a collecting surface. The detection will then be done in a conventional scintillation counter.

To achieve the highest possible accuracy in this stage of the measurement it has been necessary to investigate the adsorption efficiencies of various surfaces. This aspect of the experiment assumed particular importance for several reasons.

First, there exists firm evidence that the sticking efficiencies of different surfaces for the same beam material vary widely,[9] and for many surfaces reproducibility is low.[10] Secondly, the coefficients for adsorption of potassium have been measured on only two materials, quartz[11] and potassium.[12] Preliminary work indicated that the efficiency of quartz is appreciably less than unity under our experimental conditions. The potassium surface has the disadvantage of requiring its use immediately following its deposition under vacuum. This could not easily be accomplished in the current work. Of the twenty surfaces investigated (shown in Fig. V-28), 0.5-mil gold plate best satisfies the requirements of our system and the experimental procedures.

It should be emphasized here that no attempt was made to duplicate the adsorption coefficient for quartz as determined by Wegener. Present interest extends only to the limit of determination of the coefficient and its reproducibility under usual beam operating conditions.

The samples consisted of approximately 1 g of metallic potassium. The metal was vacuum-distilled into a quartz capsule. The capsules were fused off the distillation manifold and bombarded in the Livermore reactor. Activity after 4 hr bombardment was usually 4 to 5 roentgens.

The quartz capsule was placed intact into the oven and then broken by insertion of the oven plug. Oven temperatures ran consistently within 214 to 217°C at the coolest part. Background pressures, except in a single run, were about 2×10^{-6} mm Hg. The beam was collimated by an orifice 0.08 in. in diameter before striking the surface.

Five separate runs were conducted. In each run six surfaces of six to nine different materials were exposed, depending on how successfully the run progressed. Gold plate surfaces were exposed during all the runs.

---

[8] Forrest S. Baker, Gilbert O. Brink, and Edmund S. Chambers, in Controlled Thermonuclear Research Quarterly Report, UCRL-9393, Sept. 1960, p. 84.

[9] S. Wexler, Revs. Modern Phys. 30, 402 (1958).

[10] J. C. Hubbs et al., Phys. Rev. 104, 101 (1956).

[11] H. Wegener, Z. Physik 140, 465 (1955).

[12] F. Hock and K. Neumann, Z. Physik Chem. 2, 241 (1954).

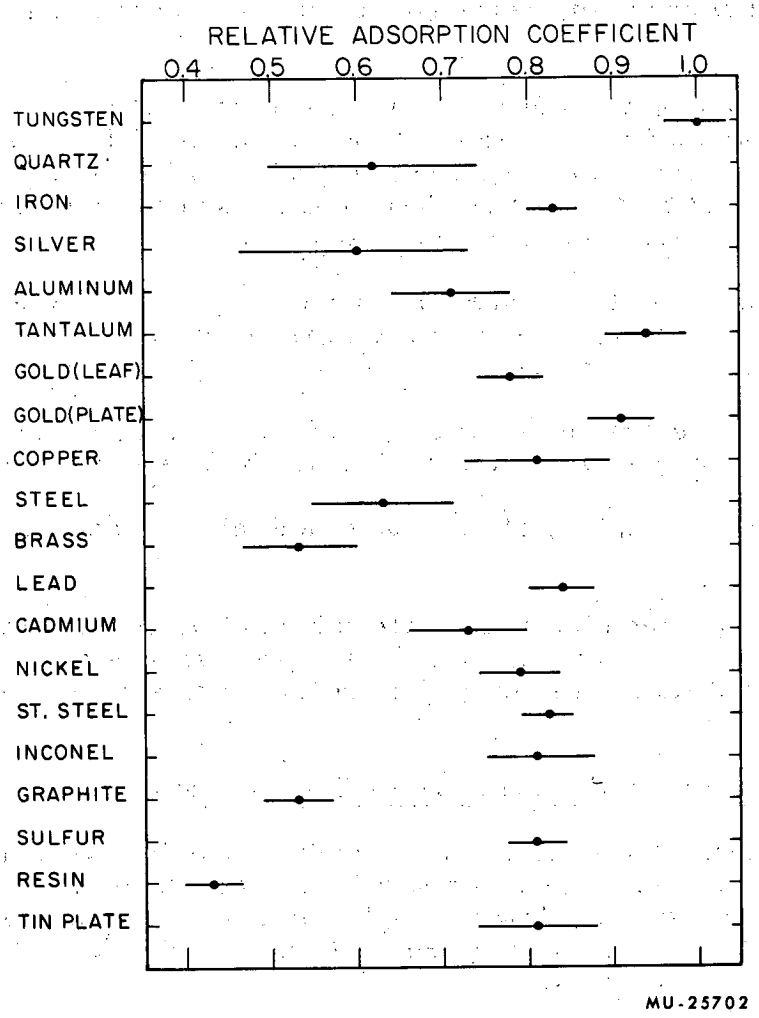

Fig. V-28. Relative sticking probabilities of various surfaces for potassium.

Tungsten was exposed to three runs and was selected as the final "standard" for normalization, since it possesses the highest efficiency and is also highly reproducible.

A few explanatory comments should be made concerning some of the surfaces:

1. The cleaning procedure for all the metals except cadmium, tin, and silver consisted of dipping into 6 N HNO_3 followed by three water rinses and then acetone. This was done about eight hours before use. Immediately prior to exposure (2 to 3 min) they were again cleaned by dipping into 1 N HNO_3, three water rinses, and acetone.

2. The sulfur surfaces were prepared very similarly to those used by Hubbs et al.[10] Although the coefficient is not unity its reproducibility is consistent within a few percent.

3. The resin surfaces were prepared by allowing a thin film of a soya-oil alkyd resin to dry for about 24 hours before exposure.

4. The reproducibility of the quartz and silver coefficients was consistently poor.

No attempt is made here to relate the relative coefficients to an absolute value. Experimental attempts to accomplish this are now in progress. A detailed comprehensive report covering this total effort is planned for the near future.

Hydrogen Ion Source for Crossed-Beam Experiments

For the experiments planned, the source should give a monoenergetic beam of about 1 μa. The energy should be variable from a few kev to 60 kev. The beam should be steady, low in ripple, and well focused several feet from the analyzing magnet. These requirements are fairly well satisfied at the present state of development.

At 1 kev about 0.07 μa H^+ and 0.7 μa H_2^+ has been obtained 1 foot from the analyzing magnet after passing through a two-plate collimator with 1/8-in. slits. These currents gradually increase to 1.3 μa H^+ and 11 μa H_2^+ at 15 kev. Somewhat higher currents are obtained up to the maximum energy of 60 kev.

A plot of ion current vs analyzer magnetic field shows peaks that are 1.4 kev wide at the base. The actual energy dispersion may be considerably smaller than this, since the above width assumes a point source and ideal focus. This source utilizes what Peterson, Cook, and Heinz[13] describe as aperture extraction. Their results show an energy dispersion of only about 50 ev for a beam energy of 2.75 kev.

---

[13] J. R. Peterson, C. F. Cook, and O. Heinz, Beam Extraction from an rf Ion Source, Stanford Research Institute Technical Report 720-1, July 15, 1960.

Figure V-29 shows an approximately full-scale drawing of the plasma source, extraction gap, and first einzel lens. Source tube 1 has a top section of Pyrex glass that is attached through a graded seal to a Kovar support tube. An rf oscillator supplies roughly 80 watts of power to the source tube. Voltage is applied between the high-voltage base plate 3 and a disc electrode placed on top of the Pyrex tube. Hydrogen is metered through a palladium leak to the source tube. A pressure of 20 μ of Hg is read on an NRC thermocouple gauge. Magnet 2 produces a field of 240 gauss (at 4 amp). The radius of curvature of the path of a 50-ev electron would be 1 mm. A 1-ev H^+ ion path would have a radius of 6 mm. Not shown are glass shields fitted into the source tube to minimize contact of dissociated hydrogen with metal.

Orifice 4, 0.1 in. diameter, allows the plasma to flow into the extraction region. The gap to the extractor 7 is 0.190 in. Teflon insulator 5 allows a few kv bias to be put on einzel electrode 8 through support 6. Extractor 7 and ground electrode 9 are connected to ground base plate 11. The moulded epoxy resin glass wool insulator 10 supports the full 60 kv. If 7 in. in diameter it is just borderline for holding 60 kv. A 9-in. -diam insulator has given no trouble.

Sylphon 12 allows the beam direction to be adjusted. A set of vertical plates just under it also provides adjustment and can be used as a beam switch.

Separation of the several ions produced is accomplished by turning the beam through 90°, using a magnet with a 6-in. pole diameter. The beam is then collimated through two 1/8-in. slits and measured in a Faraday cup. Secondary electrons are trapped by using a small permanent magnet. Recently a second einzel lens has been used between the magnet and the collimator to improve the focus.

If the H^+ ion current is measured as a function of the source magnet current, a complex curve such as Fig. V-30 is obtained. A possible explanation is that multipacting[14] is occurring. If an electron strikes a surface and produces several secondaries at the time when the rf field is changing sign, and then the same thing happens at the far end of its travel, the electron concentration can rapidly increase. The source magnet may influence the path length of the electrons and hence the transit time.

The electric field geometry at the extraction gap deflects the ions from the plasma in such a way that they appear to be coming from a virtual "point" source. The position and character of this source were investigated by placing a copper screen just below the extractor electrode and then forming an image in the plane just below the einzel electrode. MoO_3 was used as the sensitive "film." The image was sharply defined, indicating a small point source. The position, obtained by measuring the magnification, varied from 1.5 in. to 0.23 in. above the lower surface of the orifice, depending on orifice geometry. Attempts to improve einzel lens focus by restricting the angular aperture of the incoming beam were unsuccessful, however. In both the above cases the angular aperture was the same.

[14] W. D. Kilpatrick, private communication.

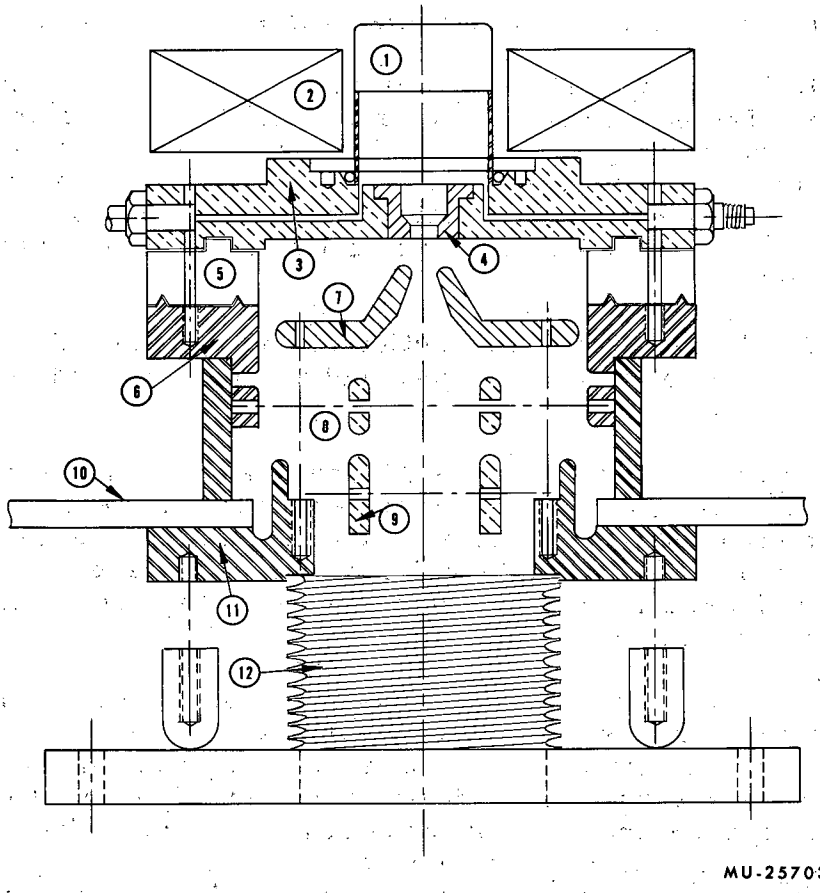

Fig. V-29. Radio-frequency ion source.

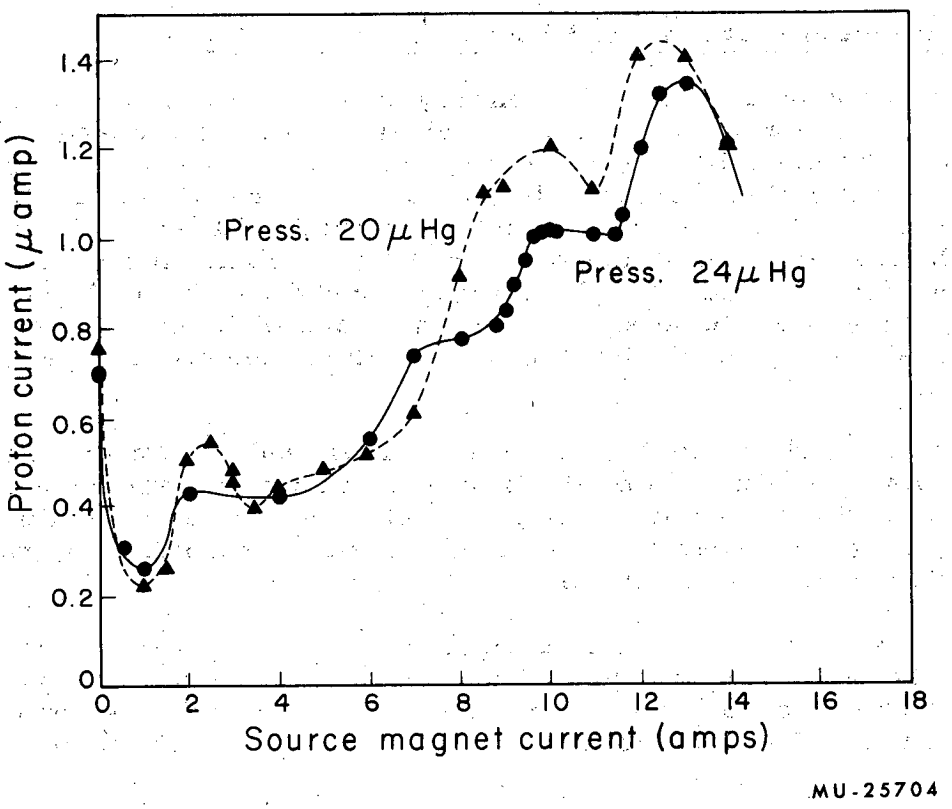

Fig. V-30. Proton current vs source magnet current.

Molybdenum trioxide has proved to be a valuable detector of both H^+ and H_2^+ ions. If a thin layer is placed on a sheet of metal and exposed to the source of ions, a detailed image of the spatial distribution of the ions is obtained. The image appears grey, and for 15 kev and 7.5 kev H_2^+ ions the optical density measured from the reflectance is 0.41 for 10^{-3} coulombs/cm^2.

The H^+ ions under similar conditions of energy and number density gave an optical density of 0.48. There is a linear region on the optical curve of density vs number density; however, it does not go through the origin. With proper calibration the method should give moderate accuracy in measuring a certain range of ion current densities.

Cross Section and Polarization Measurements in Helium

When electrons of sufficient energy excite a neutral atom, the atom may de-excite through the emission of electromagnetic radiation. This radiation is characterized by a definite discrete frequency and in general a degree of polarization. Despite the important information concerning the impact of electrons and atoms which can be obtained from a measurement of the polarization of the radiation, very little work has been done in this area. The experimental work by Skinner[15] and Skinner and Appleyard[16] on mercury, as well as the later work by Lamb and Maiman[17] on one transition in helium (λ = 3889), is not in agreement with the theory of Oppenheimer[18] and Penny.[19]

Percival and Seaton[20] have recently reviewed the theory on the polarization of light resulting from electron impact on atoms and have suggested that experiments be done using modern techniques to see if the discrepancy between theory and experiment could not in fact be resolved. It was to this end that this work was undertaken.

According to the theory on the polarization of light the polarization is related to the electronic cross section of the various magnetic quantum-number substates of the atom. For instance, the polarization of radiation resulting from a $P \rightarrow S$ transition can be shown to be of the form

$$P = G \frac{\sigma_0 - \sigma_1}{h_0 \sigma_0 + h_1 \sigma_1} ,$$

[15] H. W. B. Skinner, Proc. Roy. Soc. (London) A 112, 642 (1926).

[16] H. W. B. Skinner and E. T. S. Appleyard, Proc. Roy. Soc. (London) A 117, 224 (1927).

[17] W. E. Lamb and T. H. Maiman, Phys. Rev. 105, 573 (1957).

[18] J. R. Oppenheimer, Z. Physik 43, 27 (1927), Proc. Natl. Acad. Sci. U. S. 13, 800 (1927).

[19] W. G. Penny, Proc. Natl. Acad. Sci. U. S. 18, 231 (1932).

[20] I. C. Percival and M. J. Seaton, Phil. Trans. Roy. Soc. 251, 113 (1958).

where σ_0 is the cross section for electronic excitation to the $m_\ell = 0$ state, and σ_1 is the "electronic cross section" to the $m_\ell = 1$ state. Thus it is obvious that, if the theory is correct, measurements of the polarization of the emitted radiation give direct information on the cross sections for excitation by electrons on atoms. Further, these measurements provide a direct test of approximations used to calculate inelastic cross sections for excitation by electrons on atoms.

Because it was difficult to see how the theory could be in error, it was decided to perform experiments with great care on the monatomic gas helium. The details of the experimental arrangement and the experimental results are presented elsewhere.[21] Also, this work was described at the A. P. S. meeting in Chicago in November 1961, as well as at a symposium held at Indiana University.

The polarization of the following lines in helium has been observed as a function of the bombarding electron energy and helium gas pressure:

λ = 4713A ($3^3S \rightarrow 2^3P$)	λ = 5876A ($3^3D \rightarrow 2^3P$)
λ = 4922A ($4^1D \rightarrow 2^1P$)	λ = 3188A ($4^3P \rightarrow 2^3S$)
λ = 4388A ($5^1D \rightarrow 2^1P$)	λ = 5016A ($3^1P \rightarrow 2^1S$)
λ = 4471A ($4^3D \rightarrow 2^3P$)	λ = 3889A ($3^3P \rightarrow 2^3S$).

At the threshold energy for exciting a particular level of an atom a simple argument based upon the conservation of energy and angular momentum allows one to predict from the theory a value for the polarization independent of the cross section. Except for λ = 4713A and λ =3889, the experimental values for the polarization obtained near threshold are all zero, which does not agree with the predicted values. For the λ = 4713 A line, zero polarization was observed at all electron energies in agreement with theory. For the λ = 3889 A line, there is some indication that the predicted threshold value is experimentally obtained, but there are two anomalous extremum points for which there is no explanation.

Additional theoretical and experimental work is planned using the electron-helium system as well as the electron-neon system, since the resolution of the observed discrepancy between theory and experiment promises new insight into particle-interaction theory.

---

[21] E. A. Soltysik and R. H. McFarland, On the Polarization of Light Resulting from Excitation of Helium by Electrons, to be submitted to Phys. Rev.

VI. ENGINEERING AND TECHNOLOGICAL DEVELOPMENT

1. ULTRAHIGH-VACUUM DEVELOPMENT

Norman Milleron and Leonard L. Levenson

Introduction

Pursuing our goal of optimizing diffusion pump systems, we worked on

(a) perfecting a new heater for oil,
(b) top-jet design for a diffusion pump,
(c) a contamination analyzer,
(d) conductance measurements,
(e) design of a large bakable valve, and
(f) properties of trap materials.

A New Heater for Oil

No changes in the basic construction details of our heater have been made. Several heater failures have been traced to lack of care in the construction of the heater.

Tests are being undertaken to determine the amount of catalytic cracking of diffusion pump oils, particularly the Monsanto OS 124 fluid.

Top-Jet Design for a Diffusion Pump

Measurements were made on the probability of entrainment of light gases in a diffusion pump jet. Helium gas was pumped by a single very dense oil jet. The oil jet was dense enough to hold off a fore-line pressure of helium of about 0.5 torr. The annular space between the jet and the wall was approx 0.16 in. Helium diffusion into the jet on the molecular-flow side was entrained by the jet with a probability greater than 0.89. Within our measurement, the process of entrainment of the light gas in the heavy oil jet seemed to follow the exponential description given by Dushman.[1]

In order to pump light gases at maximum possible speeds, therefore, very dense jets are shown necessary. For example, if a Clausing factor of 0.75 were to be achieved, the mass transfer through the top jet of a pump must be greatly increased. Increasing the mass transfer through the top jet of course also increases the backscattering of oil from the jet. Two remedies for this condition are suggested: first, the top jet of the diffusion pump should take the shortest possible path to the next jet of the pump, and second, that a "skimming" or oil pumping jet be placed above this top jet of the pump.

---

[1] S. Dushman, Scientific Foundations of Vacuum Technique (John Wiley and Sons, Inc., New York, 1949) Chapter 4.

The purpose of the skimming jet would be to pump oil molecules only. The density of this skimming jet would be too small to pump light gases. The cross-sectional area of oil molecules is approximately 100 times the area of helium atoms. This large difference in cross section may make it possible to skim off the backstreaming oil from a massive-flow jet designed to pump light gases. By rearranging the relationship between the jets of a pump, two advantages might be gained; first, the change in flow density in the top jet radially outward would be minimized, and second, the overall height of the diffusion pump could be reduced substantially.

Contamination Analyzer

Air leaks and other troubles have been encountered in setting up the contamination analyzer reported last time.

Conductance Measurements

Previous conductance measurements indicated that surface roughness might possibly decrease molecular flow rates through cylinders.[2] Now the effect of surface roughness is being experimentally and theoretically studied. Two kinds of surface roughness are being examined: periodic roughness and random roughness. Examples of periodic roughness being tried are internal corrugations consisting of rings and also threads of various cross sections and depths. Both experimental and theoretical studies show that corrugations having a groove depth between 1 and 15% of the smallest inside tube radius yield conductances about 20% lower than the conductances of similar Lambert's Law plain-walled tubes. Conductance is not only insensitive to the depth of the periodic grooves but also to their cross-sectional angles of inclination between 30 and 60°. The Monte Carlo calculations made by Dr. Donald H. Davis of the theoretical group have a standard deviation of about 1%, and agree with the experimental results within about 2%. Detailed results will be given in a report in preparation.

Large Bakable Valve Design

No work was done on the large bakable valve program during this period.

Properties of Trap Materials

Details of preliminary results with a room-temperature adsorption trap have been reported.[3]

A CVC mass spectrometer using a diatron 20 has been added to the adsorption trap system. Results show that hydrogen is the major gas

[2] L. L. Levenson, N. Milleron, and D. H. Davis, Molecular Flow Conductance, UCRL-6253, August 15, 1961.

[3] L. L. Levenson and N. Milleron, Adsorption Capacities of Some Room-Temperature Trap Materials, UCRL-6396, August 3, 1961.

constituent, contributing approximately 60% of the pressure at 3×10^{-9} torr. Other gases are water and CO in about equal quantities. The partial-pressure sensitivity of the diatron 20 is about 1×10^{-9} torr.

This large hydrogen partial pressure is dependent on pump boiler power. Currently a CVC PMC diffusion pump with Convoil 20 is in use. The rated power of this pump is 1800 watts. However, a base pressure of 2 or 3×10^{-9} torr can be achieved only if the boiler power is reduced to 1000 watts. If the power to the boiler is raised, the hydrogen partial pressure increases. For example, at 1800 watts the total pressure read by the ion gauge is 8×10^{-9} torr. Of course as the power is lowered in the pump the forepressure tolerance for hydrogen is also lowered. At 1000 watts the forepressure tolerance for hydrogen is less than 10^{-3} torr.

To show that the hydrogen is originating in the boiler of the pump, another diffusion pump was placed in series with the foreline of the PMC 1440. By this means, it was shown that the hydrogen originated in the boiler of the PMC 1440 and was not due to the lowered forepressure tolerance of the pump.

In the future other diffusion pump oils will be tried in this system. Also other gases presently undetected will be looked for by an accumulation and desorption method reported previously.

2. MECHANICAL ENGINEERING DEVELOPMENT

Thomas H. Batzer

Toy Top

John R. Benapfl, Edward G. Scarlett, and James F. Ryan

Plans for moving the Toy Top experiment are now firm. The Source Test Machine will be moved into Bldg. 180, reassembled, and operated in its present form. The Toy Top Machine will be redesigned and assembled in its new location in Bldg. 180.

An internal heater probe designed to degas the final stage of the Toy Top vacuum system has been fabricated, and delivery is expected by December 31, 1961. A section of 6-inch fused quartz will be inserted in the final stage of the vacuum system. The probe is designed to be inserted remotely and to radiantly heat the interior walls of this quartz section between shots to reduce the amount of gas being driven from the walls by the plasma.

Low-Energy Neutral-Beam Experiment

William S. Neef, Jr., Eugene T. Bradley, and William T. Crothers

Alice Machine Layout and Assembly

Redesign of some beam tube components was completed and all parts were fabricated and are in operation. The redesign involved addition of a

third stage of evaporator pumping on the inlet beam tube and redesign of the collimators to prevent fringe beam from striking the hard-soldered joints. It was also decided to put two "flag" targets in the beam inlet tube on remote control and insulate them so beam current measurements could be made at these points.

Figure VI-1 indicates the stage of construction during November 1961. Some beam testing and improvements as outlined above have since been accomplished.

Assembly of the two major components that form the reaction chamber is nearing completion. The west half of the mirror with all auxiliary systems is complete. The east half is 90% complete and should be ready for use by December 31, 1961. See Fig. VI-2.

The lightweight calorimeter beam target is complete and ready for installation in the burial chamber when it is needed.

Several diagnostic instruments are being designed and constructed for use in the reaction chamber. The fast atom detector is complete and ready to install in the chamber port. The radial limiter and movable ion gauge are in the final stages of fabrication and should be ready by December 31, 1961. The axial limiter which takes measurements in the mirror loss cone is still in design, but should be released for fabrication in January.

All components for the second 10-inch bakable valve have been received and assembly has started.

Alice Magnet Coil

All sections for the mirror magnets are completed and tested. Each of eleven coil sections, eight of which constitute the full mirror, were pulsed about twelve times to 3,500 amperes and several dozen times at lower currents. Rated current is 3000 amperes. All tests were conducted at -320°F. The two halves of the mirror have been assembled and mounted on the coil carts ready to attach to the bus bars and liquid nitrogen supply line.

Pulsed Plasma Priming Experiment

This experiment utilized a portion of the Alice pumping system. To permit Alice work to proceed, the experiment had to be temporarily interrupted and a new site prepared for continuation with a new pumping system. The new pumping system and cold trap are not completely bakable, as this was not essential for this portion of the experiment. All diagnostic equipment has been built and assembled, and the entire experiment is back in operation and producing useful data.

The necessary parts were constructed for Alice to adapt an occluded-plasma source to the west end of the mirror chamber. The east end of the chamber has been equipped with a trap, diffusion pump, and cone-shaped receiver with a 1.5-in. aperture, all directly in line with the source. The burst of plasma from the occluded source is thus caught and prevented from being added to the background gas in the chamber.

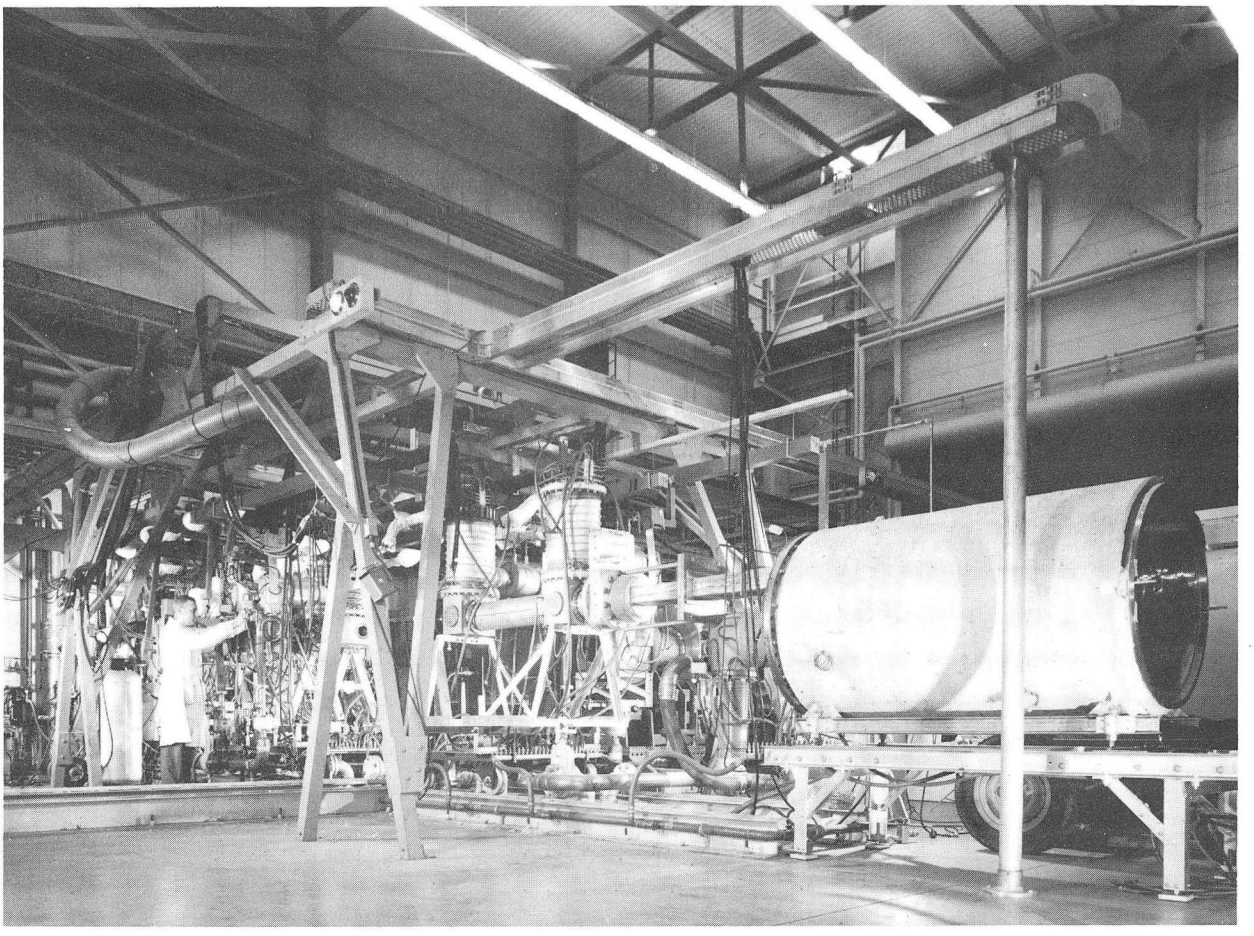

ZN-3009

Fig. VI-1. Partial assembly of low-energy neutral beam experiment, November 1961.

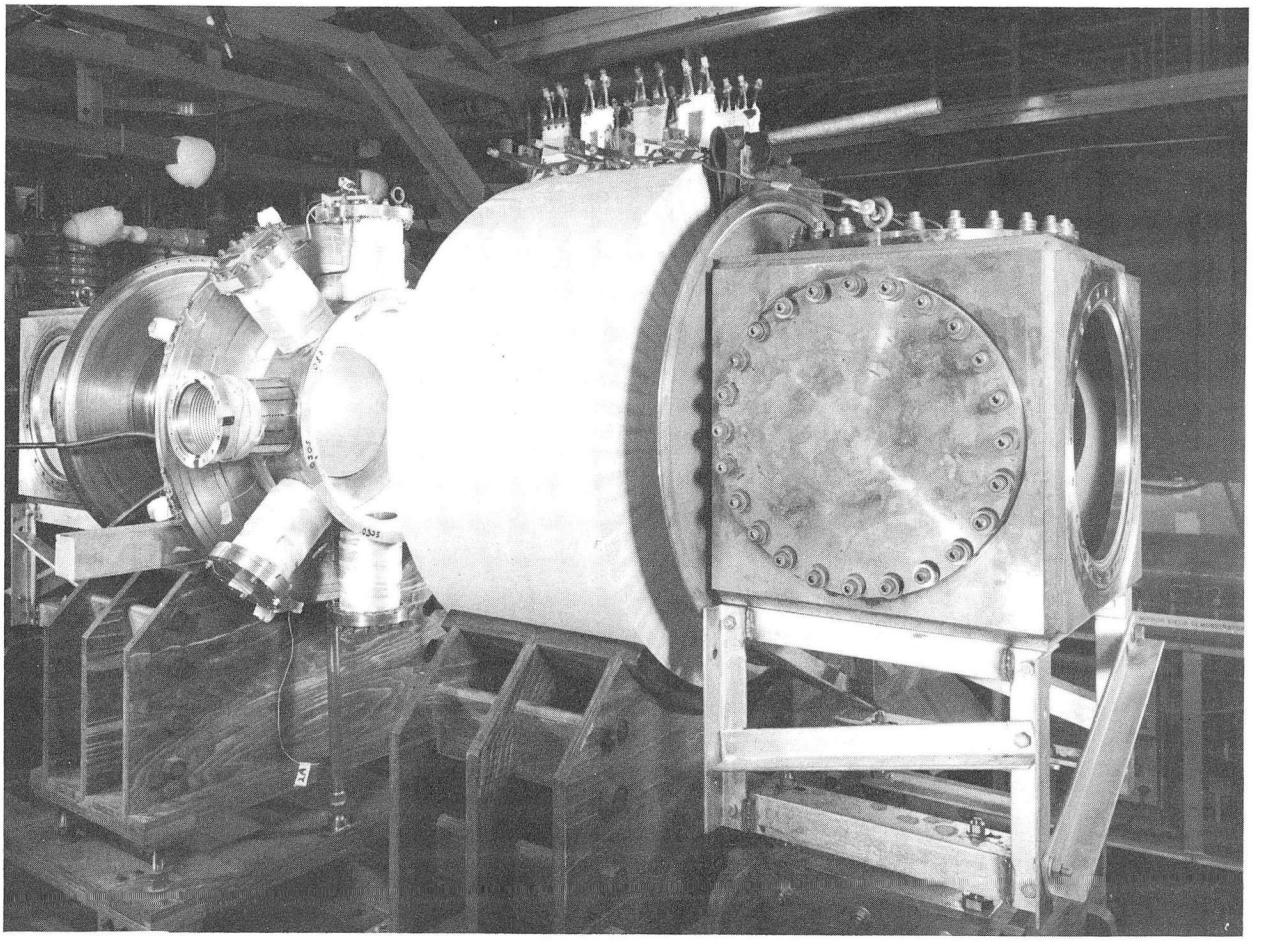

ZN-3008

Fig. VI-2. Reaction chamber and mirror magnetic components, low-energy neutral beam experiment.

Surface Bombardment Experiment

Design, fabrication, and construction of the entire machine was accomplished during the past six months. Some minor assembly work remains, but the experiment should be producing data in January 1962. The machine uses a small Von Ardenne type of source followed by a water-vapor neutralizer to generate an atomic beam at about 10 kev. Targets of various materials will be bombarded and secondary emission analyzed. It consists of a source, neutralizer, several pump tanks for molybdenum or titanium or both, and means of interrupting the beam. The entire system is bakable, using cupro-nickel pinch gaskets throughout.

Astron

Charles A. Hurley, James F. Ryan, and James E. Blades

Except for minor alterations all the structural steel work and concrete shielding necessary for the installation of the Astron machine in Bldg. 157 has been completed.

720-kv Electron Gun

All the necessary hardware for the assembly of the core stack has been fabricated and delivered. The assembly of the gun is complete, except for connections through the walls. The accelerating column used in this assembly was a reworked reject, used in the interest of saving time. The column was tested under operating conditions of pressure and temperature and found to be quite satisfactory. On this basis it was observed that the column could have been assembled with O rings rather than hard soldering. Two acceptable accelerating columns have been received from Coors Porcelain Co. These are being made ready for assembly the first time the core stack is disassembled.

Roughly 800 man-hours were required to assemble the core stack, because of the great amount of custom fitting. This was due to cutting and dorming insulation and the fact that each core was checked electrically during assembly.

The bushings for making electrical connections through the tank wall are approximately 90% fabricated. These then must be made into assemblies using 8 ohm oil-filled coaxial cable. The prototype bushings were tested in a pressurized Freon 12 atmosphere. One assembly was tested 475 hours without failure. The next assembly failed and revealed a very dangerous situation. With any amount of oxygen present during an electrical breakdown, it is possible to chemically form toxic gases, such as phosgene, chlorine, carbon monoxide, and--because of the telfon present--fluorine. A method for controlling this danger was worked out with Hazards Control. The method consists of a detection device and a sampling program. Also, whenever the system is opened the gas is to be dumped safely to the atmosphere. Another precaution is to install desiccant filters in the system to remove moisture and acids.

Pulse-Forming Network Switch Installation

Eighteen switch chassis were delivered, aligned and jigged as specified, and assembled in the jig-aligned racks. It seems reasonable to say that, with minor adjustments, 100% interchangeability is possible.

Induction Accelerator

A second revised eight-core assembly was built and tested. The previous problems of voltage holding and corona have been overcome, and orders have been placed for the mechanical parts, including insulation required for the total of eight 48-core accelerator units. Parts for two such units are to be delivered by January 30, 1962 and the balance by March 30, 1962.

The ceramic column modules required for six accelerator units are on hand. The ten modules needed for the remaining two units are on order and delivery is expected by March 30, 1962. The blowers and air ducts for cooling the accelerator units are being designed, and should be delivered by the end of February 1962.

Beam-Tube Transition Section

Tests on a straight and curved four-stage differentially pumped pressure-transition section have been completed. ENA-125, Nov. 8, 1961, has been issued covering these tests. Enough data have been obtained to let us predict the performance of various sizes and types of orifice with confidence.

Two mechanical booster (Roots Blower) pumps have been received and installed as part of a six-stage transition section. A preliminary test on this section showed 220 μ final pressure with 250 mm inlet pressure, and 700 μ final pressure for 750 mm inlet with 0.75×1.5-cm oblong orifices. Since aluminum oxide foils are now being made that hold several millimeters of mercury pressure, the transition required for the beam research facility can be obtained with the existing equipment. Design of the Beam Research Facility (Beam Tube) is to be completed by the middle of January, and the facility be assembled by the middle of April 1962.

Bumpy Torus

J. Ralph Ullman and Eugene T. Bradley

General design for the multimirror torus geometry has been completed and specific design work is in progress on the various components. The Electron Gun assembly (UCRL- Dwg. No. L15C5735) was released for fabrication on October 12, 1961 and is due to be delivered the week of December 22, 1961. The design is complete for the injector section of the torus and should be released for fabrication early in January 1962.

The North Pit of Bldg. 157 has been allocated to this experiment. The generation of 150-kv x rays necessitates the installation of a shielding wall to protect operating personnel, and lead shielding on the roof of the area to protect the rest of the building. These and other alterations necessary have been requested of the Plant Engineering Department with a completion date of February 15, 1962 for the major alterations.

Present planning is that the segments of the Torus will be fabricated outside and the coils wound by the Sherwood Coil Shop. After preliminary leak checking the segments will be welded together in the final assembly by LRL personnel. A welding fixture is being designed to facilitate this final assembly. It is expected that this method of assembly will reduce the amount of rework usually encountered when vacuum testing is not done as the assembly progresses.

Component Development

Thomas H. Batzer, James F. Ryan, and Arthur R. Harvey

The first of a new set of pulse coils for the Table Top experiment has been fabricated and tested. The specifications for this coil are 10-kv, 9 in. i. d., 20-in. o. d., and 6 in. long. It is to be operated at liquid nitrogen temperature. The coil has successfully undergone 50 pulses at 10 kv while being water-cooled and 5 pulses at 10 kv while cooled with liquid nitrogen. On the basis of these tests, the other five coils will be fabricated.

Because of size and other considerations it may be necessary to develop other nonconducting or nonmetallic materials for vacuum vessels to substitute for glass. Two approaches are currently undergoing evaluation. The first was to evaluate the vacuum characteristics of large porcelain stoneware cylinders. Two cylinders were ordered, one 3 ft in diameter and 3 ft long, and one 4 ft in diameter and 4 ft long. The 3-ft crock was installed on a vacuum pumping system having a valved-off base pressure of 1×10^{-7} mm Hg and a speed of 70 liters per second. The base pressure on the crock after 3 or 4 days of pumping was 1.2×10^{-4} torr. Bagging separate 6-in.-square areas on the outside surface of the crock indicated relatively uniform permeability to helium. Calibration of this leak rate indicated a flow of helium through the walls at the rate of 1×10^{-8} torr-liters/sec-cm^2. From these tests it was concluded that the porcelain crocks were not suitable for vacuum vessels.

The next vessel to be evaluated on this same pumping system was a fiber-glass-reinforced epoxy cylinder 30 in. long and 24 in. i. d. Previous experience with hand-layup cylinders of this type shows that they are also permeable to helium. Assuming that the leakage was along the unwetted fibers of glass, a scheme to cast a very thin epoxy liner on the inside of this cylinder was devised. The cylinder was placed in lathe end plates and a measured amount of epoxy, to give a 1/16-in.-thick liner, was poured in; the cylinder was spun and semicured in place, giving a very smooth glassy internal surface. This was then finally cured in the furnace.

The vacuum closure was made by using two 1-in. aluminum plates with Viton A O-ring seals. A vacuum outlet on the bottom plate which bolted onto the 4-in. gate valve, which was in turn bolted to the 70-liter/sec vacuum pumping system. The top aluminum plate contained hardware to evaporate a molybdenum filament inside the glass vessel.

The following table gives the results of the tests made on this epoxy cylinder.

Condition	Pressure[a] (Torr)	Outgassing rate[b] (mm-liters/sec^1 cm^2)
Before baking	5×10^{-6}	1.9×10^{-7}
After baking at 185°C	3.5×10^{-7}	5.1×10^{-10}
After evaporating molybdenum	9×10^{-9} [c]	3.5×10^{-12}

(a) The base pressure of the isolated diffusion pump and baffle was 2×10^{-7}.

(b) From rate of pressure rise, isolation valve closed.

(c) Maintained 1.0×10^{-8} pressure for 3 hr without further evaporation of molybdenum.

The final test in the evaluation of the Monsanto Fluid OS-124 in the CVC 720 diffusion pump indicated massive cracking of the pump fluid. There is reason to believe that the aluminum oxide present on the aluminum jets may be responsible for catalytic cracking. A new jet assembly has been machined from mild steel, and further tests will be made on the polyphenol ethers.

3. ELECTRICAL ENGINEERING DEVELOPMENT

Critical-Path Method

Vernon L. Smith

The design and construction of the Astron accelerator have been carefully reviewed from a scheduling viewpoint. The relatively new techniques of project planning termed Critical-Path Method have been applied. An arrow diagram has been evolved which represents the interrelation of all the jobs required to complete the accelerator.

The advantage of this diagram is in showing project members how their work relates to others' and to point out areas where rescheduling will significantly advance the completion date.

Computer programs have been evolved to analyze the diagram and present data on the longest path (critical path) through the "maze" and develop time relations of all other jobs with respect to the critical path.

The data from our first computer run will be available early in January 1962.

Astron--Systems Engineering

Clelland D. Nail

Electron Accelerator

Construction Phase

During the past 6 months the Astron Accelerator has definitely entered the construction phase. Major components are arriving and most of the design philosopy has been established.

This does not mean that design and engineering research is complete, for many details of construction are still uncertain. It should be obvious that construction on such a basis may require considerable revision. Calculated risks are necessary, however, in order to approach the completion schedule that has been established.

System Design Decisions

A few of the various major decisions that have shaped the design of the system are summarized below.

Design Parameters

The accelerator is designed for a 4-Mev output at 200 amp. This will require construction of the gun and six accelerator sections.

The 45 cores in the gun will each require three core-exciting pulsers. The 288 cores (total) of the six accelerating sections will each require one pulser for excitation.

The core-exciting pulsers will be of the line-modulator type using the 5949A hydrogen thyratron as the switch. The switch chassis will be modular, with plug-in features and interchangeability.

The pulse-forming "lines" will consist of seven parallel lengths of RG-218/U coaxial cable cut for a nominal pulse length of 0.4 μsec. These pulse-forming lines (PFN' s) will be charged to a nominal 32 kv at the command of a signal occurring about 3 msec before beam time. Pulse-repetition rate will be adjustable between 0 and 60 pulses per second.

The output of each pulser will be shaped or compensated by a network mounted in the same rack with the switch chassis. The compensated pulse outputs will be connected by six parallel RG-213/U coaxial lines to the cores.

The magnetic cores will be reset to negative saturation after each beam pulse by a 50-amp pulsed reset current. This will be applied to the regular exciting winding after the beam pulse, but before recharging the pulse-forming cables (Sequential Reset).

Present Status of the Above Design

Switch Chassis

Franklin Engineering Company of Palo Alto, California has begun construction of 518 switch chassis for the accelerator. Eighteen have been delivered and are being evaluated. Minor changes will be incorporated in the rest. Completion of this contract is expected by the end of March 1962.

The PFN Cables and Structure

Steel work for supporting reels containing the PFN cables is complete. This consists of two elevated decks over the area containing the racks for the pulser switch chassis and compensators.

The first 40% of the PFN cables is in place in the structure, with the cable descending through openings in the decks to the rear of the racks below. Most of the cable reels are completed. Approximately 1700 reels are on hand; about 175 are held up waiting delivery of additional cable.

Racks and Hardware

All the racks for switch chassis and pulse shapers are in place and sliders are being installed and jigs adjusted. These racks must be very carefully aligned and braced so that the chassis will be interchangeable.

Charging Power Supplies and Associated Equipment

Carad Corporation (Palo Alto) has completed the first of four 125-kva charging power supplies for the machine. Final checkout at the vendor's plant is in progress, prior to delivery.

Space in Building 156 has been cleared for the power supplies. Overhead conduit for the high-voltage lines and control cables is about 90% complete.

Voltage distribution and switching cubicles are designed and a prototype is being constructed. One such unit will be associated with each 8-core pulser. Contracts for construction of these 53 units will be let after evaluation of the prototype.

Pulse Shaper

The pulse-shaping network (frequently referred to as the compensator) has been redesigned. Commercial variable inductors and fixed capacitors have been assembled without use of oil or dibutyl sebacate.

The resulting chassis is much lighter and has nothing to spill or burn. It is similar in size to the switch chassis (8 3/4-in. panel) and will be mounted on slide hardware below each switch unit. A special tee connects the cables from the switch chassis to the compensator and to the load.

Presently available pulse capacitors for these networks have a large temperature coefficient. Heating in the capacitors from losses will vary with pulse repetition rate. This, with marked temperature dependence, will make readjustment of the pulse shaper necessary after each significant change in repetition rate.

Inquiries have been circulated in an attempt to obtain capacitors of reduced temperature dependence. Numerous responses have been received and samples have been ordered for evaluation. None is in full accord with both mechanical and electrical requirements.

Components, including the temperature-dependent capacitors, are ordered.

The delivery schedule for inductors is long, and it is doubtful that pulse-shaper chassis can be made available until after the gun is ready for test. Fortunately much of the initial debugging in the gun can be done without compensation. The earliest delivery estimates for better capacitors is April or May 1962.

Core Reset Pulser

The research group has completed the preliminary design of a solid-state reset pulser that delivers 50 amp to each of eight cores. The pulse duration has been set at about 100 μsec. This is short enough to minimize heating in the isolation choke. The first of these pulsers is being life-tested before final construction is ordered. The system will require 42 chassis of this type (plus spares). A production prototype should be ready by February 1 and a fabrication contract awarded by about March 1, 1962.

System-Timing Generator

Digital time-delay generators have been ordered (Hewlett-Packard Model 218A) for timing the various parts of the accelerator.

The Research Group is designing input and output equipment to be used with the delays. The beam-initiating pulse must be line-synchronized to minimize magnetic fields at the cathode due to heater current. Gating and scaling circuits will be used to secure line synchronization at repetition rates below 60 pps. Output equipment is required, since the digital delays are not capable of triggering large numbers of chassis (for example, the 42-core reset pulsers).

Construction of the input and output equipment will probably be done in local fabrication shops, since no large quantities are required. Delivery promises on delays and other items indicate the timing system can be completed by about March 1, 1962.

Controls and Interlocks

Necessary but less intriguing bits of the system include controls and safety interlocks. The thyratron switch chassis are the most numerous items requiring control. A double rack containing eight switch chassis will

be turned on by a group control panel located in each rack. Detailed drawings are being prepared for prototype construction. After test, a contract for 50 to 60 such panels can be placed, probably about March 15, 1962.

Several groups will be controlled by a division control located at the remote-control console. The details of these controls and tentative layouts have been worked out. Construction will proceed from prototype to contract as with other parts of the system. Completion is estimated for some time in late March or April. The prototype division control will be used earlier for the gun section.

Other controls for the remote operation of charging supplies, reset pulsers, timing generator, cathode heater, vacuum pumps, and cooling blowers will be constructed by local shops as required.

Areas of Continuing Research

As mentioned at the beginning, there are unsolved problems remaining. Certainly system reliability must be included in this catagory. Large numbers of identical circuits operating simultaneously require very long individual life expectancies. This has been impossible to measure accurately on a few samples, although a great deal of the engineering effort has been used for this purpose.

Based on these very limited statistics, it is probable that the overall operation of the accelerator will be moderately successful at low repetition rates. However, better components may be necessary to attain reliable operation at high repetition rates.

A method for monitoring the output of each of the pulsers is necessary. Equipment of this sort has been worked on by the computer group in Bldg. 170 and a small model has been built. It will detect pulsers producing low or poorly timed pulses and indicate this on a central light panel so that the operator may shut down or adjust faulty equipment. Without such information it will be very difficult to determine which of nearly 500 circuits have depreciated or are inoperative.

The monitoring system is partially designed and will be added after the accelerator is constructed.

The Astron Facility

Progress has been made on the design and construction of the Astron facility. This includes the equipment, apart from the accelerator, for trapping the E layer and containing the plasma.

Main Field Power Supplies

Specifications have been prepared and bids will be secured in January for approximately 100 dc power supplies. They are needed for the magnetic field structure of the main reaction tank.

These power supplies will be located on the deck over the north pit in Building 157 to minimize lead length (and line drop) at currents ranging up to 1100 amp. A total power demand for the group of power supplies will be about 1.6 megawatts.

Plant Facilities is preparing the necessary structure to support the power supplies on the decked area and to provide the utility power.

Magnet Leads

Coaxial magnet leads with water cooling are to be used for the inner coils. Samples of spirally supported coaxial transmission line have been purchased. Flow measurements are being made to test the effectiveness of cooling before the final design is contracted.

Deceleration Resistors

Special resistive elements for decreasing the axial motion of the trapped electrons have been designed by Mechanical Engineering. Six have been ordered for evaluation, and quotations for the entire quantity (825) have been requested.

Research and Development Engineering

K. Aaland

Astron

Magnetic Modulators to Power Astron Cores

A magnetic modulator with a nonlinear lumped-constant PFN with compensating properties was designed to power a 50% Ni-Fe 1/2-in. core, 8 in. i. d. × 24 in. o. d. Pulse properties were essentially the same as those obtained with the thyratron line modulator using a compensator. The effects of temperature rise at 60-pps repetition rates were not studied.

Magnetic Modulators for Triggering 500 Thyratrons Simultaneously

Two small-scale (2%) units were constructed for demonstration purposes. One was designed to have a 10% ramp ahead of the main pulse. This was to determine the effects, if any, on the thyratrons. Suppression by means of thyrite was demonstrated. The other unit had a rectangular output with about 0.03 μsec rise and a 0.5-μsec width.

A 1500-volt 0.1-ohm model was made. This was successfully expanded to two stages and driven from a single ignitron. No jitter in the nsec range was detectable between channels.

Another unit, rated 10 kv into 1.4 ohm, is under test and development. A peak power output of 100 Mw has been obtained. Temperature stabilization of the switching core has been given special attention. A regulated charging voltage is required. This power supply is finished and working and deserves a special description.

24-kv 5-kw Charging Supply

This new design of a resonant charging supply does not require a trigger, but can be gated, yet always delivers a regulated voltage, single pulse to 400 pps. The series tube, or hold-off diode, also works as a de-Q-er. The shunt coupling tube also acts as a shunt regulator. These are the only two tubes, and the balance of the circuitry is solid state (transistors).

Digital Timing System

Work proceeded on the hardware only. New plug-in chassis hardware was designed that utilizes printed circuit cards, connectors, front panel and shielding. For technical discussion of the timing system, see the quarter-year report for April - June, 1961.

Beam Flipper

This flipping can best be done by a magnetic deflection scheme, since only a few hundred gauss is required. An ON-OFF system is suggested.

All bending magnets are identical and will be machined out of high-frequency ferrite. The requirements can be satisfied by the Astron core pulsers with the type 5949A thyratron.

Beam Gater

The approach is not yet settled on the 100-kv, 2 - 3,000 amp beam gater. The new Litton switch tube appears best. An evaluation program is needed.

Core Reset Pulser, Astron Accelerator

A hard-tube 1-Mw blocking oscillator was originally developed for this purpose; however, it underwent voltage breakdown several times in the output transformer. A solid-state type was developed with silicon-controlled rectifiers (SCR). One 7-inch chassis has nine 50-amp outputs and is completely self-contained. No failures have occurred in more than one month of operations. A prototype for outside fabrication is being made.

Switch Development

David B. Cummings

Mechanical Switching

The fast mechanical crowbar relief switch has been modified to improve alignment. The testing and timing are finished. There has been no further activity on this project because of postponement of the requirement.

Ignitron Development

Tube Tests

The WX 4564 is a radical short low-inductance stackable tube designed for arc stabilization. Seven have been ordered and received, of which one had a molybdenum anode. One had a slow leak and is being replaced. With a low-inductance capacitor discharge circuit, this tube showed slower (0.5 to 1.5 μsec at 20°C) but reliable ignition with a 3-kv ignitor pulse. It also showed an inductance of 30×10^{-9} henrys as against 39×10^{-9} for the WX 4681 (below) in the same circuit. The remaining tests will be to look for arc stabilization on a major capacitor bank.

The Westinghouse WX 4681 and the General Electric GZ 7207 are identical 5-inch switching ignitrons built to LRL Specification L-1500. They have the standard 5555 outline and fittings, three rectifier ignitors, and no internal baffles. Both manufacturers failed to meet the 2200°C temperature specified for vacuum-baking the graphite anode prior to assembly. Westinghouse reached a conservative 2130°C and General Electric took their tubes back to improve the 2050°C maximum that they reached. Both tubes high-pot 5 to 10 kv better than the 5555. The WX 4681 has also held 20 kv consistently on a mild test performed by David R. Branum.

Two 2-inch ignitrons have been ordered for fabrication and testing by Westinghouse. These will be molybdenum-anode tubes with experimental ignitors designed to function when wetted. The WX 4838 will have a glass-tungsten dielectric ignitor. The WX 4839 will have a silicon carbide ignitor with the contact up into the center. These are the outgrowth of earlier work done here on nonwetting ignitors.

New Commercial Products

Westinghouse has recently registered three switching ignitron types which are essentially the most successful designs built for us by Westinghouse in the ignitron development program. Most of the innovations they embody were conceived here and incorporated into experimental designs in technical conferences with Westinghouse engineers.

The WL 7171 is an unpotted WX 3977, which was our first attempt at 2300°C anode vacuum baking. General Electric had already registered their GL 7171, which was an unpotted Z 5296 developed by them for LRL.

The WL 7740 is a WX 4233 which had a 1/4-in. radius in the throat and a vacuum-melted molybdenum anode.

The WL 7703 is a simplified version of the GL 7703 developed by General Electric under a development contract from LASL. The simplified glass seal was first built in the WX 4388.

In addition to these types they are registering the WX 4231, which has a 1/4-in. radius in the throat and has been used extensively here.

Technical Conferences

A meeting was held with General Electric tube engineers on the problem of improving their ovens to meet LRL Specification L-1500 for the GZ 7207.

Pinch-and-Collapse Program

Hugh W. Van Ness

Gamma Bank Area

Successful operation of most of the electronics equipment involved in the Levitron experiment has been obtained. However, internal insulation damage in the experimental device has necessitated shutdown for repairs. During this shutdown, tests are being run on the capacitor bank in order to determine the source of numerous small problems and to upgrade the bank in general.

The original 450-kc rf induction heating equipment was modified to operate at 10 kc. Successful liner heating to 500°C was obtained with the modified equipment. In addition, a 30-kw 10-kc motor generator system has been purchased and installed for future induction heating requirements.

The 1.5-farad electrolytic bank has been repaired. A great number of capacitors were found to have excessive leakage current which did not improve with charging. These have been replaced and a maintenance schedule has been instituted of weekly charging the bank to full voltage for approximately 15 min. This treatment helps to maintain the capacitors in good condition, even though their pulse service is infrequent.

Energy Storage System Investigation

The repaired unipolar generator was tested running as a motor and found to be in excellent condition. Machine balance at all speeds up to 10,000 rpm was very good and required no rebalancing. The starting torque required to overcome bearing friction has been reduced from its original value because of better centering of the rotor.

The load and megampere switch were assembled, tested, and installed in the pit with the machine.

Because of other program commitments, no further effort has been expended in testing of this system since the end of September. When the manpower situation eases sufficiently, this program will be reactivated.

Pyrotron Program

Cryogenics Coil Experiment

All bus installation has been completed. The battery supply and current metering have been operated successfully into a dummy load. About one-half the control valve cabling remains to be completed. The diagnostic

system design is complete, with equipment being fabricated. Installation of the diagnostic system will complete the system.

Alice

Load testing of the Alice modular coil sections has been completed. Out of ten modular sections charged to 3,000 amp or more, only one failed by shorting. This section was subsequently repaired and successfully tested. These coil sections have now been assembled to form the Alice Mirror field coil pair, mounted on their support cradle trucks, and are now awaiting installation with the confinement chamber vacuum system.

These preliminary coil tests have shown that the rise in coil temperature rise and, hence, rise in coil resistance during the long current charging time is greater than was anticipated. The results of a dummy load test run on one of the existing 300-kw selenium-rectifier Perkins power supplies showed that the present dc supply system would not be capable of supplying 6,000 amp at the required voltage of 750 volts. A load test was run on a 300-kw Perkins supply in Berkeley which had been converted to silicon diode rectifiers. The results of this test showed that this type of supply could furnish the required output in the Alice dc supply system. In addition, the kva demand would be less for the converted supplies at all load conditions. Silicon diode conversion kits have been ordered for the five Alice Perkins supplies.

Alice Ion Source Development

Operation of the ion source is continuing to maximize the beam current. A neutral ion beam current of 40 to 60 ma has been produced down the full length of the Alice beam tube to the extreme end of the beam burial chamber.

The ion-source high-voltage equipment cage installation has been reworked to minimize the electrical noise produced when the source arcs down. This is still a problem and further modifications are in progress.

A 30-kv 1-amp regulated accelerator supply has been successfully used with the ion source, although it is vulnerable to arc-down transients. The source can now be conveniently switched to run with the above-mentioned supply or with a 40-kv 2-amp Kenotron type supply unregulated, or through the hard-tube series regulator.

Owing to faulty components and electrical noise problems, considerable difficulty has been experienced in getting the J. C. Carter Rotating-Coil Fluxmeter to perform properly in the ion-source magnetic-field regulator system. Work on this is continuing.

Alice P-3 Ion Source (Occluded-Gas Ion Source Development)

Initial experiments on this equipment were concluded in August. The experiment was originally built in the Alice machine area, using part of the Alice machine vacuum and electrical systems. This experiment has now been relocated and rebuilt in an area where operations can continue independent of the Alice machine proper. Three 200-kw Bart-Messing dc supplies have

been installed in the East extension of Bldg. 156 to supply the power for the field coils on this setup. A new efficient hv supply has been built to charge the PFN used with this ion source. A 1200-volt 60-amp pulser has been built and successfully used with diagnostic equipment in this experiment.

Alice DDT (Diagnostics Development and Test)

The initial construction of this experimental complex is essentially complete. The Duo-Plasmatron ion source purchased from High Voltage Engineering has been operating satisfactorily. The need for well-regulated high-voltage accelerator and lens supplies is evident. Borrowed unregulated supplies are presently being used.

High-Vacuum Research

Development work was very ably done during the summer by Mr. Kenneth Hatch (summer graduate engineer employee) on ion gauge emission regulator circuits. The transistorized, dc filament power, emission regulator for the Westinghouse Schultz high-pressure ion-gauge tube was improved (LE 5110-1C). The above circuit was also adapted to the Veeco RG-75 ionization gauge tube (LE 8310-1). A versatile Veeco ion gauge chassis was also designed (LE 8309-1).

Pyrotron

David R. Branum

Table Top

During the past six months, the experiment has been operated for a total of 13,792 pulses. The average level for bank No. 1 has been ± 10 kv.

July and August were spent in getting the bank to fire and crowbar reliably into a high-inductance load coil. Several of the pulse load coils failed during this test period. The main bank, bank No. 1, was made more reliable by removing all but two of the series "firing" ignitrons.

From September on, the bank has been operating satisfactorily.

The capacitors for the added energy to the gate bank, bank No. 2, and bank No. 3 have been received and are stored awaiting the decision to build the two new bank sections.

Various small capacitor banks were constructed for the side experiments in this area.

The old Geneva exhibit bank is being installed in the Table Top area. The output pulser was modified for the new improved type A ignitrons, Type 4231. The old exhibit bank was discharged by conventional type A 5550 ignitrons that were not reliable above 10 kv.

An old dual Lee-type 60-volt 200-amp dc supply has been installed for one getter system, and a higher-output model is under design for another getter system on the main experiment.

Various types of photomultiplier bases have been designed and built for the experiment. Some are fast bases and some are bases that will accept fast signals that last 100 msec or longer.

Toy Top III

The experiment has been pulsed for 16,314 pulses at the run levels of the five energy-storage banks.

There have been a few capacitor explosions in bank No. 3; this bank uses the old 7.5-μf General Electric capacitors.

There have been several machine modifications that required new potted-type transmission lines from the bank main transmission line terminals to the coil load. For this use we now have gone to $1/4 \times 4$-in. solid copper potted-bus transmission lines.

The source bank continued to destroy the General Electric 7.5-μf 20-kv capacitors. Two new types of 7.5-μf 20-kv capacitors were ordered and installed in the source bank for an operating test. Now installed are units from Cornell-Dubilier and Sangamo. These units have been operating satisfactorily for more than 2 months.

Six Cornell-Dubilier 7.5-μf units were installed on bank No. 1. A new mounting arrangement is under design to try to increase the operating level of bank No. 1 from ± 14 kv to ± 17 kv, and later on, when the moly-anode type A ignitrons are received, to a maximum run level of ± 20 kv.

Two new delay generator types were designed and constructed for use on the experiment. The first type uses commercial lumped-constant push-button delays with input and output drivers installed. Ten channels are now in use on the experiment. This delay is a dual-channel 0- to 50-μsec delay generator and has proven very reliable. The second type is a 3-μsec to 1-msec phanastron dual-delay generator. Three models now in use on the experiment have proven reliable and accurate delay generators.

A third type of delay generator with a range from 3 μsec to 1 second is now under design.

The energy storage banks and associated control systems for the 2X Toy Top experiment in Bldg. 180 are now under engineering design. These designs include a new control room, 1.5×10^6 joules of new ± 20 kv capacitor banks, and 100,000 joules of new fast banks. The control work design includes controls for the above banks plus controls for 1.3×10^6 joules of capacitor bank now in use in Bldg. 157 and 5×10^6 joules of capacitor bank now partially installed in Bldg. 156 (the old Squash Court bank).

Two additional Kenotron-type 25-kv 4-amp kc charging supplies will be installed in Bldg. 156 to charge the added energy storage banks to be used in 2X Toy Top.

A special capacitor charging supply was designed and built that will charge fifty 7.5-μf capacitors to 10 kv in 10 seconds every 15 seconds. This

power supply will be used in the source bank of 2X Toy Top. A second supply is now under construction for the source trigger bank of 2X Toy Top. Both these supplies are small portable units.

P-4

The small amount of electronics engineering support needed for this experiment has been for a few diagnostic-type circuits. The main electrical electronic complex has been functioning normally.

High-Vacuum Lab

There has been a moderate amount of engineering effort expended in this area. The main portion of the work has been the development of an ion gauge power supply for the special nude gauge in use in this area. The model from the University of Illinois was found unsatisfactory and could not be modified to fit the gauge used. A new model is now under design.

Atomic and Molecular Physics

The electronics engineering effort for the past 6 months has been applied to design and construction of diagnostic tools for the experimental physicists. These design circuits included such units as six-channel dc amplifiers, pulse adders for ion detector, and reference signal gate delays.

Diagnostic Development

Charles B. Wharton, Joseph Katz, and Ronald Hawke

Astron Electron Beam Experiment

General

The vacuum system of the small discharge experiment has been improved, so that consistent, reproducible pressures of air, hydrogen, and helium can be maintained. A sketch of the vessel is shown in Fig. VI-3.

The reflectionless compound indicated was concocted from Sauereisen ceramic cement, powdered iron, Aquadag, and carborundum powder. The reflections from a 0.5- to 1.0-mm-thick coating, on either glass or metal, of 70- and 90-Gcs waves are less than 10% (compared with bare aluminum) at any angle. The vapor pressure is low, and after an overnight 100°C bakeout its presence in a 10^{-6}-mm vacuum chamber is not noticeable. The surface is refractory and hard, and does not deteriorate under plasma bombardment. Only one very faint spectral line of iron (5014 A) and one of carbon (4267 A) were identifiable when hydrogen was used as a filling gas. Aside from lines associated with the filling gas the spectrum was relatively clean. The nonreflective (microwave) coating was felt to be necessary after plots of the microwave fields inside the chamber showed some evidence of diffraction effects. These plots were made with a small probe carried by an x-y motion table. The presence of the coating and a careful alignment of the radiating horns eliminated virtually all stray interferences due to scattering of the microwaves.

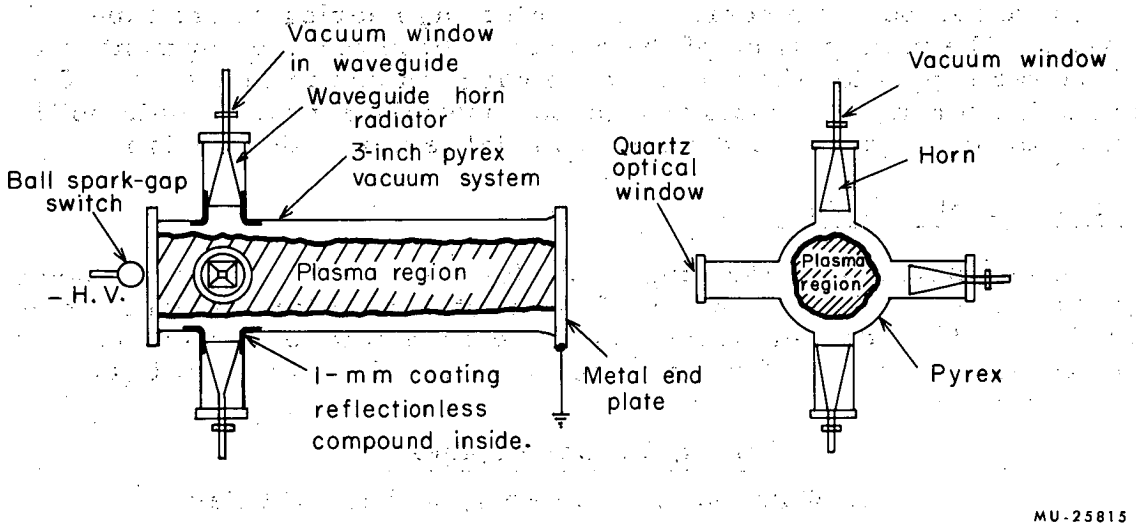

Fig. VI-3. Sketch of the vacuum chamber, with diagnostic ports.

Optical Spectroscopy

Spectroscopic observations have been made with a Bausch and Lomb monochrometer-and-multiplier phototube. To date only relative intensities, as a function of time, of the various ion and excitation lines have been made. No absolute intensity calibration was done; the value of making absolute intensity measurements in this experiment is dubious, since the plasma probably is not in thermal equilibrium.

With air we observed a hopeless multitude of lines. Some ionized states of oxygen were present early in time, indicating qualitatively that the electron temperature is at least a few ev.

With hydrogen as a filling gas we observed strong Balmer lines out to H_δ (4102 A), and faint molecular lines, such as 5812 A, 4634 A, and 4461 A. The molecular lines had disappeared within 20 μsec, but the ion lines (Balmer) persisted 70 or 80 μsec, indicating that the H_2 was rapidly dissociated (requiring at least 10 ev electrons) and that the electron temperature remained high long enough that the ion recombination was not excessively fast, as shown in Fig. VI-4A. The ionization had a tendency to be delayed in nearly all cases, but after 5 μsec built up at a fast rate, to a peak at 10 μsec. The impressed voltage and the plasma current are falling during that time and are very low by 10 μsec. Apparently the current early in time is being carried by relatively few high-velocity carriers (25 ka could be carried by a density of 2-kev electrons of about $10^{12}/cm^3$, corresponding to about 0.01% ionization) flowing through a weak, charge-neutralizing background, much like runaways. As the voltage across the tube and the current fall, the electrons begin coupling to the plasma, and rapid ionization occurs. The microwave observations, discussed below, bear out this conjecture.

With helium as a filling gas the delay of the He II lines was even more pronounced, the intensities actually falling and then rising again as shown in Fig. VI-4B. This behavior is probably due to the population of metastable states (during the fall) which later become ionized (giving the second increase). The electron temperatures deduced from the intensity ratios out to 10 μsec or so are thus suspect, since the metastable transitions cannot be accounted for in relating populations to intensities. The He II populations are probably underestimated by the 4686-A line intensity and the electron temperatures indicated in Fig. VI-5 are too low. It may be possible to quench the metastables by adding a small impurity of argon, which leads to a reaction

$$He^{met} + A \rightarrow He + A^+ + e^-$$

having a very large probability. We plan to try this.

Microwave Diagnostics

Extensive microwave transmission observations were made, under a wide variety of conditions, until we felt that we understood how the plasma density, spatial distribution, decay rates, collision rates, etc. scale with bank voltage and filling-gas pressure. Measurements were made at 35, 70,

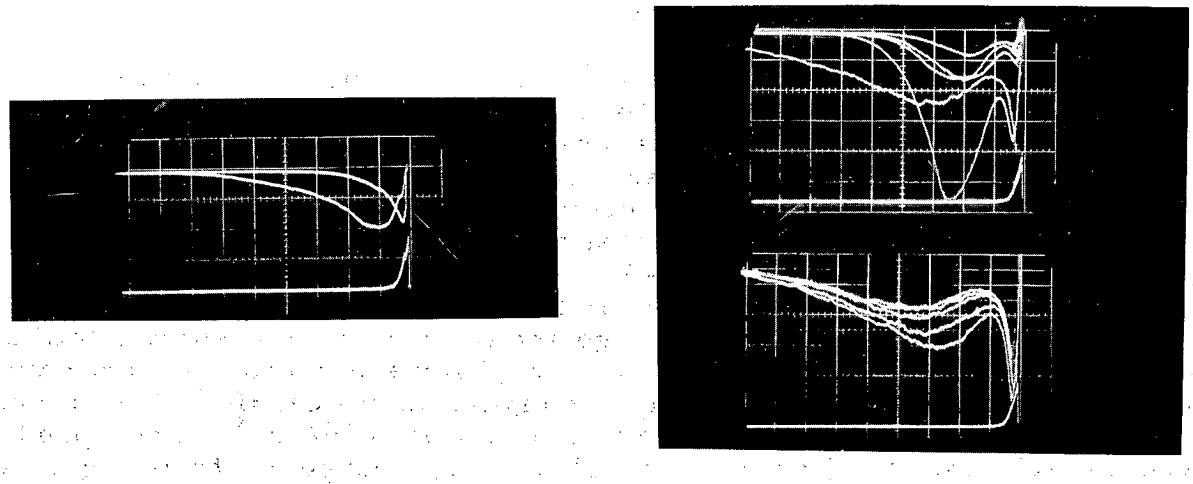

ZN-3011

Fig. IV-4. Spectroscopic diagnostics of the transient discharge.
(left) Hydrogen spectral line intensities.
Top traces: 4634-A H_2^* (short duration),
4861-A H_β (long duration)
(4861 intensity is attenuated 5 times).
Bottom trace: discharge current, 15 ka/cm.
Time: 10 μsec/cm. Pressure: 150 μ.
(right) Helium spectral line intensities.
Top picture: 4686-A He II.
Bottom: 5015-A He I.
Multiple exposures at different bank voltages,
top to bottom. 4.5 kv, 5 kv, 6 kv, 7 kv, 9 kv.
Current trace at bottom of each picture: 15,000 amp/cm.
Time: 10 μsec/cm.

and 90 Gcs, allowing central densities between 10^{11} and $10^{14}/cm^3$ to be inferred as a function of time. At low bank voltages (4 to 6 kv) the profile seemed roughly a cosine or J_0 Bessel shape. At higher bank voltages (8 to 10 kv) it seemed more peaked, like a cosine-squared or Gaussian distribution. The current densities are hardly sufficient to cause self-pinching ($< 10^3$ amp/cm^2); the change in shape must have more to do with plasma temperature (for example, radial variations in metastable densities) or the formation of cathode spots (although none were visible to the eye). Typical microwave interferometer fringes are shown in Fig. VI-6. The plasma density is very high after a microsecond or so, cutting off the transmission of both signals. (For these simultaneous measurements a microwave horn was installed in place of the optical window.) The 91-Gcs signal returns (in Fig. VI-6A) at about 50 μsec, corresponding to a central density of approx $10^{14}/cm^3$; the 70-Gcs signal returns a little later, corresponding to $6\times10^{13}/cm^3$. By counting fringes (one fringe denotes a phase change of 2π) and measuring the envelope amplitude one obtains the complex transmission coefficient as a function of time, which is related to the central density and the profile by well-known methods. By extending the curves of density in the top frame of Fig. VI-5 to early times, one might guess that the maximum density reaches $10^{15}/cm^3$. Original plans were to install equipment operating at 120 Gcs (cutoff density of $2\times10^{14}/cm^3$), and some of the components have been developed or acquired, but the technical difficulties seem to outweigh the gain in information at the moment.

Early attempts to measure the electron temperature by microwave radiometry were disappointing. No obviously "thermal" radiation could be seen at the time the plasma was "black" (i. e., just coming out of cutoff), and annoying spikes of high-intensity radiation were observed just at the end of the current pulse. After the 70-Gcs receiver had been improved somewhat and the attenuation in the waveguide had been decreased, the thermal signal showed up occasionally (see Fig. VI-6B) and, by estimating and measuring several quantities, we arrived at a calibration relating amplitude to electron temperature. The early signal is still somewhat puzzling, since at times its amplitude is so large as to correspond to 15 kev "noise temperature." From this one concludes that it is nonthermal radiation and probably is associated with an instability. A good guess might be a two-stream type, which excites plasma oscillations. The oscillating frequency would be at the plasma frequency, but the waves are longitudinal and thus nonradiating. If steep density gradients were present, however, some mode conversion to radiative electromagnetic waves could occur and a small radiation field might escape the plasma. (See the section on P-4 Instability Experiment below.) At the plasma frequency the microwave transmission changes from propagating to cutoff. Careful scrutiny of the transmission data (see Fig. VI-6B) shows that an "opening up" of the plasma occurs at the time of each radiation burst. Also the path is not completely opaque until several microseconds after the current begins; in fact it first becomes opaque at the same time the intense radiation burst begins, suggesting that the critical density has been reached at that time. Radiation burst at 35 Gcs were also seen, but earlier in time, a fact also in agreement with the low initial density conjecture. Comparison of the temporal behavior of ionization light (such as the Balmer lines for hydrogen or the He II lines) and the radiation pulses shows that in nearly all cases the onset and ending of the radiation pulses (typically 3 and 9 μsec, respectively) and the rise times of the ion line intensities correspond exactly.

Fig. VI-5. Composite data analysis for hydrogen filling gas.
a. Peak electron density in a cosine spatial distribution, as determined by microwave interferometry. Pressure: 150 μ H_2. Bank voltage: 9 kv (Gives approx 25 ka)

b. (left) Electron temperature, as estimated from rate of population of ionized states and rate of dissociation of H_2, determined by optical line intensities.

b. (right) Electron temperature, as estimated from the intensity of microwave radiation, the reflectivity, and the absorptivity of microwaves at 70 Gcs.

c. Microwave radiation intensity at 70 Gcs, 9 kv, 150 μ.
$I = \sqrt{P}$, where P is the noise power equivalent in ev; $P = kT \Delta f$
(I = 40 corresponds to 1600 ev;
I = 3 corresponds to 9 ev)

d. Microwave transmission through the plasma at 70 Gcs.

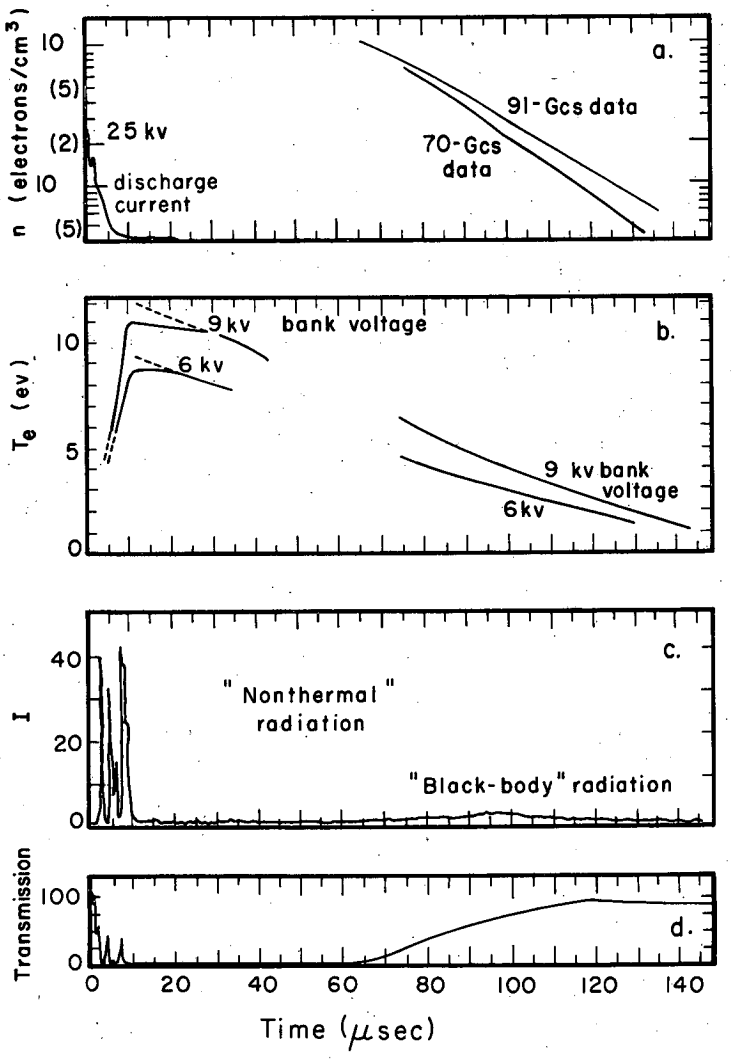
n (electrons/cm³)
10
(5)
(2)
10
(5)
25 kv
discharge current
a.
91-Gcs data
70-Gcs data
Te (ev)
10
5
0
9kv bank voltage
6 kv
b.
9 kv bank voltage
6kv
I
40
20
0
"Nonthermal" radiation
"Black-body" radiation
c.
Transmission
100
0
d.
0
20
40
60
80
100
120
140
Time (μsec)
MU-25863

Fig. VI-5.

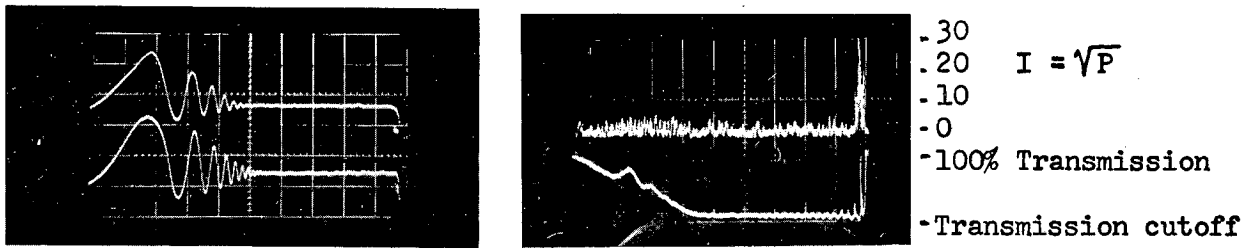

Fig. VI-6. Microwave diagnostics of the transient discharge.
(left) Microwave interferometer responses.
Top trace, 70 Gc; bottom, 91 Gc.
Time, 20 μsec/cm.
(right) Microwave radiation-transmission.
Top trace, 70-Gc radiation; bottom, 70-Gc transmission.
Time, 20 μsec/cm.

A possible conclusion then is that (a) the early current, up to about 3 μsec, is carried by "runaway" electrons in a weakly ionized background; (b) as the voltage and current fall off an instability is excited, which couples the high-velocity electrons strongly to the plasma electrons, (c) the ionization increases rapidly from some 0.01% to about 10% and the electrons become thermalized at a few ev, depending upon the initial voltage and current density.

Further measurements with probes, rotating-mirror cameras, and a 90-Gcs radiometer may shed more light on the question.

Pyrotron

Toy Top III

No plasma microwave measurements have been made by us in this period. A considerable amount of development of components and techniques has been accomplished with the hope that we could get some machine time in order to continue the radiation measurements begun at the beginning of the year.

Electroformed thin-wall horns were made and tested in pulsed magnetic fields. Low-conductivity nickel gives the horns mechanical strength and damps induced eddy currents. A thin film of copper gives them good microwave properties.

Resonant slot radiators have been made at 8-mm (35-Gc) and 4-mm (70-Gc) wavelengths and installed on a teflon ring to be slipped inside the machine for electron density and profile measurements (see Fig. VI-7). The slots have radiation patterns very much like small horns, and allow inaccessible regions to be reached.

Low-loss waveguides in the TE_{11} ⊙ mode were developed for 35, 70, and 90 Gcs. Ten-foot sections and 90° elbows were fabricated from hard-drawn copper tubing. Special choke-joint flanges and mode transitions were electroformed. Typical performance at 70 Gcs was: VSWR, < 1.05; loss, ~2 db for a 10-foot run plus two transitions. This compares with 18 db for an equivalent run of RG-98/U coin silver waveguide.

Vacuum waveguide windows for 70 and 90 Gc were made by splitting mica down to approx 1 mil thickness and fastening it with low-vapor-pressure epoxy in a 6-mil-deep spot on the waveguide flange. VSWR is < 1.4, and losses as low as 1 db are typical; 35-Gc windows have better performance.

Voltage isolation sections in the 35-, 70-, and 90-Gc waveguides, to break up ground loops and permit floating horns, have been made to hold off 10 kv and introduce only 1 db of loss.

The radiometers made up for Toy Top were used in the experiment discussed above but are available for Toy Top's use at any time.

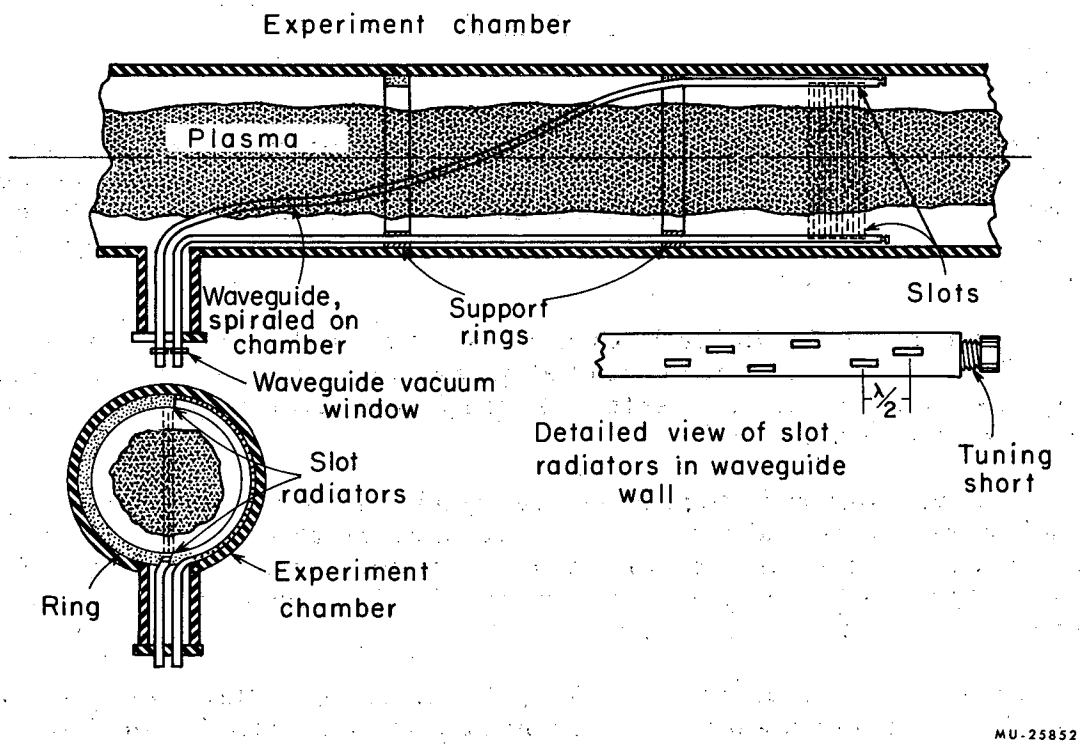

Fig. VI-7. Slot radiators in waveguide, used for plasma diagnostics in regions not accessible to horns.

Table Top

A microwave interferometer system has been installed to measure the electron density as a function of time. The expected density and spatial distribution are in an awkward range for microwaves, in that the density is only about 10^{11} and the diameter only a few centimeters. Ideally one should use resonant-cavity techniques at S band (3 Gc), but it is hard to see how to put a cavity inside a plasma-compression experiment. A compromise was made, viz., 7.9 Gc (3.8 cm), which has a cutoff density of $7\times10^{11}/cm^3$. In a 5-cm path of $n = 10^{11}/cm^3$ plasma, an interferometer will see a change in phase of only 0.16 fringe (60°) if the density is uniform and only half that if n has a cosine distribution. To be able to measure such small changes in phase one must stabilize the klystron frequency. A very simple frequency-stabilization system (AFC) has been built. The stabilizer is a tunable resonant cavity, whose frequency is swept back and forth at a 500-kc rate by modulating the capacity of a varactor diode mounted in one end wall. The reflected signal from the cavity is detected by a crystal diode. When the transmitter klystron is tuned slightly to one side of the cavity's response frequency the detector has a 500-kc output, which is amplified by a tuned amplifier and fed to a phase bridge. The dc output of the bridge is connected to the klystron repeller in the proper sense to pull the frequency toward the center of the cavity response frequency. To get greater stability, the gain characteristic of the 500-kc amplifier is nonlinear, i.e., it has greater gain at small signals (near the null). The overall stability is being checked against a Stalo system. So far it looks quite good.

The microwave interferometer is quite standard, except that the video amplifiers are direct-coupled differential amplifiers. Here dc amplifiers are needed because of the very slow time scale of the Table Top experiment. The differential amplifier rejects the common mode (dc level) resulting from biasing the crystal detectors up into their linear range with a large reference path signal (milliwatt level). Small changes in phase then give a linear output voltage response instead of square-law.

Some very preliminary measurements have yielded puzzling data. A maximum deflection corresponding to about 0.25 fringe (90°) is seen, denoting an n maximum of approx $2\times10^{11}/cm^3$, but the time dependence is wild. There may be internal reflections or resonances from the vacuum chamber or other effects. We are now attempting to single out the real from the spurious effects, by trying reflectionless coatings and different radiators.

P-4 Instabilities Experiment

Our equipment for measuring the bursts of microwave radiation, presumably due to instabilities, has been in use by Andrew L. Gardner, who is presenting his observations elsewhere in this report (Section I. 9). We have assembled additional 8-mm radiometers and plan to look at several locations along the column, both upstream and down, to see how the radiation varies with position. We also will do some experiments directed at understanding how the instability waves (which are nonradiative) can couple to external radiation fields.

VII. TALKS AND PUBLICATIONS

San Francisco Wescon Conference, San Francisco, Calif., August 22-25, 1961

V. L. Smith, Development of 32-Megawatt Modulators for the Astron 1000-Megawatt Electron Accelerator, UCRL-6469-Abst., May 5, 1961.

Gas Dynamics Symposium, sponsored by the American Rocket Society and Northwestern University, Evanston, Ill., Aug. 23-25, 1961.

Alan W. DeSilva, John M. Wilcox, William S. Cooper III, and Forrest I. Boley, Experiments on Alfvén-Wave Propagation, UCRL-9523 Abst., Jan. 1961, and UCRL-9523, June 27, 1961.

Fifth International Conference on Ionization Phenomena in Gases, Munich, Germany, Aug. 28-Sept. 1, 1961.

Wulf B. Kunkel, Hydromagnetic Ionizing Waves (invited paper), UCRL-9612 Rev., August. 14, 1961.

IAEA Conference on Plasma Physics and Controlled Fusion Research, Salzburg, Austria, Sept. 4-9, 1961.

R. F. Post, Critical Conditions for Self-Sustaining Reactions in the Mirror Machine, UCRL-6377, June 10, 1961.

E. J. Lauer, G. Gibson, and W. C. Jordan, Containment of Positrons in an Asymmetric Mirror Geometry, UCRL-6380, June 8, 1961.

F. H. Coensgen, W. F. Cummins, W. E. Nexsen, Jr., and A. E. Sherman, Production and Containment of Hot Deuterium Plasmas in Multistage Magnetic Compression Experiments, UCRL-6381, June 7, 1961.

John Killeen, Warren Heckrotte, and Garret Boer, Energy Transfer from Hot Ions to Cold Electrons in a Plasma, UCRL-6383, June 12, 1961.

Harold P. Furth, The "Mirror Instability" for Finite Particle Gyro-Radius, UCRL-6384, June 5, 1961.

S. A. Colgate, H. P. Furth, C. W. Hartman, and R. L. Spoerlein, Particle Motion on Magnetic Flux Surfaces in "Stabilized" and Hard-Core Pinches, UCRL-6385, June 12, 1961.

William A. Newcomb, Lagrangian and Hamiltonian Methods in Magnetodydro-dynamics, UCRL-6387, June 12, 1961.

Nicholas C. Christofilos, Energy Balance in the Astron Device, UCRL-6390, June 15, 1961.

Nuclear Instrumentation Symposium, sponsored by ISA, AIEE, and IRE, at North Carolina State College, Raleigh, N. C., Sept. 6-8, 1961

W. F. Cummins, Diagnostic Techniques of the High-Compression and Neutral-Injection Experiments (invited paper), UCRL-6492-T, June 30, 1961.

C. B. Wharton, A Survey of Plasma Instrumentation (invited paper), UCRL-6521-T, August 1961.

Brookhaven International Conference on High Energy Accelerators, Upton, Long Island, N. Y., Sept. 6-12, 1961.

C. E. Taylor and R. F. Post, Cryogenic Superconducting Techniques, UCRL-6601, Aug. 29, 1961.

14th Annual Gaseous Electronics Conference, General Electric Research Laboratories, Schenectady, N. Y., Oct. 11-13, 1961.

Melvin J. Bernstein and Wulf B. Kunkel, Electron Drift and Diffusion Measurements in Hydrogen in a Transverse Strong Magnetic Field, UCRL-9818 Abstract, Aug. 15, 1961.

Second International Congress on Vacuum Technology, Washington, D. C. Oct. 16-19, 1961.

Norman Milleron, Preliminary Pumping Results with Penning-Type Discharges Supported on Condensable Metal Vapors, UCRL-5598, July 26, 1961.

Norman Milleron and Leonard L. Levenson, Progress on Optimization of Oil Diffusion Pump Systems for Ultrahigh Vacuum. III, UCRL-6407, July 26, 1961.

Leonard L. Levenson and Norman Milleron, Adsorption Capacities of Some Room-Temperature Trap Materials, UCRL-6396, July 24, 1961.

T. H. Batzer, Evaluation of a High-Temperature Functional Fluid in a Conventional Diffusion Pumping System, UCRL-6577-T, Aug. 10, 1961.

J. R. Ullman, Commercial Seals as Seats in a Bakable Valve, UCRL-6565-T, Aug. 10, 1961.

American Institute of Electrical Engineers General Fall Meeting, Detroit, Mich., October 19, 1961.

R. F. Post, Present Feasibility Picture for Fusion Power Generation with Mirror Machines (invited paper).

Sherwood Vacuum Conference, Washington, D. C., October 20, 1961.

A. L. Hunt, Adsorption on Condensed Films (informal talk).

International Conference on High Magnetic Fields, Massachusetts Institute of Technology, Cambridge, Mass., November 1-4, 1961.

F. H. Coensgen, Plasma Confinement in Magnetic Mirror Fields (invited paper), UCRL-6566-T, July 27, 1961.

H. P. Furth, Pulsed Magnets (invited paper), UCRL-6551-T Abst., July 21, 1961.

C. E. Taylor and R. F. Post, Cryogenic Coils (invited paper), UCRL-6672-T, October 26, 1961.

APS Division of Plasma Physics 3rd Annual Meeting, Colorado Springs, Colo., Nov. 15-18, 1961.

S. A. Colgate, Recent Experiments in Pinch Confinement (invited paper).

Harold P. Furth, Hydromagnetic Instabilities in Fluids of Finite Conductivity (invited paper).

H. P. Furth, Instability of Thermally Anistropic Plasmas, UCRL-6591-T Abst., Aug. 18, 1961.

R. F. Post, Critical Parameters for Some Plasma Instabilities in the Mirror Machine, UCRL-6587-T Abst., Aug. 16, 1961.

C. C. Damm, J. F. Steinhaus, and N. L. Oleson, Cold Plasma Trapping in Neutral Injection Experiments, UCRL-6614-T Rev. Abst., Sept. 20, 1961.

T. O. Passell, Calorimetric Studies of Plasma Heated by Adiabatic Magnetic Compression, UCRL-6610-T Abst., Sept. 1961.

F. H. Coensgen, W. F. Cummins, W. E. Nexsen, Jr., and A. E. Sherman, Observed Transverse Plasma Drift in a Magnetic Mirror Field, UCRL-6593-T Abst., Aug. 22, 1961.

W. B. Kunkel and R. A. Gross, Hydromagnetic Ionizing Fronts, UCRL-9854 Abst., Sept. 1961.

S. A. Colgate, D. H. Birdsall, H. P. Furth, and C. W. Hartman, A Hard-Core Toroidal Pinch, UCRL-6592-T Abst., Aug. 21, 1961.

J. R. Hiskes, F. E. Harris, and G. A. Paulikas, Formation and Electric Dissociation of the Helium Hydride Isotopic Molecular Ions, UCRL-6618-T Abst., Sept. 12, 1961.

A. L. Gardner, Localized Determination of Electron Density in the Plasma of the P-4 System, UCRL-6620-T Abst., Sept. 14, 1961.

C. W. Hartman, High-Q Magnetosonic Oscillations, UCRL-6613-T Abst., Sept. 8, 1961.

APS 1961 Thanksgiving Meeting, University of Chicago, Chicago, Ill., Nov. 24-25, 1961.

R. H. McFarland and E. A. Soltysik, Polarization of Light Resulting from the Excitation of Helium by Electrons, UCRL-6623-T Abst., Sept. 18, 1961; Bull. Am. Phys. Soc. Ser. II 6, 423 (1961).

Sixth Lockheed Symposium on Magnetohydrodynamics, Palo Alto, California, Dec. 15-16, 1961.

Wulf B. Kunkel and Robert A. Gross, Hydromagnetic Ionizing Waves, UCRL-9936 Abst., Nov. 1, 1961.

R. F. Post, Plasma Instabilities and the Mirror Machine, UCRL-6705-T Abst., Nov. 30, 1961.

APS 1961 Winter Meeting in the West, University of California, Los Angeles, Calif., Dec. 27-29, 1961.

Wulf B. Kunkel, Production of Highly Ionized Gases in the Laboratory for Basic Plasma Research (invited paper).

F. H. Coensgen, Production and Containment of Hot Deuterium Plasmas (invited paper).

Willard C. Jordan, Containment of Positrons in an Asymmetric Mirror Geometry (invited paper).

Angus L. Hunt, Clyde E. Taylor, and John E. Omohundro, Adsorption of Hydrogen on Solidified-Gas Films, UCRL-6626-T Abst., Sept. 28, 1961; Bull. Am. Phys. Soc. Ser. II 6, 512 (1961).

H. F. Rugge, G. A. Paulikas, Robert V. Pyle, and J. W. Stearns, Hollow-Cathode Strontium Plasma Source, UCRL-9899 Abst., Oct. 1961; Bull. Am. Phys. Soc. Ser. II 6, 517 (1961).

Publications

American Journal of Physics

Allan N. Kaufman, Definition of Macroscopic Electrostatic Field, 29, 626 (1961) (UCRL-6273, Jan. 1961).

Annals of Physics

T. G. Northrop, The Guiding-Center Approximation to Charged Particle Motion, 15, 79 (1961) (UCRL-5708-T, Mar. 15, 1960).

Journal of Applied Physics

Angus L. Hunt, Charles C. Damm, and Earl C. Popp, Attainment of Ultra-high Vacua, Reduction in Surface Desorption, and the Adsorption of Hydrogen by Evaporated Molybdenum, 32, 1937 (1961) (UCRL-5889 Rev., Feb. 1961).

Journal of Nuclear Energy, Part C, Pergamon Press

B. J. BenDaniel, Plasma Potential in a Magnetic Mirror System, 3, 235 (1961) (UCRL-6235, Jan. 21, 1961).

R. F. Post, Impurity Radiation Losses from a High-Temperature Plasma, 3, 273 (1961) (UCRL-6130, Sept. 1960).

The Physics of Fluids

Richard F. Post, Equilibrium Ambipolar Potentials in a Mirror Machine, 4, 902 (1961) (UCRL-6342-T Rev., March 6, 1961).

John M. Wilcox, Alan W. DeSilva, and William S. Cooper III, Experiments on Alfvén-Wave Propagation, 4, 1506 (1961) (UCRL-9613, May 10, 1961).

Physical Review Letters

Selig Kaplan, George A. Paulikas, and Robert V. Pyle, Dissociation of H_2^+ Ions by a Magnetic Field, 7, 96 (1961), (UCRL-9763, June 26, 1961).

Review of Scientific Instruments

Robert E. Ellis and Norris W. Carlson, A Calibrated Scintillator Probe for Determining Energy Distribution, Density, and Mean Energy of the Electronic Component of Pyrotron Plasma, 32, 1367 (1961) (UCRL-6412, April 17, 1961).

Other UCRL Reports Issued in 1961

Lewi Tonks, Magnetic Field Reversal by Relativistic Electrons Which Slow Down While Circulating in a Uniform Impressed Magnetic Field (final report of consultant), UCRL-5733 (Rev.), Sept. 7, 1961.

James F. Steinhaus and Charles C. Damm, Trapping and Confinement of 20-kev Hydrogen Atoms in a Magnetic Mirror Machine, UCRL-6131, Dec. 1960.

David J. BenDaniel, A Theory of Scattering Loss from a Magnetic Mirror System, UCRL-6236, March 7, 1961.

Stirling A. Colgate, Aerodynamic Turbulent Skin Friction, UCRL-6256, Feb. 8, 1961.

Harold P. Furth, Hard-Core Pinches, UCRL-6266, January 1961.

David B. Cummings,Minimum Rise Times of Current in Ignitrons, UCRL-6276, January 10, 1961.

Laurence S. Hall, Thermodynamic Cycling in Magnetic Pumping, UCRL-6355, March 16, 1961.

William L. Barr, A Method for Computing the Radial Distribution of Emitters in a Cylindrical Source, UCRL-6440, June 9, 1961.

Laurence S. Hall, Probes and Magnetic Pumping in Plasma (Thesis), UCRL-6535, July 19, 1961.

David J. BenDaniel, Asymptotic Scattering Loss from a "Long" Magnetic Mirror System, UCRL-6554, Oct. 12, 1961.

Laurence S. Hall and Andrew L. Gardner, P-4, a Steady-State Plasma System, UCRL-6561, Sept. 27, 1961.

Andrew L. Gardner, William L. Barr, Raymond L. Kelly, and Norman L. Oleson, Diagnostic Measurements on the P-4 Steady-State Plasma, UCRL-6562, Oct. 24, 1961.

Alvin M. Saperstein, Stability of Cylindrical Plasmas for Axial Perturbation Wavelengths Less than the Radial Thickness of the Equilibrium Plasma, UCRL-6585, Aug. 7, 1961.

Edmund S. Chambers, Ion Cyclotron Resonance Heating of Deuterium Plasma Using a Radial Electric Field, UCRL-6668, Oct. 24, 1961.

Angus L. Hunt, Clyde E. Taylor, and John E. Omohundro, Rates of Hydrogen Adsorption on Solidified Gas Films, UCRL-6679, Nov. 3, 1961.

Alan W. DeSilva, William S. Cooper III, and John Wilcox, Alfvén-Wave Reflections and Propagation Modes, UCRL-9496, Feb. 2, 1961.

William S. Cooper III, Alan W. DeSilva, and John M. Wilcox, Ion Density Measurements in a Decaying Hydrogen Plasma, UCRL-9509, Mar. 1, 1961.

Theodore G. Northrop, The Adiabatic Motion of Charged Particles in Electromagnetic Fields, UCRL-9517, January 1961.

John M. Wilcox, Alan W. DeSilva, William S. Cooper, III, Pierre F. Pellissier, and William R. Baker, A Device for Generating a Highly Ionized Hydrogen Plasma, UCRL-9528, Jan. 16, 1961.

George A. Paulikas, The Positive Column in a Longitudinal Magnetic Field (Thesis) UCRL-9588, Feb. 27, 1961.

Alan W. DeSilva, Experimental Study of Hydromagnetic Waves in Plasma, (Thesis) UCRL-9601, March 17, 1961.

Melvin J. Bernstein, Electron Drift, Diffusion, and Ionization Measurements in Hydrogen with Crossed Electric and Strong Magnetic Fields, (Thesis) UCRL-9865, Oct. 4, 1961.

Gordon Gibson, Willard C. Jordan, and Eugene J. Lauer, Steady Injection of a Beam of Energetic Charged Particles into the Bumpy Torus, Design of a Proposed Electron Experiment, UCID-4241, Feb. 28, 1961.

Charles W. Hartman, An Electrostatic Plasma Accelerator, UCID-4243, March 8, 1961.

N. W. Hetherington and C. H. Woods, Adiabatic Motion Near the Center of a Magnetic Mirror, UCID-4246, April 3, 1961.

Warren Heckrotte and John R. Hiskes, Decay of the Magnetic Field Components Generated by a Relativistic Electron Stream Moving Through a Plasma, UCID-4251, March 21, 1961.

John R. Hiskes, Lorentz Dissociation in Neutral Injection Systems, UCID-4261, April 13, 1961.

Nicholas C. Christofilos, Note on the Stability of the E Layer, UCID-4274, May 12, 1961.

Nicholas C. Christofilos, Marginal Stability of an Infinite, Cylindrical E Layer of Finite Thickness, UCID-4277, May 18, 1961.

V. Kelvin Neil, Electromagnetic Coupling Instabilities in Astron, UCID-4288, June 1, 1961.

Harold P. Furth, Spontaneous Generation of Azimuthal Magnetic Field in the E Layer, UCID-4297, June 6, 1961.

A. M. Saperstein, The Stability of Plasmas Having Cylindrical Symmetry Using the Linearized Collisionless Boltzmann Equation, UCID-4337, July 5, 1961.

Harold P. Furth, Finite-Conductivity Flute Instabilities, UCID-4374, Oct. 12, 1961.

Information Division
sa